

**Development of a Cold End and High-Efficiency Valves
for a One-Watt 10 Kelvin Cryocooler**

by

Matthew J. Traum

B.S., Mechanical Engineering (2001)

B.S., Aerospace Engineering (2001)

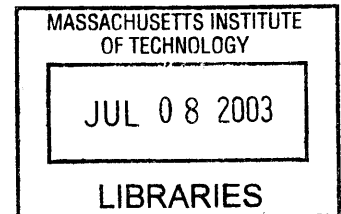
University of California, Irvine

**Submitted to the Department of Mechanical Engineering in
Partial Fulfillment of the Requirements for the Degree of
Master of Science in Mechanical Engineering**

at the

Massachusetts Institute of Technology

June 2003



© 2003 Massachusetts Institute of Technology
All Rights Reserved

Signature of Author.....

Matthew J. Traum
Department of Mechanical Engineering
May 9, 2003

Certified by.....

John G. Brisson
Professor of Mechanical Engineering
Thesis Advisor

Accepted by.....

Ain A. Sonin
Chairman, Department Committee on Graduate Students

BARKER

Development of a Cold End and High-Efficiency Valves for a One-Watt 10 Kelvin Cryocooler

by

Matthew J. Traum

**Submitted to the Department of Mechanical Engineering on
May 9, 2003 in partial fulfillment of the requirements for the
Degree of Master of Science in Mechanical Engineering**

ABSTRACT

The comprehensive mechanical design for a feasible cold end unit capable of executing the expander portion of one-stage of a multistage Collins cycle is presented. This device is a working demonstration prototype for a three-stage cryocooler that will be capable of lifting one Watt at 10 Kelvin. Emphasis is placed upon the development of the cryogenic cold valves and their integration into the cold end. An evolutionary design iteration process based on finite-element modeling is pioneered and posited. This process allows convergence to optimal valve geometry via computer modeling without the necessity of building or testing hardware. An experimental process for static benchmarking is described, and the sensitivity of the valve to various geometric tolerances is explored. The finite element model is combined with other analytical models and utilized to develop a series of first-order modeling approximations for several aspects of the cold end operation and performance.

Thesis Supervisor: John G. Brisson

Title: Professor of Mechanical Engineering

ACKNOWLEDGEMENTS

I would like to extend my appreciation to Professor Joseph L. Smith, Jr. and Professor John G. Brisson, for selecting me to take on this project. Developing a working machine from a concept in our imaginations allowed me to take marvelous excursions into disciplines that I had never explored before. I have no doubt that the analytical and practical engineering skills I gleaned from this experience will serve me throughout the rest of my career. Professor Smith and Professor Brisson displayed tireless effort to assure I used this opportunity to exercise my education, learn how to think, and understand problem solving in a more rigorous way.

The success of this project is also indebted to Mike Damaree. Mike's expertise and skill as a technician is matched only by his ability as a teacher. Mike taught me that it is much more fun to solve a problem by getting your hands dirty than to push numbers around a page.

For being my role models and helping me work my way through the most difficult moments of this project, a special thank you goes out to my laboratory mates Franklin Miller and Fritz Pierre. For their infinite support throughout my difficult process of growing into an MIT graduate student, Franklin and Fritz have earned my lifelong respect and friendship.

Finally, for their financial support, I would like to thank Advanced Mechanical Technology, Incorporated of Watertown, Massachusetts. They were always a valuable resource of engineering know-how, and their participation served as a continuous reminder of the practical applications my work had to offer. None of the cold end development would have been possible without their support.

BIOGRAPHICAL NOTE

Matthew J. Traum graduated Cum Laude from The Henry Samueli School of Engineering at the University of California, Irvine in June 2001. He holds a B.S. in Mechanical Engineering and a B.S. in Aerospace Engineering from UC Irvine; he is also the recipient of a minor in Women's Studies. Traum attended the University of Bristol in the United Kingdom as an exchange student in 2000 where he was a non-matriculating member of the Master of Engineering Program within the Department of Aerospace Engineering. While in the UK, Traum co-authored an M.Eng thesis entitled "Autogyro Pitch Sensitivity in Low-Speed Forward Flight."

Traum is a lifetime member of Phi Beta Kappa national honor society, Tau Beta Pi national engineering honor society, and Pi Tau Sigma national mechanical engineering honor society. Traum is also a lifetime member of the Association of Energy Engineers (AEE). His professional affiliations include the American Society of Mechanical Engineers (ASME), the American Institute of Aeronautics and Astronautics (AIAA), and the National Society of Professional Engineers (NSPE).

TABLE OF CONTENTS

Chapter 1 — Introduction.....	6
1.1 Project Motivation.....	6
1.2 Collins Cycle Overview.....	7
1.3 Rationale for Miniaturization.....	10
1.4 Enabling Technologies.....	11
1.5 Contribution of this Thesis.....	11
Chapter 2 — Background and Hardware Description.....	13
2.1 Previous Work.....	13
2.2 Valve Hardware Description.....	14
2.3 Description of Design Constraints.....	26
2.3.1 <i>Benefit Tradeoffs of Electromagnetic Valves</i>	28
Chapter 3 — Valve Geometry Optimization.....	30
3.1 Physical and Material Parameters.....	31
3.1.1 <i>B-H Curves, Machine-ability and Material Selection</i>	33
3.1.2 <i>Modeling the B-H Curve</i>	34
3.2 Translating Operational Requirements.....	35
3.3 Design by Evolutionary Iteration.....	36
3.3.1 <i>Outlet Valve Iterative Design Process</i>	37
3.3.2 <i>Inlet Valve Iterative Design Process</i>	54
3.4 Permanent Magnets as Valve Springs.....	55
3.4.1 <i>Magnet Material Selection</i>	55
3.4.2 <i>Determining Dimensions for the Magnet Valve Spring</i>	56
3.4.3 <i>Modeling the Magnetic Valve Spring Via Finite Element</i>	59
Chapter 4 — Valve Manufacturing Process.....	62
4.1 Steps in Valve Disk Manufacturing Process.....	62
4.2 Steps in Valve Manufacturing Process.....	63
4.3 Fabrication Results.....	68
4.3.1 <i>Electrical Testing</i>	69
4.4 The Epoxy Potting Process.....	70
4.4.1 <i>The Importance of Vacuum</i>	70
4.4.2 <i>The Epoxy Dipping Process</i>	73
4.4.3 <i>Evaluating Success of Epoxy Potting Results</i>	76
Chapter 5 — Static Modeling and Static Benchmarking.....	78
5.1 Static Force Measurements.....	78
5.1.1 <i>Static Test Rig Mechanical Description</i>	79
5.1.2 <i>Static Test Rig Electrical Description</i>	80
5.1.3 <i>Force Measurement Experimental Procedure</i>	81
5.1.4 <i>Experimental Hysterisis in Force Measurement</i>	83
5.2 Developing AN Advanced Finite Model.....	84
5.2.1 <i>Tolerance in Magnetic Properties of Material</i>	84

5.2.2	<i>Modeling Metal-to-Metal Interface Tolerance</i>	86
5.2.3	<i>Modeling Part Alignment Tolerance</i>	88
5.2.4	<i>Modeling Shim Gap Tolerance</i>	90
5.2.5	<i>Sensitivity of the Model to Geometric Tolerances</i>	91
5.2.6	<i>Value of Modeling to Future Work</i>	92
5.3	Stray Field Assessment.....	93
5.4	Valve Inductance Measurements.....	94
5.4.1	<i>Description of Experimental Technique</i>	94
5.4.2	<i>Inductance Measurement Experimental Procedure</i>	96
Chapter 6 — System Integration and Cold End Design.....		97
6.1	The High Pressure Assembly.....	99
6.1.1	<i>Welding The High-Pressure Assembly</i>	101
6.1.2	<i>Cold End Flanges and Fittings</i>	102
6.2	The Cold End Housing.....	105
6.2.1	<i>Expander Space Dead Volume Minimization</i>	109
6.3	The Valve Assembly.....	110
6.3.1	<i>Valve Seat Swaging Process</i>	113
6.4	Fabricating Indium Seals.....	115
Chapter 7 — Valve Dynamic Operation.....		118
7.1	Valve Disk Dynamics and Operational Time Scales.....	118
7.2	Valve Seat Sealing Effectiveness.....	122
7.2.1	<i>Valve Bulkhead Deflection Analysis</i>	124
7.2.2	<i>Valve Seat Deflection and Sealing Analysis</i>	127
7.3	Valve Seat Lifetime.....	132
7.4	Control, Energy Consumption, and Dissipation.....	134
7.4.1	<i>Triple-R Valve and Energy Consumption</i>	134
Chapter 8 — Reflections and Conclusions.....		136
8.1	Technologies This Work May Enable.....	138
8.2	Conclusion.....	138
References.....		140
<i>Appendix A — Paramagnetic Material Properties</i>		141
<i>Appendix B — Static Force Data</i>		143
<i>Appendix C — Valve Model Performance Data</i>		152
<i>Appendix D — Valve Disk Dynamics</i>		161
<i>Appendix E — Valve Bulkhead Deformation Analysis</i>		171
<i>Appendix F — Valve Sealing and Deformation Calculations</i>		179

1.0 INTRODUCTION

Cryogenics is the production of low temperatures and the study of low-temperature phenomena. There is a hazy temperature division line between refrigeration and cryogenics, which occurs at about 123 Kelvin (-150° Celsius). Applications of cryogenics span from industrial processes such as gas liquefaction to studies of basic phenomena in physics and chemistry. The discipline presents a unique set of challenges encompassed by basic property changes that occur in most substances and materials when they are exposed to extremely low temperatures.

The work covered by this thesis focuses on the development and principal analysis of the cold end for a prototype cryogenic machine, a cryocooler, capable of demonstrating the feasibility and implementation of a miniaturized, multistage Collins cycle. This machine is a proof-of-concept test rig used to unite several pre-existing technologies into a single device. The machine will be used to validate analytical thermodynamic results as well as to work through unanticipated challenges that may arise through the integration of various independent technologies into a single system.

The machine developed in part through this work is the precursor to a modular, three-stage cryocooler capable of achieving 1 Watt of cooling at 10 Kelvin. If successful, the three-stage machine will represent a two-fold increase in efficiency over existing cryocoolers capable of achieving sustained cooling at 10 Kelvin.

1.1 PROJECT MOTIVATION

The availability of a small machine capable of sustained cooling at 10 Kelvin will enable many technologies reliant upon cheap, reliable cryogenic working fluid. Current applications include chilling military sensory equipment and enabling better resolution for astronomical observatories. However, foreseeable applications include cheap, low-temperature superconductors as well as desktop-sized supercomputers.

Many classes of small cryocoolers are currently in use today. These systems include pulse tubes, sterling machines, and Gifford-McHahon cycles. However, each of these cryocooler types is either prohibitively wasteful with respect to energy usage or is simply impractical for substantial cooling applications at 10 Kelvin.

The motivation of this project is to combine various technology advances made in the Cryogenics Engineering Laboratory at the Massachusetts Institute of Technology into a single small machine capable of executing a Collins cycle. The focus of the current effort is to develop cryogenic valve technology and the supporting cold end geometry to engender the operation of the machine.

1.2 COLLINS CYCLE OVERVIEW

The Collins cycle is an industrial-scale helium liquefaction process usually carried out by large machines. The Collins cycle is essentially a three-stage machine with each intermediate stage made up of a mechanical expander and a heat exchanger. The final stage of the cycle employs a Joule-Thompson valve to expand and liquefy the helium. A schematic showing the various parts of this cycle is provided in Figure 1.1. Samuel C. Collins pioneered development of this cycle in 1946 to provide practical helium liquefaction without the need for hazardous cryogenic hydrogen as pre-coolant. Since hydrogen freezes at 13.8 Kelvin and most other substances freeze at higher temperatures, helium is the only working fluid available for applications below about 14 Kelvin.

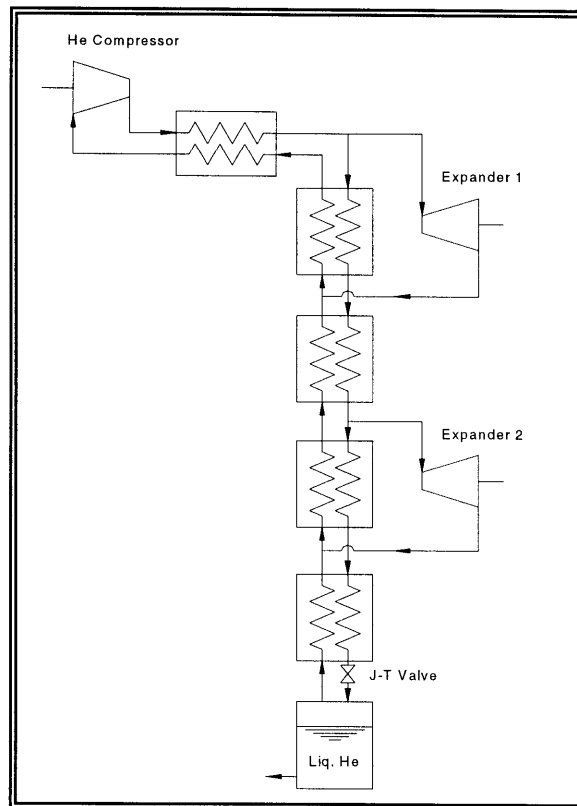


Figure 1.1: The Collins cycle is a multi-stage machine consisting of counter flow heat exchangers and adiabatic expanders

Many working fluids have a positive Joule-Thompson coefficient; the fluid temperature reduces as the fluid expands at constant enthalpy – as with a throttle valve. However, cryogenic helium has a negative Joule-Thompson coefficient. Expansion at constant enthalpy causes the fluid to warm up. The only way to induce helium to cool in the 10-Kelvin regime is to take work out of it – an adiabatic expansion. Thus, a mechanical expander is necessary to execute a helium liquefaction cycle where helium is the working fluid.

As shown by the temperature-entropy diagram, Figure 1.2^{4*}, the idealized Collins cycle consists of several distinct but similar mechanical expander stages and a final Joule-Thompson expansion process. The mechanical expansion processes are identical at each stage and are repeated down the temperature scale between two isobars. These stages chill the gaseous helium below its Joule-Thompson inversion temperature. Once the inversion temperature is passed, the gas can be expanded to generate liquid helium.

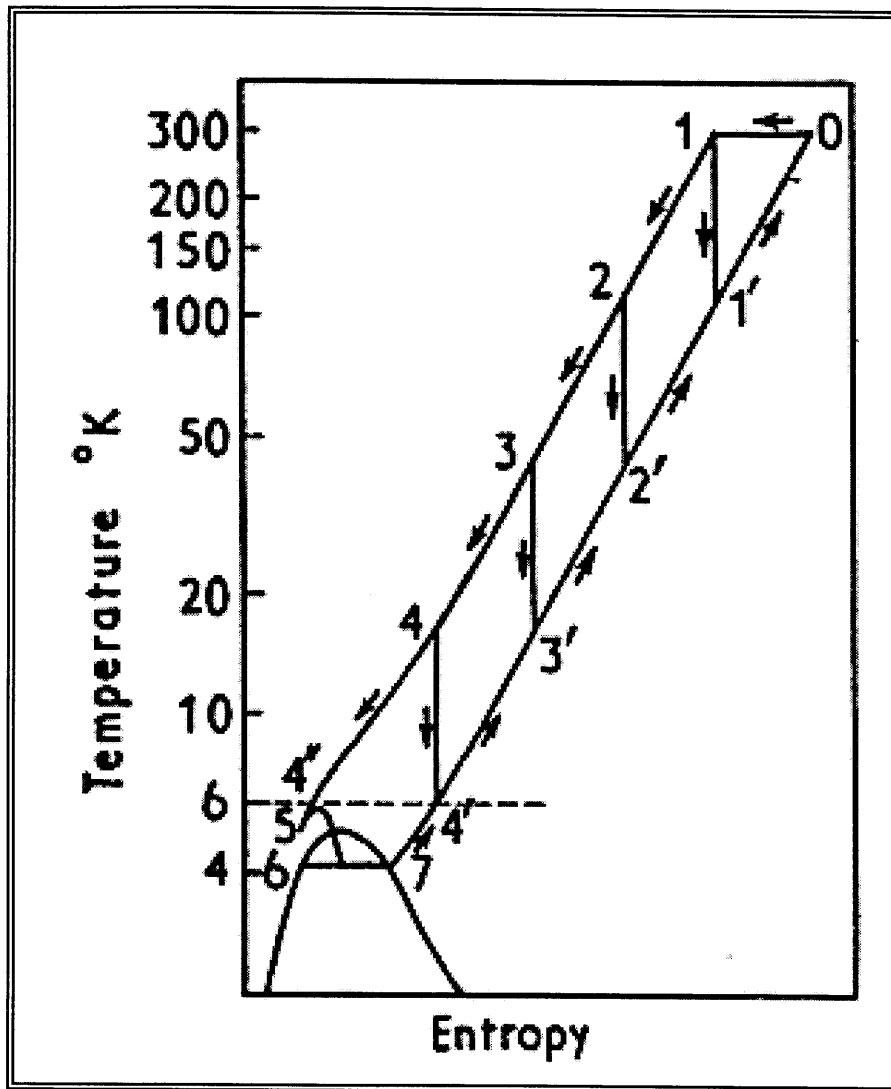


Figure 1.2: The ideal Collins cycle on a T-S diagram shows the distinct mechanical stages and the final expansion to liquid

The research effort described in this thesis focuses on the development of the cold end and expander section for a single stage of the Collins cycle. Since all of the mechanical expander stages in the overall cycle will carry out similar processes, this single expander component will be used to benchmark and develop a multi-stage machine as the research evolves.

* All superscripts in the text body refer to the number of the reference appearing in page 140

As with any cryogenic machine, it is absolutely necessary to thermally isolate the working components of the cold end to mitigate thermal leaks, which detract from the cycle's cooling power. In conventional helium liquefaction machines, thermal isolation is achieved by driving all mechanical components via cams connected to long, thin linkages. These long linkages retard heat transfer from room temperature to the cold end and avoid mechanical friction at low temperature, but they necessitate a machine of large size.

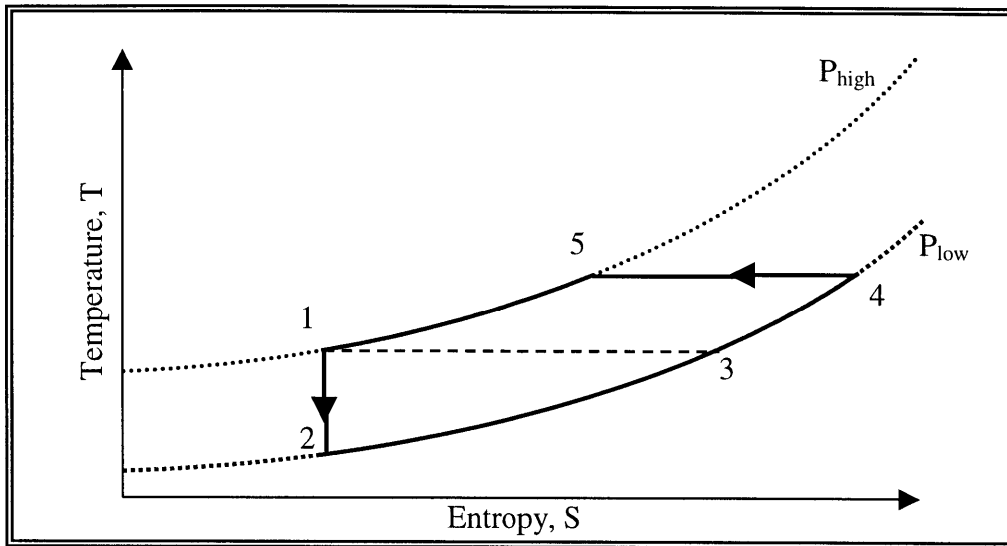


Figure 1.4: The single-stage expander unit executes a five-stage cooling process when attached to a helium compressor.

1.3 RATIONALE FOR MINIATURIZATION

The motivation for compacting an industrial-scale machine into a device a few cubic feet in volume is threefold. First, it is desirable to capture the positive attributes of the Collins cycle in a device small enough to be dedicated to a single electronics package or capable of being plugged into a standard wall outlet. Second, a miniaturized Collins cycle would be competitive with existing small cryocoolers used in military and astronomical applications. Third, shrinking the system's size allows a number of technologies to be used to facilitate the cycle that would be impractical in a larger machine. These technologies include the electromechanical valves upon which this thesis focuses.

The primary means of miniaturizing the cycle is removing the various cams and linkages operating the valves and piston expander in favor of other driving mechanisms. In fact, the mechanical complexities associated with conventional actuation mechanisms make them impossible to implement as the size of the system drops. To operate the scaled-down cryocooler, alternate mechanisms must be developed.

1.4 ENABLING TECHNOLOGIES

The current effort at miniaturizing the Collins cycle is focused on the cold end and the expander, which contain all of the hardware to carry out the adiabatic expansion of the working fluid to drop its temperature, Process 1-to-2. This process is the coldest part of the cycle, and all of the mechanisms must be able to operate through a huge temperature range from room temperature down to the cooling temperature of the apparatus.

The cold end and expander can be broken down into a number of simpler parts, each of which must be modified to operate without mechanical linkages. A reciprocating floating piston expander is utilized to take energy out of the working fluid. The floating piston travels within a cylinder extracting work from the helium in the cold volume by compressing helium in a room-temperature warm volume. The motion of the floating piston is controlled by the flow of room-temperature helium into and out of the warm volume through conventional valves.

Directing the flow of working fluid through the expander at the cold end is a pair of cold valves of novel electromagnetic design. These valves are actuated by a control current generating a magnetic field that attracts the valve disk away from the valve ports. This action allows the valves to be mechanically opened and controlled very precisely by a pulse of electrical current. When the control current is not on, the cold valves act as check valves. They are held closed by the gas pressure difference across the valve ports and by a permanent magnet acting as a valve spring.

Both the cold and warm valves are controlled by a digital data acquisition and control board in a PC. The PC board monitors the warm-volume pressure and piston position. A LabView program actively controls the opening and closing of each valve so that the expansion of the helium in the cold volume approximates a reversible adiabatic process, Process 1-to-2 shown in Figure 1.4.

1.5 CONTRIBUTION OF THIS THESIS

This thesis makes several significant contributions to the field of cryogenics. The comprehensive mechanical design of a feasible cold end unit capable of executing the expander portion of one-stage of a Collins cycle is presented. Emphasis is placed upon the development of the cryogenic cold valves and their integration with the cold end. Various advantages and disadvantages of this design concept are discussed and the difficulties encountered during the development process of this new machine are catalogued.

An evolutionary design iteration process based on finite-element modeling coupled with analytical solutions is pioneered and posited. This process supplants pre-existing cryocooler valve design methodologies by allowing the experimenter to converge on an optimal valve geometry without having to build and test hardware. When the right design is ultimately found, this thesis provides a robust, repeatable, comprehensive set of valve manufacturing processes and instructions to create a quality electromagnetic device.

An experimental process for static benchmarking is described. The sensitivity of the valve to various geometric tolerances is explored and modeled, and it is demonstrated that the finite element modeling method can be utilized to reliably bound a set of experimental data. The finite element bounds are then utilized to make first-order modeling approximations for several processes of the cold end including the following: electromagnetic, mechanical, dynamic, thermodynamic, and tribological. These first-order performance calculations are instrumental in breaking down the various processes affecting the operation of the cold end. These analyses will be used as a baseline to develop more sophisticated cycle models and design rules as the cryocooler evolves from a single-stage prototype to a commercial device.

This thesis ends with a set of observations and suggested improvements for future iterations on cryocoolers of similar design. It is hoped that outlining the pitfalls and successes encountered in this development effort will facilitate accelerated advancement towards an operable three-stage Collins cycle cryocooler.

2.0 BACKGROUND AND HARDWARE DESCRIPTION

The most significant components in the cryocooler's cold end are the two cold valves, which facilitate and check the flow of working fluid in the cold end. These valves represent the third generation in design of electromagnetic cryogenic valves for machines developed at the Cryogenics Engineering Laboratory at MIT. The basic configuration of both valves is the same. They each consist of a toroidal valve yoke and valve disk made of solenoid-quality stainless steel. The valve disks create a seal on three Kel-F plastic valve seats that are embedded within a valve bulkhead. The valve ports are small-diameter holes drilled through the valve bulkhead, which allow gas to pass through when the valves are opened.

2.1 PREVIOUS WORK

The pioneering work to develop electromagnetic valves for cryogenic applications was conducted by J.A. Crunkleton² in the 1980s. Crunkleton's work focused on modifying the original Collins cycle with a wet expander. Crunkleton was also interested in miniaturizing the industrial-scale Collins cycle for small-scale commercial use, and his motivation for utilizing an electro-mechanical valve was to reduce size and mechanical complexity at the cold end.

In Crunkleton's original machine, the electromagnetic solenoid was placed outside of the cold end, and a long valve stem that pierced through the cold end actuated the valve disk. This configuration proved difficult to effectively seal at low temperatures, and the mechanical complexity was not substantially reduced. Crunkleton later replaced the external solenoid with an internal low-loss solenoid as part of a cryocooler developed by the Boreas company³. Substantial reduction in complexity was achieved because only current carrying wires to energize the valve coil had to penetrate the cold end.

Additional significant work in utilizing electromagnetic valves for cryogenic applications was performed by K. M. Ceridon in 2001¹. The focus of this project was to modify a Gifford-McMahon cryocooler to deliver remote cooling via an addendum flow loop. Electro-mechanical valves were devised to check the oscillating pressure of the cycle to provide unidirectional flow in the external loop. Ceridon pioneered electromagnetic valve force analysis and measurement methods as well as a valve design methodology that forms the foundations of the current work. Although her valve was adequate to perform the required task, her analytical model lacked the convincing general predictive ability achieved in the current effort through finite element modeling.

The feasibility of a dry floating piston expander was demonstrated by R.E. Jones in 2000⁷. Jones showed that a piston without any linkages driven solely by pressure differences could be used in a controlled adiabatic expansion of gas. Jones also developed a rudimentary computer control routine to run the expander cycle without any mechanically actuated timing mechanisms.

Ceridon's work on electromechanical valves molds naturally with Jones's work on the free piston expander and points to an integration of the two projects to develop a miniaturized cryocooler devoid of any mechanical linkages as outlined in this thesis.

2.2 VALVE HARDWARE DESCRIPTION

A majority of the hardware development work in this project has focused on the cold valves. The cryocooler's cold end, which is represented schematically in Figure 2.1, contains two cold valves. The inlet valve regulates flow from the high-pressure reservoir into the expander displacement volume, and the outlet valve channels expanded, cooled gas to out of the cold end the load.

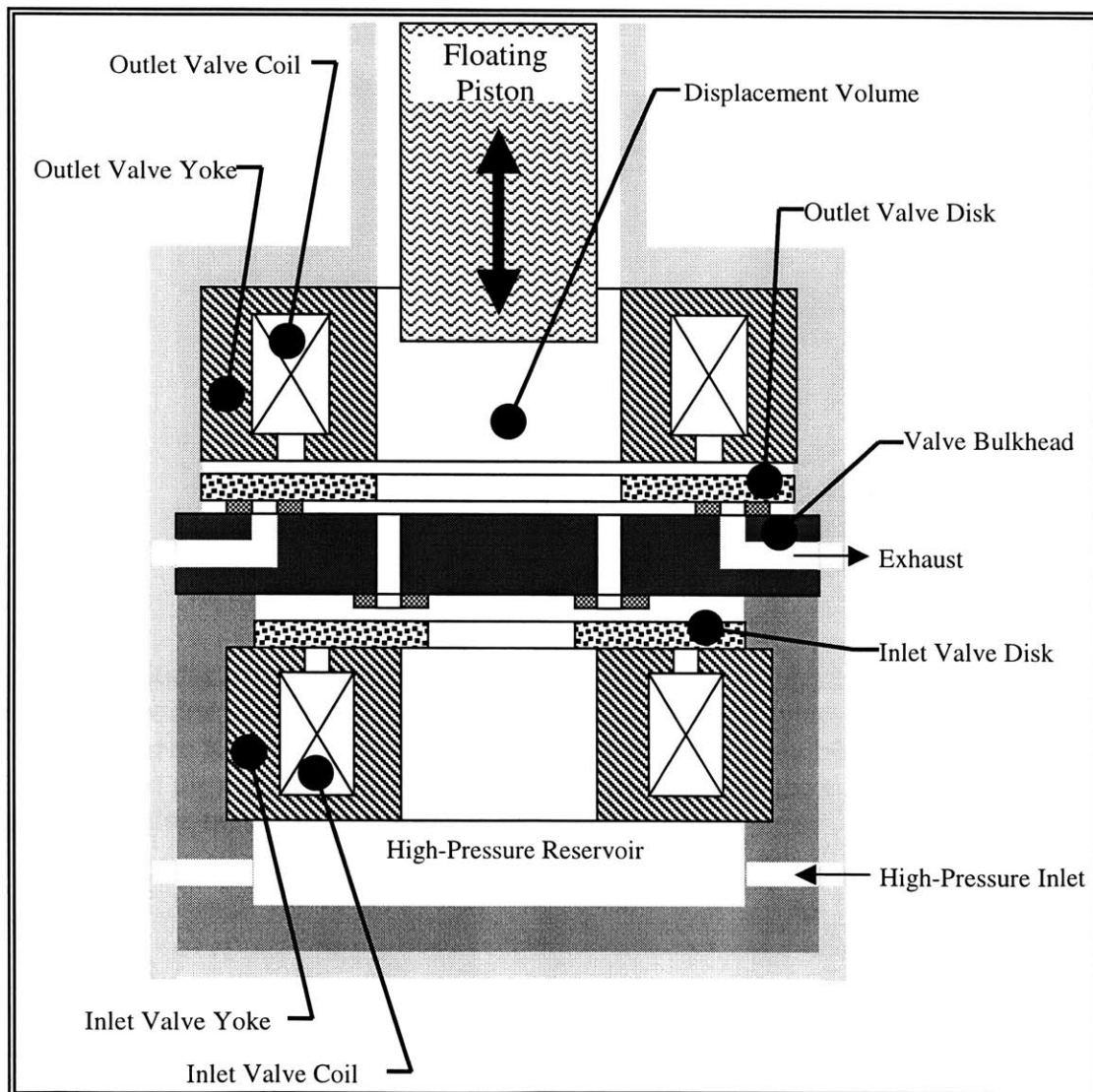


Figure 2.1 This cold end schematic shows how the cold valves are positioned and how they function with respect to other key components

To open a valve, a command current is sent into the copper winding of the valve coil. This current sets up a magnetic field in the axial direction with respect to the valve. The field is magnified by the high-permeability steel yoke and draws the valve disk away from the valve seats, allowing working fluid to pass.

Before assembly, the valves consist of three separate parts. The valve yoke is made up a spool and a cover piece, as shown in Figure 2.5. The spool is used as a fixture upon which the copper wire of the valve coil is wound. Once the spool is completely wound, the cover piece slides over the spool to protect the valve coil and complete the magnetic circuit. The third part of the valve is the valve disk, which remains free-floating below the valve yoke when all the parts are assembled in the cold end. The valve disk is skirted by a special non-permeable spacer ring that keeps the valve disk radially centered with respect to the valve yoke and minimizes accidental cocking of the valve disk as it moves.

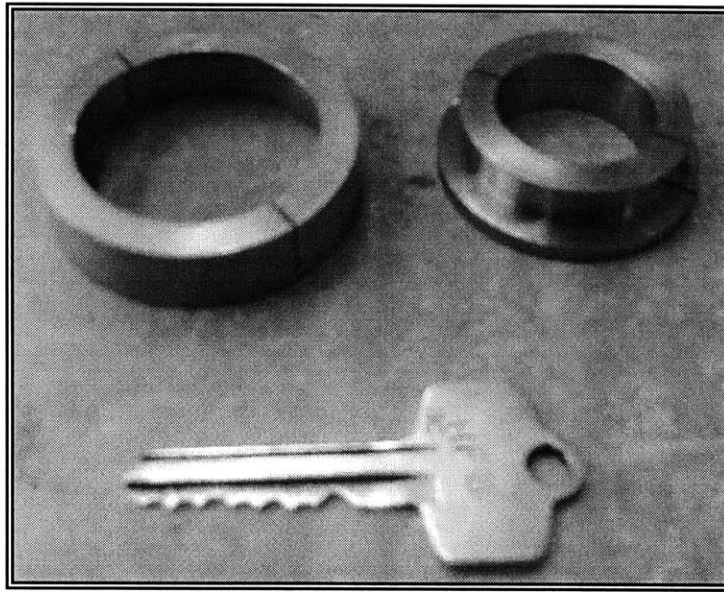


Figure 2.5 The valve yoke is made up of two pieces

The assembled inlet valve yoke is shown in a technical drawing in Figure 2.6. The constituent parts of the inlet valve, the spool, cover, and disk are shown in Figures 2.7, 2.8, and 2.9 respectively. The assembled outlet valve yoke is shown in a technical drawing in Figure 2.10. The constituent parts of the inlet valve, the spool, cover, and disk are shown in Figures 2.11, 2.12, and 2.13 respectively.

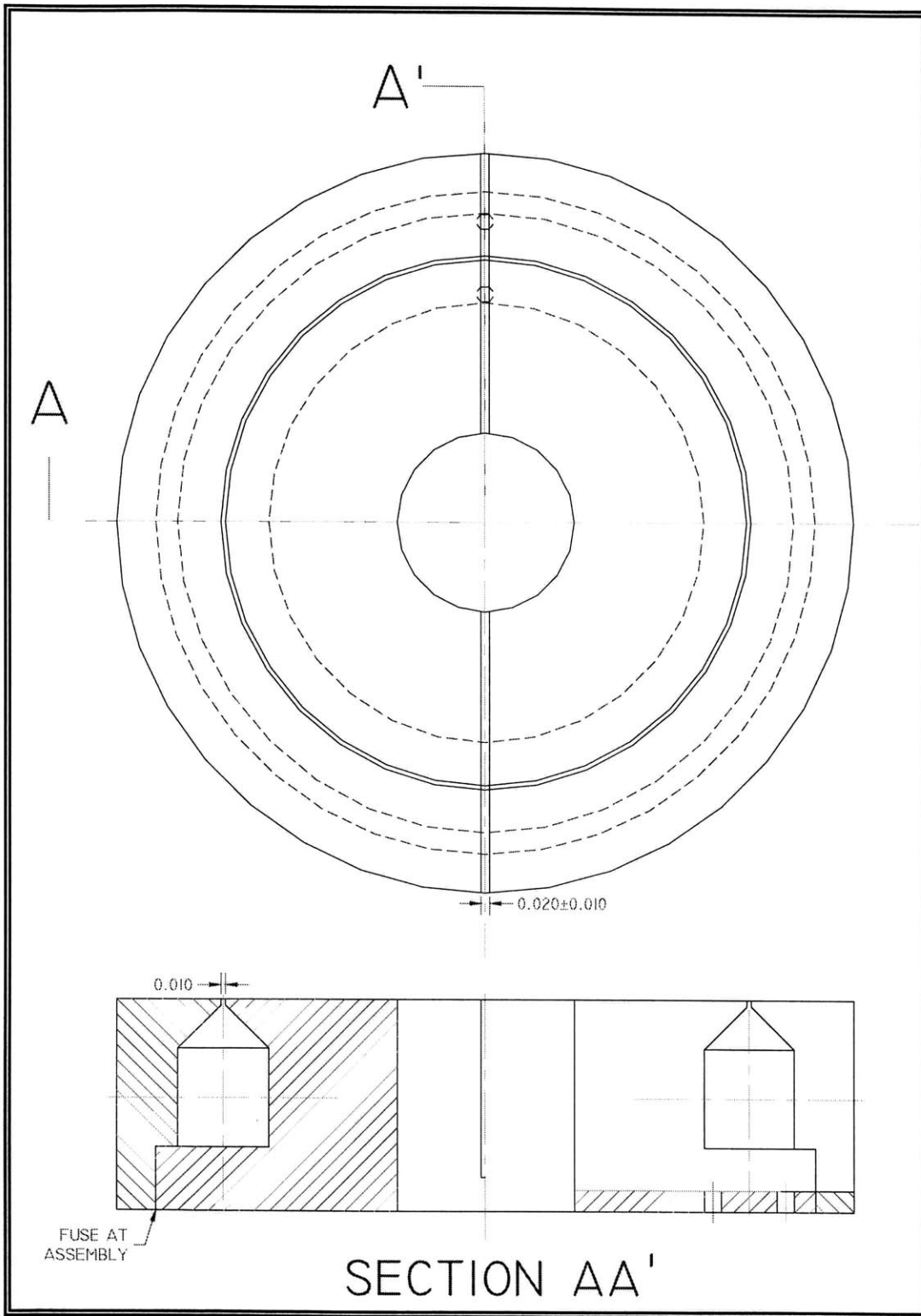


Figure 2.6: The inlet valve yoke is an annular electromagnet with a small inner diameter providing much permeable material to strengthen the magnetic field

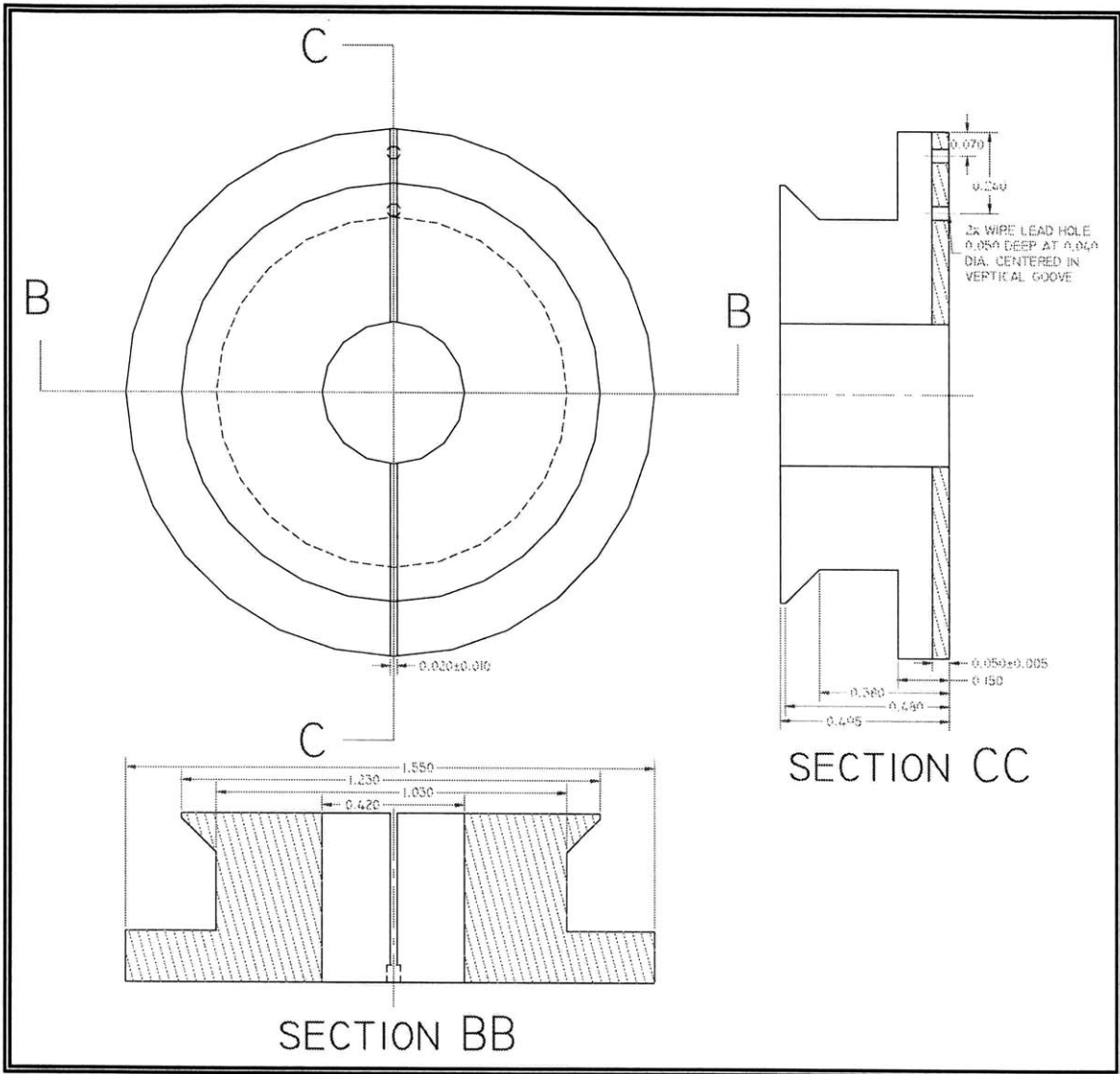


Figure 2.7: The inlet valve spool is shown in quarter section to relate the detail of the eddy current groove and the wire lead holes

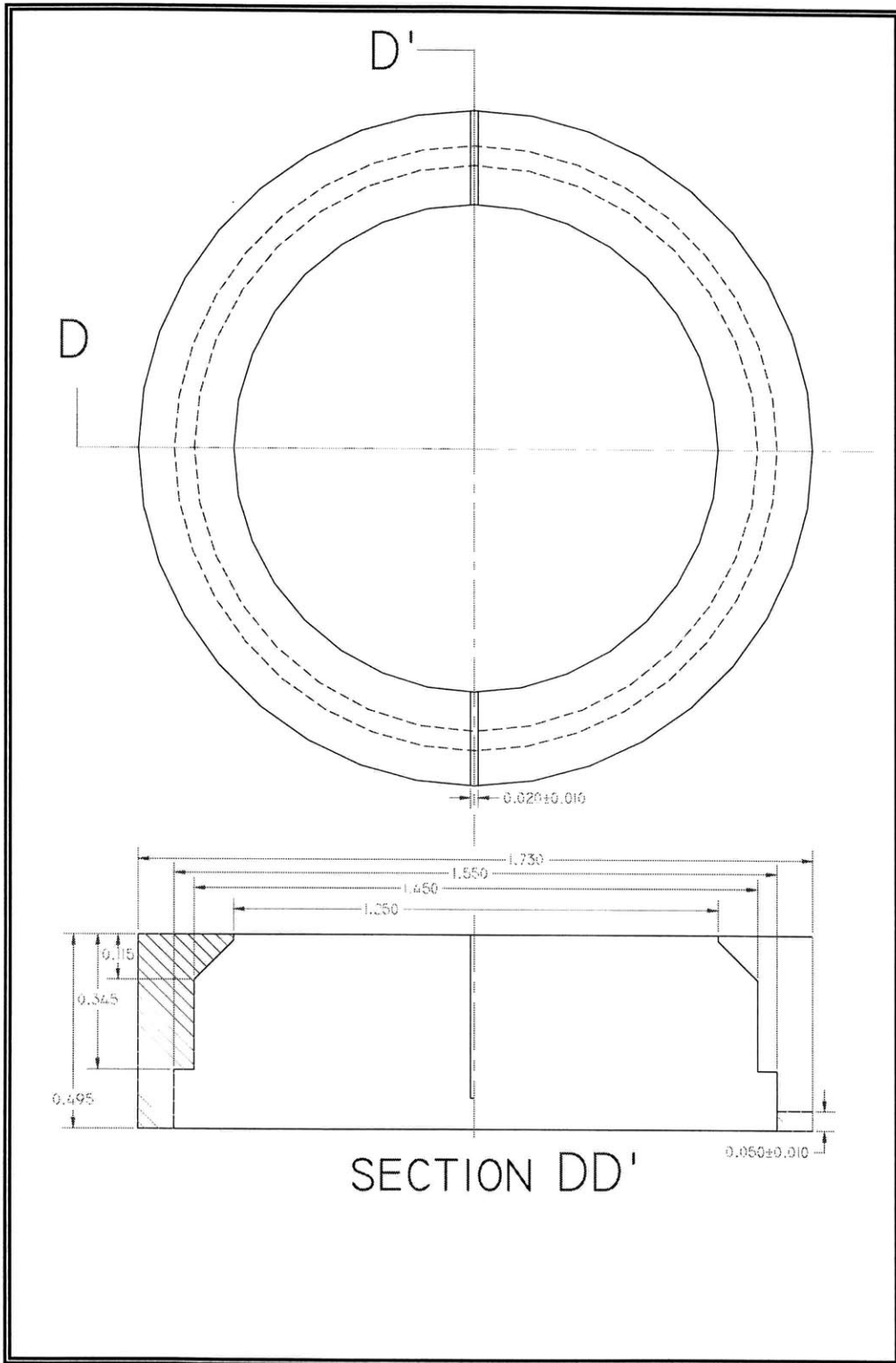


Figure 2.8: The outer diameter of the inlet valve cover is constrained by the necessity of passing small tubes past it to the high-pressure reservoir

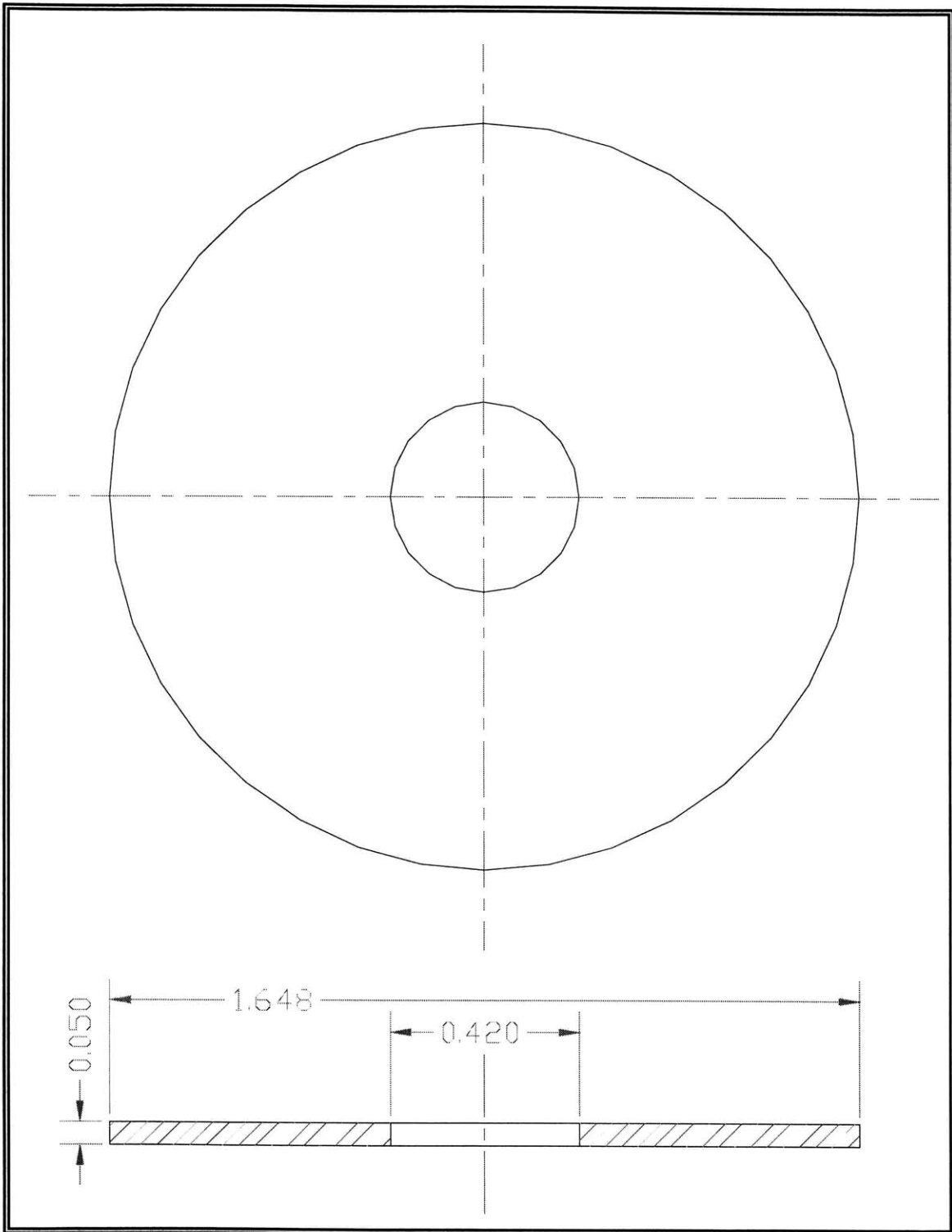


Figure 2.9: The inlet valve disk checks high-pressure flow into the expander and its inner and outer diameters are similar to those of the assembled inlet valve yoke

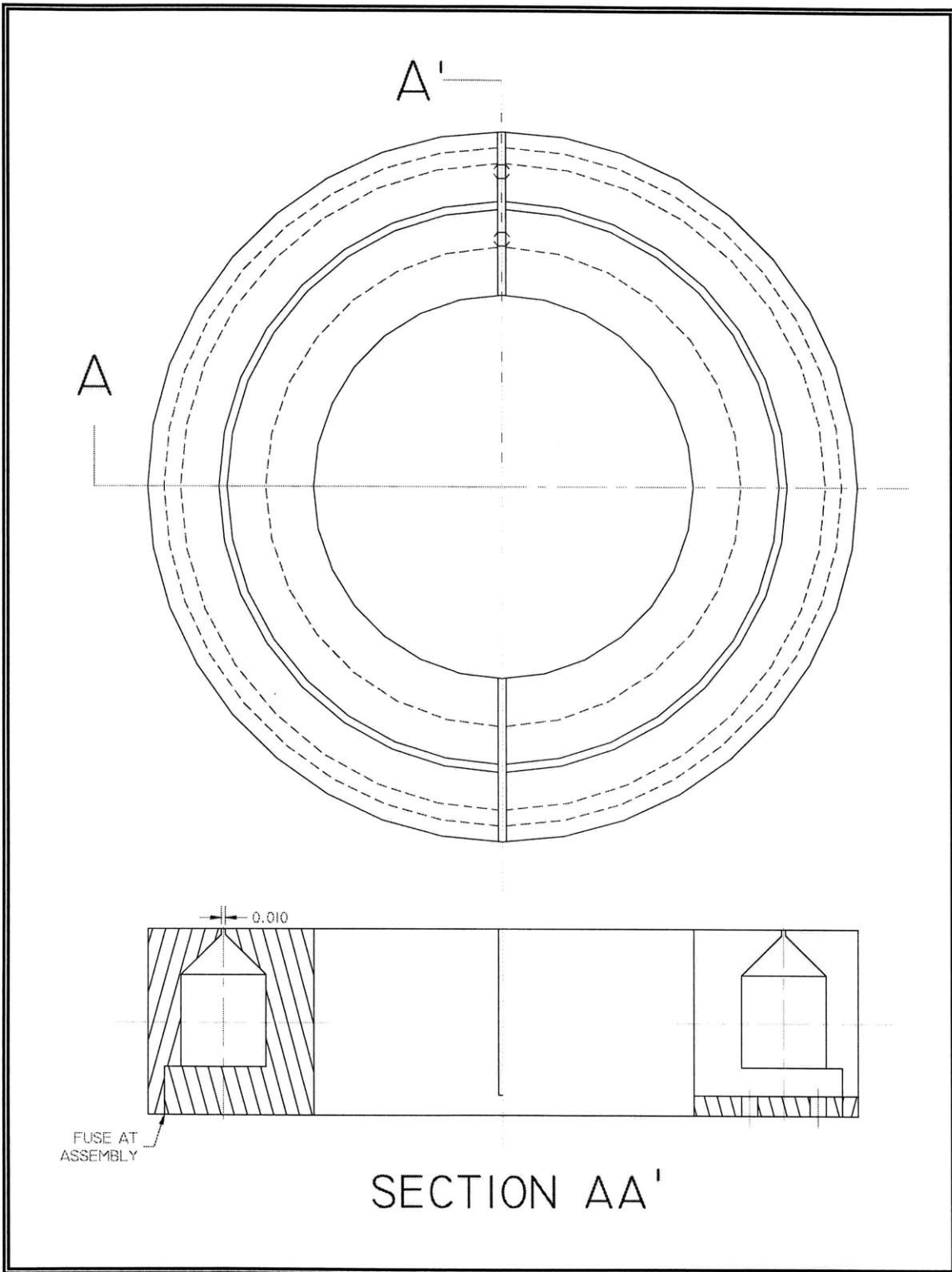


Figure 2.10: The outlet valve yoke is constrained to a 0.96-inch inner diameter because during its stroke, the expander piston travels through the outlet valve's center

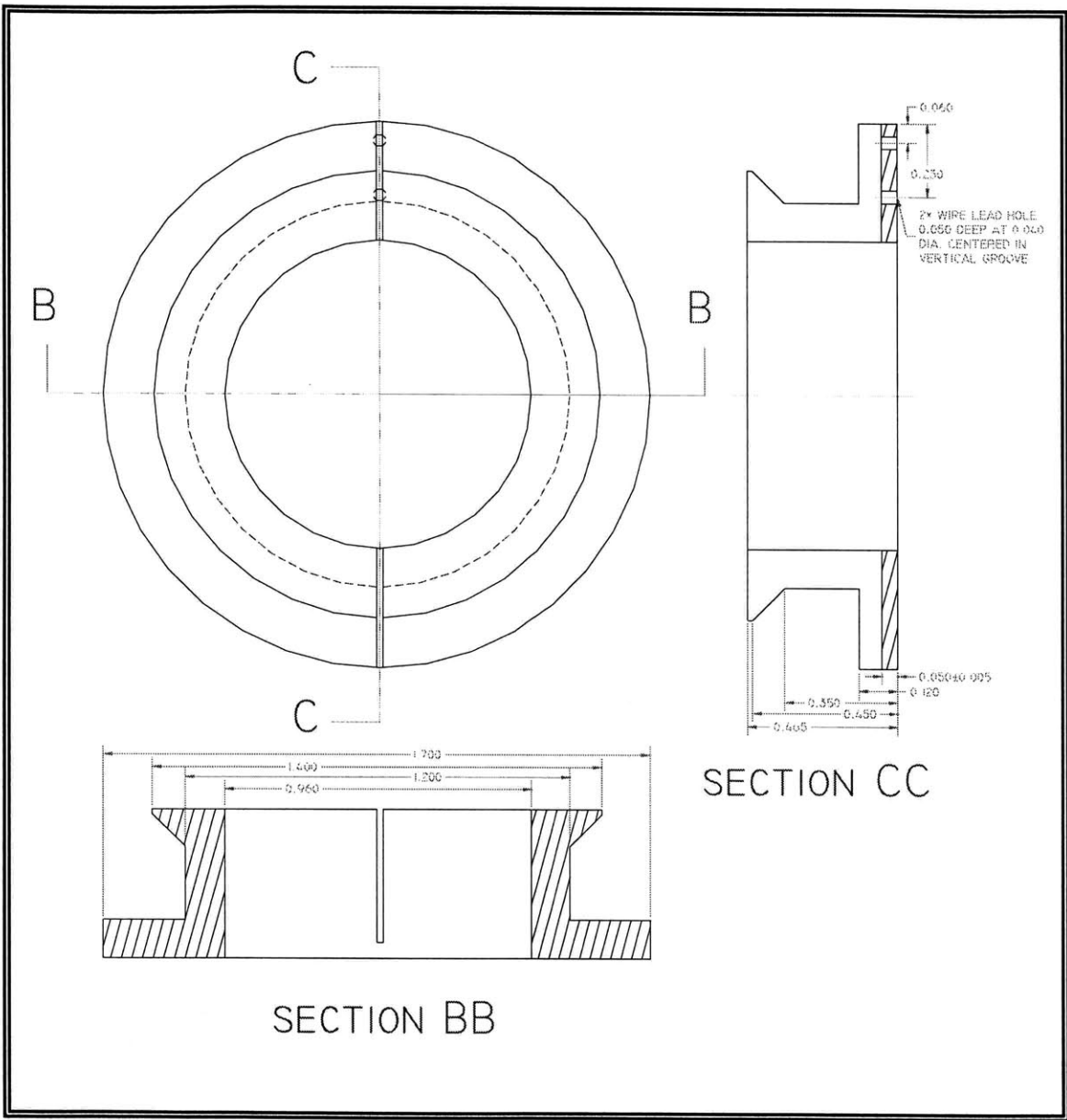


Figure 2.11: The outlet valve spool has the same valve coil area as the inlet valve, although the outlet valve coil contains a greater length of wire because its diameter is greater

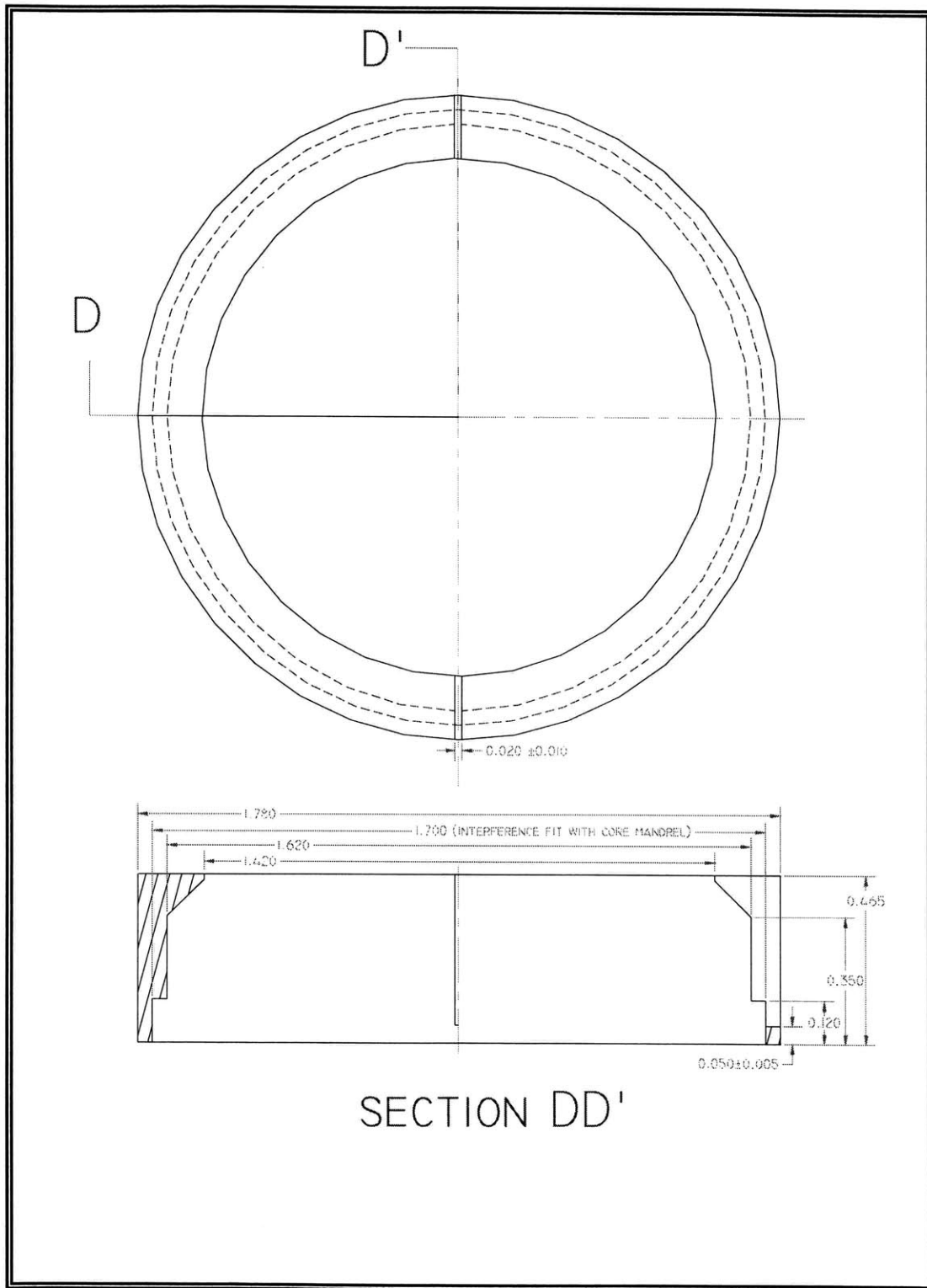


Figure 2.12: The outlet valve cover contains a step in its inner radius to assure proper alignment with the valve spool piece when the two are assembled

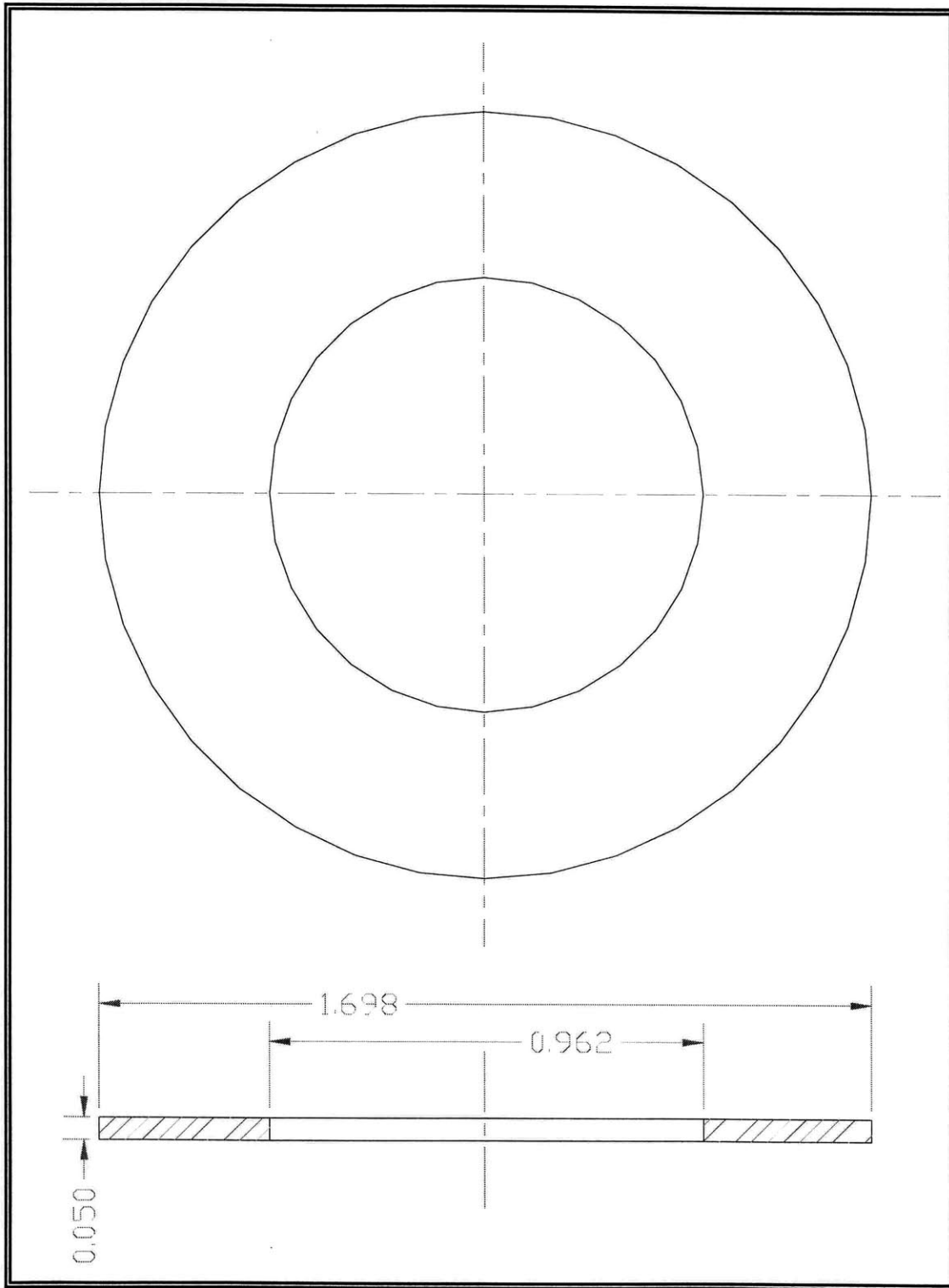


Figure 2.13: The inner diameter of the outlet valve disk is slightly larger than 0.96 inches, assuring the expander piston does not strike it when passing through

2.3 DESCRIPTION OF DESIGN CONSTRAINTS

A number of preliminary design constraints are imposed on the geometry of the valves by the specific requirements of minimization. The major geometric design goal is to squeeze the cryocooler cold end into a vacuum tube two inches in diameter. This constraint assures that the expander wall presents the minimum possible cross sectional area normal to the axial direction. Reducing this area minimizes the heat leak path down the expander wall from the warm to the cold end. The extent of thermal isolation required for the cold end also sets the length of the expander housing. The piston stroke and frequency must be set accordingly to achieve the desired cryocooler heat lift, one Watt. A one-inch piston stroke at one expansion per second was selected to achieve the proper cooling and mass flow rate of working fluid.

The valve port area from the industrial-scale helium liquefier at the Cryogenics Engineering Laboratory at MIT is used as a baseline to develop the required valve port area of the miniaturized cryocooler. The large helium liquefier operates with the Collins cycle and has demonstrated satisfactory performance for over 30 years. Thus, the ratio of piston area to valve port area on the existing machine is used to determine a satisfactory valve port area for the miniature machine, which has a 0.96-inch diameter piston.

The valve port scale ratio matching the piston scale ratio yields a valve port area of about 0.0127 square inches. This flow area must be divided evenly between the valve ports. The individual valve ports are sized to assure minimum pressure drop through the valve ports while maintaining a geometry that can be machined. As a first estimate, this condition means keeping the working fluid velocity constant through the ports. To minimize pressure drop, the port inlet area, A_{inlet} , must match the port outlet area, A_{outlet} . To meet this requirement, equation 2.1 is employed to solve for the necessary valve lift, L . From this analysis, the valve disk lift requirement of 0.01 is determined. Figure 2.14 graphically shows the simple valve port model used to estimate the required valve lift to assure A_{inlet} matched A_{outlet} .

$$A_{inlet} = \pi \left(\frac{d}{2} \right)^2 = \pi(dL) = A_{outlet} \quad (\text{Equation 2.1})$$

To assure the pressure drop across the valve bulkhead remains small, the valve bulkhead design originally contained sixteen valve ports, eight for the inlet valve and eight for the outlet valve. However, three ports per valve proved to be the preferable final design because they provide three points in a true plane upon which the valve disk must seal. The size of the individual ports was not increased to accommodate the required expander mass flow because the valve lift would need to increase to accommodate the constant velocity constraint. Thus the three valve port configuration as built causes a larger pressure drop on the working fluid entering the expander section than with the eight-port design.

Second, there are practical diminishing returns in the net cross sectional area of copper in a coil of wire as the wire diameter decreases. At very small wire diameters, the wire's insulation area is as large as the copper area. As the wire size decreases further, the current-carrying material in the valve coil volume decreases and the insulation area begins to dominate the copper area.

Third, there is a practical limit imposed by on coil manufacturability. The wire must be large enough to manually manipulate during the manufacturing process, and it must have enough durability to be wound onto the valve spool with reasonable tension without breaking. This third condition ultimately proves to be the limiting factor on wire size. Several trial valve coil winding tests were performed with progressively smaller wire at 26-, 28-, 32-, and 34-gauge to determine where the manufacturing envelope ends. It was found that 34-gauge wire is as small as could be reasonably handled in a manual manufacturing process. Thus 34-gauge wire became the standard wire size for cold end valves built for this project.

2.3.1 Benefit Tradeoffs of Electromagnetic Valves

The main benefits of electromagnetic valves include eliminating the need for heat flux mitigation with long linkages, reducing the mechanical complexity in the cold end, and facilitating an infinitely variable valve control strategy. In a system with mechanical linkages, the valve timing is set to optimize cycle performance at its operating temperature. This hard-wired optimization for a single temperature elongates cool-down time because the cycle is not operating at peak efficiency as it cools. Electromagnetic valves can facilitate dynamic adjustments in the cycle diagram while the cryocooler is running. This feature allows the cycle to be tuned for highest efficiency during cool down as well as temperatures other than the design temperature. These features should be explored in more detail in future projects with this cryocooler as they will provide a significant advantage when the cryocooler is marketed as a commercial product.

The benefits of electromagnetic valves also bring some disadvantages. With no physical connection to the valves disks, they cannot be mechanically unstuck if they cock or jam during operation. The maximum force that can be applied is limited by the electrical tolerances of the valve yoke. In addition, all of the mechanical complexity that was removed must be replaced by electronic complexity in the cryocooler's control routine and valve actuation equipment. When considering valve lifetime, controlling the energy with which the valve disk strikes the valve seats is much more difficult through electromagnetic actuation than it is with mechanical linkages.

Although the heat leak through mechanical linkages is eliminated, it is replaced to some extent by the heat leakage through the valve coil leads. In addition, the current driving the electromagnet is dissipated in the cold end by joule heating. This addition of heat to the cold end must be precisely controlled to assure the cold end does not begin heating the load instead of cooling it.

The electromagnetic components of the valves consist of a valve yoke, a valve disk, and an array of permanent magnets. The valves are normally closed as the permanent magnets hold the valve disk against a set of valve seats, blocking flow through the valve ports. To open the valves, a valve coil in the valve yoke is energized with current, creating a magnetic field. This field draws the valve disk away from the permanent magnets to open the valve port. To close the valves, the current through the valve coil is removed. The magnetic field generated by the valve yoke disappears, and the permanent magnets attract the valve disk to its closed position on the valve seats.

To prepare a faithful model of the actual valves, significant research had to be conducted to assure material properties, performance requirements, and numerous other parameters were well understood. Many of these parameters had to be translated in some fashion to be entered into the finite element model. It was also important to check that the finite element code returned values consistent with conventional analytical approximations.

3.1 PHYSICAL AND MATERIAL PARAMETERS

Perhaps the most important aspect of the valve's design is selection of the material used to build the valve yoke. Where electromagnetism is concerned, materials are divided up into two broad categories. Nonmagnetic materials are those unaffected by the presence of a magnetic field, and examples include plastic and brick. Paramagnetic materials, in contrast, respond to magnetic fields by generating fields of their own. This response can be thought of as an alignment of small magnetic domains in the material such that the magnetic poles of the domains point in the same direction.

Paramagnetic materials are used in engineering applications to amplify the strength of magnetic fields generated by the electric current carried through wires. In these applications, the magnetic flux lines link the wire coil and the material amplifying the magnetic field. This combination of paramagnetic material with coils of current carrying wire is called an electromagnet. When designing an electromagnetic, some choices of paramagnetic material are better than others. The magnitude of a material's ability to enhance magnetic fields is contained in a plot of magnetic flux density in the material, H , versus the resulting magnetic field density, B . This plot is commonly referred to as a B-H curve, and an example B-H curve is presented in Figure 3.2.

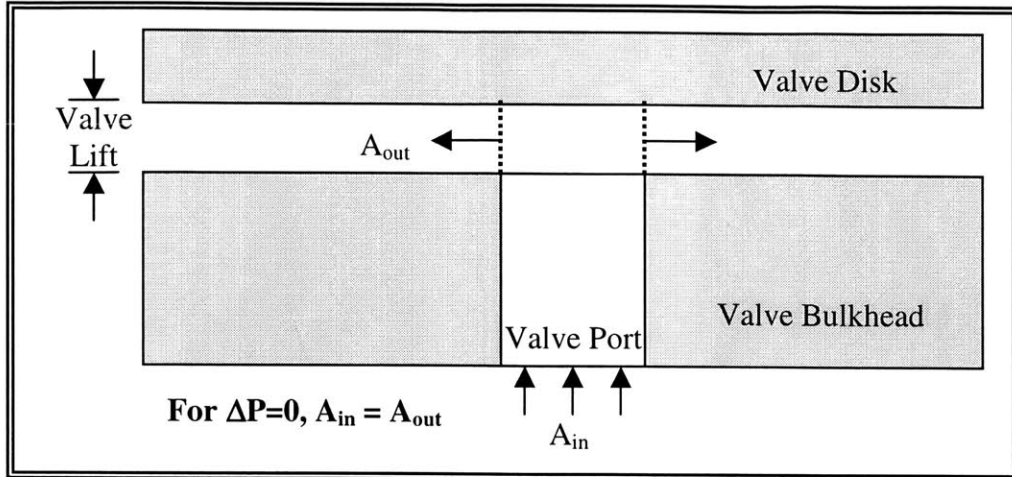


Figure 2.14: Equilibrating the areas of the valve ports determines valve lift

The maximum pressure differential in the cycle, 250 pounds-per-square-inch, creates several mechanical and electrical design requirements. The valves must open against 250 pounds-per-square inch multiplied by the total cross sectional area of the valve ports. The valves are designed to overcome the force induced on the valve disk by the pressure difference across eight 0.045-inch diameter valve ports. Each valve yoke is built to generate at least 14.2 newtons of opening force on the valve disk when in its closed position. This level of performance is used as the benchmark design value throughout this thesis, and it yields the requirement that 110 amp-turns is the opening current used in valve static finite element modeling. Regardless, it is important to note that after the valves were built, the valve bulkhead design was modified to reduce the number of valve ports, from eight to three. Thus, the valves need only open against 5.55 newtons of force, and as a result, they are severely over designed in the current application.

Two components make up the value of amp-turns that can be applied to the valve coil: 1) the number of wire turns wound on the valve coil and 2) the number of amps driven through the valve coil circuit. It is important to minimize the number of input amps to keep joule heating in check. Thus, maximizing the number of wire turns in the valve coil is desirable. Since the space set aside for the valve coil in the valve yoke is limited, it is attractive to select the smallest possible wire gauge size to maximize the number of wire turns. However, there are three practical limits preventing unlimited reduction of wire size.

First, a coil wound with small gauge wire has many more windings than a coil of larger wire wound into the same volume. Thus, the coil of smaller wire has a higher resistance, and more voltage is required to push current through it. There is a voltage at which current jumps through the wire's insulation and short-circuits the coil. This voltage is the maximum that can be safely imposed upon the leads of a coil. For small-gauge wire the practical voltage limit occurs at about 100 volts.

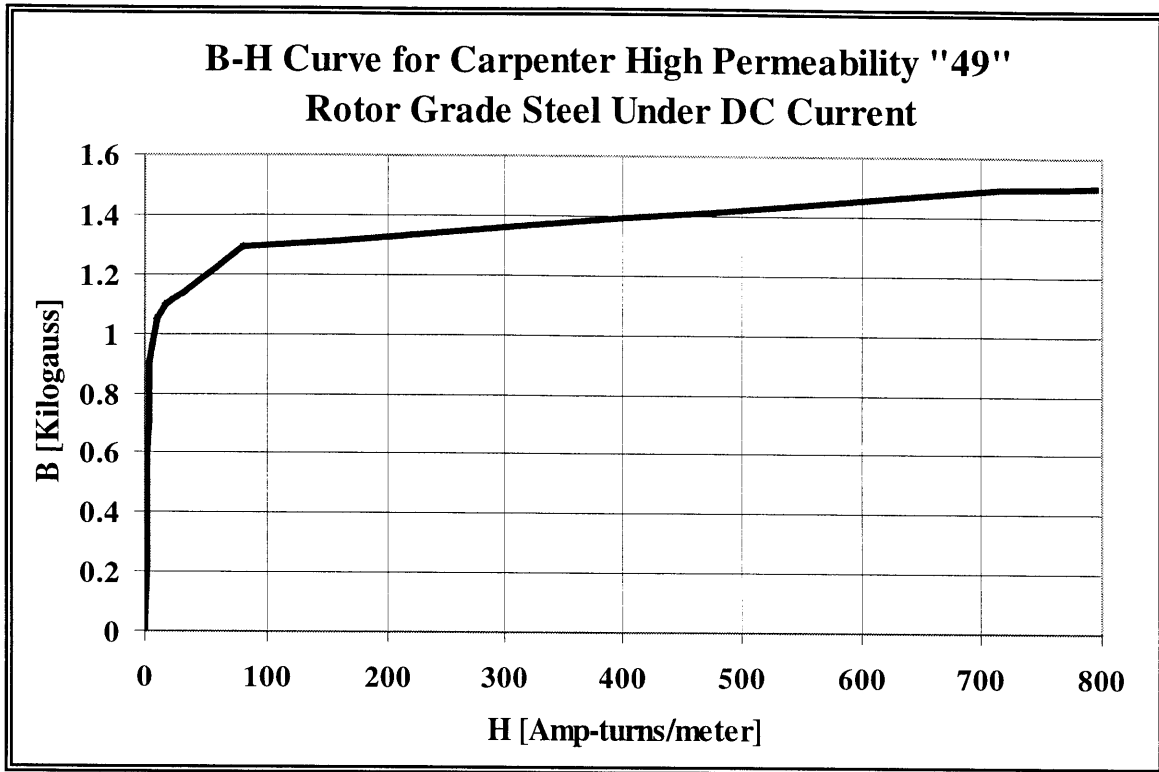


Figure 3.2 This B-H curve represents the electromagnetic properties and behavior of a good paramagnetic material, HP49, which is used to make the solenoid cores.

B-H curves have two important properties that can be used to determine which material is preferred when creating an electromagnet. The first property is magnetic permeability, μ , which is represented by the slope of the line on the B-H curve. This property dictates the extent of magnetic field density generated in a material for a particular input magnetic field intensity and can be found from Equation 3.1. Physically, permeability can be thought of as the extent to which the poles of magnetic domains in the material align for a given input magnetic field intensity.

$$\mu(H) = \frac{dB(H)}{dH} \quad \text{Equation (3.1)}$$

Once all of the domains align to the greatest extent possible, addition of magnetic field intensity does not induce any greater magnetic field in the material. This property is called the magnetic saturation density, B_{sat} , and it is the second important feature of a B-H curve. This property is manifested when the slope of the B-H curve dramatically changes from steep to very shallow, and the value of B increases only slightly even when the input H increases substantially. Saturation density is important to material selection in electromagnets because it dictates the maximum flux enhancement that can be derived from a particular paramagnetic material.

Another disadvantage of the current design is that the outlet valve resides in the expander space. A substantial amount of dead volume arises from the thin space surrounding the valve, which detracts from the cryocooler's performance. Although great measures were taken to reduce the extent of this dead volume, the design geometry makes it unavoidable.

One possible solution to this problem is to put both valve coils in the high-pressure space and actuate one of the valve disks through the valve bulkhead using push rods, as shown in Figure 2.15. While eliminating dead volume, this concept will have some severe sealing, and size restriction issues that must be overcome if it is to be practically implemented in future designs.

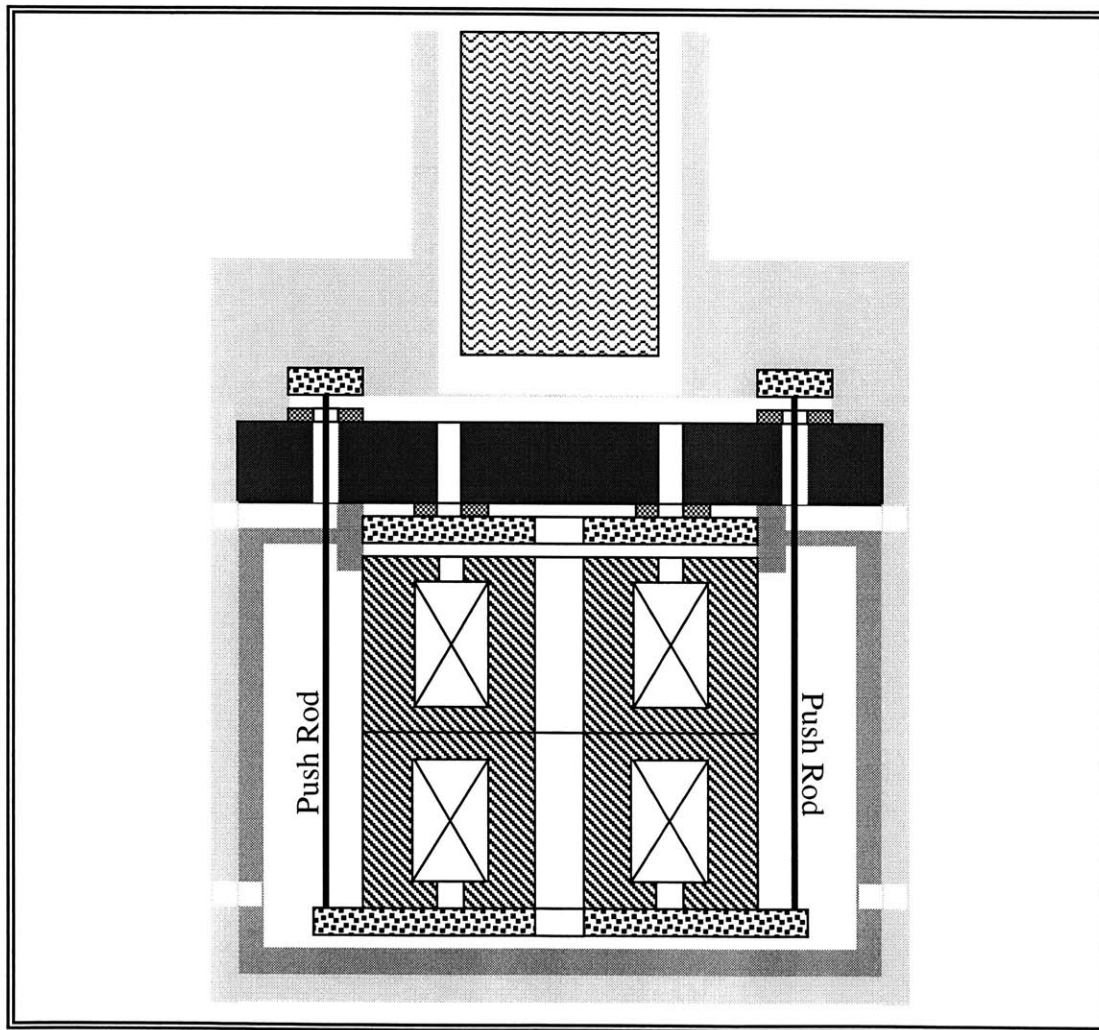


Figure 2.15: Although awkward, removing the valve from the expander space and placing it in the high-pressure space allows reduction in expander dead volume

3.0 VALVE GEOMETRY OPTIMIZATION

Previous cold valve designs have been hindered by lack of an adequate performance prediction technique. Classical magnetic modeling methods such as the one-dimensional circuit approximation are idealizations that break down because geometric considerations, material properties, and flux leakage become complex or uncertain. Using only these rudimentary models, uncertainties in performance are large and gross over design is necessary to assure adequate performance.

An alternative approach explored in this thesis is the use of a magnetostatic finite element modeling code to explore valve performance before any hardware is built. The code of choice to perform this analysis is Quickfield 4.3 by Tera Analysis. The drivers for selecting this code over other packages include its reasonable cost, \$950 per year academic license, and its relative ease of use. The code is not as sophisticated as other packages because it does not allow true three-dimensional modeling. However, axi-symmetric systems can be modeled. Although the cold valves are not perfectly axi-symmetric, results produced by Quickfield provide a performance approximation of far greater accuracy than any simple analytical method.

In the axi-symmetric mode, Quickfield's user interface only allows the user to draw model cross sections with the centerline running horizontally. This restraint causes the model to be rotated 90 degrees so that it lays vertically instead of horizontally, which is how the machine sits in actual operation. Figure 3.1 denotes the important magnetic components of the valve design whose Quickfield models are described throughout this thesis. Figure 3.1 shows the components in the orientation used to model them.

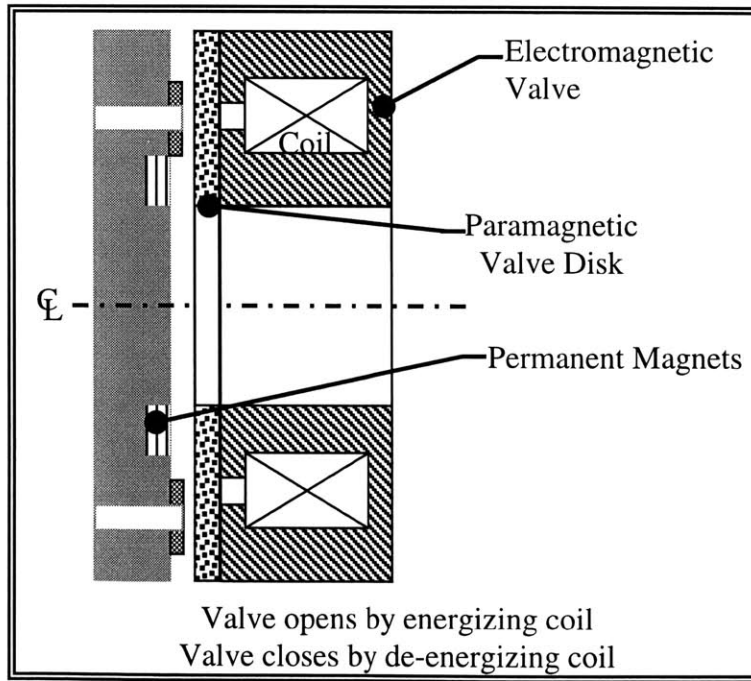


Figure 3.1 The components created via finite element are shown here oriented horizontally as they were modeled

3.1.1 B-H Curves, Machine-ability, and Material Selection

The ideal material for an electromagnet yoke has high permeability and a high magnetic saturation density. It also must be a soft magnetic material with low hysteretic loss associated with changing the magnetic field. Such a material would create a powerful magnetic field for little input magnetic flux density and the magnetic field density would continue to increase rapidly even for very high values of H. In addition, when H is removed, the magnetic field density would also go to zero instead of lingering at some non-zero value. This point is significant because the magnetic field produced by the valve yoke must return to zero if the valve is to close properly when the current is de-energized.

Since electromagnetic coil windings are prevalent in modern machines, many candidate materials have been developed that provide a good union of desirable magnetic and mechanical properties. In general, these materials are referred to as solenoid-quality steel. The Carpenter company produces several such metals, and two specific types were explored for this valve application: HP49 and 430FR. Although HP49 has the superior magnetic properties, it has higher tensile strength than 430FR, making it more difficult to machine. In addition, 430FR has a higher electrical resistance, which makes it better at managing eddy currents and the associated losses that arise in the material when transient conditions exist. Thus, 430FR was selected as the material of choice for the valve yoke. A sample B-H curve for 430FR is presented in Figure 3.3 and technical data on this material from the manufacturer is presented in Appendix A.

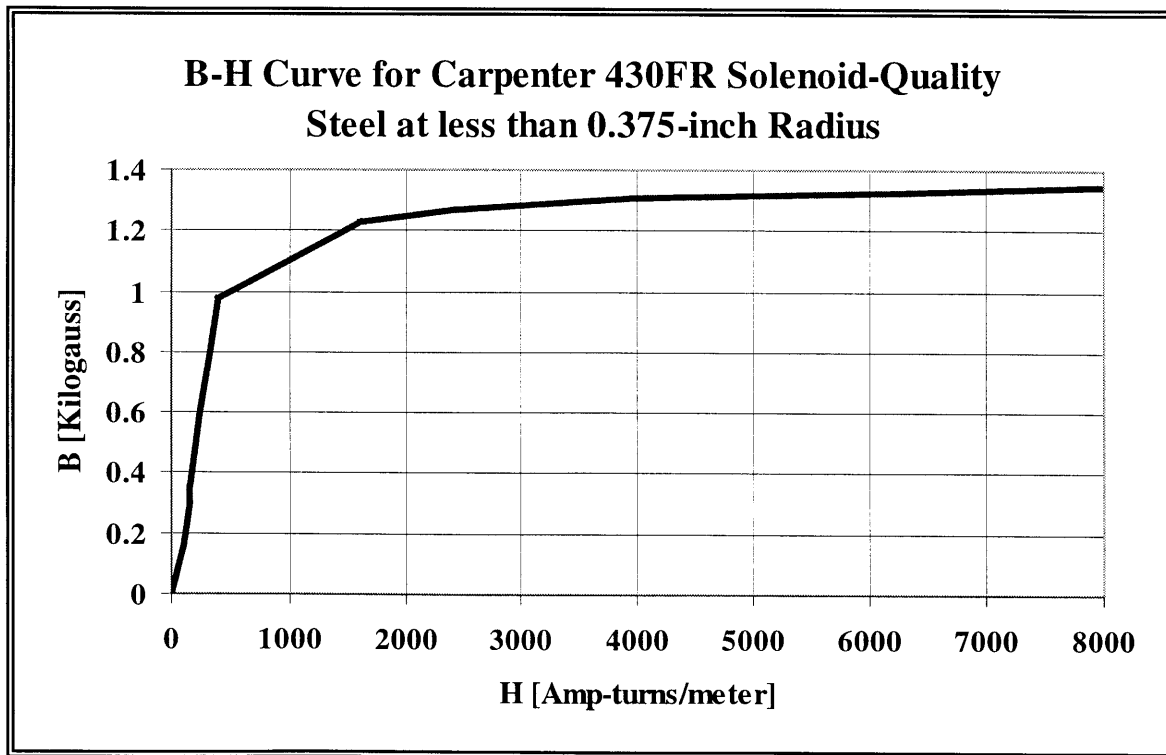


Figure 3.3 This B-H curve is for 430FR, a commercially available ring coil-quality steel that can be annealed after machining to restore lost paramagnetic properties.

3.1.2 Modeling the B-H Curve

With the valve yoke material selected, its magnetic properties can be entered into the Quickfield finite element code to begin building up the model. The program has a user interface allowing points from the material's B-H curve to be entered. The software then references this data as it creates the field solution.

Several methods of modeling the B-H curve were considered. The classical method used to deal with these curves is to represent the major portions of the plot with two intersecting straight lines as shown in Figure 3.4. This method characterizes a majority of the data very well. However, the transition region to magnetic saturation is not well captured. Thus, this modeling method was discarded because it is anticipated that with good design, the valve yoke would skirt the material saturation envelope.

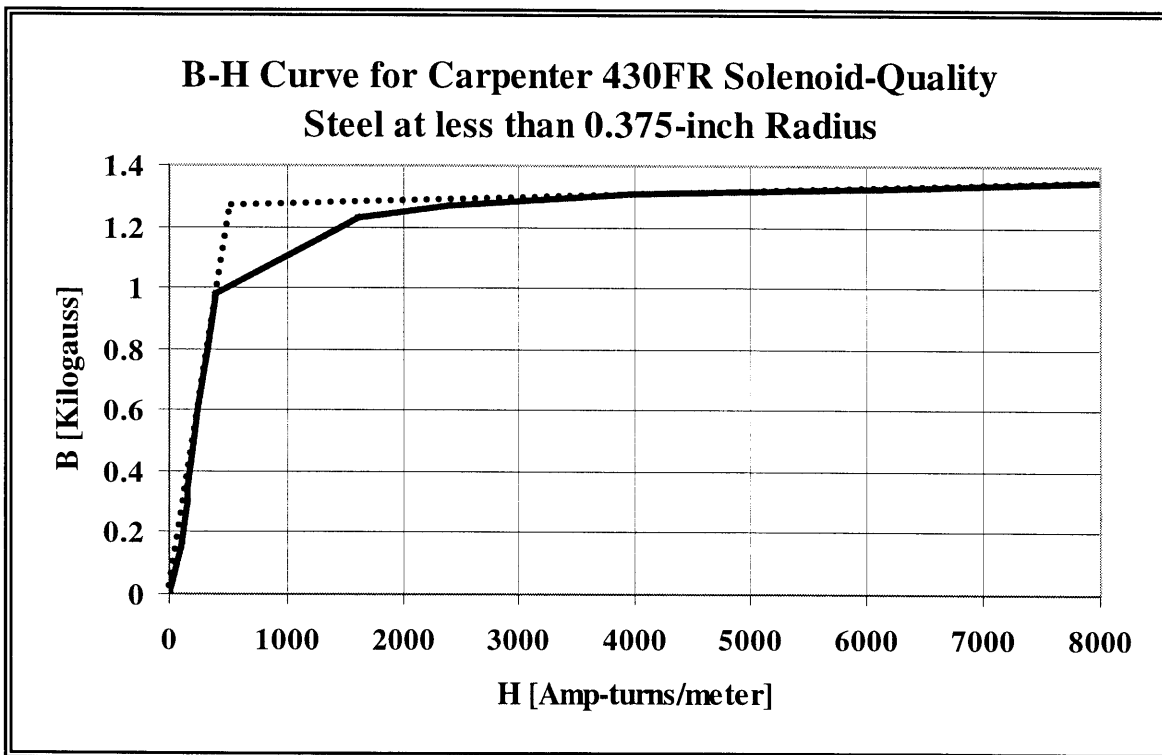


Figure 3.4 The B-H curve can be well represented by two straight lines, but the details of the transition to saturation region are not captured by this approach

Another modeling method that can be employed is to pick as many points as possible from the manufacturer's B-H curve and enter these points into the finite element code user interface. This method is problematic because B-H curves usually appear in manufacturer literature on semi-logarithm plots and the potential for error in picking points is substantial. In addition, Quickfield is highly sensitive to nonphysical features in user-defined B-H curves, and the program will not solve most problems unless the B-H curve is a completely smooth array of points. User-defined curves with many points were found to be relatively unphysical and caused Quickfield to fail.

The ideal B-H curve modeling method for finite element codes is a combination of the two-line approximation with the point-picking method. Seven to eight total points are used to define the B-H curve. The plot is principally made up of two long straight lines with the transition between the lines defined by a detailed set of points. This approach provides a simple but accurate material B-H curve for the finite element code to utilize.

It turns out that the valve's performance is relatively insensitive to the material's magnetic saturation density because the valve is over designed. Under normal operation, most of the paramagnetic material in the yoke does not saturate, and Section 5.2.1 discusses this finding in more detail. The permeability of the material's B-H curve, however, is important. Once the valve yoke parts are machined, they are annealed to restore the metal's paramagnetic properties. This annealing process, covered in Section 4.1, assures that the material's actual B-H curve is similar to the manufactures curve used to create the finite element model.

3.2 TRANSLATING OPERATIONAL REQUIREMENTS

In Chapter 2, all of the valve design requirements are outlined as they relate to the physical constraints on the miniaturized cyrocooler. Once these requirements are defined, they can be translated into the finite element model. Quickfield employs a graphic user interface that allows the programmer to draw in two dimensions a characteristic cross section of the axi-symmetric solid of revolution that makes up the model. All geometric features of the valve are entered into the finite element code by drawing them.

The valve opening force requirement based on the maximum cycle pressure differential is outlined in Chapter 2. The finite element code's post processing analyzer allows the user to determine the force generated on various pieces of the geometry in the model. In the model, as in the real valve, the force on the valve disk increases as the valve coil is energized to higher amp-turn values. Thus, an amp-turn value must be set as a benchmark to determine whether adequate force is being generated on the valve disk, and the following methodology was utilized.

Initial valve coil winding tests with 28-gauge wire demonstrate that about 250 turns can be placed on the prototype valve ring coil. These coils have an average resistance of about 6.25 ohms. The design calls for the cyrocooler to lift one Watt of heat at 10 Kelvin. The cyrocooler can lift more heat at higher temperature, and the valve coil resistance will drop with operating temperature. Regardless, it is assured that the valves will never dissipate more power than the cooler can lift if the maximum valve coil power is set to one Watt. One watt through a resistance of 6.25 ohms results in a maximum current of 0.4 amps, and 0.4 amps multiplied by 250 winding turns yields 100 amps-turns. Thus, this value is selected as the benchmark input for the finite element model. Quickfield allows the user to define any solid geometric component as an electrical coil and the amp-turns through that coil can be set to any value. The value of 100 amp-turns is utilized in all finite element benchmarking model tests to determine the optimum valve geometry.

The evolutionary approach proceeds so that the range for each type of improvement is exercised individually. To determine the order of exploration, the experimenter must make educated engineering judgments about which factors will most influence the valve's performance. In general, the most favorable value for the characteristic being explored is incorporated into the geometry and carried into the next iteration. In this way, the valve design evolves from the baseline model to the final geometry.

It is important to note that this development process may not have captured the best possible combination of properties in the design space because not all combinations of characteristics were examined. The selection of the order in which the characteristics were explored may have a substantial influence on the final outcome. In some cases, it is not clear which characteristics have the most influence on performance and the selection of which to explore first is somewhat arbitrary. Regardless, this process provides a substantial improvement over previous design methods based on simple analytical models. It allows the designer to exercise and explore the affects of many geometry changes that might be too small to model accurately model with a less sophisticated method.

3.3.1 Outlet Valve Iterative Design Process

The following section covers each of the geometric improvements made to the baseline model in the order they were explored. It explains the trends gleaned from changing characteristic values of each property and why a particular geometry was selected over another one. Following the figures showing the valve configuration with each evolutionary improvement, a depiction of the evolution of the valve from the baseline to the final design can be realized.

The baseline model is characterized by a cross-sectional area square in shape. When swept around 360 degrees, this shape generates an annular volume of rotation with an outer diameter of 1.8 inches and an inner diameter of 0.96 inches. The wall thickness of the valve yoke and valve disk is 0.03 inches on all sides. The cross sectional area of the valve coil has a 1:1 width to length aspect ratio, and there is no rounding or filleting of the valve coil corners. In the closed position, the valve disk sits 0.01 inches away from the valve yoke. The valve disk force produced by this design is 3.6837 newtons.

1) Valve Yoke Outer Diameter

Increasing the outer diameter of the yoke was found to increase the force generated on the valve disk. Analytically this result follows because increased outer diameter yields an increased surface area normal to the magnetic flux lines. More area for the flux to travel through translates into a drop in the equivalent flux resistance of the valve yoke in the one-dimensional circuit model. Unfortunately, the valve's outer diameter is limited by the 2-inch constraint imposed in the design specifications. Although the outer diameter was made as large as possible, it was reduced to 1.78 inches to accommodate the thickness of the cold end wall housing.

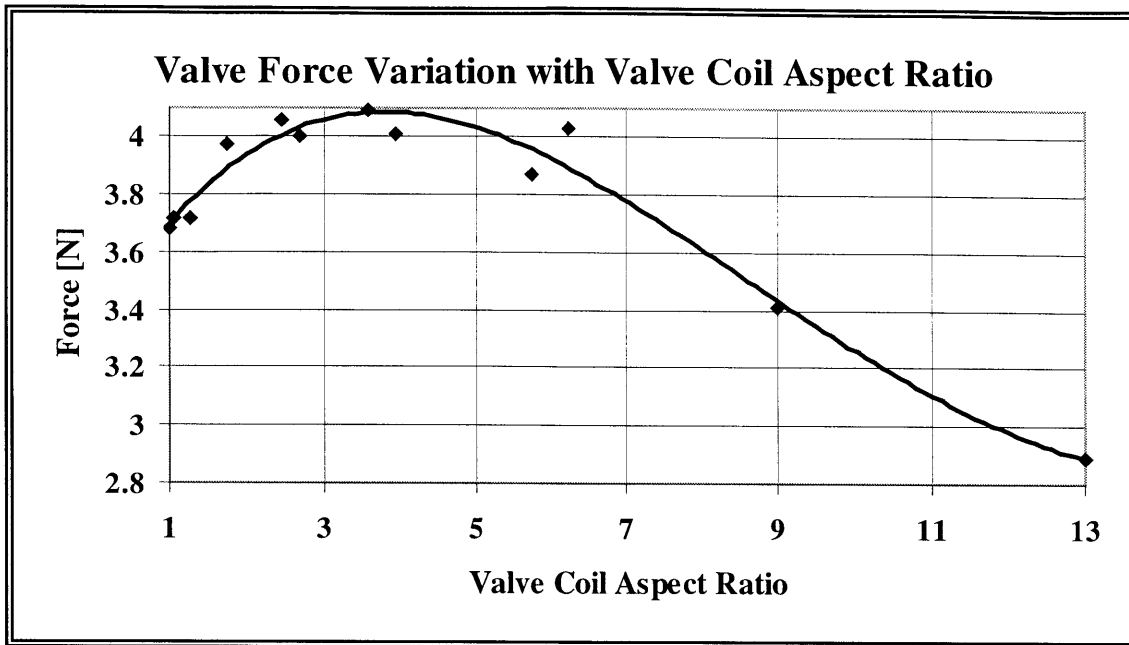


Figure 3.8 The optimal coil ratio is difficult to pinpoint because the data is severely scattered; a fourth-order polynomial fit was used in an attempt to find the maximum

In general, it is expected that valve force will increase with aspect ratio because a greater volume of copper conductor is placed in the valve yoke as the aspect ratio goes up. As described above, the benefits of this affect disappear when the valve coil becomes thin because magnetic flux jumps across the coil instead of traveling around the valve yoke. According to a fourth-order polynomial fit to the severely fluctuating data, the analysis indicates that a valve coil aspect ratio of about 4 provides the best performance. However, the data is highly scattered owing to second-order affects, and the actual band of possible optimal coil aspect ratios lies between about 1.5 and 6.5.

When the aspect ratio study was originally conducted, the aspect ratio was truly isolated from all other factors by holding the outer diameter of the valves constant and fixing the volume of copper wire. Holding the copper volume constant instead of cross sectional area yielded the conclusion that aspect ratio alone has little affect on valve performance. Instead, it is the additional volume of copper in the valve coil winding engendered by higher aspect ratio that provides the true enhancement of valve performance.

Unfortunately, this analysis was conducted early in the development stage of the valve and the experimenter did not realize the supplemental benefit of adding additional copper volume when exploring the coil aspect ratio. Since aspect ratio alone has no effect, the valve remained unchanged from the geometry presented in Figure 3.6 after the aspect ratio analysis. It is suggested that future cold valve development projects explore the performance benefits afforded by additional conductor volume for valve coils with aspect ratios between 1.5 and 6.5.

3.3 DESIGN BY EVOLUTIONARY ITERATION

The majority of the valve development work took place on the computer by exercising the finite element model through various geometric iterations to converge on the final design. A simple baseline model was selected and used to benchmark all iterations. This model, shown in Figure 3.5 meets the basic geometric design constraints but does not meet the opening force requirements outlined in Chapter 2. Note that all finite element models presented in this thesis are characteristic cross sections representing a volume of rotation. The boundaries of each model have been greatly truncated to allow the figures to fit on the page. The actual model boundary in all cases as a square eight inches on each side that allows no flux to pass through it.

A matrix of possible geometric improvements was developed to dictate how the baseline model could be enhanced to provide better performance. Early on, it was realized that the number of parameters requiring exploration was large and the range of characteristic values for each parameter was even larger. Checking every possible combination of geometric improvements for the optimal combination would have taken much more time than was available to complete the development effort. Thus, the exhaustive approach was abandoned and an evolutionary iteration process that could be completed in the appropriate timescale was adopted.

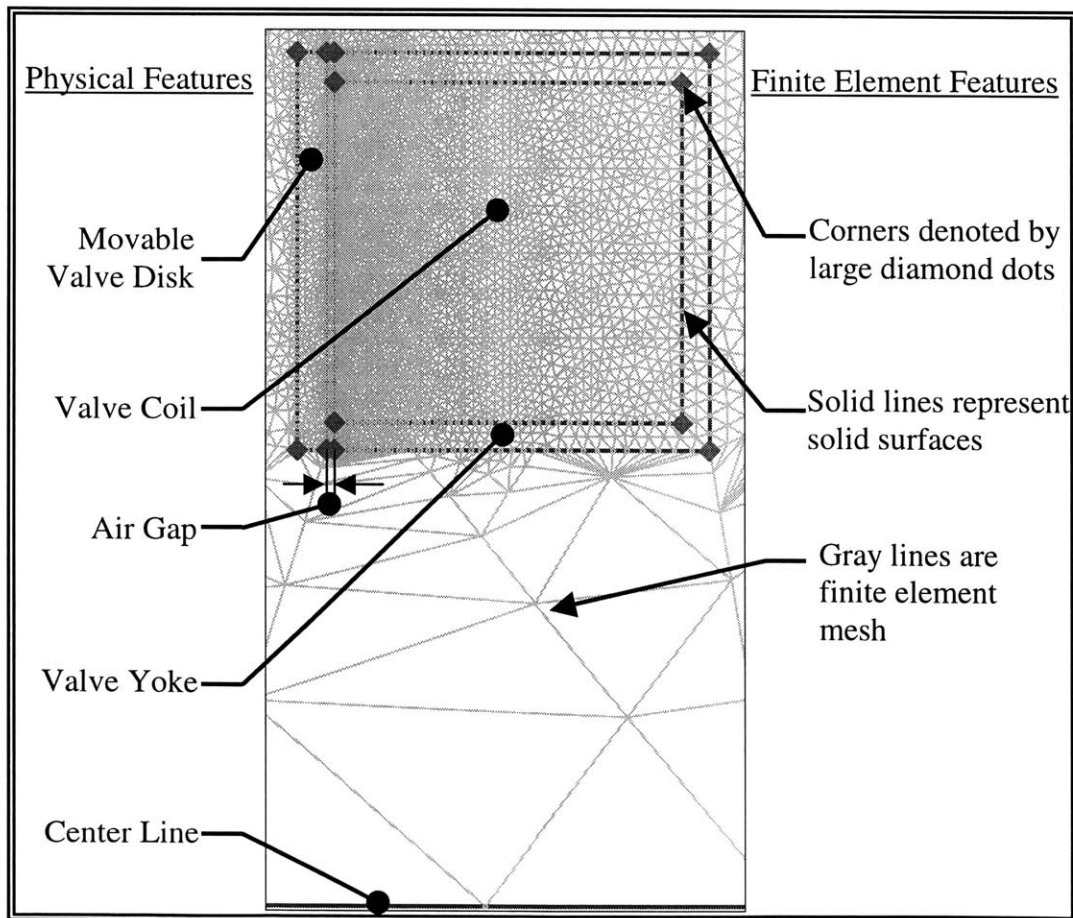


Figure 3.5 The baseline model benchmarks performance for sophisticated designs

According to Quickfield, the inlet valve design is capable of generating 25.003 newtons of force with an input current of 100 amps-turns. This performance represents an increase of about 7.35 times over the inlet valve baseline model and an opening force 189 percent in excess of the required value. The inlet valve model will require much less than 100 amps-turns of input current to meet the design force requirements.

3.4 PERMANENT MAGNETS AS VALVE SPRINGS

Opening the valve ports is accomplished by energizing the valve coil, which magnetically attracts the valve disk away from the valve ports toward the valve yoke. However, a method is required to assure the valve disk returns to the closed position when the valve coil is de-energized. Gravity is ruled out as a primary restoring force because the cryocooler may ultimately see service in satellites where it will have to function in the absence of gravity. In addition the vertical orientation of the valves causes gravity to act against the closing direction of the inlet valve. The pressure differential across the valve ports is employed to seal the valve disk to the valve ports. However, if there is no sealing force on the valve disk when the pressure difference across the valve ports is zero, back pressure cannot build up to engender further sealing.

Many conventional electromagnetic valves utilize a spring or flexure to return the valve disk to its normally closed position. Ceridon¹ utilized a spiral flexure to generate the restoring force and maintain lateral stability against unstable magnetic forces in her cyogenic valve. The current design enjoys natural lateral stability of magnetic forces. To reduce mechanical complexity, the valve disks are not physically connected to anything and are free floating in the magnetic field.

An array of small permanent magnets acts as a magnetic valve spring. An arbitrary force of 2 newtons on the valve disk was selected as the target for incorporating permanent magnets into the design. The selection of this performance metric is not without thought, however. During normal cryocooler operation the permanent magnets impose a force on the valve disk in addition to the force generated by the pressure differential across the valve ports. This added force is a supplemental burden against which the valve ring coil will have to act to open the valve ports. Thus, the force generated on the valve disk by the permanent magnets has to be as small as possible while providing adequate force to close the valve and seal the valve ports in the absence of backpressure.

3.4.1 Magnet Material Selection

Two types of hard magnetic material were considered to make the magnetic valve springs: SmCo18 and NdFeB. The materials are attractive candidates because they both can carry strong permanent magnetic fields, they are commercially available, and they come in very small sizes.

2) Valve Yoke Inner Diameter

Decreasing the inner annular diameter increases the amount of paramagnetic material for the magnetic flux to travel through and thus increases the valve's induced force. The outlet valve's inner diameter is constrained to be no smaller than 0.96 inches because the expander piston, which has an outer diameter just less than 0.96 inches, must travel through the outlet valve's inner hole. The inlet valve, which was developed after the outlet valve geometry was fixed, has no practical limit on the minimum size of the inner diameter. An inner diameter of 0.42 inches was selected because the finite element model exhibited diminishing returns on performance for further decreases in inner diameter.

Figure 3.6 demonstrates how the valve cross-section appears after both inner and outer diameters are selected. This design keeps the wall thickness of the yoke and valve disk at 0.03 inches, but the decrease in outer diameter modifies the cross sectional area of the coil to an aspect ratio of 1.06. The force produced by this design is 3.7175 newtons. Despite the reduced outer diameter, this increase in force is due to the change in valve coil aspect ratio, which will be examined next.

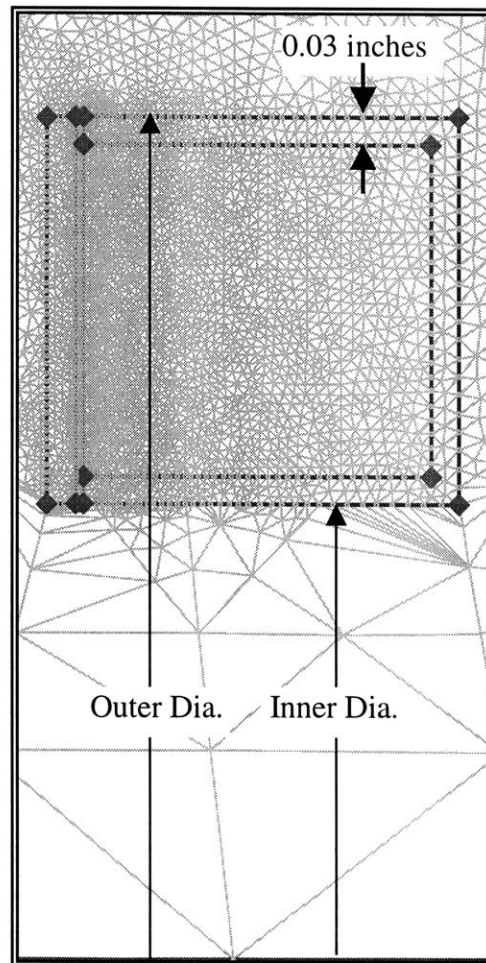


Figure 3.6 The valve model evolves with fixed inner and outer diameters

3) Valve Coil Cross Sectional Size and Aspect Ratio

The valve is constrained in diameter but not in length. One early idea was to develop a valve with a long, thin cross section allowing large amounts of wire to be wound into the valve coil without taking up much radial space. A characteristic magnetic flux line plot for a valve with this geometry is presented in Figure 3.7. This thin valve has a coil cross sectional area equal to the one presented in Figure 3.6, but the aspect ratio is 13 instead of 1.06. The force generated on the valve disk by this configuration is 2.3485 newtons, substantially less than the previous design. This decay in valve performance stems from the leakage of magnetic flux out of the valve yoke across the valve coil. This flux leakage is evident in Figure 3.7. Flux leakage is not well accounted for in simple analytical models, but its affects can be well-quantified using finite element tools.

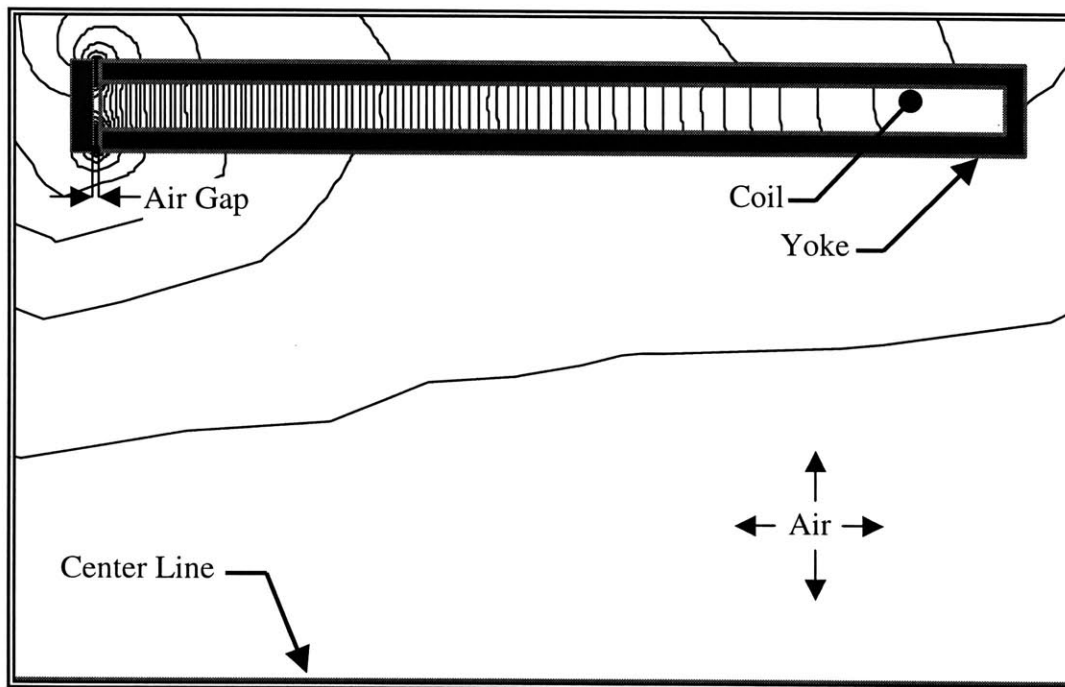


Figure 3.7 At a resolution of 8×10^{-7} Webers, a substantial number of flux lines are seen leaking through the thin valve coil, which retards valve performance

The thin valve model suggests that the valve's performance is strongly dependant upon the aspect ratio of the valve coil and that there is some global maximum in valve performance between a coil aspect ratio of 1 and 13. Thus, the location of this aspect-ratio-dependant maximum was examined via finite element. To perform these tests, the outer diameter of the valve was fixed and the cross sectional area of the coil was held constant at 0.1295 square inches. The aspect ratio of the coil was altered from 1 through 13 by varying the coil's length and width. The length of the valve and the inner diameter were modified accordingly to match the change in coil geometry. Figure 3.8 shows the results of this process.

Although the magnetic qualities of NdFeB are slightly inferior to SmCo18, NdFeB was ultimately selected because it can be ground to cylindrical buttons of very specific thickness without fracturing or losing its field strength. This feature adds a degree of flexibility to the design process. The magnets ultimately selected for the machine are small cylindrical buttons about 0.095 inches in diameter and about 0.040 inches in height.

The magnetic behavior of permanent magnets is described by three properties. The permanent field density is a measure of the strength of the magnetic field created by a substance when no electric current is applied. The coercive force is the magnetic field intensity required to cancel out the permanent magnetic field of the substance. The permeability is the slope of the line that connects these two points on a plot of magnetic field density versus magnetic field intensity, a B-H curve. The B-H curve provided by the manufacturer for NdFeB is shown in Figure 3.28.

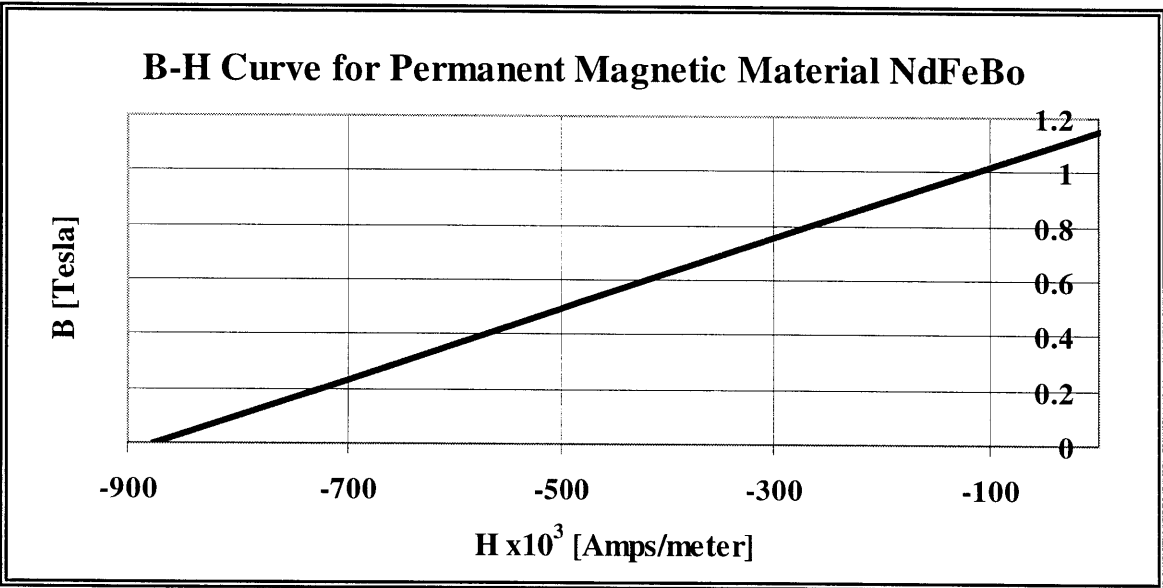


Figure 3.28 The line connecting the coercive force to the permanent magnetic field density on a B-H curve represents the behavior of NdFeB permanent magnet material

3.4.2 Determining Dimensions for the Magnet Valve Spring

The main challenge in modeling permanent magnets via the Quickfiled finite element package is the software’s constraint that all three-dimensional objects be axi-symmetric. The permanent magnets must be embedded into the valve bulkhead in such a way as to not interfere with the valve ports. One approach is to secure an annular permanent magnet with specific dimensions matched to the valve bulkhead. However, with an eight-port valve bulkhead, the easiest way to accomplish the design is to stagger an array of eight button magnets between the valve ports at regular intervals. Conveniently, NdFeB magnets are commercially available in button magnet form at sizes applicable to the magnet array design approach.

4) Valve Yoke Jump Gap

The valve yoke jump gap is the distance between the inner and outer prong of the valve yoke. In electromagnetic machines, this gap is usually bridged to some extent by paramagnetic teeth to facilitate the flow of magnet flux, as shown in Figure 3.9. For this application, these teeth have the benefit of providing more surface area for the magnetic flux to move through to link the valve yoke to the valve disk, and this effect increases with decreasing valve yoke jump gap. To their detriment, these teeth shorten the distance the magnetic flux must jump to travel from one yoke prong to the other without passing through the valve disk. This detriment increases with decreasing yoke jump gap.

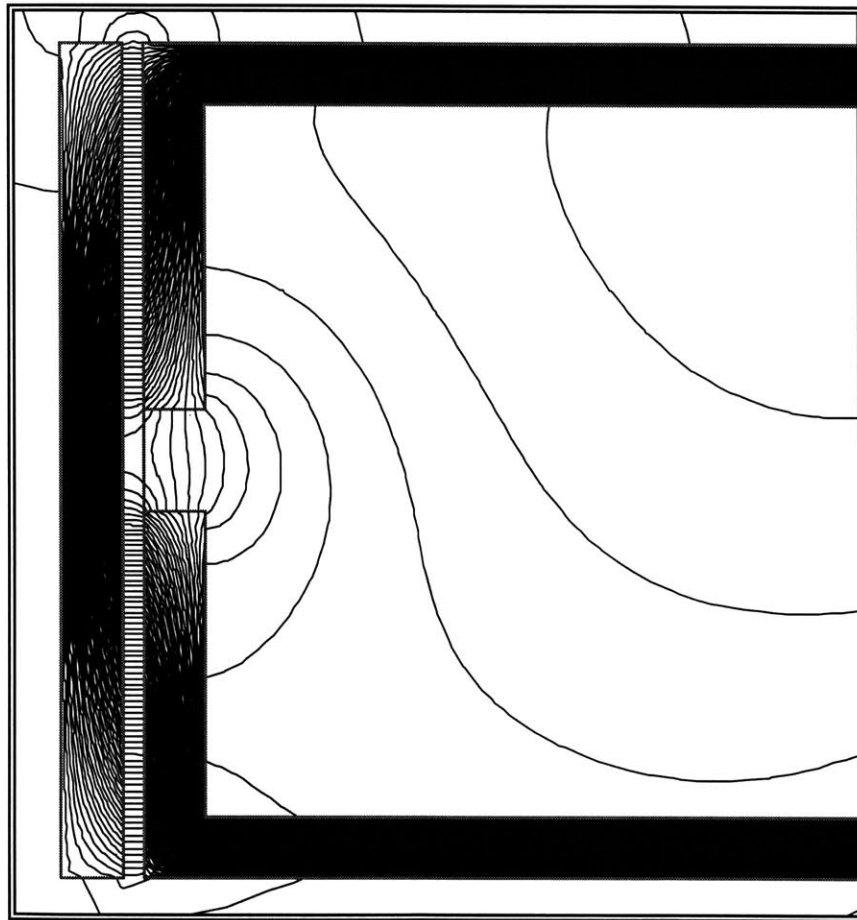


Figure 3.9 At a resolution 1×10^{-6} Webers many magnetic flux lines are seen jumping from the valve yoke and the valve disk

Between the two competing factors, the finite element code was exercised to find the optimum valve yoke jump gap. Figure 3.10 shows that the optimum valve performance is achieved for a valve yoke jump gap of about 0.21 inches. Thus, this dimension was incorporated into valve geometry, as shown in Figure 3.11.

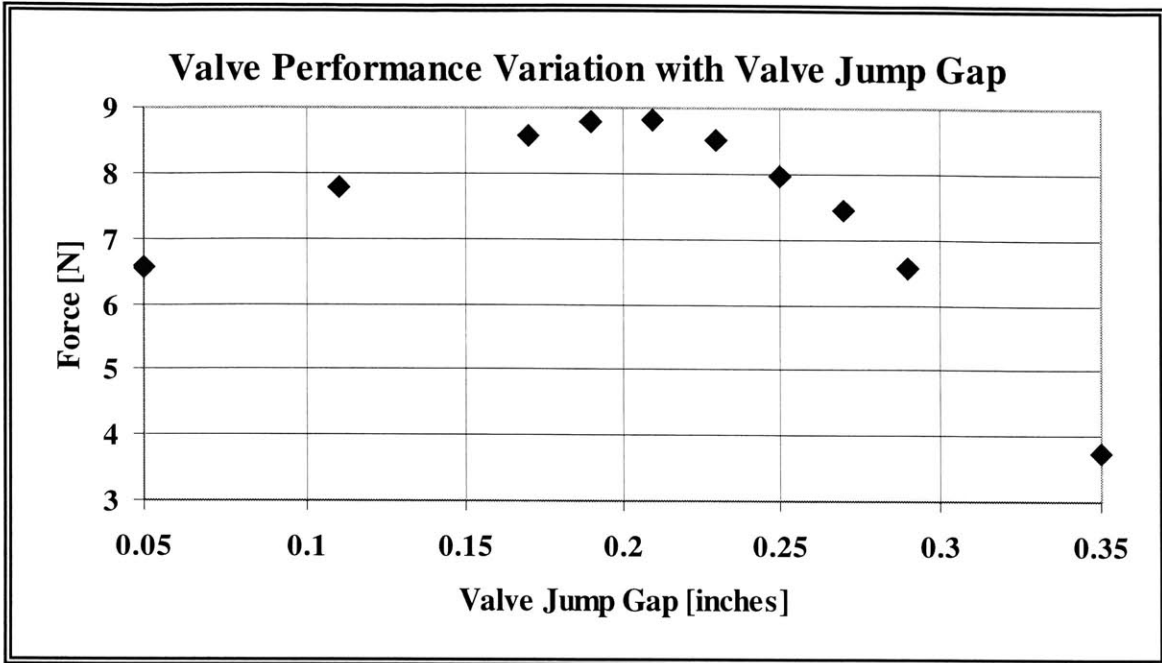


Figure 3.10 An optimal balance between the positive and detrimental factors of changing the valve yoke jump gap is reached at the maximum point of this plot

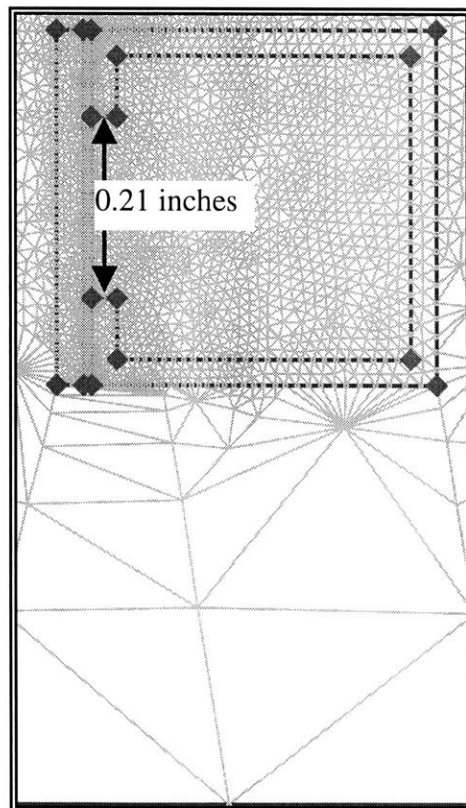


Figure 3.11 The valve yoke jump gap is set to 0.21 inches

5) Valve Yoke Prong Flux Area

Simple analysis shows that as magnetic flux travels the resistance it experiences is inversely proportional to the normal cross-sectional area of paramagnetic material through which it travels. By design, the cross sectional areas of the inner and outer valve yoke prongs perpendicular to the magnetic flux flow remain the same. However, because the two prongs are at different radii, their cross sectional areas normal to the flow of flux are different. This situation is demonstrated graphically in Figure 3.12. The magnetic flux experiences less resistance traveling through the outer prong than through the inner prong because the outer prong has a larger area normal to the flow of flux. This disparity in resistance reduces the valve's performance, and the first corrective measure is to increase the inner prong thickness to match the outer prong.

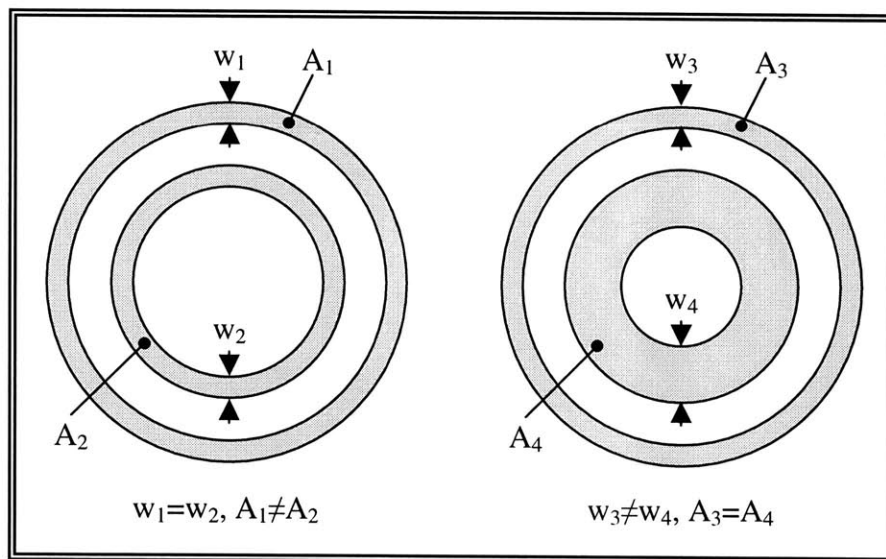


Figure 3.12 When viewed from above, the valve yoke prongs are coaxial annuli, and if their widths are the same, their areas must differ

To determine what area yields the best valve performance, a study of valve yoke prong thickness was performed; it was conducted by fixing the inner and outer diameters of the valve. The major internal diameter of the valve yoke was adjusted by increasing the wall thickness of the outer prong. The wall thickness of the inner prong were then adjusted to keep the area normal to the flux the same in both prongs. As the wall thickness increased, the yoke teeth moved towards the center of the coil closing the valve yoke jump gap.

Increasing the prong thickness reduces the volume of copper in the valve coil and increases the coil's aspect ratio. Despite these changes, the finite element model maintains a constant amp-turn value on the valve coil. In addition, the flux leakage through the valve coil is an increasing problem as coil aspect ratio increases.

Adjusting the yoke flux area weighs the relative value of placing paramagnetic material versus copper conductor in the valve ring coil. The results of this study are provided in Figure 3.13, and there is a clear maximum point on this parameter.

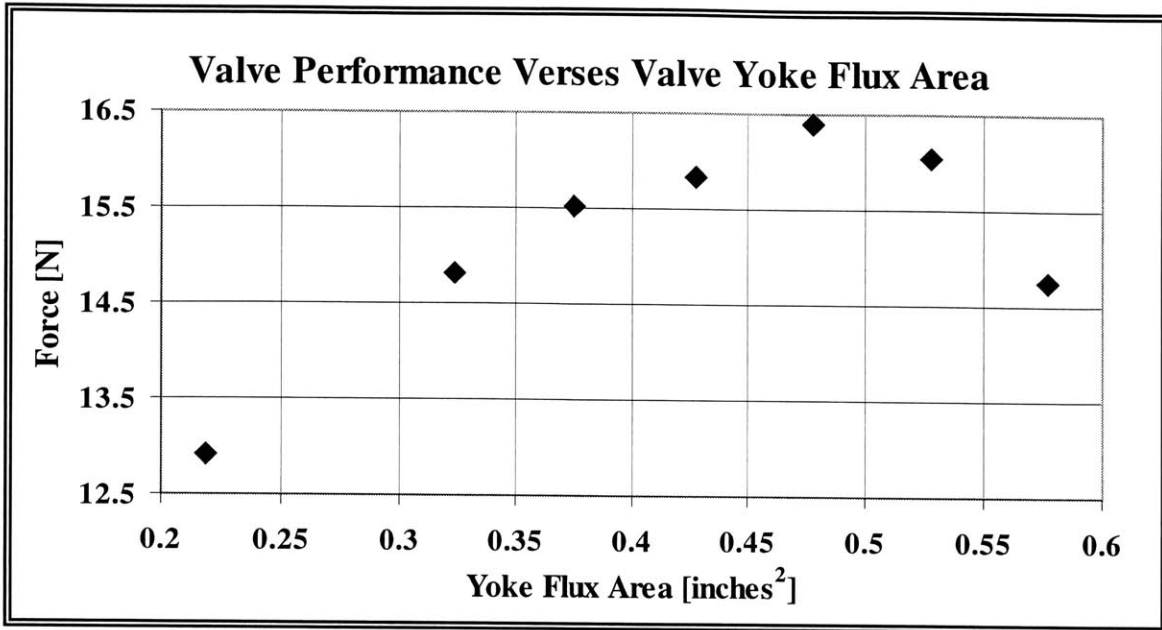


Figure 3.13 Increasing the area normal to magnetic flux flow is generally beneficial; in this case, increasing the valve yoke flux area contributes to flux leakage through the coil

Although the maximum valve performance is found at a yoke flux area of about 0.48 square inches, it is important to recall that the copper conductor volume in the valve coil falls linearly as the yoke flux area is increased, as shown in Figure 3.14. Reduced copper volume translates to fewer turns of wire wound on the valve coil. This deficit requires that more current be driven through the coil to achieve the same amp-turn value.

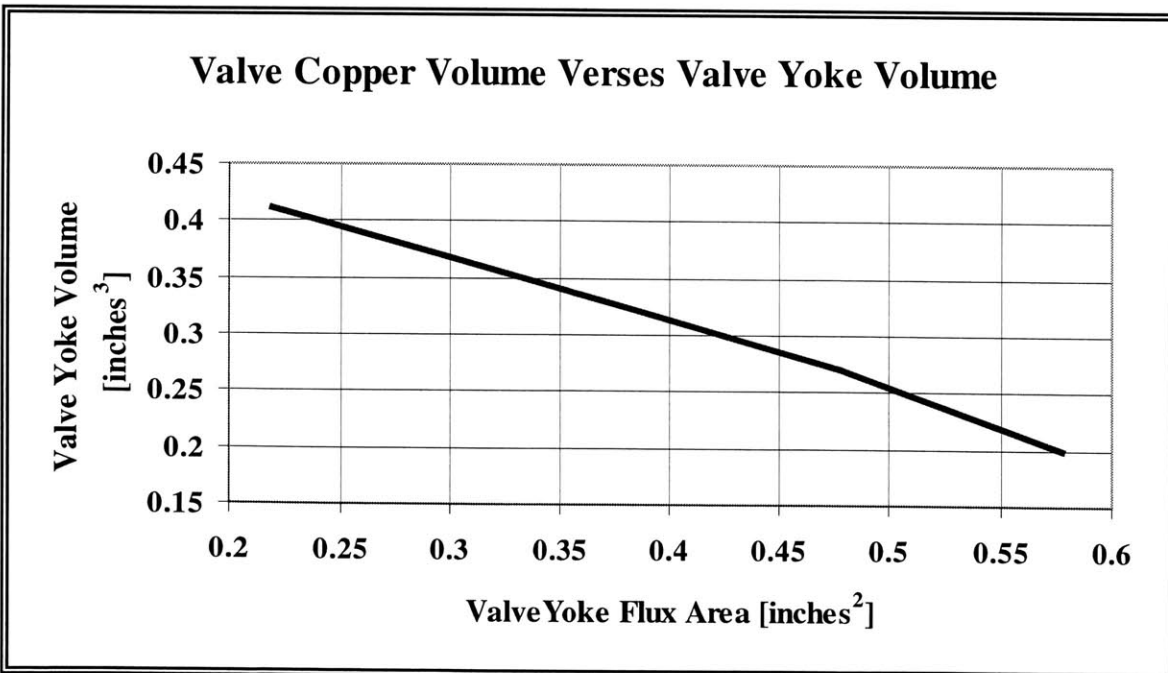


Figure 3.14 With the valve ring coil's fixed outer dimensions, increasing the internal volume of paramagnetic material yields an identical decrease in valve coil volume

Ultimately, a compromise is reached to assure that adequate internal volume remains in the valve yoke to accommodate the copper wire. The flux area of 0.43 square inches is selected yielding an available copper volume of just under 0.3 cubic inches. The valve geometry arising after this study is shown in Figure 3.15.

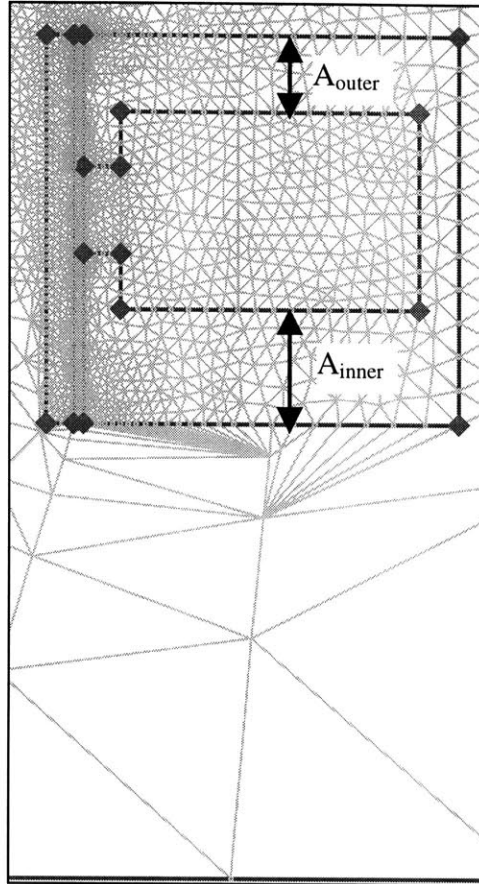


Figure 3.15 The yoke's walls are bulked up to increase flux flow area

6) Valve Yoke Base Flux Area

The magnetic flux, in addition to passing through the valve yoke prongs, must also pass through the base of the valve yoke as it moves in the radial direction from the outer prong to the inner prong. Due to the annular geometry of the valve, it is difficult to make this area constant normal to the path of the flux. However, there is no significant penalty for making this area very large by thickening the base of the valve.

A range of thickness values was exercised with the finite element model until a point of diminishing returns was reached at a thickness of about 0.06 inches, as shown in Figure 3.16. A sharp jump in valve performance between 0.03 inches and 0.4 inches was noted accompanied by an additional slight increase up to 0.12 inches. At this value, the performance gains level off. This dimension was incorporated into the evolving valve design, shown in Figure 3.17.

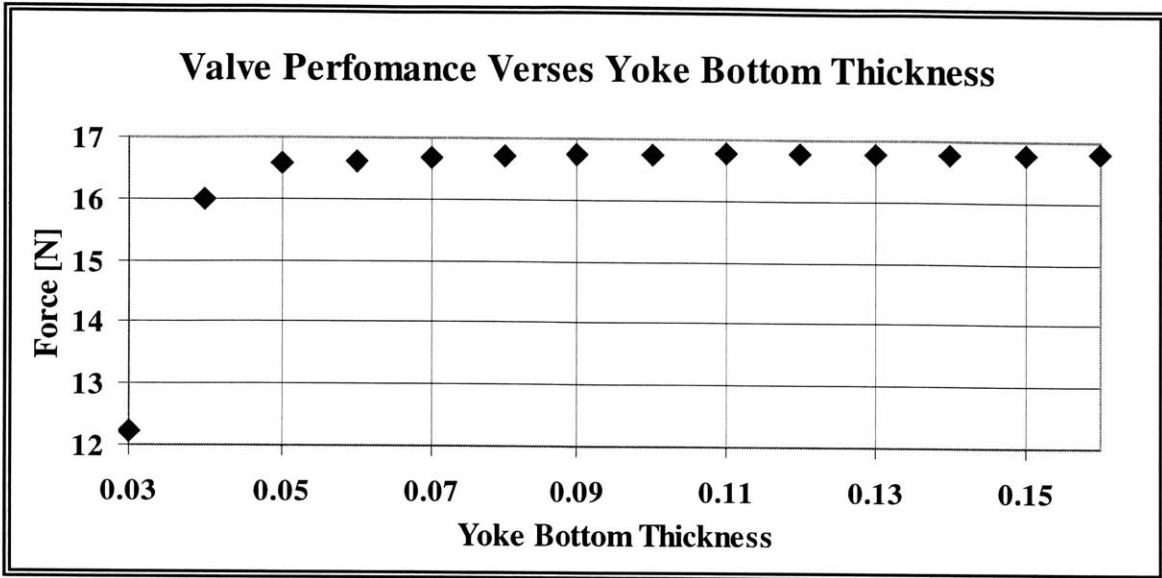


Figure 3.16 Although there is no performance penalty for making the valve base very thick, the benefits of doing so quickly drop off as the base area matches prong area

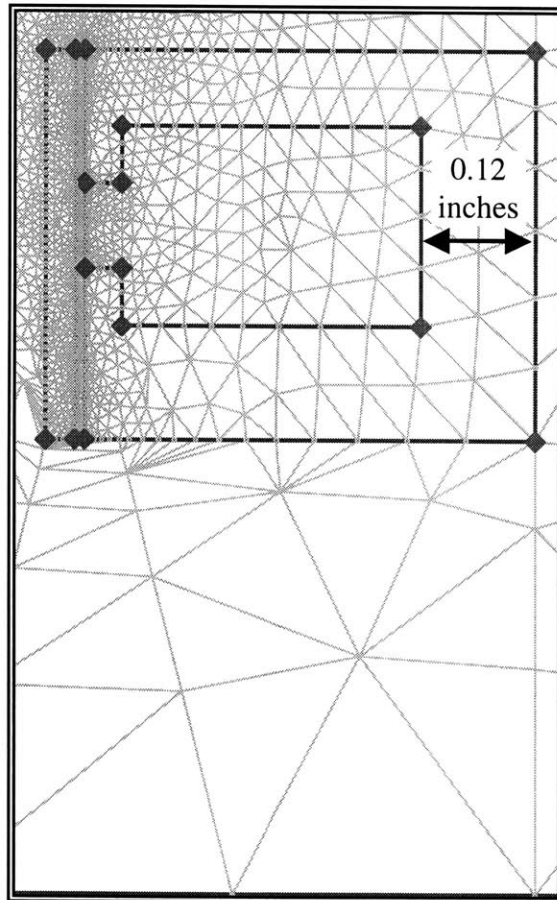


Figure 3.17 The base thickness is increased to aid radial flux flow

7) Valve Disk Thickness

Magnetic flux resistance in the valve disk can be decreased as with the valve yoke base by increasing its thickness. This measure increases the area through which the magnetic flux can flow, and it has no negative impacts on the valve's performance. The valve disk thickness can essentially be increased until diminishing returns are realized.

There are, however, some negative implications to increasing the valve disk thickness indefinitely. First, an increase in valve disk thickness corresponds an increase in the height of the space between the valve yoke and the valve seats. Although the valve disk fills most of this space, the increased height of the gap between the valve disk and the spacer ring causes a small increase in expander dead volume. Second, the mass of the valve disk increases as it becomes thicker. Doubling the valve disk thickness, and hence its mass, increases the time the valve disk takes to traverse the lift gap by more than 40 percent, according to the simulation method outlined in Chapter 7. Although this increased time span is still much faster than other processes in the cycle, the more massive valve disk strikes the valve seats harder, leading to decreased valve seat lifetime and entropy generation in the cold end. This analysis illustrates that valve thickness cannot be increased indefinitely without consequences to other functions of the cycle.

Figure 3.18 shows the results of the finite element model exercised through various values of valve thickness. As the plot illustrates, diminishing returns are realized at a valve disk thickness of about 0.04 inches. Figure 3.19 shows the modified valve geometry where a valve disk thickness of 0.05 inches is selected to assure the real valve disk is safely within the optimal valve disk thickness region above 0.04 inches.

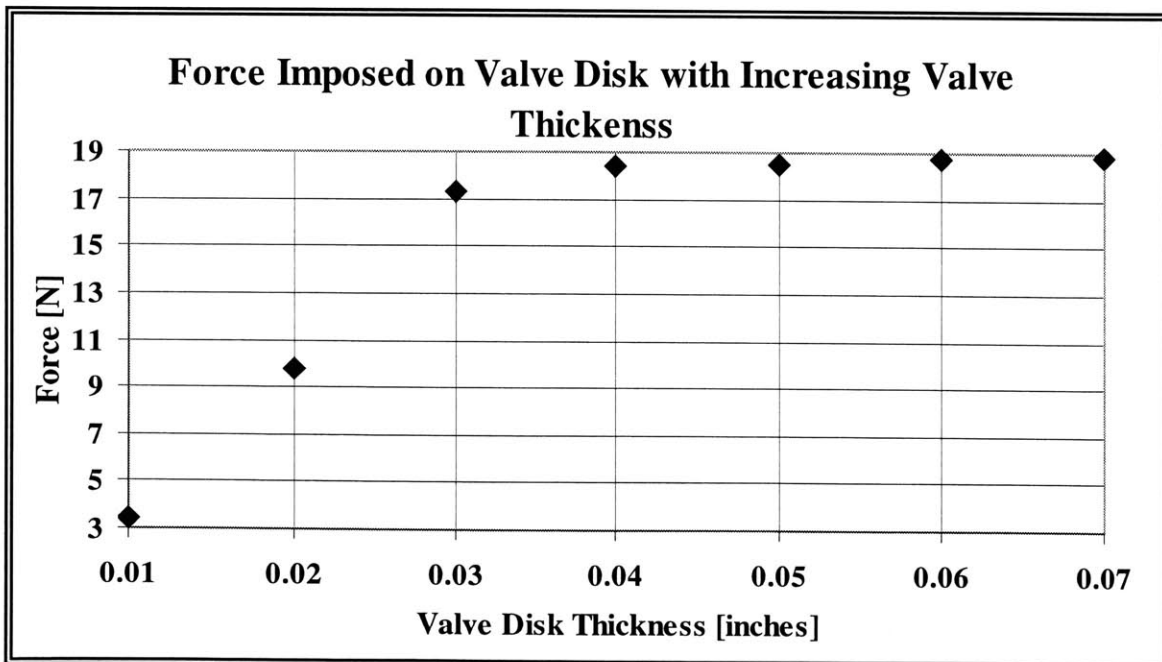


Figure 3.18 Increasing valve disk thickness reduces the resistance to flux flow through the valve disk and enhances the force generated on the valve disk by the valve yoke

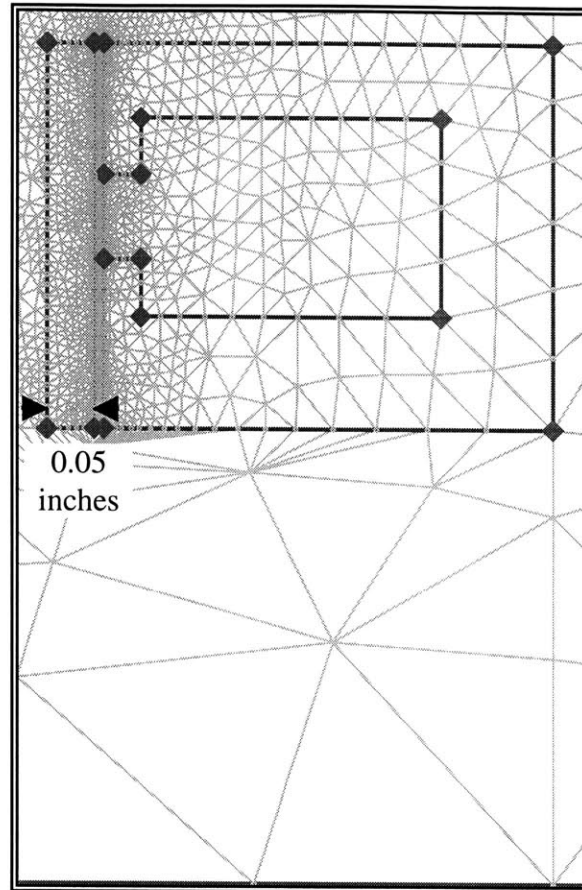


Figure 3.19 The valve design evolves with Increased valve disk thickness

8) *Filleting Coil Corners*

As with all types of potential flow, corners in the magnetic flux path create resistance to the flow. The square corners surrounding the valve coil create flux concentrations that promote flux leakage out of the valve yoke, detracting from the performance of the valve.

The potential performance enhancement gained from filleting the corners was explored using the finite element code. Filleting a corner removes the geometric flux concentrator at the 90-degree bend in the valve yoke and increases the area normal to the flow of magnetic flux around the bend. These factors enhance flux linkage between the valve yoke and the valve disk.

To quantify the degree of filleting, a fillet factor is defined to provide an easy way to identify different magnitudes of filleting from one another. As demonstrated in Figure 3.20, the fillet factor is the distance in inches between the corner of the fillet and the hypothetical location the corner would be if no fillet were applied.

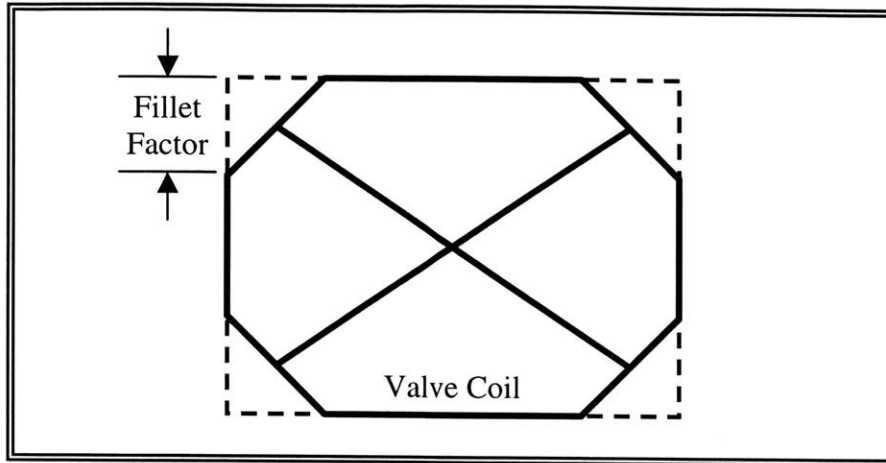


Figure 3.20 The distance between the fillet corner and the imaginary corner if no fillet were present is defined as the fillet factor

The finite element model was exercised through a number of fillet factors, and as is shown in Figure 3.21, filleting has an enormous positive effect on the force generated by the valve yoke on the valve disk. Identical fillets with the same fillet factor were placed on all four corners of the valve coil, and no attempt was made to mix different size fillets at various corners to reap further optimization. Fillets with angles other than 45 degrees were also tried, and in some cases, these alternatives returned better performance than 45-degree fillets. However, these alternate geometries were abandoned because of fabrication difficulty. Fillets on the open side of the valve yoke were allowed to cut through the teeth in the valve yoke. When the fillets became so large that they closed off the valve yoke jump gap completely, as shown graphically in Figure 3.22, the fillets were artificially truncated to preserve a 0.01-inch gap between the valve yoke teeth. The optimum size of this gap is addressed in the next portion of analysis.

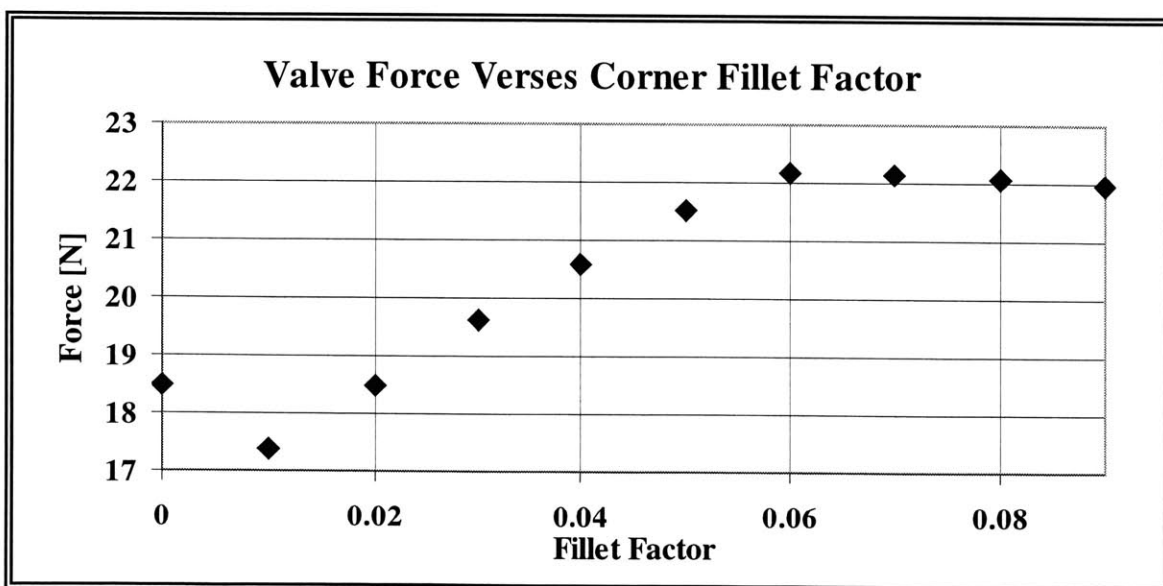


Figure 3.21 Filleting the valve coil corners enhances flux flow and valve performance

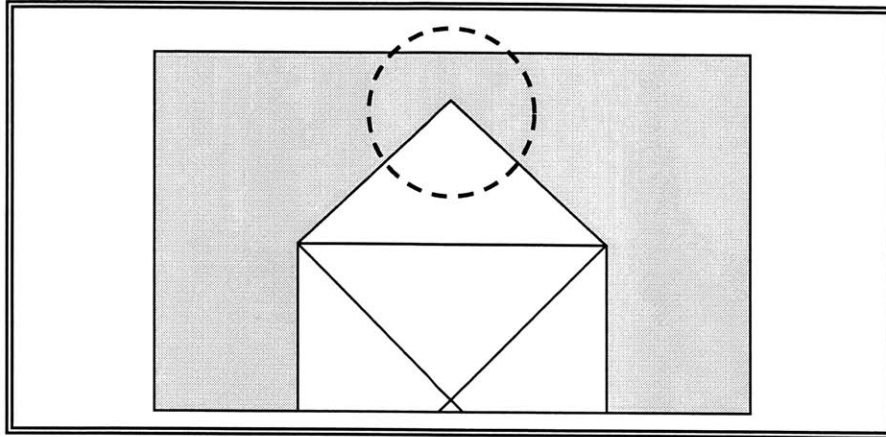


Figure 3.22 Too much filleting can close the valve yoke jump gap

Figure 3.22 shows the geometry of the valve with the fillets in place. A fillet factor of 0.07 is selected because it demonstrates near-optimum valve performance. Also, the point is far enough within the level performance region to assure the benefits of filleting are captured in the real valve regardless of small errors in the model.

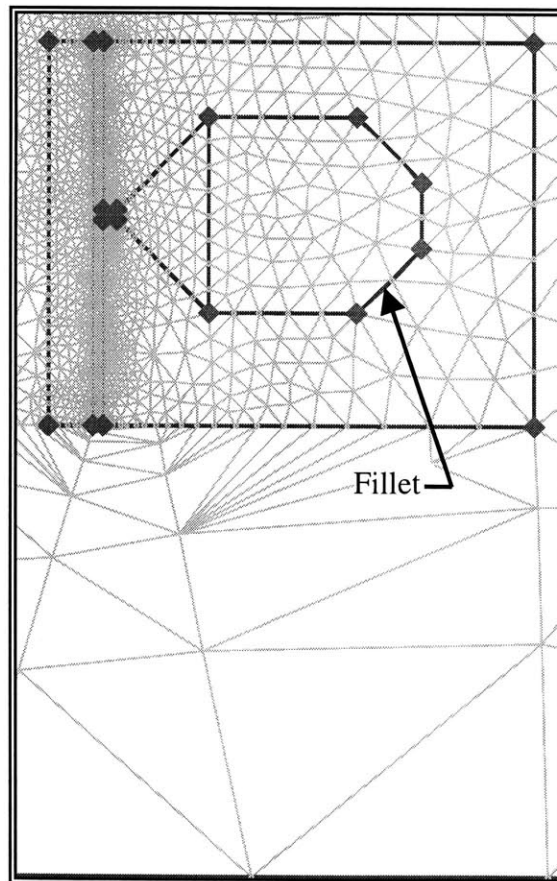


Figure 3.23 The valve model evolves to include valve coil corner filleting

Filleting the valve yoke reduces the volume of copper that can be wound into the valve coil. This consequence has the effect of increasing the required coil input current to deliver the same magnitude of amp-turns. Thus, filleting the valve yoke represents a trade-off between valve performance and the heat dissipated into the cryocooler cold end by joule heating in the valve coil.

9) Valve Yoke Jump Gap

The fillet factor selected to provide optimum performance creates a geometry demonstrated in Figure 3.22 where the fillets are large enough to close the natural jump gap at the open end of the valve yoke. Closing this gap will short the magnetic circuit created by the valve yoke and cause a significant reduction in valve performance. To reap the full benefit of filleting despite this problem, an artificial valve yoke jump gap was arbitrarily selected at 0.01 inches for the benefit of the fillet calculation. Exercising the finite element model through a range of possible jump gaps assures this geometry is optimized. Figure 3.24 shows the results of this analysis, which indicate that the original value of 0.01 inches is the optimum geometry. Thus, the valve was not modified from the configuration shown in Figure 3.23 as a result of this exercise.

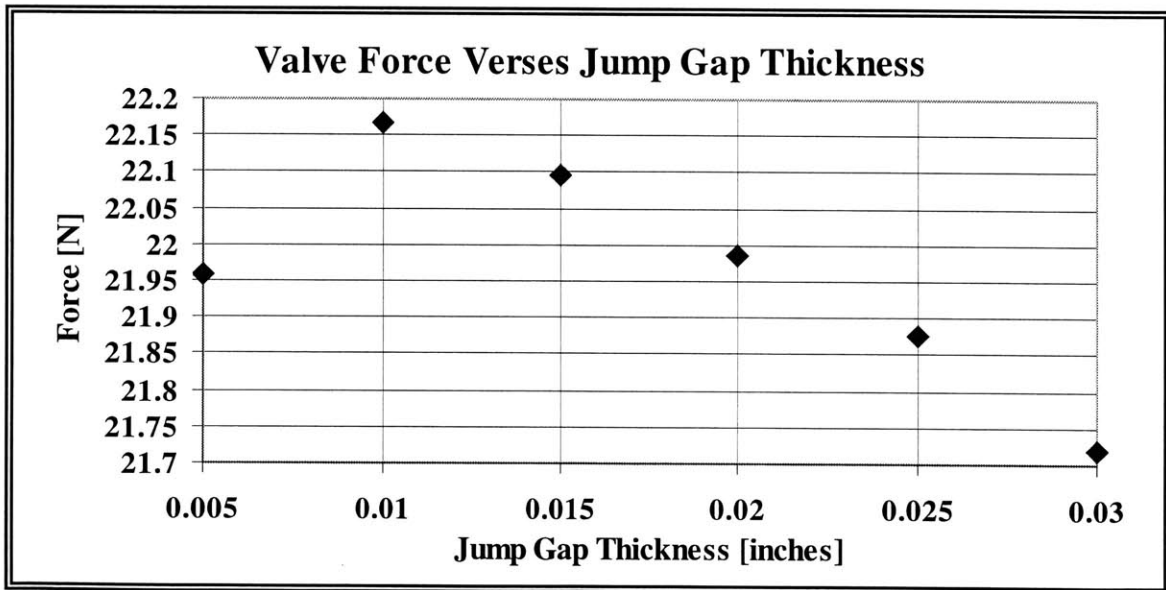


Figure 3.24 Verifying that the synthetic valve jump gap thickness is optimal, this plot shows that further increase in the valve jump gap more detracts from valve performance

At this point, it is important to note that the force scale in Figure 3.22 is on the order of tenths of newtons. This observation illustrates that small modifications in geometry such as jump gap thickness have a very tiny effect on valve performance with respect to the previously explored parameters. Once the major geometric variables above have been considered, the design converges to a local maximum in the design space. Due to diminishing returns reaped from further small modifications, it was decided to cap the evolution of the valve at this point and begin the construction process.

10) Un-Filleting Coil Corners

Having arrived at a finalized valve design via finite element modeling, an effort was made to develop a machining process to assure the parts could be built using conventional machine tools and processes available in the lab. The finite element model was used to develop the technical drawings presented in Chapter 2, and the spool component of the outlet valve yoke was machined out of aluminum. Tooling and machining methods were identified to cope with making the complex geometry of the filleted coil within the yoke. This process required a cutting tool thin enough to probe past exposed features of the valve yoke without touching them. The tool also required the delicately to be manipulated on the lathe's compound axis.

The practice spool was wound with 28-gauge copper wire to test whether the valve coil winding process was feasible. It was found that wire could not be wound up the inside of the angled face associated with the fillet at the base end of the valve yoke. The wire became scrambled and failed to fill the space. This result was unsatisfactory, and ultimately the fillets at the base were abandoned to ease the winding job and increase the copper volume in the coil. Figure 3.25 shows the final resulting geometry.

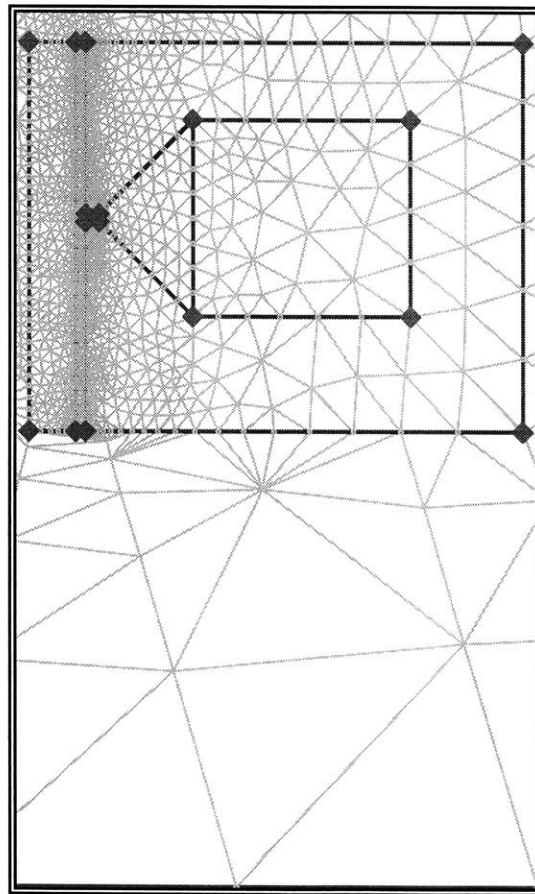


Figure 3.25 The fillets at the base of the valve coil are removed to facilitate the winding process

11) Final Modifications

Placing the final outlet valve design in the cryocooler cold end requires two small modifications. A nonmagnetic spacer ring has been added to assure the valve lift remains at exactly 0.01 inches during valve operation. This spacer ring also keeps the valve disk centered with respect to the outlet valve so the expander piston does not strike the valve disk during its exhaust stroke. Accommodating the spacer ring requires a reduction in the valve disk outer diameter from 1.78 inches to 1.648 inches. In future designs, the spacer ring is not necessary if LocTite® is used to hold the valve yoke in place and the cold end wall assembly is modified to properly center the valve disk.

The final design for the outlet valve, modified with the spacer ring, is presented in Figure 3.26. According to the finite element model, this final valve design develops 21.886 newtons of force with an input current of 100 amp-turns on the valve disk in its closed position. This performance represents over 165 percent of the required opening force and a nearly six-fold increase in opening force over the baseline outlet valve model presented at the beginning of the evolutionary design process. Thus, the outlet valve model requires much less than 100 amp-turns input current to achieve the opening force design requirement.

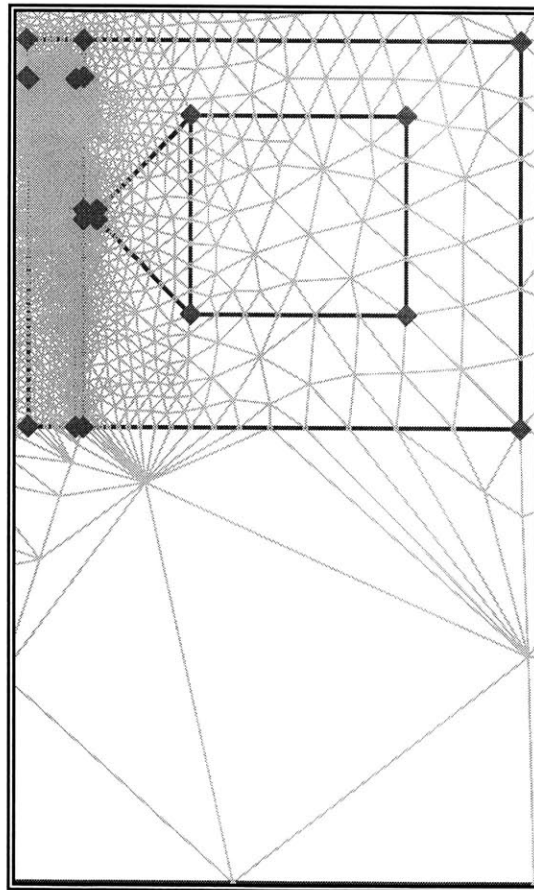


Figure 3.26 The final outlet valve finite element model design

3.3.2 Inlet Valve Iterative Design Process

With the information gleaned from the iterative design process outlined above for the outlet valve, a similar approach was developed to converge on a final design for the inlet valve. This final design is presented in Figure 3.27. A baseline model with dimensions similar to those of the outlet valve baseline was used to seed this process. However, the outer diameter of this baseline was modified to reflect the dimensional constraints of the inlet valve.

Several important features were taken from the outlet valve design and transposed directly to the inlet valve model. The valve coil dimensions and aspect ratio are identical to the outlet valve, and the fillet factor is preserved along with the jump gap thickness. There is a large volume of material added on the inner prong of the yoke to increase the cross sectional area normal to the travel of magnetic flux in the inner leg. The final inner diameter dimension was selected by iterating on the inlet valve finite element model until diminishing returns were realized.

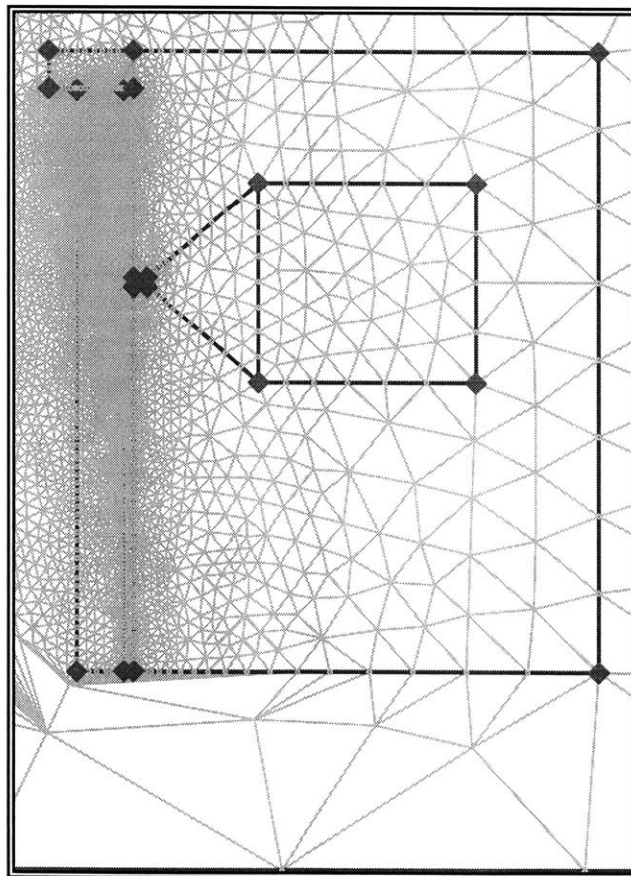


Figure 3.27 The final inlet valve finite element model design

Finally, it is important to note that the magnet configuration was developed for an eight-port valve bulkhead. No redesign of the permanent magnet array was attempted when the number of ports was reduced to three. However, a magnet configuration based on multiples of three might be more conducive to the final geometry of the valve bulkhead.

While annular valve components are easily modeled in axi-symmetric space, the arrayed arrangement of button magnets described above is not. To accommodate permanent magnets into the finite element model, the button magnets must somehow be modeled with an annular shape. Thus, two problems are solved in parallel. First, a mounting arrangement has to be divined to place real magnets in the valve bulkhead to deliver 2 newtons of force. Second, a method has to be developed to describe the force induced on the valve disk by the magnet array within the finite element software.

It was unknown whether the presence of the de-energized valve yoke would perturb the results of the magnet-array/valve-disk interaction. Thus, a test was developed to determine its effect. The valve yoke finite element model was utilized with the valve coil de-energized and the valve disk placed in the closed position. A variety of permanent magnets of different strengths and sizes were modeled in the finite element code and placed at various distances between 0.005 and 0.025 inches from the valve disk on the side opposing the valve yoke. The forces induced by the magnets were recorded. The same set of tests was repeated with the valve yoke removed from the finite element model. A comparison of the force results shows that the force induced on the valve disk by the various permanent magnets varies by no more than 1 percent between the cases with and without the valve yoke present. The conclusion this study yields is that the presence of the valve yoke can be ignored in all finite element force modeling conducted between the valve disk and any permanent magnets within 0.025 inches of the valve disk.

To estimate the force induced on the valve disk by the button magnet array, a finite element model was devised consisting of a single button magnet acting on a solid paramagnetic disk with a diameter matching the width of the valve disk annulus. The thickness of the modeled disk also matches the thickness of the real valve disk. This approach correctly isolates as many dimensions as possible given the axi-symmetric constraint of the modeling software. In this case, the radial width of the valve disk annulus and its thickness are preserved while the rotational distance is ignored. An arbitrary distance of 0.01 inches between the button magnet and the valve disk is selected in this simulation. A characteristic field solution for this geometry is given in Figure 3.29.

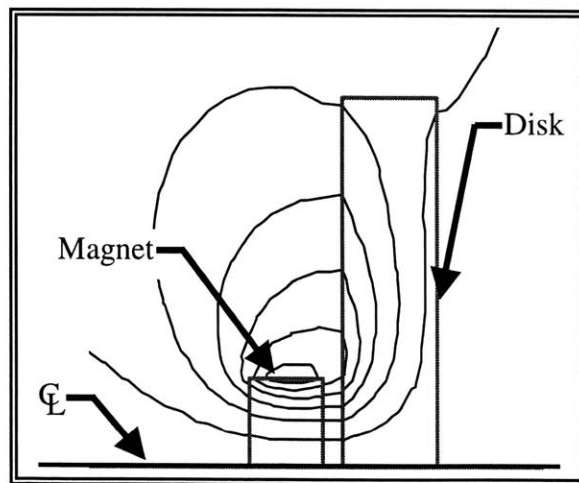


Figure 3.29 At a resolution of 5×10^{-7} webers the flux lines linking the magnet and valve disk are seen

To gauge the importance of the ignored radial direction in the one-magnet finite element model, the button magnet was allowed to act on a disk of essentially infinite radius. The infinite disk case yielded a force of 0.44027 newtons on the disk while the finite case yielded a force of 0.43888 newtons. The difference of 0.32 percent indicates that neglecting the infinite radial distance may not be too detrimental to the model's accuracy.

To develop an estimate of the force an array of eight button magnets imposes on the valve disk, the force on the finite disk determined above is multiplied by eight. Exercising this model through a span of valve disk locations away from the permanent magnet yields an approximated force curve for the valve disk as it traverses through the permanent magnetic field.

To compare these simulations to real data, a magnet test rig was built consisting of eight permanent magnets spaced evenly on a 0.6-inch diameter circumference. A force measuring test stand, described in more detail in Chapter 5, was utilized to determine the force generated on a prototype valve disk by the permanent magnetic array. The valve disk was held at different distances from the magnets by a series of shims to generate a force versus distance curve similar to the one generated from the finite element data. These data are presented together in Figure 3.30.

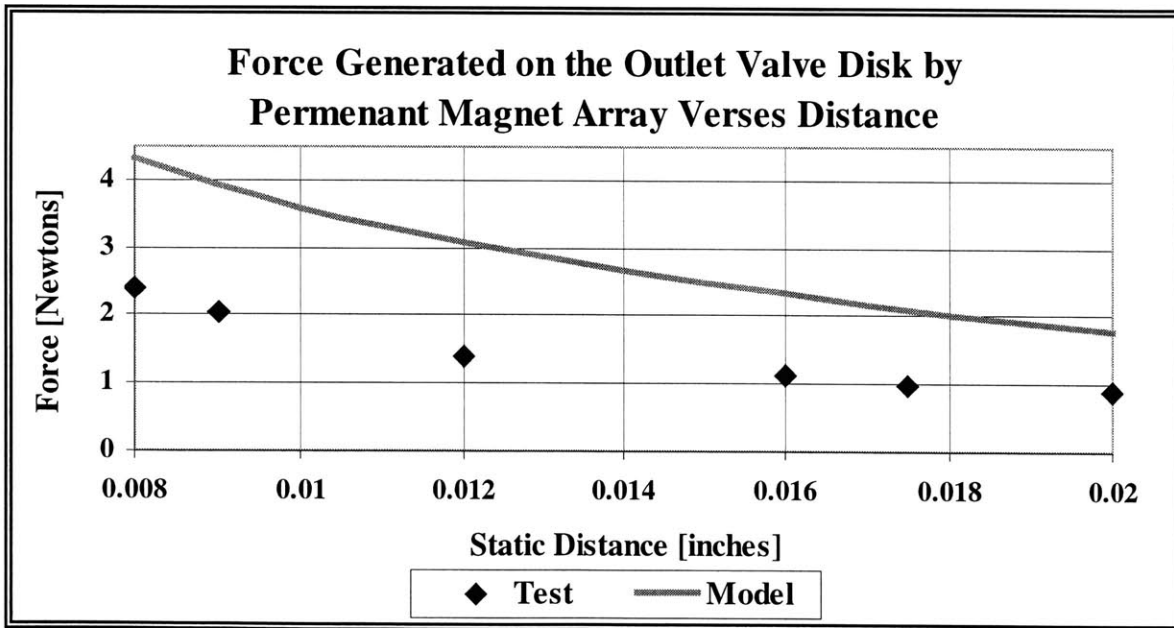


Figure 3.30 A comparison of the modified single magnet model to actual data shows that the model severely overestimates the magnitude of force generated on the valve disk

A comparison of the real data to the modified single magnet model shows that the model preserves the correct general trend, but over predicts the force generated on the valve disk by a factor of about 1.8 for all distances considered. This poor result is to be expected based on the number of assumptions that went into developing the model. For example, in addition to ignoring the radial dimension of the valve disk, the flux linkage between the fields of adjacent magnets is also ignored.

The major design question is how far to distance the magnet array from the valve disk to provide 2 newtons of sealing force on the valve disk, and the test rig force versus distance data in Figure 3.30 provides the answer. The geometry selected places the magnet array 0.01 inches from the valve disk by providing 0.04-inch-deep holes for the magnets in the valve bulkhead. This design should provide a permanent magnet sealing force of about 1.75 newtons.

3.4.3 Modeling the Magnetic Valve Spring Via Finite Element

It is desirable to developing a more representative version of the finite element model that includes an accurate representation of the permanent magnet array. A complete, accurate magnetic model can be exercised to learn about the behavior of the valve disk behavior in the actual machine. To address this goal, a model for the permanent magnet array must be developed whose properties match those of the magnetic test rig presented in Figure 3.30.

Due to the axi-symmetric constraint imposed by the finite element modeling code, an annular magnet must be modeled, and a first attempt to determine the dimensions of an annular magnetic model that solves this problem was developed. This method places the mean diameter of the annulus, r , at the diameter of the circle upon which the real magnets are placed. The model requires the area of annular magnet normal to the magnetic flux flow to match the summed area of the faces of the real magnets in the array. The width of the annular magnet, $2w$, reduces as its mean diameter increases to assure the same area is always presented to the valve disk. The thickness of the annulus is taken to be the same thickness as the permanent magnets. Through geometric manipulation, the value of w can be determined for any mean radius using Equation 3.2. The geometry associated with this calculation is presented graphically in Figure 3.31.

$$w = \frac{A_{magnets}}{\pi 4r} \quad (\text{Equation 3.2})$$

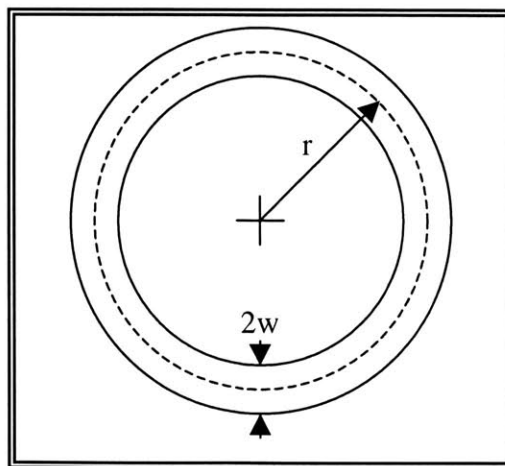


Figure 3.31 These annulus geometric definitions are used with Equation 3.2 to yield the model magnet dimensions

To build a comparison between the annular magnet model and the real test data, an annular model was developed as described above and exercised with the finite element software for the outlet valve case. A comparison of the results is presented in Figure 3.32.

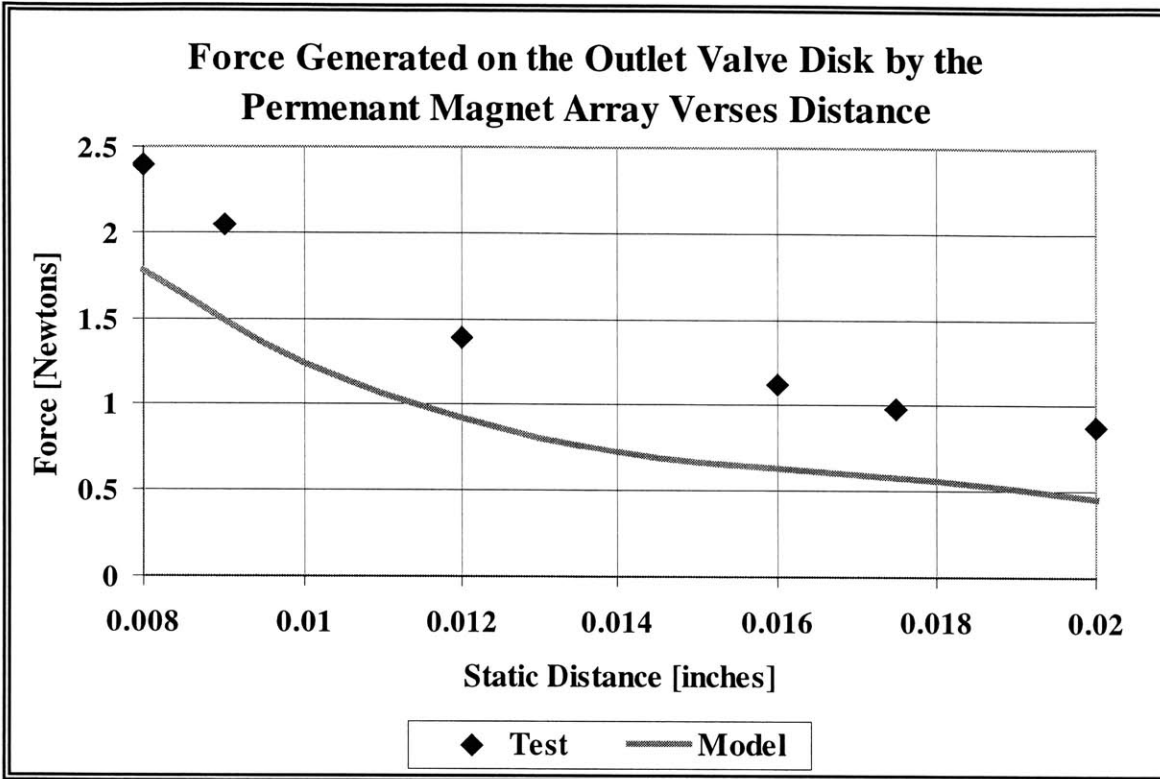


Figure 3.32 A comparison of the annular magnet model to actual data shows that this model slightly underestimates the magnitude of force generated on the valve disk

Clearly, this annular magnet model underestimates the force induced on the valve disk. In addition, the error increases from about 25 percent less than the proper value at 0.008 inches to over 50 percent less than the proper value at 0.020 inches. Thus, the force trend is not adequately captured. Regardless, the force values generated by the permanent magnets are an order of magnitude smaller than the force generated by the valve yoke. So long as some reasonable contribution from the permanent magnetic array is utilized in the finite element model, the errors associated with that model are essentially lost against the total force generated on the valve disk. Thus, this annular magnet model was incorporated into the final finite element geometry and used in conjunction with valve model to predict the actual forces on the valve disk during its traverse.

In the future, deeper explorations into the modeling process may benefit from revisiting this permanent magnet model and refining it to better predict the force induced on the valve disk by the permanent magnet array. When the force test experiment was conducted only the outlet valve disk was used and no data was ever taken for the inlet valve. This lack of data prevented a comparison of the annular magnet model to be made for the inlet valve case.

1) Machine Parts

Drawings for both valve disks, developed from the finite element model, were utilized to machine the valve disks out of Carpenter HP430 magnetic stainless steel. This material was selected as described in Section 3.1.1 for its magnetic properties and its ability to be easily machined.

2) Anneal Parts

To enhance the magnetic properties of the disks, they were annealed using the procedure recommended by Carpenter, the material manufacturer, for development of magnetic properties.

- a) Anneal at 1450 °F to 1550 °F for 2 hours
- b) Cool at 100 °F per hour to 800 °F, then cool freely to ambient

Carpenter recommends using a dry hydrogen or vacuum environment to reduce oxidation. Instead, a special stainless steel heat-treating envelope was utilized. This envelope is coated with a material that oxidizes preferentially to the part being heat-treated. The results of this process modification were found to be satisfactory.

The soak temperature in the magnetic annealing cycle (1450 °F to 1550 °F) is higher than the annealing cycle temperature recommended to soften the material (1250 °F to 1400 °F), and the temperature range is more tightly prescribed. Also, the softening cycle does not prescribe a controlled cooling rate. Thus, the material cannot be first annealed for magnetic enhancement and then machined. The heating process makes the steel gummy and difficult to cut on a lathe.

3) Grind and Lap the Disk

The completed valve disks were ground with 600-grit wet-dry sandpaper on both sides. Then a mirror-smooth finish was put on the sealing faces with a fine lapping compound.

4.2 STEPS IN VALVE MANUFACTURING PROCESS

In their final form, the valve yokes are short annular cylinders marked by several magnetic groove features over the active faces. Stranded power wires exist the base end of the valve yokes. These wires lead to internal copper wire coils of about 900 turns impregnated in epoxy. Applying current to the wires causes a strong magnetic field to develop in the coil and the surrounding stainless steel valve yoke.

The valve yokes are made out of two pieces, a spool and a cover, as shown in Figure 4.2. Once the copper wire is wound to create a coil on the spool, the two pieces are pressed together to make the final component. The total process utilized to create these yokes is described below.

5) Cover the Spool with Insulating Tape

There are also a number of imperfections on the radial coil-winding surface of the spool that can cause shorts in the wire. To provide a level of protection for the wire as it is wound, a layer of electrical tape is stuck to each of the three spool surfaces, radial, conical, and cylindrical, that skirt the valve coil. Three special metal dies were machined to precisely cut strips of tape to the proper dimensions to fully cover the three inner surfaces spool.

6) Mount the Assembly on the Winding Lathe

The prepared spool piece is placed into a lathe modified for electrical coil winding. The spool piece slides over a long winding mandrel, held in place on the lathe by a three-jaw chuck. The mandrel keeps the winding assembly a safe distance from the chuck, assuring the wire does not accidentally get caught. The spool is secured to the mandrel with a small metal disk threaded into the top of the mandrel.

The winding lathe is modified in a number of ways to engender coil winging. First, it is attached to a variable-speed motor, controlled via a foot pedal on the floor. This modification allows the user to precisely control the speed of the lathe as well as to stop and start it with both hands free. Second, a small wooden rest for winding tools has been fashioned to sit on the lathe's ways. Third, a spring-loaded wire spool is mounted to the base of the lathe along with a Teflon and metal wire guide to assure the wire does not get cut during the winding process. Third, an optical microscope capable of 100x resolution is mounted on the lathe to allow the user a detailed view of the spool and the winging process. Finally, a revolution counter is mounted on the chuck to keep track of how many turns of wire are placed on the spool.

7) Solder Stranded Wire Leads to Solid Wire

Stranded insulated wire is used for the coil leads because it is robust when bent and provides an additional level of protection for the wire. Originally, solid copper wire was used for both winding and the leads. However, solid leads were easily broken and proved totally unsatisfactory to endure the amount of abuse they would likely encounter when the device was in operation.

The first stranded wire lead is pushed through the inner wire lead hole. Once through the hole, this wire is stripped and soldered to the solid copper winding wire. A sleeve of Teflon tube is used to cover the solder joint to prevent shorts to ground.

The stranded wire is wound about three-quarters of a turn around the spool to assure it stays in place, and the lead end is pulled taut and taped to the winding mandrel so it does not get caught on the lathe or destroyed during the winding process.

4.0 VALVE MANUFACTURING PROCESS

Once the iterative finite element process described in Chapter 3 converged onto a final design, an intricate procedure was developed to evolve the design from CAD drawings to working parts.

This evolution was not a one-way process, however. There are substantial links between the final valve design and the manufacturing process. Several optimizations suggested by the finite element model had to be abandoned because it was found that the geometry in question could not be built. Thus, the computer model had to be revised and tested many times until convergence on a practical design meeting the system parameters was achieved.

All valve parts were hand-machined and fabricated by technicians at Advanced Mechanical Technology, Inc., and both AMTI and the Cryogenics Engineering Laboratory shared the manufacturing procedure. The process described herein evolved as obstacles and challenges were met in creating the final product. In most cases, solutions were found allowing the process to move forward. However, in several cases the procedure or valve design itself had to be altered to make the entire process feasible.

4.1 STEPS IN VALVE DISK MANUFACTURING PROCESS

In their ultimate form, the valve disks are thin, annular rings with a mirror finish on the sealing side and a ground finish on the magnetically active side facing the yoke. The valve disks are shown in Figure 4.1 juxtaposed against a key for scale. The process utilized to make these components is described below.

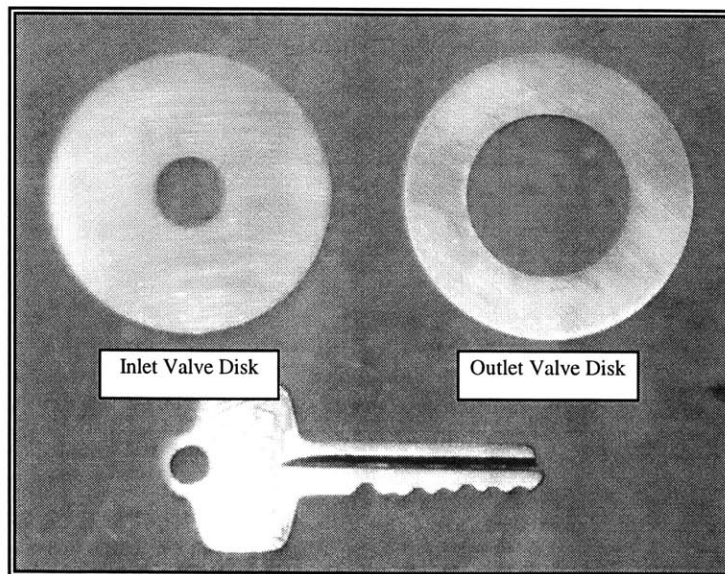


Figure 4.1: the cold end valve disks are thin, annular slices of metal roughly 2 inches in diameter

8) Wind the Copper Coil on the Spool Piece

The solid copper wire is wound onto the spool by hand. It was found that delicate control of the wire is possible given a small set of specialized tools. Early on, it was discovered that metal tools strip the insulation off the wire. Thus, a set of plastic tools was fashioned out of cable ties. The two most useful tool types are the wire guide tool and the pick tool. The wire guide tool has a smooth rounded tip, and the pick tool has a sharp, pointed end. Along with the optical microscope, these tools were used with a modest degree of success to control the wire as it is wound out onto the spool.

The wire is wound as regularly as possible for as long as possible to maximize the wire-packing factor and the amount of copper cross section in the coil. Special care must be taken when winding up the angle of the valve yoke fillet as well as when winding near the stranded wire. The initial two or three layers of solid wire can be laid down in a smooth, uniform pattern. However, small, geometry-induced imperfections in the packing quickly arise. Despite all efforts to maintain smooth layers, after about six layers of wire are applied, it becomes impossible to mitigate all the small errors and keep the wire layers smooth.

Once layer continuity breaks down, the lathe can be sped up and the coil scramble-wound. The general goal of this phase of winding is to keep the levels of winding as uniform as possible while burying the stranded wire under several layers of solid wire.

9) Adding Maverick Fixtures

In an attempt to get as much copper as possible wound around the spool, special brass fixtures were made to specially shape the coil windings to the yoke at the winding margin. Called, maverick fixtures, these brass pieces replace the simple flat disk holding the spool to the mandrel when the coil nears its final radial size.

There are two maverick fixtures added in the middle and later stages of winding. To place a maverick fixture on the spool, the winding lathe is stopped, and the wire held in place with electrical tape. The simple flat disk holding the spool is then replaced by maverick fixtures, which are mounted in place by the same screw that held the metal disk.

10) Tape the Coil in Place

The ultimate maximum diameter of the coil is determined visually by slipping annular sizing rings machined to the right inner diameter over the coil. The annular rings are designed to be five thousandths of an inch smaller in diameter than the valve yoke cover piece to assure the cover slides over the valve coil without compromising it.

Once the valve coil maximum diameter is achieved, the second piece of stranded wire is soldered to the solid copper wire. As before, the joint is protected with a Teflon sleeve. The stranded wire is threaded out of the second wire lead hole and secured to the winding mandrel with tape.

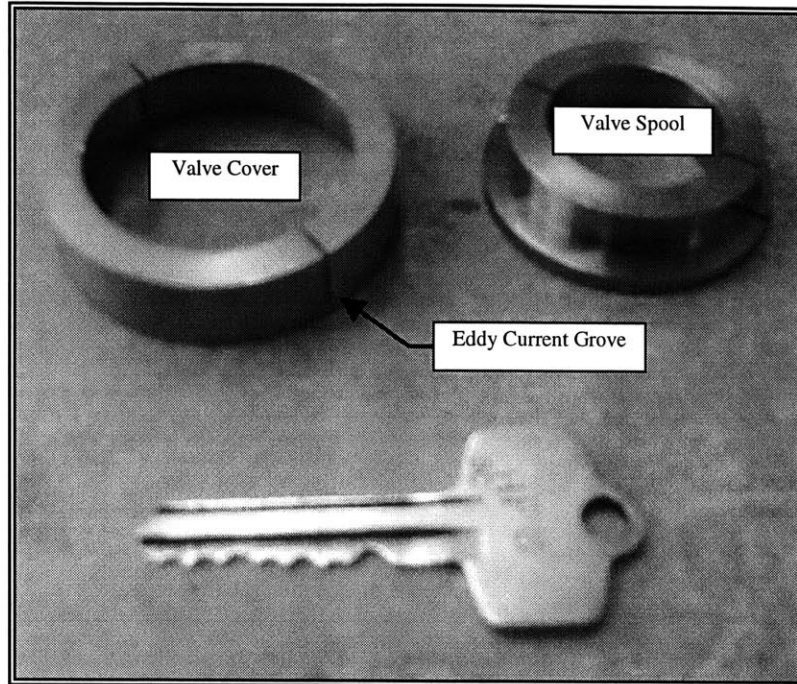


Figure 4.2: the valve bodies consist of two parts that are press fit together to create a magnetic yoke

1) Machine Parts

Drawings for each of the components, developed from the finite element model, were used to machine the cover and spool parts out of Carpenter's HP430 magnetic stainless steel. A few thousandths-of-an-inch were left on all active faces in anticipation of later grinding and lapping. The preservation of this extra material is not reflected in the drawings provided in this thesis.

2) Anneal Parts

To enhance the magnetic properties of the yokes, they were annealed using the procedure recommended by Carpenter for development of magnetic properties described above for valve disks.

Note again that the material cannot be first annealed and then machined. The heating process makes the steel gummy and difficult to cut on a lathe.

3) Machine Active Faces

The spool and cover pieces were press fit together and clamped to assure proper seating and alignment. The additional material left on the active face was machined away until the parts reached the height specification in the component drawing.

This step assures that the faces of the magnetic circuit are flush so the entire active area of the valve yoke face acts equally on the valve disk. The flush faces also assure that the magnetic pull of the valve yokes on the valve disks are equally maximized.

4) Epoxy Spool Eddy Current Groves

Each valve yoke piece includes a pair of eddy current grooves that run vertically into the part, dividing it in two. This feature is highlighted on the valve cover in Figure 4.2. The purpose of these grooves is to retard the flow of residual electrical flux in the circumferential direction about the valve yoke. Slicing this conduction path cuts the propagation of transient eddy currents through the valve yoke and reduces losses in the valves.

It was found in early iterations that the wire would crimp into the spool's eddy current grooves during the winding process, as demonstrated by Figure 4.3. Due to the geometry of the grooves, it was difficult to assure that all burrs were removed and the groove corners were not sharp. Hence, these crimping locations almost always caused the wire insulation to be compromised, exposing the copper underneath directly to contact with the spool. At these spots, the wire shorted to ground.

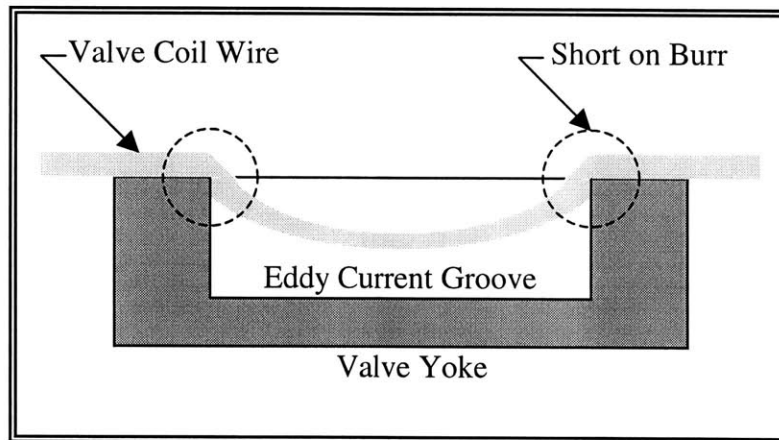


Figure 4.3: Edges of eddy current grooves have burrs that tend to foul the wire insulation, shorting the coil

Epoxy was used to solve this problem. A bowl to hold epoxy was built into the grooves by covering the axial slots of the eddy current groove with Teflon tape secured by electrical tape. The wire lead holes were also plugged with Teflon tape. With the tape in place, the eddy current groove acted like an epoxy reservoir, and uncured epoxy was dribbled in through the radial groove opening along the active face. The epoxy-filled grooves were allowed to cure, and then the tape was removed.

The cured epoxy prevents wire crimping by making a continuous solid surface for the wire to wind over. In addition, the cured epoxy adds significant structural robustness to the spool and prevents it from deforming or folding when pressed into the valve yoke cover.

To keep the valve coil from unwinding once the maverick fixtures are removed, pieces of electrical tape are stuck around the circumference of the valve coil. With the tape in place, the maverick fixtures are removed as delicately as possible.

11) Press the Cover over the Spool

The valve yoke cover piece is slipped over the valve coil onto the spool and pressed into place. A step in the cover piece assures accurate axial alignment of the two parts. If the fit is very tight, an aluminum ring can be fitted over the cover piece to assure it does not bend, deform, or spray outwards as it is press fit.

With the cover on, the valve yoke can be safely removed from the winding lathe and handled without and danger of unwinding.

12) The Major Valve Yoke Potting Process

To prepare the assembled valve solenoid for final potting, bee's wax is stuffed into the wire lead holes around the stranded wire to assure no epoxy leaks out of the holes. The eddy current groves in the valve yoke cover piece are covered in Teflon tape secured with electrical tape. The valve yoke thus becomes an annular bucket prepared to hold the liquid epoxy in place as it cures over the coil.

The potting process includes its own series of individual steps, which are outlined in Section 4.4 of this chapter. Once this process is complete, the resulting epoxy-impregnated assembly is heated slightly to remove the bee's wax from the wire lead holes.

13) Grind and Lap the Assembled and Potted Yoke and Coil

To assure proper axial alignment of active faces of the assembled pieces, the competed yoke is ground with 600-grit wet-dry sandpaper until the surfaces of both parts begin to wear. A smooth finish can be put on the active faces with a lapping compound.

4.3 FABRICATION RESULTS

Using the valve yoke design presented herein and 34-gauge copper wire wound as described above, Table 4.1 shows the typical results for wound coils.

Table 4.1: Characteristic Valve Winding Statistics

	Coil Turns	Legnth of Coil	Coil Resitance	Coil Inductance
	[turns]	[meters]	[ohms at 20 °C]	[Henries]
Inlet Valve Coil	899	85	82.5	0.273
Outlet Valve Coil	908	100	97.1	0.334

4.3.1 Electrical Testing

In many of the initial winding runs, a complete method for protecting the copper wire had not evolved. Thus, it was typical to complete a winding job and find that the valve coil had shorted electrically to the valve yoke. A method to approximate where on the valve coil this short occurred allowed problem spots to be identified and dealt with. Many of the wire-protection processes outlined above were put in place because of problem spots identified via this method.

Most often, wire shorts occur in only one location on a valve coil. Thus, it is possible to measure the resistance of the valve coil by attaching an ohmmeter across the leads (resistance A-B). Secondary resistances can be measured from each wire lead to the valve yoke (resistances A-C and B-C). These measured resistances can be combined in a series of linear equations to determine the actual resistance of each leg in the model circuit shown in Figure 4.4.

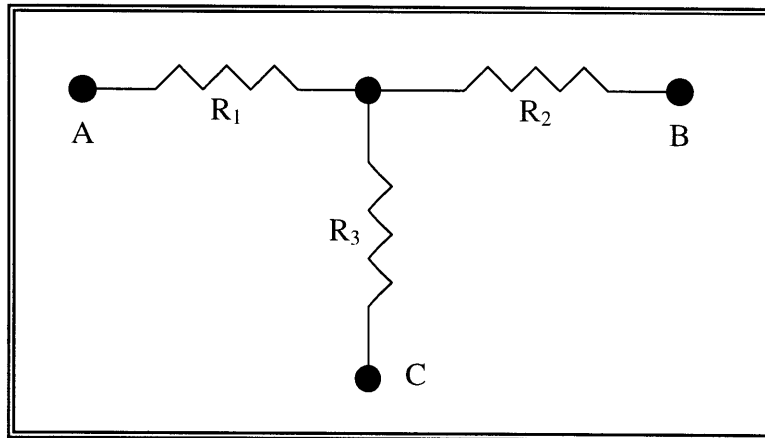


Figure 4.4: A valve coil with one short to the yoke can be modeled as three electrical resistances

The three appropriate linear equations are as follows:

$$A-B = R1 + R2 \quad \text{(Equation 4.1.1)}$$

$$A-C = R1 + R3 \quad \text{(Equation 4.1.2)}$$

$$B-C = R2 + R3 \quad \text{(Equation 4.1.3)}$$

If a set of real number resistances, R1, R2, and R3 can be found to solve the set of linear equations, it is known that a valve coil short to the valve yoke occurred in only one location. Using the resistivity of 34-gauge copper wire, the exact distance along the length of the wire could be ascertained. Finally, using the number of turns placed on the coil during winding, the exact turn on which the short occurred could be identified.

This analysis led to the conclusion that the wire was most often shorting on the initial 30 turns in the vicinity of the eddy current groove. Thus, potting the groove before winding became a standard practice along with taping the spool to provide an extra degree of protection.

It was found that valve coils with only one short to the valve yoke could be used for static testing purposes, provided no electrical path between the leads and the valve yoke was created to complete the shot circuit. Despite their value for tests, these faulty valve yokes cannot be used in the real machine because all the metallic components, including the valve yokes, will be electrically grounded to prevent valve control and data monitoring complications. These ground paths would short-circuit the faulty valve yokes and prevent them from working properly.

4.4 THE EPOXY POTTING PROCESS

The valve coil potting process is important to the valves for two primary reasons. First, the epoxy provides an additional measure of structural robustness and protection for the valve coil. Second, the epoxy fill reduces the dead volume of the expander space in the cold end, reducing entropy generation.

In order to pot the valve coil effectively, an epoxy and hardening agent combination with the proper material qualities must be utilized. The following properties are favorable:

- 1) The un-cured mixture must have very low viscosity to assure it wicks into the valve coil
- 2) The epoxy must cure at room temperature
- 3) The material must display no electrical conductivity, nor any magnetic properties
- 4) The cured epoxy must demonstrate sealing capability against fluid at 10 Kelvin
- 5) The material must be entirely non-reactive once it is cured
- 6) The cured epoxy should have temperature expansion characteristics similar to metal

The epoxy of choice is STYCAST® 1266 distributed by GRACE Specialty Polymers. It exhibits all of the favorable properties described above and is commercially available.

4.4.1 The Importance of Vacuum

When epoxy is mixed by hand in open air under a fume hood, a substantial number of air bubbles are formed in the mixture. If allowed to remain, these bubbles would severely detract from the favorable properties of the epoxy. Thus, steps must be taken to remove as much air from the material as possible.

1) Set up Valve Assembly on Dipping Rod

The valve assembly is placed on the rod mounting cradle. The lead wires are pulled taut from underneath the valve yoke and wrapped around the rod. They are secured to the rod with electrical tape. It must be assured that the dynamic o-ring inside the sliding-seal valve is well greased. The rod is slid through the sliding-sealing valve until the valve yoke wires touch the top of the desiccator. This placement assures the valve yoke will not prematurely dip into the epoxy.

The large o-ring creating the seal between the two desiccator hemispheres must also be well-greased and sitting in its groove in the bottom half of the apparatus.

2) Mix Epoxy

The two components, the epoxy and the curing agent, are each measured by weight on a simple balancing scale to obtain proper proportions. Enough epoxy must be used to assure the valve is completely submerged in the bath when dipped. It was found that between 50 and 75 grams of epoxy component A are adequate, if a standard plastic glass is used to hold the epoxy. The two components are mixed together in a small disposable plastic dish under a fume hood. A metal mixing implement is used. Once the components are well mixed the resulting substance is a clear liquid filled with air bubbles with a viscosity just noticeably higher than water.

When moving the epoxy out of the fume hood, it must be assured that the hood remains running to create a high air change in the room and minimizing exposure to epoxy fumes.

From the moment of mixing, curing of the epoxy begins in about 40 minutes at room temperature. Thus, the remaining processes must be completed briskly.

3) Place Epoxy in the Vacuum Chamber

The mixed epoxy is transferred from the mixing dish to a tall plastic cup and placed on the floor of the vacuum vessel. The lip of the plastic cup must be substantially higher than the surface of the epoxy because the material tends to boil up over the sides of a shallow glass.

4) Seal the System

The top of the desiccator assembly is placed over the bottom half, and it must be assured that the valve yoke does not prematurely dip into the epoxy bath. The desiccator hemispherical top should be twisted to assure the o-ring seals properly. The sliding-seal valve is closed tightly, and the vacuum tube line is connected to desiccator valve. The electronic pressure gauge is plugged in and checked to confirm a reading of 1 atmosphere.

5) Pump Epoxy Down in Vacuum

The vacuum pump is turned on, and the associated pressure drop is monitored. The epoxy will froth and boil violently at first, and it may attempt to spill over the sides of the plastic cup. If spilling is imminent, the vacuum pump may be turned off, but the vacuum should not be released. The air boiling out of the epoxy will increase the chamber pressure and rapidly subdue the boiling. Once the fluid has settled, vacuum pumping can begin again.

Once a substantial amount of air has been removed from the substance, it will boil gently without danger of spilling. Once this state is achieved, the steady-state pressure measured inside the vacuum chamber should be about 60 torr. From this steady state, the pumping process should be timed. It was found that the desirable duration is about 15 minutes.

The goal of this pumping process is to remove the air bubbles from the epoxy, but there is also a danger that the volatiles will be removed from the epoxy mixture. This situation is undesirable because the epoxy fails to cure correctly if too many volatiles are sucked away. Thus, it is important to not exceed a 15-minute initial pumping time.

6) Dip Valve in Epoxy Bath

Once the bath is de-aired, it is ready for valve dipping. With the vacuum pump still running, the torque on the sliding-seal valve is relieved. There should be a corresponding increase in pressure inside the vacuum chamber to about 100 torr.

The rod is eased downwards, immersing the valve assembly fully into the epoxy bath. The openings at the top of the valve should be completely covered by the bath or impregnation will not occur.

The sliding-seal valve is retightened on the rod, and the pumping on the vacuum chamber continues.

7) Allow Epoxy to Impregnate Valve

Once the valve yoke is immersed in the epoxy bath, another timing of the pumping process begins. The valve should remain under the epoxy for 15 minutes at a background pressure between 60 and 100 torr. Small air bubbles can be observed migrating away from the valve coil.

After 15 minutes has elapsed, the vacuum pump is turned off. The desiccator valve is slowly opened to let atmospheric pressure back in. The surface of the epoxy should be closely watched to assure the rush of air does not disturb it. Most of the filling of the coil occurs when atmospheric pressure is applied to the bath. Air pressure acting on the epoxy surface forces the liquid into all the evacuated pockets. Any small amount of gas left in the pockets dissolves into the liquid epoxy.

The method utilized for this manufacturing process was to subject the mixed epoxy to a low vacuum to boil the air bubbles out before the mixture cured. A special vacuum chamber was designed and built for this purpose. As shown in Figure 4.5, this chamber is made out of a modified chemical desiccator with a specially designed sealing-sliding valve on the top. Using a clear desiccator is desirable because it allows visual access to the de-airing process. Vacuum is generated using a standard vacuum pump whose hose can be seen trailing on the left side of Figure 4.5. The pump is set continuously running while vacuum was desired. A small electrical gauge placed in the vacuum line measures the pressure. When properly sealed with vacuum grease, the chamber proves capable of holding a vacuum as low as 60 torr (0.08 atmospheres) for extended periods of time.

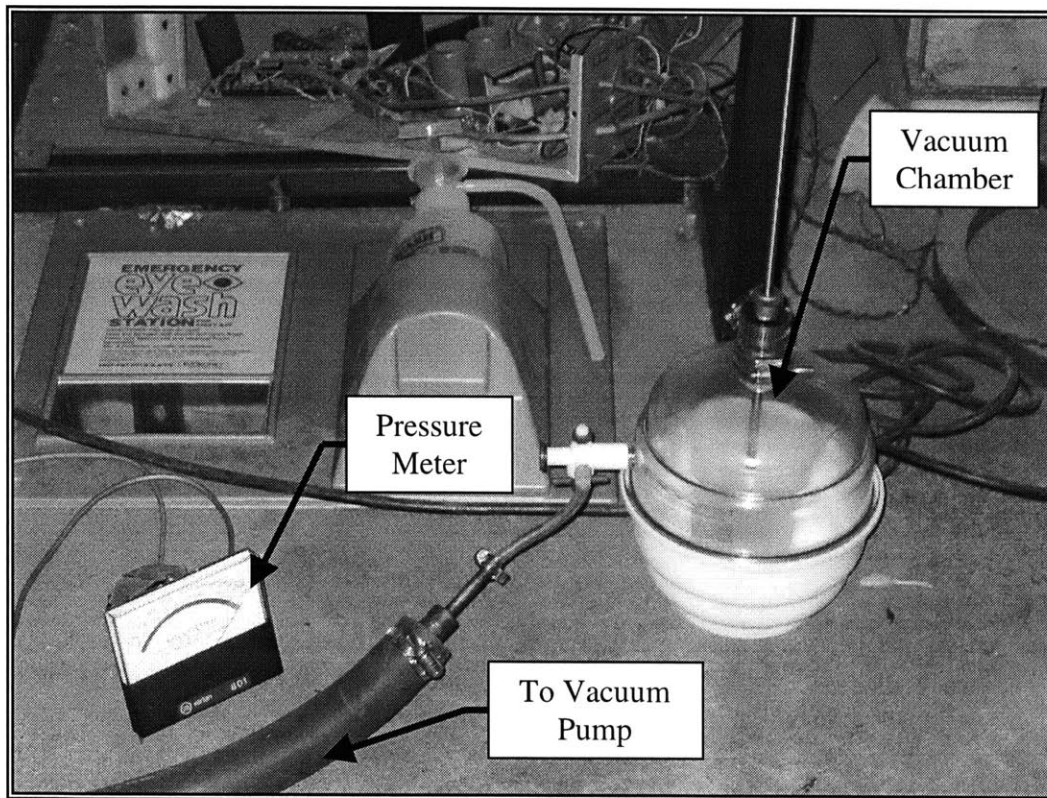


Figure 4.5: A chemical desiccator was modified to create a vacuum chamber for epoxy impregnation of the valve coil

The mixed epoxy is placed in a deep plastic cup inside the vacuum chamber. The use of both glass and plastic dishes were explored to determine which is best for this process. The disadvantage of plastic is that the epoxy cures exothermically and ultimately melts the container. However, the advantage of plastic is its disposability. Provided steps are taken to keep the plastic cool throughout the epoxy curing process, the excess epoxy and the plastic cup can be thrown away.

The advantage of glass is that it does not melt at the epoxy's exothermic curing temperature. Regardless, the disadvantage of glass is that it is not disposable: epoxy cannot be allowed to cure in a glass container or the entire container must be thrown out. Disposing of epoxy in an environmentally benign manner before it is cured is difficult without a container to store it in.

In addition, the shape of available plastic cups is more conducive to the dipping process. Their diameter tapers from large at the mouth to small at the bottom while typical glass containers have the same diameter along their entire height. The taper allows the plastic cup to hold the same volume of epoxy in a deeper bath than glass. In addition, the plastic taper provides better containment for bubbling epoxy in the initial stages of pump-down if it boils over. Thus, plastic was ultimately selected as the container of choice.

The valve assembly is placed in the vacuum chamber mounted on the end of a long rod as shown in Figure 5.6. The rod is actuated vertically from outside through the sealing-sliding valve. The valve's wires are wrapped around the rod to keep them out of the way throughout the dipping process. The system is designed to allow the epoxy to de-air as well as dip the valve into the epoxy without breaking the vacuum seal.

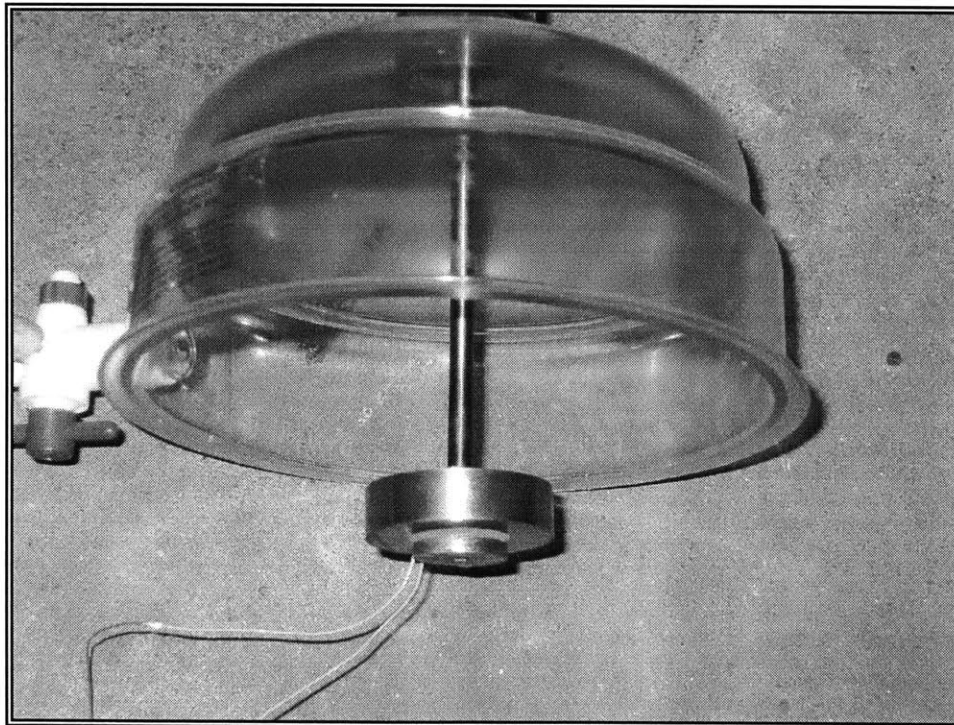


Figure 5.6: The valve assembly is mounted on a long metal rod inside the desiccator vacuum chamber in preparation for epoxy impregnation

The valve yoke is placed inside the vacuum chamber while the epoxy de-airs under vacuum. The valve yoke is then dipped into the epoxy and impregnated. This continuity of processes assures that no air is trapped in the coil or allowed to creep back into the epoxy between de-airing and valve impregnation. It also assures that most of the air is removed from the valve coil, making the epoxy impregnation process much more rapid.

The dipping rod slides through a standard sliding-sealing valve from Nupro®. This valve is bootstrapped onto the desiccator's top using a plug of steel fitted into a Tygon tube and held in place with hose clamps. A hole machined in the desiccator top allows the rod to pass. This assembly is shown in detail in Figure 5.7. A dynamic sliding o-ring allows the rod to move while holding vacuum within the desiccator chamber.

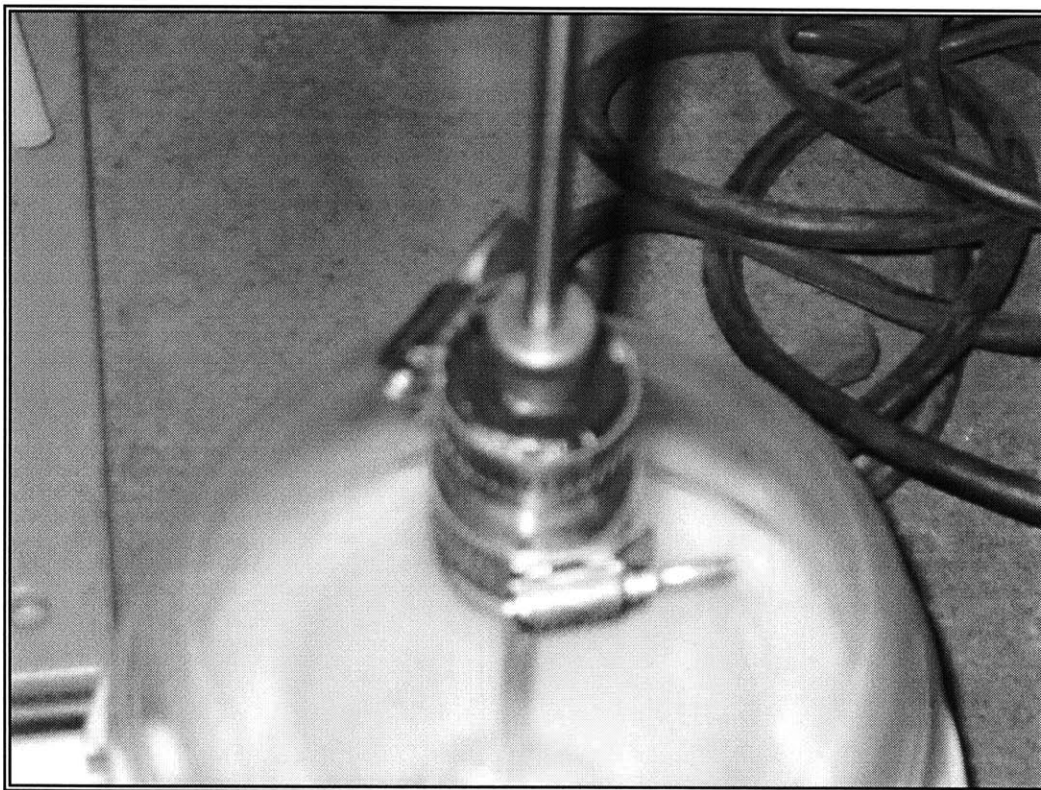


Figure 5.7: The sliding-seal valve allows the desiccator chamber to hold a high vacuum while the valve assembly is submerged into an epoxy bath

It was observed that the system holds vacuum down to about 100 torr (0.132 atmospheres) when the rod is sliding and about 60 torr (0.079 atmospheres) when the rod is static.

4.4.2 The Epoxy Dipping Process

The dipping process that utilizes the apparatus described above to fill all voids within a fully assembled valve yoke and valve coil with epoxy.

8) Remove Valve Yoke from Epoxy Bath

The upper half of the desiccator is removed by sliding it all the way off of the sliding seal valve. The electrical tape that holds the valve yoke wires in place is removed from the rod. Using the rod to keep the valve yoke upright, the cup with the epoxy bath and valve yoke is lifted out of the desiccator, and the assembly is transported to the curing location.

The valve assembly is lifted off of the sting, assuring that the top of the part stays level and no epoxy drains out. It was found that latex-gloved fingers work best for this process because epoxy is slippery and any tool that could apply enough clamping force to overcome the slippery surface with friction might deform the valve yoke.

The valve assembly is rested atop a clean, dry, non-epoxy-bonding surface, providing an outlet for the wires. It was found that two overturned plastic epoxy mixing dishes provide an adequate base of the valve yoke. Caution should be taken to assure paper towels are laid out beneath the base because epoxy tends to drip off the valve yoke and ruin the surface below.

A paper towel is used to remove the droplets of epoxy remaining on the insulation of the stranded wire. In addition, excess epoxy is removed from the open face of the valve assembly by scarping it off with the metal mixing instrument.

9) Let Epoxy Cure

The epoxy will shortly begin to cure, and it becomes warm, viscous and gummy. It was found that epoxy tends to leak out of the eddy current groves regardless of how well they are filled with wax. Thus, epoxy from the bath excess is spooned into the top of the valve yoke to replace the material that leaks out. After about 30 minutes of spooning, the epoxy becomes thick enough that it not longer leaks out of the valve yoke.

The valve assembly is left for eight hours, allowing the epoxy to cure to its final hardness.

The plastic cup containing the excess epoxy is placed in a plastic epoxy mixing dish and allowed to melt. After curing, the waste epoxy was disposed of in the garbage.

4.4.3 Evaluating Success of Epoxy Potting Results

It was found that the valve yoke potting process outlined above meets the goals laid out for the potting process. Figure 4.8 shows a potted spool with the cover forced off to examine the effectiveness of the process. A house key skirts the spool to provide a sense of scale.

A different mounting block must be specially machined for each valve tested. Mounting blocks must be built to assure the yoke assembly rests snugly and the valve disk has as little radial clearance as possible without touching the mount walls. This small clearance allows the valve disk to be placed concentrically with the valve yoke. Radial offset must be minimized because it creates an asymmetrical magnetic field, increasing the torques applied to the disk and causing it to prematurely drop. It is important, however, to assure that no contact exists between the disk and the mount wall because static contact friction would also skew the force measurements.

In the real machine's cold end, the distance the valve disk must travel from the fully closed position to the fully open position, is 0.010 inches. This travel is called the valve lift. If parts in the machine are not aligned properly, the lift can be as high as 0.012 inches. Thus, force measurements for various separation distances between the disk and the valve yoke face ranging from zero inches to 0.012 inches were taken. Values smaller than 0.010 inches are important because the disk traverses through these values every time it opens. Hence, an idea of the force induced on the disk when it is in the middle of its stroke can be ascertained.

Placing a thin, annular brass shim between the valve disk and the valve yoke while performing the static tests creates the desired separation distances. Shims of various thicknesses were built to encompass the possible range of motion encountered by the valve disk. Shims are built with an outer radius less than that of the valve disk and an inner radius greater than the hole in the valve disk. This design assures that the shims do not interfere with any of the other test rig parts while maintaining the correct separation distance between the valve yoke and the disk.

Brass is a sub-optimal material to use for these test shims because although it is nonmagnetic, it is a good conductor and can carry transient electrical currents that may disrupt the lifting magnetic field. Non-conducting materials including paper and Teflon were also tried as shims. Paper proved too spongy to provide a reliable separation distance under compression, and it was also difficult to measure the width accurately. Teflon proved impossible to machine into the thin annular shape necessary for the shim. Thus, brass was utilized because it proved the best material readily available, despite the small transient magnetic fields it created.

5.1.2 Static Test Rig Electrical Description

The electrical components of the test rig include a power supply to drive current through the valve coil and two meters measuring the potential across the coil and the current through it. Valve coil current was measured via a shunt placed in the circuit and wired to a voltmeter. The shunt also supplies an additional protective resistance to assure the coil could not easily burn out if overpowered. The wiring diagram for the electrical system is provided in Figure 5.3.

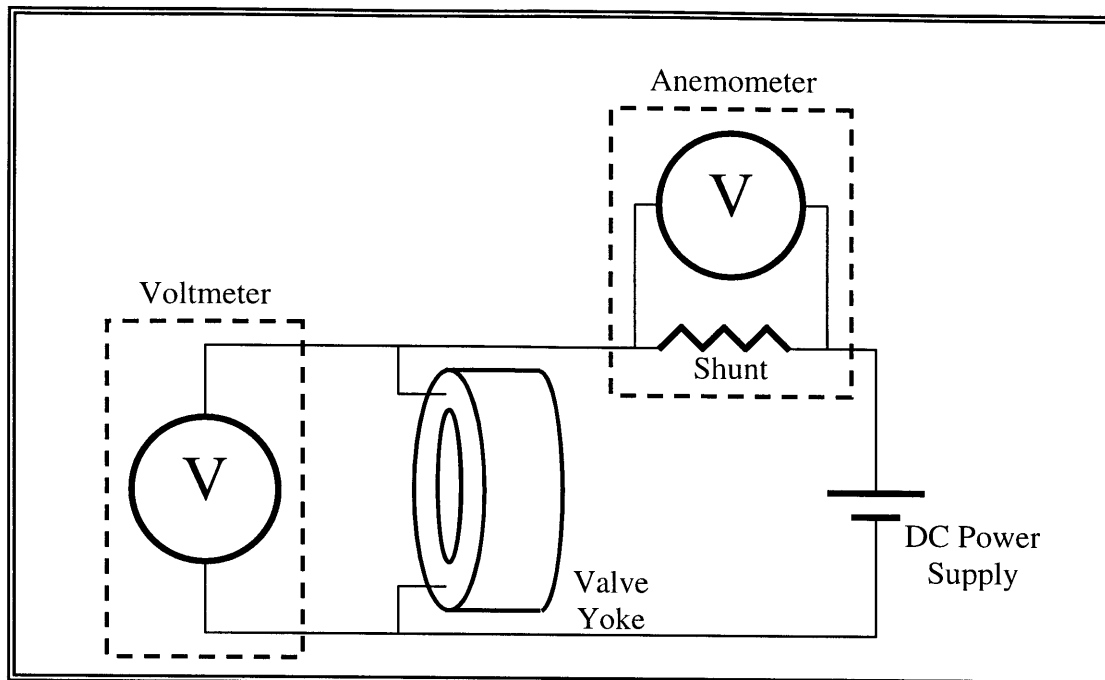


Figure 5.3: The wiring associated with the static force test rig allows the electrical properties of the valve coil to be measured while it is exercised through tests

The rig is configured to allow the experimenter to finely vary the input current using a control on the power supply. The supply provides variable levels of voltage to meet the power demand of the coil at any given current setting.

5.1.3 Force Measurement Experimental Procedure

Once the test rig has been set up to accommodate a particular valve, force measurements can be taken for various current inputs to generate data points determining valve performance. The experimental procedure used to generate this data is as follows.

1) Set up the Test Weights

Place a pre-measured set of weights in the basket tied to the valve disk. The total weight held aloft against gravity represents the force the valve yoke imparts to the disk. This force is the opening force of the valve if the shim is selected as 0.010 inches. Each weight added to the basket represents a new data point on the current-force curve.

2) Place the Appropriate Shim into the Rig

A variety of brass shims ranging from 0.004 inches to 0.012 inches can be placed between the valve yoke and the valve disk. These shims recreate the air gap distance that the valve yoke's magnetic field must cross through to impart force upon the valve disk. Theory dictates that magnetic force varies inversely as the square of the distance across the air gap. Thus, the measured force is highly sensitive to small changes in the shim width.

There are several important features of this image that indicate a good coil potting. 1) The cured epoxy has taken on the shape of the air space indicating reduced dead volume. 2) There are very few bubbles embedded in the epoxy signifying that most of the air was successfully removed by the vacuum process. 3) The epoxy completely embeds the coil, assuring it remains physically and electrically protected. 4) The epoxy fills the space to the top, assuring that all the material that may have leaked out was replaced before the epoxy cured.

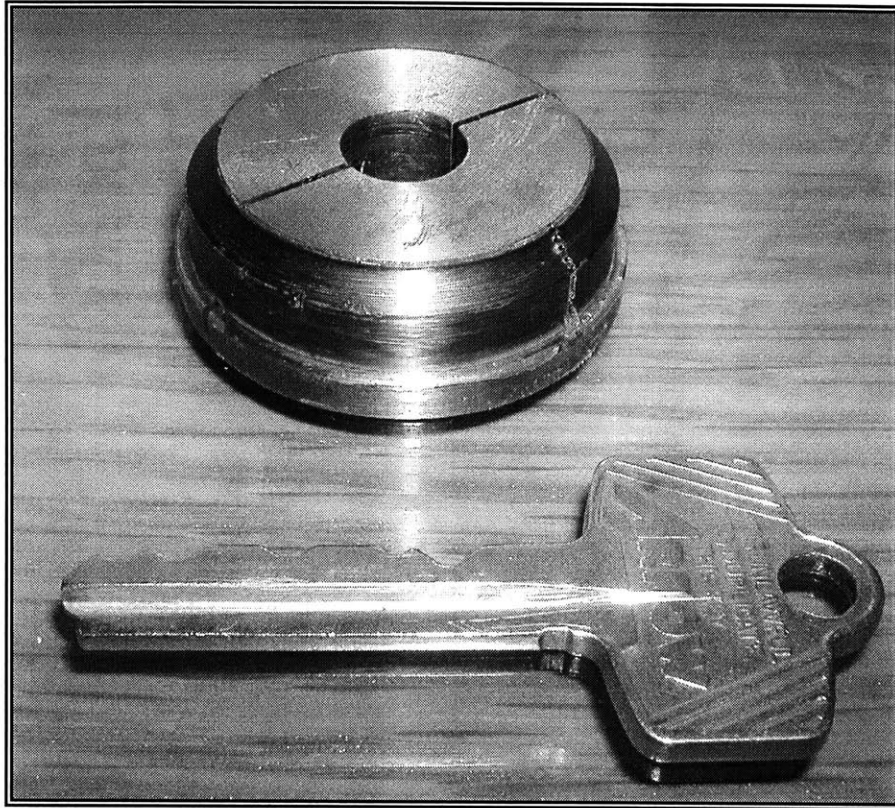


Figure 4.8: The inside of a potted spool demonstrates the successful epoxy coil impregnation and potting process

Since this method of determining the success of the epoxy potting process is destructive, it cannot be used to test the effectiveness of each run. However, it can be used to empirically demonstrate that the process developed to pot the valve coils returns the desired results.

5.0 STATIC MODELING AND STATIC BENCHMARKING

Once the electromechanical valves were completed, they were statically tested both mechanically and electrically. These tests allowed a comparison to the finite element computer model detailed in Chapter 3. The main objective of these tests was to demonstrate that the magnetic valve core could develop the force required to open the valves against the maximum pressure differences encountered in the cold end. Additional finite element modeling was conducted to identify the sensitivity of the valves to geometric and material tolerances. This work suggests future improvements and augmentations that might increase performance further. In addition, the rate of the valves' response to input signals was measured electrically to assure they would function with the speed required to execute the cycle.

5.1 STATIC FORCE MEASUREMENTS

A test apparatus was developed to take static measurements of the valve opening force for various current inputs. This test rig is shown in Figure 5.1 and consisted of both mechanical and electrical components.

The data resulting from the static force tests described below is presented herein in Appendix B.

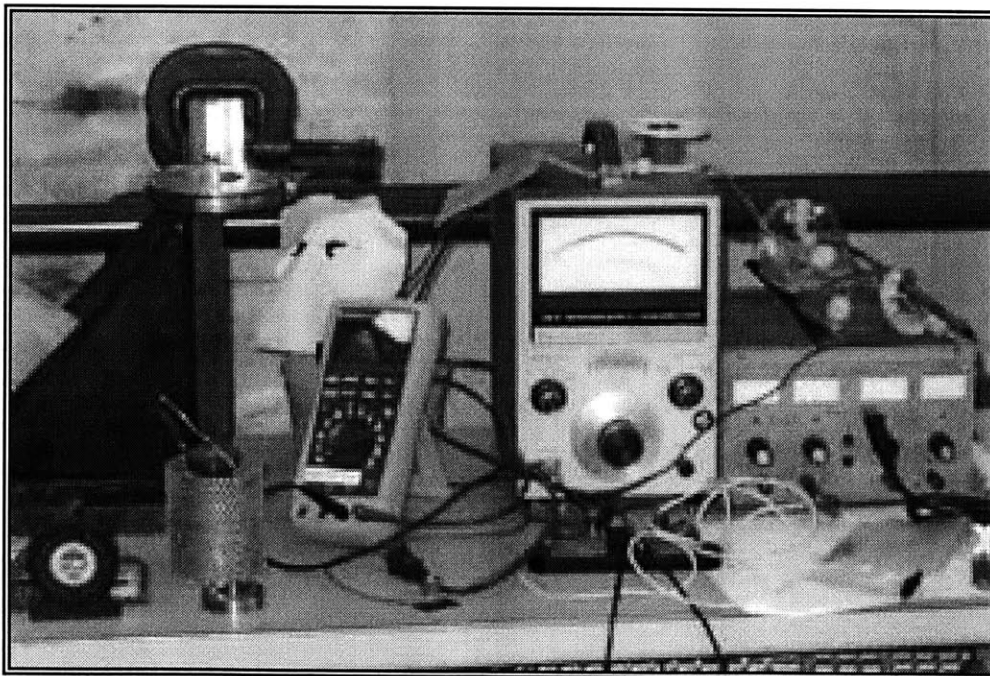


Figure 5.1: The static force measurement rig was used to develop real force-current curves for the cold end valves

5.1.1 Static Test Rig Mechanical Description

Mechanically, the rig included a large mounting stand with a ridged cantilevered mounting block. The rig was capable of holding over 1500 grams without any perceptible bending in the cantilever. The valve assembly was rested in the mounting block for testing. The block was made completely from non-magnetic material so as not to interrupt the valve's magnetic field.

The rig was designed to assure that the valve could be mounted entirely level with respect to Earth's gravitational field because torques imposed on the valve disk due to mis-leveling during static tests would severely skew the results. In addition, the rig held the valve assembly far enough off the ground to assure the weight basket utilized to test performance was totally suspended from the valve disk with no other contact.

Variable force is imposed on the disk by suspending from its center a weighted basket, as shown in Figure 5.2. Adding progressively heavier weights to the basket increases force. The basket is tied to the disk via 28-gauge copper wire that is threaded through a brass plug in the disk and tied in a simple knot. The plug fits into the hole at the center of the valve disk and is prevented from falling through by a thin lip machined into the plug.



Figure 5.2: A brass plug is used as an anchor for the weight basket below as the valve disk is inserted into the aluminum mounting block

Shims should be placed atop the valve disk concentrically with the hole in the disk to maintain as much axial symmetry as possible. They cannot overlap or interfere with the brass plug holding the weights to the disk, as this interference would create an oversized or axially asymmetrical gap.

3) Find The Sticking Current

Originally, only the current at which the disk dropped under the force of gravity was taken as a data point. However, substantial hysteresis was found between this drop current and the sticking current where the sticking current is defined as the minimum current required for the disk/shim/weight combination to be placed against the yoke and stick. Ultimately both sticking and drop currents were recoded as data points and averaged to approximate the actual opening force imparted to the disk.

Setting the current to a low value and pressing the disk/shim/weight combination against the yoke allows the experimenter to find the sticking current. If the valve disk does not stick at the set current, the current can be slightly increased and the process iterated until the valve disk sticks. Once the sticking current is located, the current and voltage running through the valve coil are measured as a data point.

It is observed that both the drop and sticking voltage are repeatable. It is also found that if the experimenter pulls the disk assembly away before the dropping current is achieved, it will not stick again until the current is increased to the sticking current. This combination of experimental observations requires the superposition of at least two of four hysteresis sources outlined below in Section 5.1.4. However, it is not clear to what extent each of the factors contributes to the hysteresis.

4) Reduce the Current to Find the Drop Current

The valve disk assembly will hang indefinitely at the sticking current. However, the current can be slowly lowered through a region where the disk will stay affixed if already stuck, but will not reattach if pulled loose. At the fringe of this region is the drop current, the value of amp-turns at which the disk assembly finally drops under the force of gravity.

Once the valve drops under the force of gravity, the current and voltage running through the coil are measured as a data point.

5) Average the Sticking Current and Drop Current to Generate a Data Point

The process described above should be repeated for all shim widths and disk weights of interest to generate pairs of raw data points, sticking current and dropping current, for each combination of inputs. The two points represent a range of valve coil input currents required to achieve a given valve opening force. For simplicity of analysis, the average of these two currents is utilized to estimate the actual performance of the valves.

5.2 DEVELOPING AN ADVANCED FINITE MODEL

The idealized finite element model used to develop the valve geometry as described in Chapter 3 does not provide an adequate representation for the performance of the valves as built and can not reproduce the measured results of the force test described above. There are a number of physical aspects of the real valve that were not properly represented in the idealized model. Thus, an effort was made to identify these features, determine their magnetic characteristics, and incorporate them into a more sophisticated finite element model to test against the actual valve.

Quickfield, a finite element software code by Tera Analysis, was utilized to create a realistic static model of the valves. This code was also used during the valve geometry development phase described in Chapter 3. Throughout the development phase, the finite element code was used because no analytical model of the valve's magnetic characteristics could be developed to accurately describe flux leakage. Once the primary geometry was developed and built, Quickfield was again utilized to identify physical characteristics that detracted from the valve's performance to demonstrate whether the valve performance could be accurately modeled via finite element.

Three primary physical characteristics were explored for additional advanced modeling: 1) metal-to-metal interface, 2) axial alignment tolerance, and 3) tolerance in shim gap. Models for each of these characteristics were developed and added to the original, ideal finite element model to return more accurate results. In addition to these physical characteristics, the sensitivity of the valve to magnetic materials properties was explored.

5.2.1 Tolerance in Magnetic Properties of Material

A magnetic field density verses field intensity plot, or B-H curve, is developed and described in Chapter 3 to represent the magnetic properties of the valve yoke. This curve is utilized in the ideal finite element model and is based on manufacture's specifications for the material, FR430, when heat-treated for magnetic properties.

The real material used to build the valve may contain significant property departures from the idealized model. Owing to heat treating, machining, and magnetic hysteresis not included in a model with a single-valued B-H curve function, the magnetic properties of the material may not be homogeneous throughout the material, they may be anisotropic, and the material may simply not have the same saturation limit as modeled.

Thus, a sensitivity analysis was conducted to ascertain what effect altered saturation would have on the performance of the valves. The B-H curve used in the ideal model was scaled as shown in Figure 5.5. Scaling was conducted equally on both axes to preserve the shape of the curve and the permeability at low B while modifying the saturation limits. The parameter h represents the percentage of scaling with $h=100\%$ being the original curve. The result is a series of seven similar curves with h values ranging from 50% to 150% spaced across an envelope of possible values.

Magnetic force on the valve disk is theoretically inversely proportional to the square of the distance between the disk and the active valve yoke surface. Thus this 5 percent tolerance in the measurement of distance results in theoretical 20 percent error in the force measurement. The effect on valve performance for shim tolerances of ± 0.0005 inches is graphed in Figure 5.10.

Although this type of uncertainty is similar in magnitude to other geometric tolerances encountered using the force test rig, the lift may vary by much more than ± 0.0005 inches when the real machine is actually assembled. The exact size of all the parts as well as the deformation of the seals sets the valve lift. Once the machine is assembled, it is impossible to accurately measure whether the proper lift has been achieved. Thus, it is expected that lift tolerance will be the primary factor to valve performance when the machine is assembled.

5.2.5 Sensitivity of the Model to Geometric Tolerances

The valves were originally designed to open against the full pressure differential of the cycle acting on eight 0.045-inch diameter ports. However, after the valves were completed, the bulkhead design changed to include only three 0.045-inch diameter ports. Thus, the valves must now open against only about 5 newtons instead of 13 newtons. This opening force is achieved for all of the modeled cases between about 55 amp-turns and 60 amp-turns of driving current.

Table 5.1 explores the relative sensitivity of the model performance to each of the geometric tolerance parameters studied in the vicinity of the maximum opening current, about 57 amp-turns. Relative sensitivity is gauged by the change in force the model generates over the range of the tolerance of a particular parameter. Thus, a comparison can be made between the parameters.

Table 5.1: Sensitivity of the Valve Model to Parameter Tolerance Ranges

	Geometric Tolerance	Range @ 57 amp-turns	Geometric Sensitivity
	[inches]	[newtons]	[newtons/inch]
Metal Interface	(+) 0.003	6.2 - 4.5	580
Axial Offset	(+) 0.003	6.2 - 4.7	502
Shim Gap	(\pm) 0.0005	6.9 - 5.7	1,216

In this operating regime, the valve performance is about twice as sensitive to lift gap tolerance as it is to the other parameters. Unfortunately, the lift gap is the most uncertain of the three parameters owing to the alignment complications that will be encountered when the machine is assembled.

Although it is impossible to measure the contribution of each tolerance type to the total valve performance, it is possible to predict the limits on performance by exercising the model through the various possible permutations of the variables and identifying the worst- and best-case scenarios. These cases, shown in Figure 5.11 bind the limiting upper and lower levels of valve performance and encompass the actual measured performance.

5.1.4 Experimental Hysterisis in Force Measurement

Static hysteresis is a commonly observed phenomenon in magnetic materials that undergo cycling in magnetic fields, such as electromagnets. One physical interpretation is that the domains on the magnetic material do not totally randomize to their original state when the current is removed. In effect, the magnetic material becomes a permanent magnet that displays a field even with no driving current. There are also a number of dynamic hysteresis affects that are active in this experiment.

The hysteresis between the drop and sticking currents is primarily the result of forces induced by dynamic changes in the magnetic field. This hysteresis can be characterized by a raw set of data, as presented in Figure 5.4. These transient forces result from four primary sources: 1) eddy currents running around the valve yoke and valve disk, 2) transients in the current caused by experimenter adjustment, 3) changes in the shape of the magnetic field induced by the proximity of the valve disk to the valve yoke, and 4) the hysteresis in the magnetization of the valve coil.

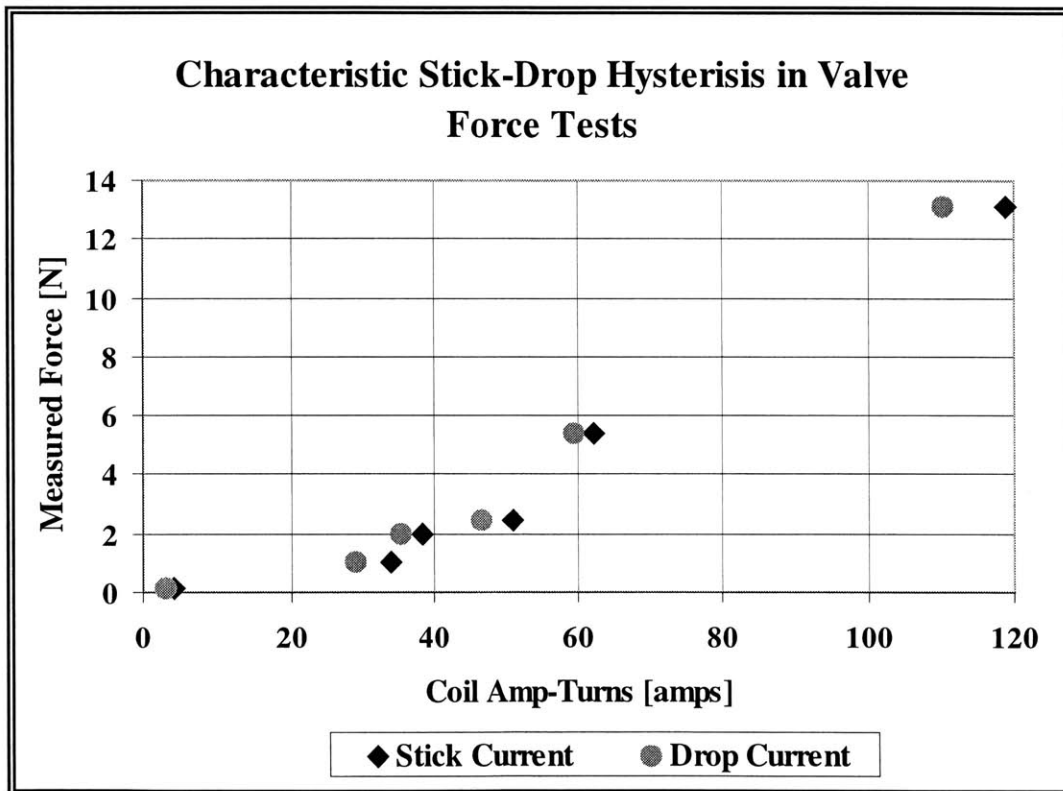


Figure 5.4: The distance between each data point at the same force quantifies the level of hysteresis between the experimental sticking and drop currents

Given that the background field density of the Earth's magnetic field is about 5.0×10^{-5} Tesla at the planet's surface, the valve field intensity reaches background levels at a distance of about 2 inches radially from the surface of the tube.

This model indicates that all electronic components should function normally in the presence of the valve if placed at least two inches from the vacuum can. Additional magnetic shielding can also be implemented in the final design to further damp the field if active components must be placed in close proximity to the vacuum can.

5.4 VALVE INDUCTANCE MEASUREMENTS

A necessary feature of the valves is that they must react to input and output signals at a rate much faster than the cycle frequency of the cryocooler. If the valves are slower than the cycle, they will not be able to regulate the flow of working fluid fast enough for the cycle to run.

Electrically, the property that directly reflects the valves' reaction time to input current is inductance. Inductance is the constant relating voltage as a function of time to the time rate of change of current via Equation 5.4.1.

$$V(t) = L \frac{di}{dt} \text{ (Equation 5.4.1)}$$

The magnitude of the current in the valve coil directly controls the force developed on the valve disk. Hence the valve's inductance indicates how much instantaneous voltage must be applied for the valve to develop force rapidly enough to open faster than the rate of the cycle. The practical limit on the voltage that can be applied is the arcing voltage of the coil wire, the voltage at which current will jump through the wire insulation. This voltage is roughly 100 volts. The higher the voltage that one can apply, the more turns can be wound onto the coil for the same current. In other words, more voltage yields more amp-turns and hence more valve opening force. The upper limit on the possible voltage is driven by the size of the wire that can be manageably wound around the yoke. One must be able to apply enough voltage to drive current through the coil.

5.4.1 Description of Experimental Technique

To generate a reasonable first approximation of a valve's inductance, it is appropriate to use the resonant characteristics of a standard CL circuit as shown in Figure 5.13 where the inductor is the valve coil. This circuit can be constructed such that an oscilloscope reads the amplitude of the voltage across the coil.

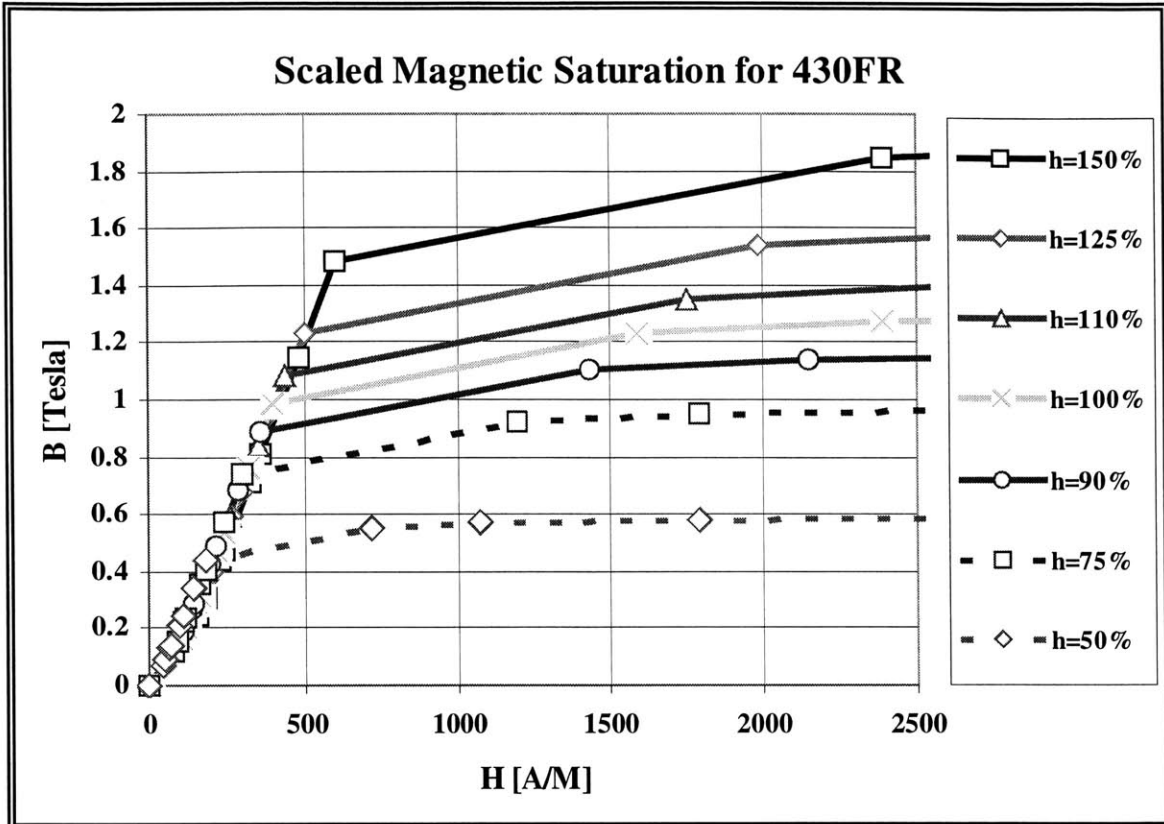


Figure 5.5: An array of scaled B-H curves for the magnetic yoke material is exercised via finite element to determine the effect of the magnetic field density at saturation

These B-H curves were utilized in conjunction with the ideal finite element model to determine the possible range of performance linked to uncertain saturation. All of the resulting valve performance curves from $h=150\%$ to $h=75\%$ aligned exactly, within the error expected in from finite element software. The notable exception was the $h=50\%$ curve, and this material displayed identical performance to the others until it experienced magnetic saturation at about 80 amp-turns.

Theses results indicate two important conclusions. First, a large portion of the material in the yoke must experience current density less than 300 amps per meter when the coil is energized to 100 amps-turns. Second, the magnitude of the B-H curve does not have a significant effect of valve performance because all of the activity occurs on the far left-hand side of the curve, below 300 amps-per-meter.

This finding is an expected result of the valve design process. A core feature of that effort was to assure that the yoke did not saturate when energized with the maximum opening current. If the $h=100\%$ case is utilized, saturation would occur if parts of the yoke experienced current density exceeding 400 amps-per-meter. In addition, because all the scaled B-H curves have the same slope at low current densities it is not surprising that the valve model performs identically for each curve in the low current density region.

Radical changes in the slope of the curve on the left-hand side of the plot will affect the performance of the valves. However, significant changes in slope will only be encountered if a metal of different permeability replaces the yoke material, or if there is a serious departure from the metal annealing process described in Chapter 4. Thus, it can be concluded from this analysis that the model is not sensitive to uncertainty in magnetic properties in the region of interest to the experiment.

5.2.2 Modeling Metal-to-Metal Interface Tolerance

When the valve parts are assembled, the cover is press fit over the spool piece to complete the valve's magnetic yoke. Ideally, a perfectly smooth and uniform pair of contact surfaces characterizes the interface between these two parts where the total wetted area of both parts is in full contact. In short, the pieces join at their intersection to create one continuous part. This situation exists in the idealized Quickfield model and represents the upper limit of magnetic performance for the joint.

In reality, the interface between these two metal surfaces is not smooth. Instead both surfaces are immensely rough at the microscopic level such that myriad air pockets and foreign particles interrupt the interface and reduce the areas of direct metal-to-metal contact. A visual representation of this non-ideal interface is presented in Figure 5.6.

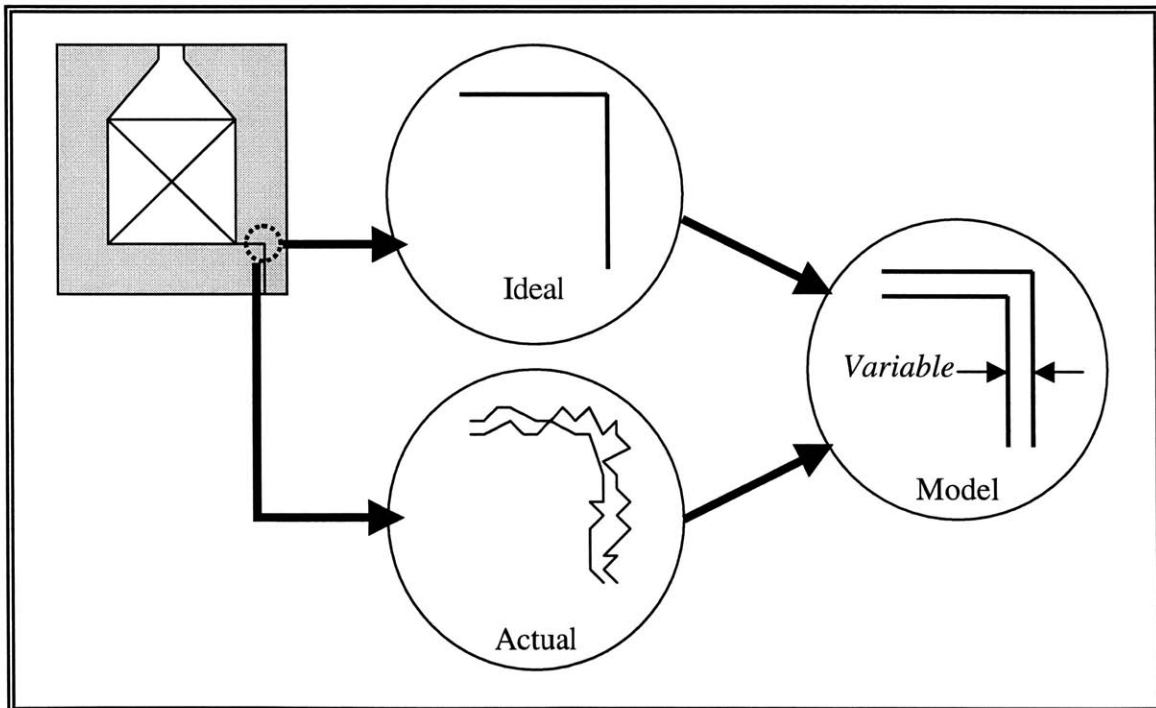


Figure 5.6: At the microscopic level, the interface between the spool and cover pieces is characterized by irregularity, which is modeled by a tiny air gap of variable width

The resulting interface creates additional resistance in the valve yoke's magnetic circuit impeding the flux through the valve yoke. It reduces the available potential pushing the flux across the air gap between the active face of the valve yoke and the valve disk.

The intricacy and complexity of this interface belies any attempt to model it with geometric accuracy. However, it can be well approximated by an equivalent magnetic resistance, a gap of permeability equal to unity placed between the two metal components at the interface. The width of this gap can be adjusted accordingly to reflect the performance of the joint. The poorer the flux linkage through joint the greater the corresponding width of the low permeability gap. The characteristic affect of this modeling approximation on valve performance is demonstrated in Figure 5.7.

Model gaps ranging from 0.001 inches to 0.003 inches in width were considered during the development of the model. Over the operational range of the valve, the performance difference between an ideal model and a model with the largest interface gap is substantial: about 2.5 newtons at 50 amp-turns and almost 8 newtons at 110 amp-turns. The same kind of degradation from ideal behavior is observed in actual force measurements.

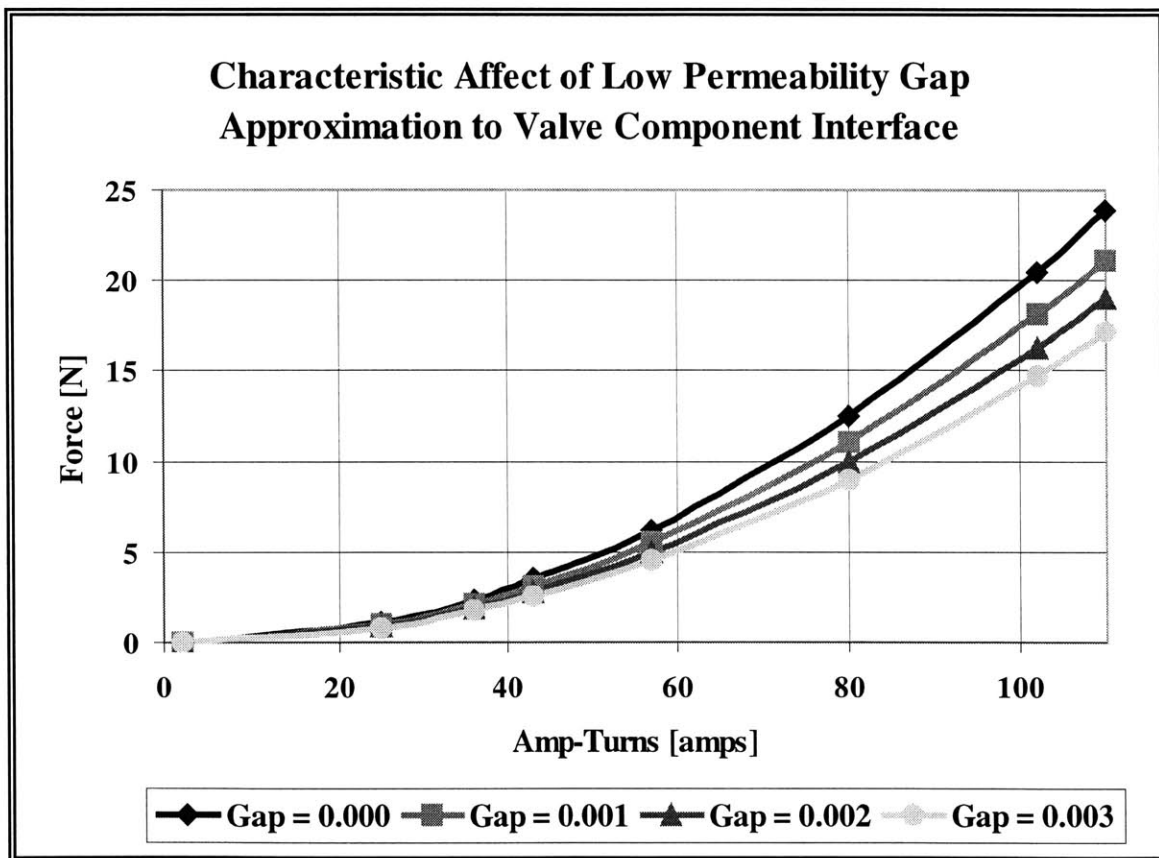


Figure 5.7: The effects of some characteristic gap values on performance of the outlet valve show a wide spread sensitivity to this parameter

It is very difficult to quantify exactly what gap width should be used in this model to approximate the actual interface. This difficulty arises because there are several magnetic loss mechanisms in the valve and the design does not allow the mechanisms to be isolated and quantified individually. Future improvements to the valve design may involve work to quantify individual loss mechanisms.

5.2.3 Modeling Part Alignment Tolerance

As the cover piece slides over the spool during valve assembly, it is important to align the magnetically active faces. Unfortunately, the interference fit between the two components makes it difficult to assure the parts align exactly, and thus there is a tolerance uncertainty on the location of the parts with respect to one another. Improper alignment increases the flux path length and reduces the contact area between the two pieces. Both factors increase the resistance of the valve yoke's magnetic circuit and reduce the force the valve yoke can apply to the valve disk. Figure 5.8 shows a highly exaggerated representation of the difference in flux paths between properly aligned and misaligned parts.

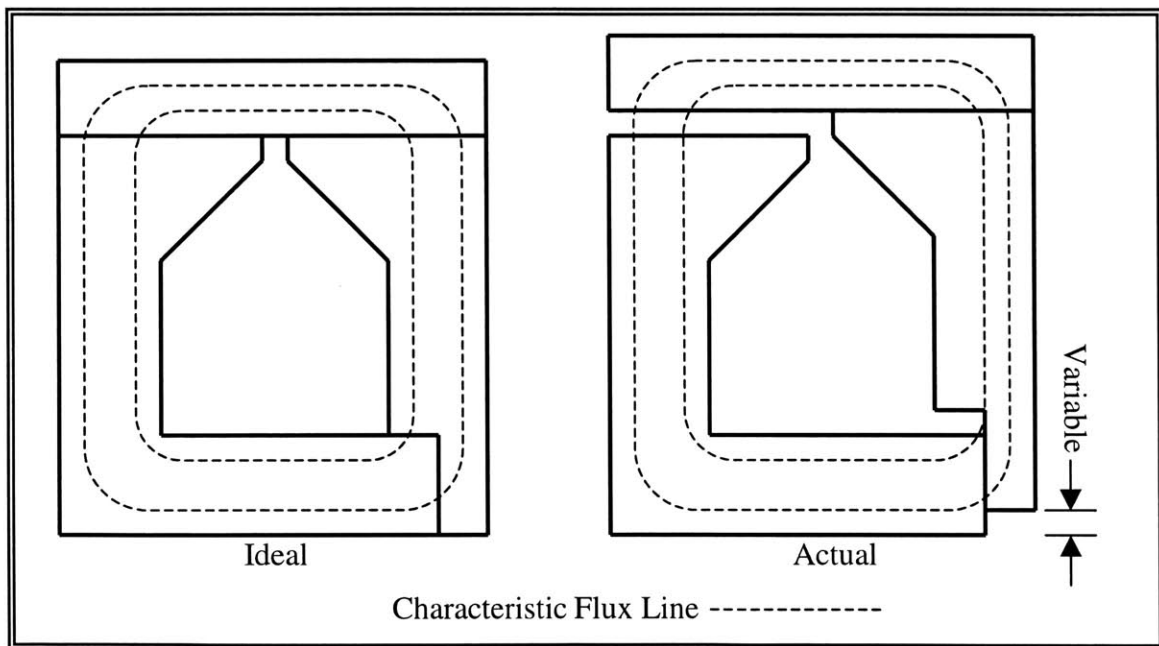


Figure 5.8: In an ideally aligned valve yoke, the flux lines are uniformly spaced about the valve coil; if the parts are misaligned, the flux lines become elongated and pinched

When prototype valve parts were originally built, they contained no surfaces to aid axial alignment. Thus, large alignment tolerances were difficult to avoid. The analysis of losses due to axial alignment demonstrated the necessity to incorporate some kind of alignment scheme into the valve design. Thus, a step was added into the cover piece to reduce the tolerance in axial alignment upon assembly.

This case represents the most prominent example of the value this post-manufacturing modeling exercise holds because it suggested a simple change in geometry that increased the valve performance substantially.

The surface that engenders axial alignment is a step in the cover piece that allows the parts to be press fit until the spool piece seats on the step in the cover. The parts can be clamped together during the epoxy curing process to assure axial alignment is maintained when the epoxy hardens. However, this additional step is not currently utilized in the manufacturing process. Even without clamping, the typical error in axial alignment is diminished from about 0.010 inches to less than 0.003 inches. This improvement reduces the need to sand a substantial amount of material off the active face of the misaligned part and generally increasing the valve's performance.

The magnitude of this increased performance is demonstrated analytically in Figure 5.9. An axial offset tolerance of 0.000 inches to +0.003 inches was utilized in the modeling process.

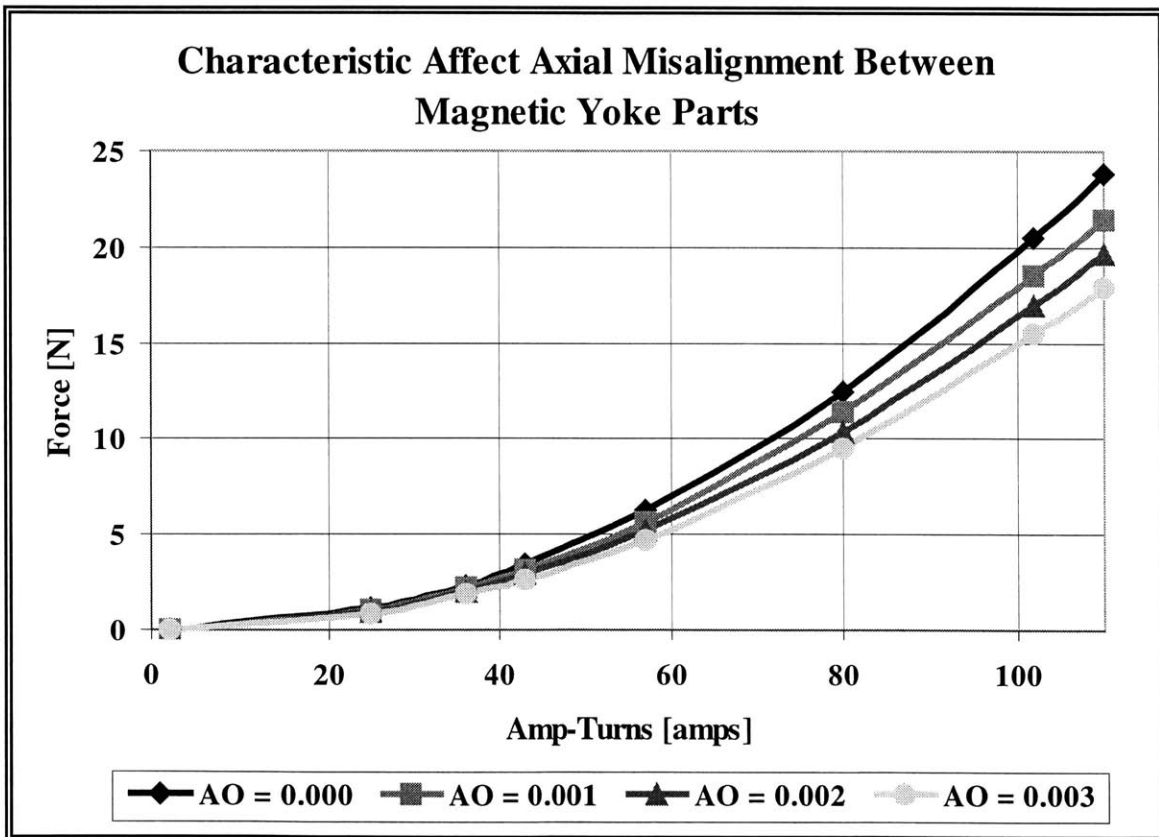


Figure 5.9: The characteristic effect of axial offset (AO) in the outlet valve shows that performance is substantially improved when the valve parts are in exact alignment

Over the operational range of the valve, the performance difference between the ideal model and the model with the largest axial offset about 2 newtons at 50 amp-turns and almost 6 newtons at 110 amp-turns. The same kind of degradation from ideal behavior is observed in actual force measurements. However, as with metal-to-metal interfaces, it is difficult to separate the axial offset tolerance from other geometrical loss mechanisms to determine the magnitude of this effect alone.

5.2.4 Modeling Shim Gap Tolerance

The shim holding the valve disk away from the active surface of the valve yoke in the test rig was made of brass and measured at 0.010 inches via micrometer. However, this dimension was taken at only three locations on the shim and could be affected by many factors. Imperfections on the surfaces, folds in the shim, and uncertainty in the micrometer used to take the measurement are all uncertainties that could skew the accuracy of the measurement. It is estimated that these factors could combine to upset the actual distance between the disk and the active surface by as much as ± 0.0005 inches.

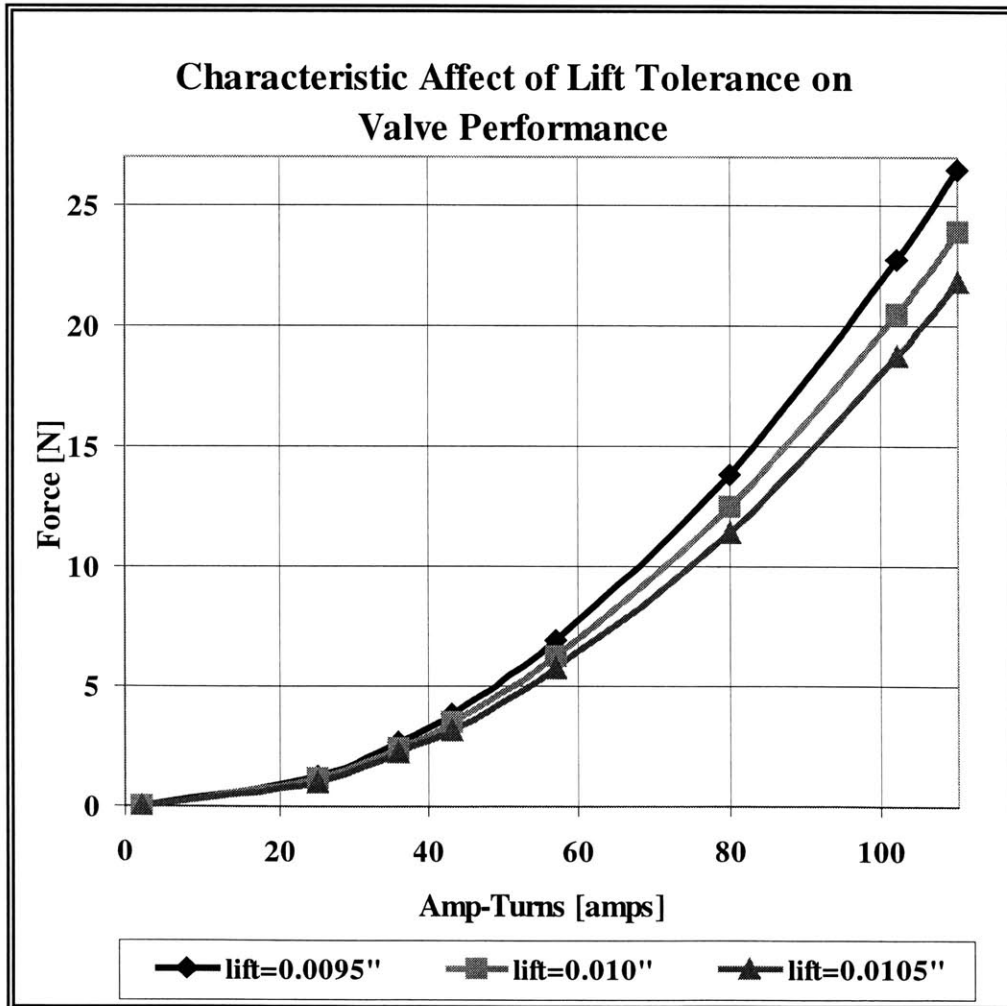


Figure 5.10: Differences of one-half of one thousandth of an inch in the lift height can sway the modeled valve performance by as much as 20 percent

Magnetic force on the valve disk is theoretically inversely proportional to the square of the distance between the disk and the active valve yoke surface. Thus this 5 percent tolerance in the measurement of distance results in theoretical 20 percent error in the force measurement. The effect on valve performance for shim tolerances of ± 0.0005 inches is graphed in Figure 5.10.

Although this type of uncertainty is similar in magnitude to other geometric tolerances encountered using the force test rig, the lift may vary by much more than ± 0.0005 inches when the real machine is actually assembled. The exact size of all the parts as well as the deformation of the seals sets the valve lift. Once the machine is assembled, it is impossible to accurately measure whether the proper lift has been achieved. Thus, it is expected that lift tolerance will be the primary factor to valve performance when the machine is assembled.

5.2.5 Sensitivity of the Model to Geometric Tolerances

The valves were originally designed to open against the full pressure differential of the cycle acting on eight 0.045-inch diameter ports. However, after the valves were completed, the bulkhead design changed to include only three 0.045-inch diameter ports. Thus, the valves must now open against only about 5 newtons instead of 13 newtons. This opening force is achieved for all of the modeled cases between about 55 amp-turns and 60 amp-turns of driving current.

Table 5.1 explores the relative sensitivity of the model performance to each of the geometric tolerance parameters studied in the vicinity of the maximum opening current, about 57 amp-turns. Relative sensitivity is gauged by the change in force the model generates over the range of the tolerance of a particular parameter. Thus, a comparison can be made between the parameters.

Table 5.1: Sensitivity of the Valve Model to Parameter Tolerance Ranges

	Geometric Tolerance	Range @ 57 amp-turns	Geometric Sensitivity
	[inches]	[newtons]	[newtons/inch]
Metal Interface	(+) 0.003	6.2 - 4.5	580
Axial Offset	(+) 0.003	6.2 - 4.7	502
Shim Gap	(\pm) 0.0005	6.9 - 5.7	1,216

In this operating regime, the valve performance is about twice as sensitive to lift gap tolerance as it is to the other parameters. Unfortunately, the lift gap is the most uncertain of the three parameters owing to the alignment complications that will be encountered when the machine is assembled.

Although it is impossible to measure the contribution of each tolerance type to the total valve performance, it is possible to predict the limits on performance by exercising the model through the various possible permutations of the variables and identifying the worst- and best-case scenarios. These cases, shown in Figure 5.11 bind the limiting upper and lower levels of valve performance and encompass the actual measured performance.

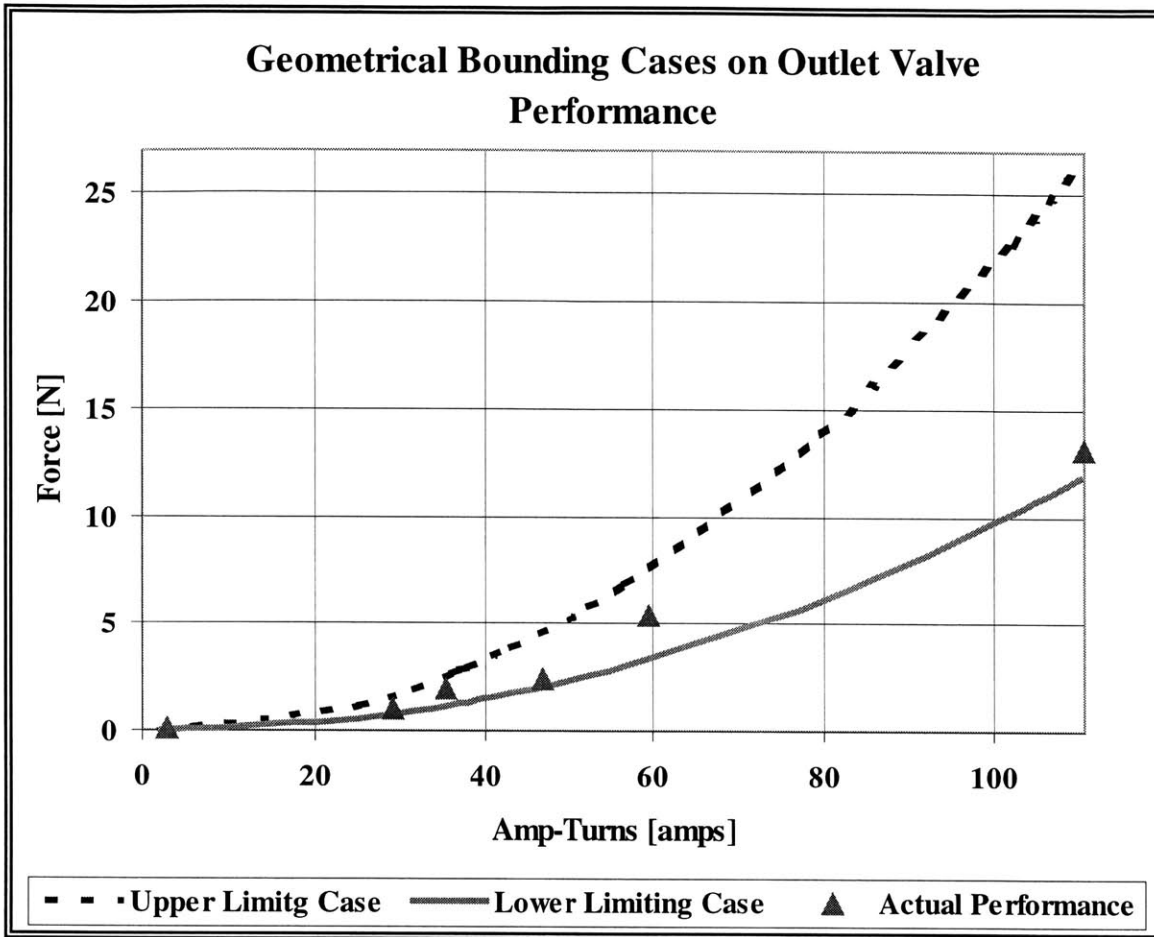


Figure 5.11: A limiting case analysis shows that the sophisticated valve model does not encompass the valve's actual performance

A set of tables representing the performance of the outlet valve for a complete set of characteristic tolerance variables is available in Appendix C of this document.

5.2.6 Value of Modeling to Future Work

Although the original purpose of deploying a finite element code for this project was to derive guidance in determining the optimal geometry of the valve, there is additional value added in enhancing the model to capture the real characteristics and behavior of the valves as built. The original goal of achieving 13 newtons of opening force was achieved. However, a substantially higher input current was required than predicted by the idealized model. Quantifying the effects of the real valves' physical characteristics has provided enormous insight into improvements that should be made in future iterations. This analysis has also identified pitfalls that should be avoided.

For example, an important discovery arising from this analysis is the sensitivity of the valve performance to axial alignment tolerance between the spool and the cover piece. This finding led to an easy fix, the incorporation of a step in the cover piece, to assure the two parts aligned axially within a few thousandths of an inch of perfection.

5.3 STRAY FIELD ASSESSMENT

A secondary, but important, consideration is the stray magnetic field generated by the valves during their normal operation. This factor will become more significant as the cold end and cryocooler go into actual use. If the cooler is used to chill sensitive avionics or electronic instruments packaged in close proximity, the field given off by the valves may disrupt the accurate function of these devices.

Hence, a calculation was run on Quickfield utilizing the idealized outlet valve model to determine the extent and strength of the magnetic field outside a typical vacuum can in which the cooler might be placed. For this simulation, the vacuum can was modeled as an effectively infinite stainless steel tube with a 2-inch outer diameter and 0.020-inch wall. The valve coil was charged to 110 amp-turns, the highest value it could be ramped to in normal operation in an eight-port bulkhead design. A quantitative plot of the field intensity versus distance from the outside surface of the stainless steel tube is displayed in Figure 5.12.

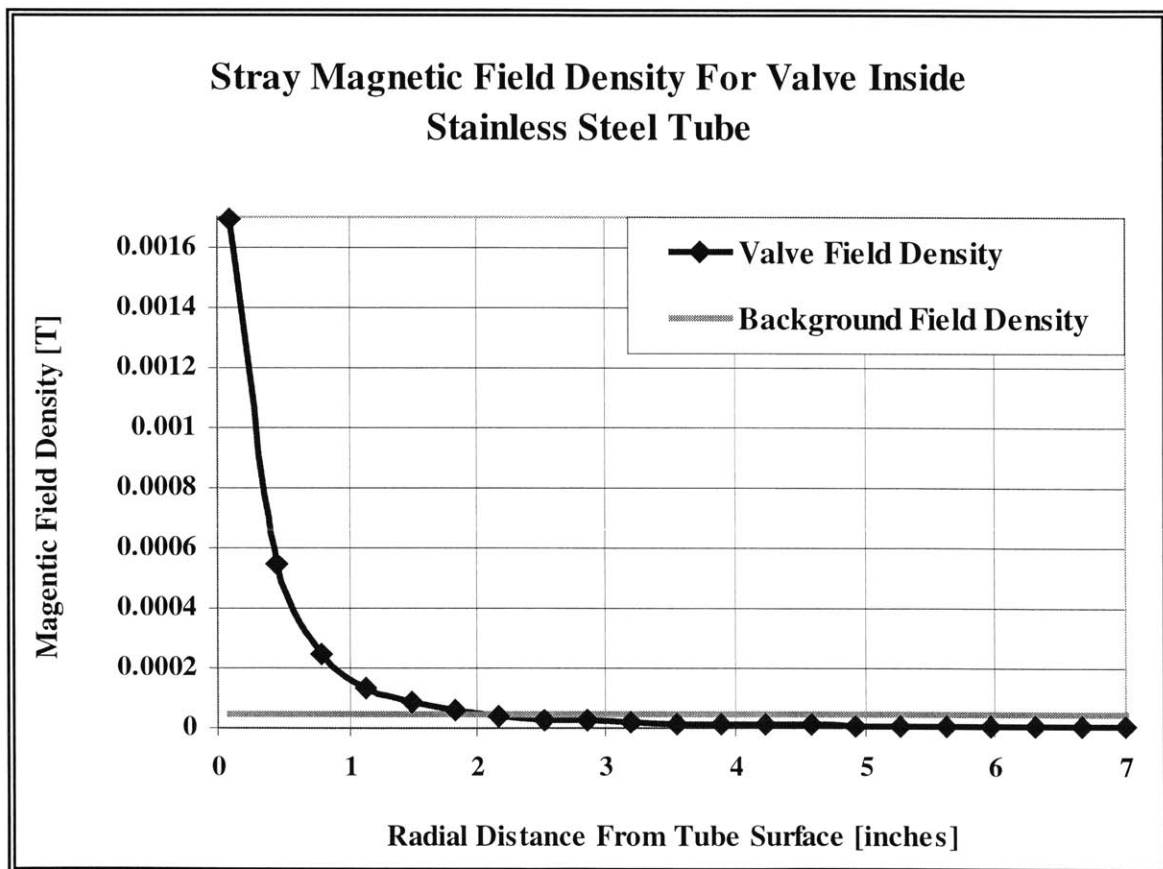


Figure 5.12: The magnetic field density induced by the valves will decay to background levels about two inches away from the cryocooler’s vacuum can

Given that the background field density of the Earth's magnetic field is about 5.0×10^{-5} Tesla at the planet's surface, the valve field intensity reaches background levels at a distance of about 2 inches radially from the surface of the tube.

This model indicates that all electronic components should function normally in the presence of the valve if placed at least two inches from the vacuum can. Additional magnetic shielding can also be implemented in the final design to further damp the field if active components must be placed in close proximity to the vacuum can.

5.4 VALVE INDUCTANCE MEASUREMENTS

A necessary feature of the valves is that they must react to input and output signals at a rate much faster than the cycle frequency of the cryocooler. If the valves are slower than the cycle, they will not be able to regulate the flow of working fluid fast enough for the cycle to run.

Electrically, the property that directly reflects the valves' reaction time to input current is inductance. Inductance is the constant relating voltage as a function of time to the time rate of change of current via Equation 5.4.1.

$$V(t) = L \frac{di}{dt} \text{ (Equation 5.4.1)}$$

The magnitude of the current in the valve coil directly controls the force developed on the valve disk. Hence the valve's inductance indicates how much instantaneous voltage must be applied for the valve to develop force rapidly enough to open faster than the rate of the cycle. The practical limit on the voltage that can be applied is the arcing voltage of the coil wire, the voltage at which current will jump through the wire insulation. This voltage is roughly 100 volts. The higher the voltage that one can apply, the more turns can be wound onto the coil for the same current. In other words, more voltage yields more amp-turns and hence more valve opening force. The upper limit on the possible voltage is driven by the size of the wire that can be manageably wound around the yoke. One must be able to apply enough voltage to drive current through the coil.

5.4.1 Description of Experimental Technique

To generate a reasonable first approximation of a valve's inductance, it is appropriate to use the resonant characteristics of a standard CL circuit as shown in Figure 5.13 where the inductor is the valve coil. This circuit can be constructed such that an oscilloscope reads the amplitude of the voltage across the coil.

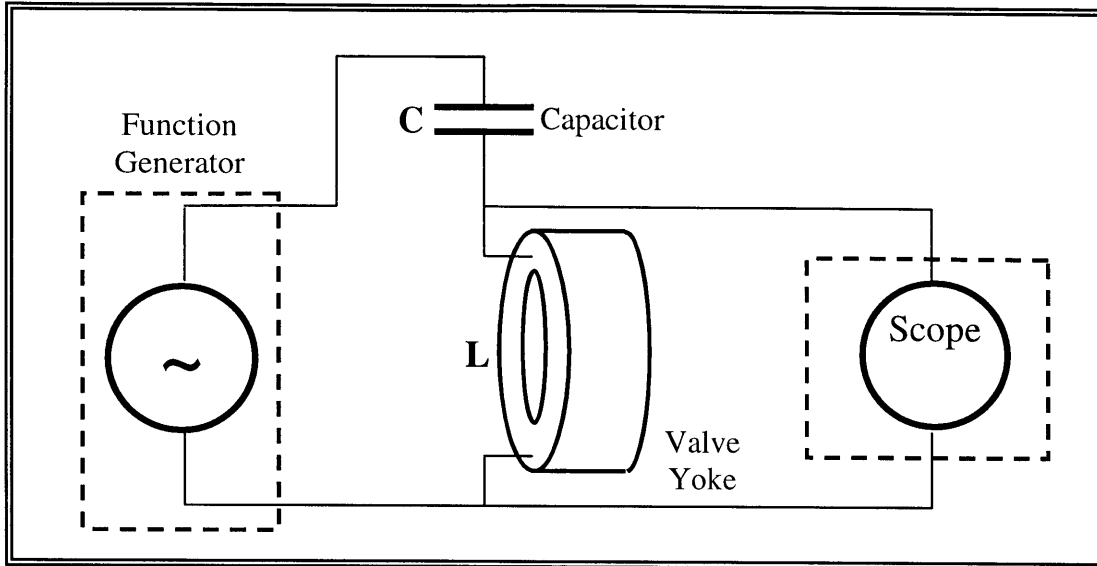


Figure 5.13: A simple CL circuit can be utilized to measure the inductance of the valve coil

This ideal circuit is governed by the second order ordinary differential equation, Equation 5.4.2 developed from applying Kickoff's voltage law around the circuit.

$$\frac{d^2V(t)}{dt^2} + \frac{1}{CL}V(t) = 0 \text{ (Equation 5.4.2)}$$

Solving this ordinary differential equation yields solutions of the form illustrated in Equation 5.4.3.

$$V(t) = 2 \cos\left(\frac{t}{\sqrt{CL}}\right) \text{ (Equation 5.4.3)}$$

In this form, the resonant frequency, ω , of the circuit is recognized as the term involving inductance and capacitance acting in the cosine expression, as per Equation 5.4.4.

$$\omega = \frac{1}{\sqrt{CL}} \text{ (Equation 5.4.4)}$$

The resonant frequency, ω , represents the frequency at which the circuit will naturally resonate if perturbed by an impulse. It also represents the driving frequency at which the voltage amplitude of the circuit's response will be highest.

To measure the valve's inductance, the circuit shown in Figure 5.14 was wired with the valve coil as the inductor in series with a 1-microfarad capacitor with a ± 10 percent error. The circuit was driven by a sine wave using a variable frequency AC current source. The voltage response of the circuit was monitored via an oscilloscope wired across the valve's coil leads.

5.4.2 Inductance Measurement Experimental Procedure

Ideally, the valve disk is placed atop the valve yoke to complete the magnetic flux path. This configuration represents the highest inductance the valve coil can produce because the magnetic flux enjoys an uninterrupted closed-loop path through the yoke and the disk. Hence the magnetic field is most at liberty to resist changes in the coil current. Unfortunately, the valve disks are not utilized in the results presented here because disassembly of the machine is required to make this type of measurement. It was deemed more important to continue the cryocooler test regimen than disassemble the machine to make inductance measurements.

With the circuit in Figure 5.13 set up and the oscilloscope set to measure voltage amplitude across the valve coil, the experiment begins. The driving frequency on signal generator is slowly increased while the amplitude response of the coil is observed on the oscilloscope. By inspection, the maximum amplitude can be determined, and this amplitude corresponds to the resonant frequency of the coil.

Knowing the resonant frequency and the value of the capacitor in the circuit, Equation 5.4.4 can be solved to estimate the valve coil inductance. Using this process, the outlet valve was shown to have an inductance of about 0.334 Henries while the inlet valve has an inductance of 0.273 Henries.

Coil inductance can also be estimated using the Quickfield finite element package. For the valve disk configuration described above, the outlet valve model has a value ranging between 1.18554 and 1.08125 depending on which set of characteristic tolerances are selected. The inlet valve has a range between 1.09927 and 1.02086 Henries depending on which set of characteristic tolerances are selected. The significant differences between the measured and modeled values can be attributed to uncertainties in the capacitance used in the test circuit, the crudeness of the inductance measurement method, and small physical differences between the real valve and the model that have not been captured.

6.0 SYSTEM INTEGRATION AND COLD END DESIGN

The valves described herein are a significant part of a larger cryocooler machine. The cold end of the cooler is designed to house the valves, facilitate all the necessary static sealing, and support electrical and fluid supply lines.

The cold end is made up of three main components: the high-pressure assembly, the housing assembly, and the valve assembly. These parts are laid out in order in Figure 6.1. Figure 6.2 is an un-dimensioned assembly drawing of the cold end hatched to show each individual component.



Figure 6.1: The cold end consists of several components that when assembled together support the function of the valves in the context of the larger machine

The cold end is designed within constraints that were laid out for the system in the concept development phase. Geometrically, it fits inside a vacuum can with an outer diameter of 2 inches. Structurally, the cold end has demonstrated integrity to hold up to 250 pounds-per-square-inch of pressure. It can provide many more times that pressure as sealing force against the various helium-tight Indium seals between the internal components. The cold end is also relatively easy to disassemble so that the moving parts can be easily accessed, swapped out, or repaired. The cold end also has to demonstrate mechanical robustness and survivability at temperatures as low as 10 Kelvin.

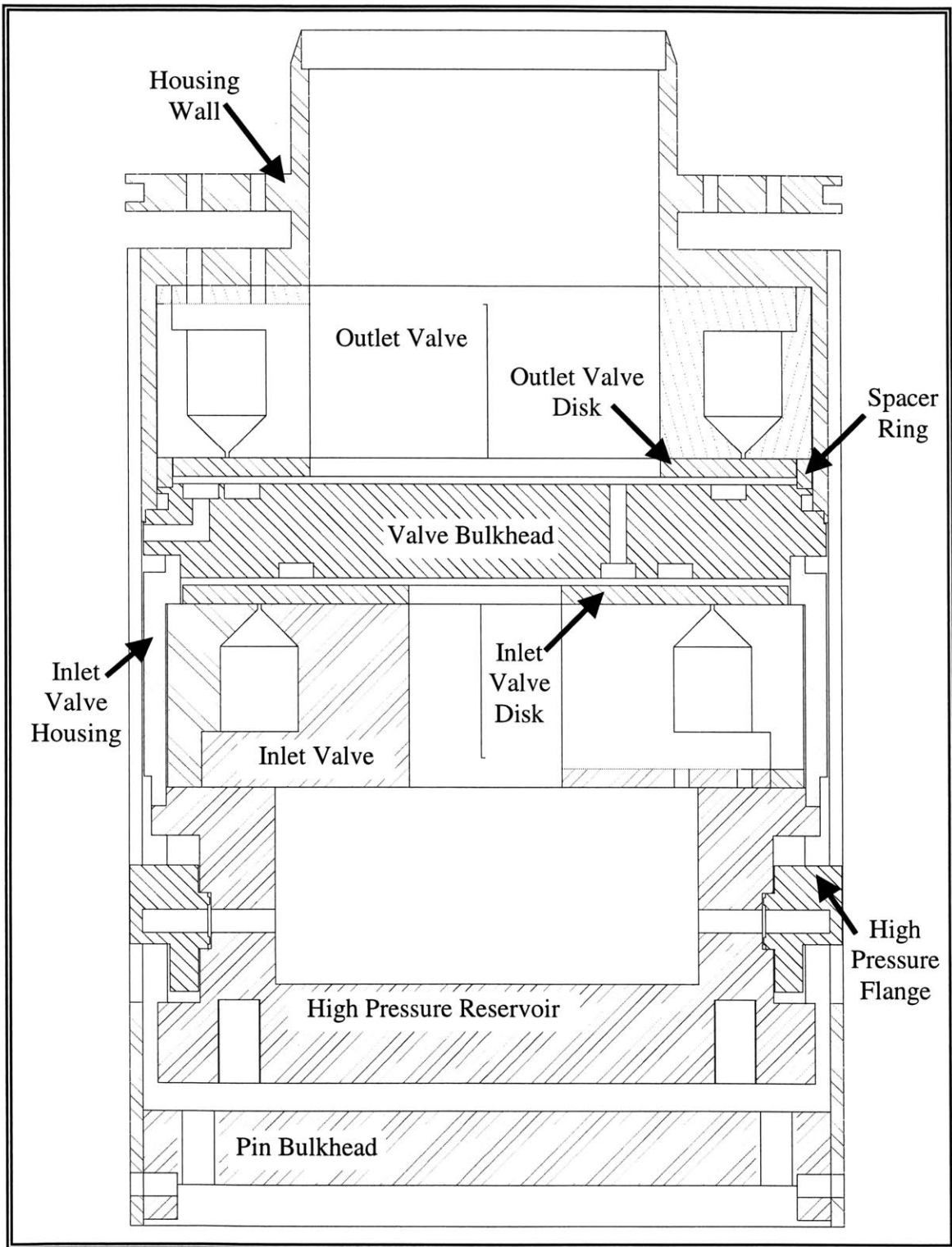


Figure 6.2: An assembly drawing of the cold end shows its various constitutive internal parts as discussed in Chapter 6

6.1 THE HIGH-PRESSURE ASSEMBLY

The high-pressure assembly, pictured in its completed form in Figure 6.3, serves as the reservoir of high-pressure working fluid for the cold end. It also contains the female fixtures for two high-pressure flanges, which port the working fluid into the reservoir.

The inlet valve yoke is completely contained within the high-pressure assembly, and the power wires to actuate the valve emanate from a third fitting on the part. The inlet valve lift is determined by the interface between the high-pressure assembly and the valve bulkhead and this interface is designed to accommodate a high-pressure Indium seal.

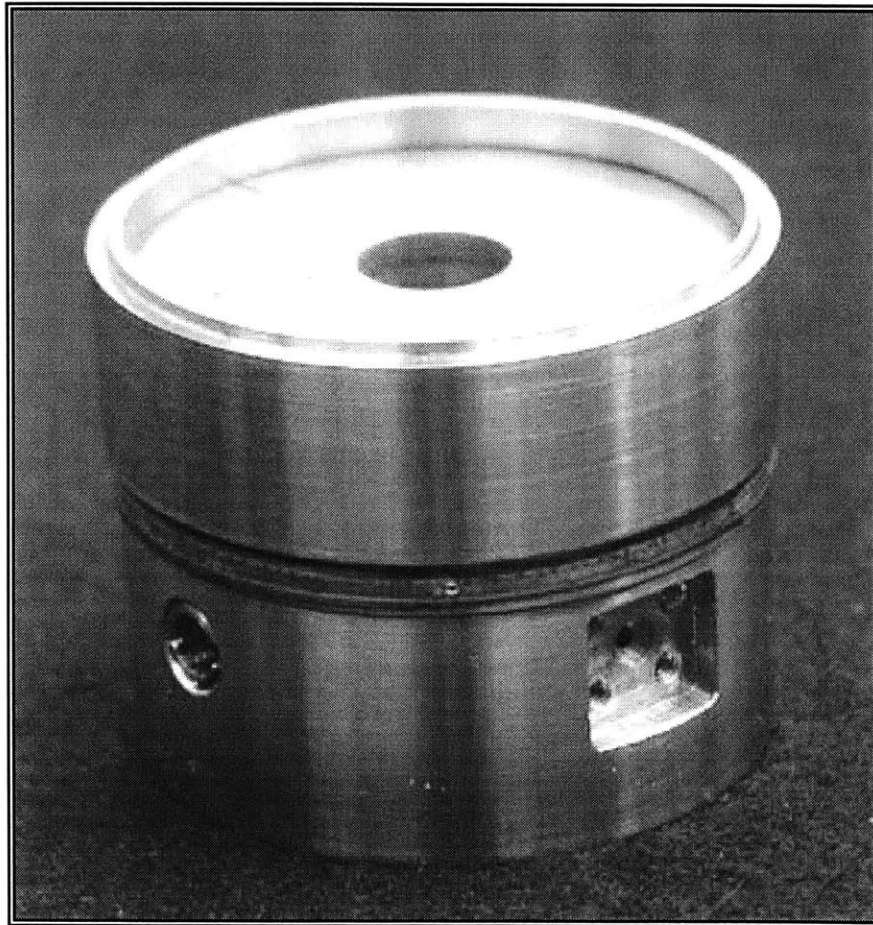


Figure 6.3: The high-pressure assembly consists of the inlet valve sandwiched between two welded pieces

In addition to the inlet valve, the finished assembly is made up of two other major components: the high-pressure reservoir and the inlet valve housing. These parts are made out of non-ferrous stainless steel to assure no interference with the magnetic field generated by the inlet valve. Figure 6.4 presents a technical drawing of the high-pressure reservoir while Figure 6.5 shows the inlet valve housing. These parts are designed to fit together, sandwiching the inlet valve between them. A weld preparation is built into each part at this interface so they can be permanently welded together.

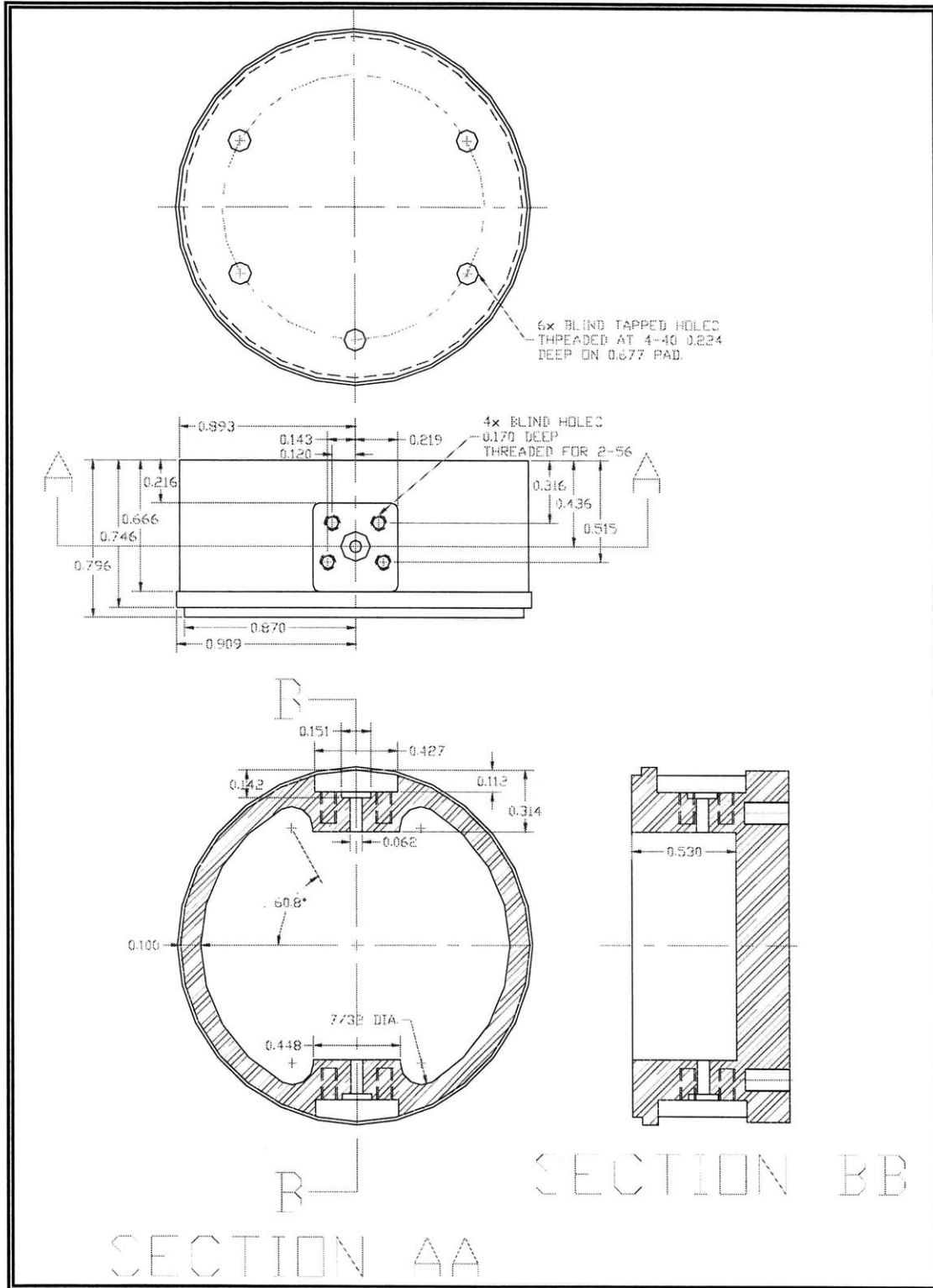


Figure 6.4: This technical drawing of the high-pressure reservoir shows the detailed machine work that goes into the high-pressure flange fixtures

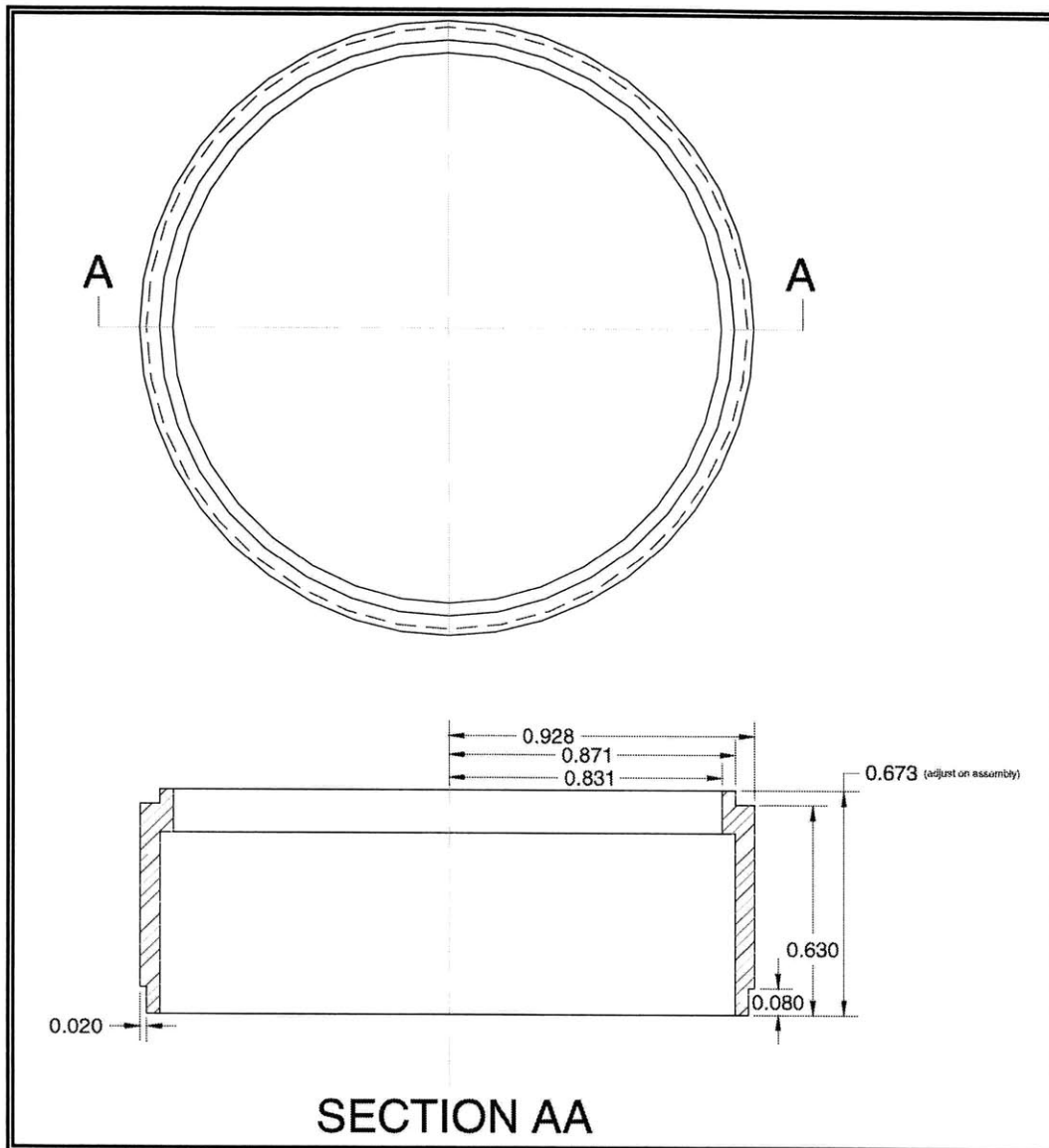


Figure 6.5: The height of the inlet valve housing can be shorted by sanding for refined control over the lift of the inlet valve

6.1.1 Welding The High-Pressure Assembly

Creating the completed high-pressure assembly component required intricate welding work to seal the inlet valve between the two parts without damaging it. Since, the entire assembly is required to seal against helium gas at 250 pounds-per-square-inch, the parts were precision arc welded on a lathe, which was converted for the job.

Before welding occurred, the inlet valve was hard-wired to the electrical flange inside the high-pressure reservoir because the completed weld makes this wiring connection inaccessible. The valve leads were soldered to a tiny sealed connector and protected with Teflon sleeves. The hard-wired pieces are shown together before welding in Figure 6.6.

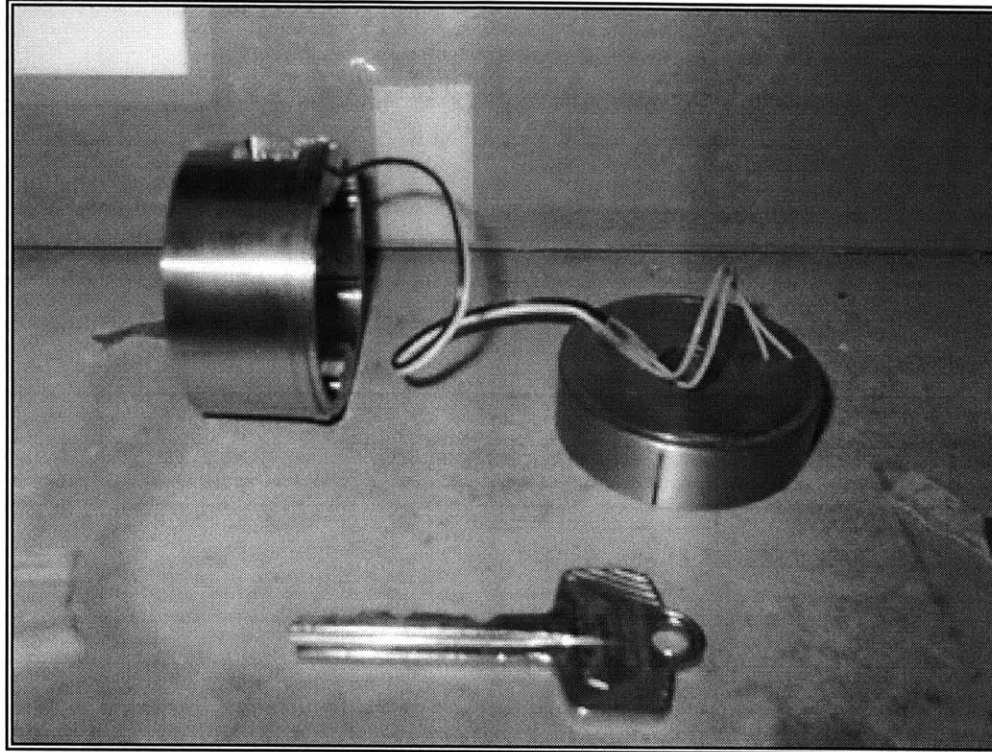


Figure 6.6: In advance of welding, the inlet valve is wired to the high pressure reservoir piece because this connection cannot be made later

The welding setup is shown in Figure 6.7. The controls on the welding lathe allow the user very precise control of the tungsten welding electrode. A microscope capable of 100X magnification was utilized, allowing the user to see the weld preparation in fine detail. The microscope's optics were covered with an arc welding filter plate to allow the user to see the weld in progress.

The major concern with this procedure was that the valve coil would get too hot or the wire insulation would begin to melt before the weld was complete. To address this issue, a pair of copper heat sinks was built. These high-thermal-mass collars were placed around the high-pressure reservoir piece and the inlet valve housing to conduct heat away from the weld site. To assure the principle was thermally sound, a set of steel test pieces was built similar in geometry to the real parts. The practice parts were test-welded together with the heat sinks in place but without the valve coil inside. This test case, without the valve, represented a lower bound on the thermal mass of the real components. It was found that the pieces remained cool enough to the touch after the welding process was complete, indicating the weld could occur without damaging the valve coil.

The real weld was performed successfully. With the added thermal mass of the valve, it was found that the parts were cool enough to handle comfortably after the weld was complete. An electrical test confirmed that no damage had been done to the valve or the wire coil during the weld.

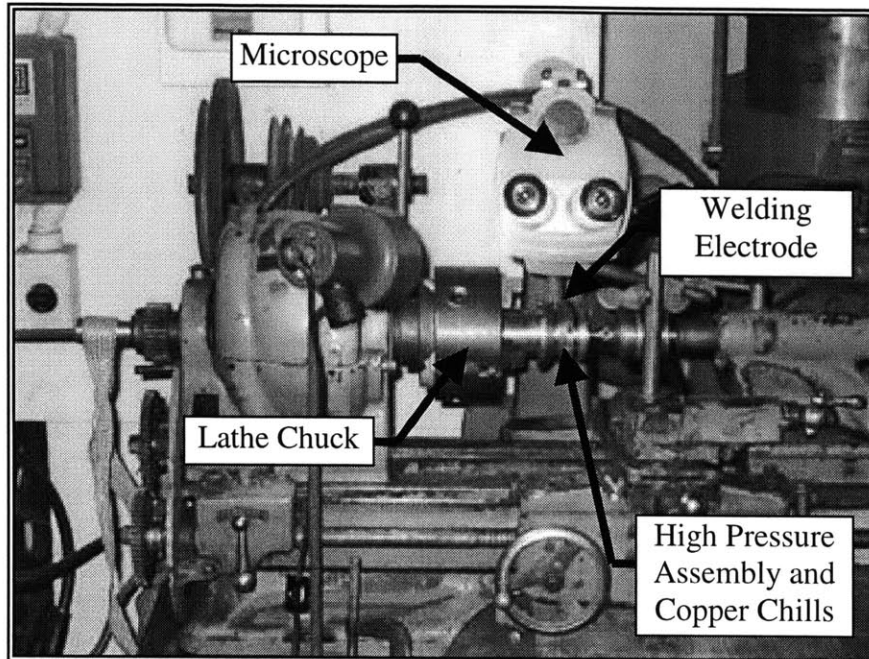


Figure 6.7: The copper chills can be seen in place on the modified lathe before welding commences on the high-pressure assembly

6.1.2 Cold End Flanges and Fittings

The high-pressure assembly accommodates two types of fittings. A pair of tiny flanges designed to bring high-pressure, pre-cooled working fluid in from the cryocooler's heat exchanger connect to female fittings machined into the side of the high-pressure reservoir. These flanges, pictured in Figure 6.8 are designed to accommodate four 2-56 screws used to crush a copper gasket between the flange and the fittings on the high-pressure assembly. This gasket assures proper sealing at this interface.

In future versions of the cold end, these flanges should be redesigned to accommodate an Indium seal. Although copper proves effective in sealing the interface against Nitrogen gas at 150 pounds-per-square-inch, it is not clear whether such a seal can provide adequate sealing against helium at higher pressure.

As can be seen in the technical drawing, Figure 6.9, these fittings have two tiny holes perpendicular to the main port. These holes support two 0.045-inch-diameter capillary tubes made of copper-nickel alloy that are hard soldered into the flange. The tubes are tiny by necessity because they must slip around the outer diameter of the cold end in a groove machined in the wall housing. However, they are restricted because they cannot increase the outer diameter of the cold end so that it does not fit into a 2-inch vacuum can. Ultimately, these tubes will need to be slightly crushed in the housing wall groove to meet this outer-diameter specification.

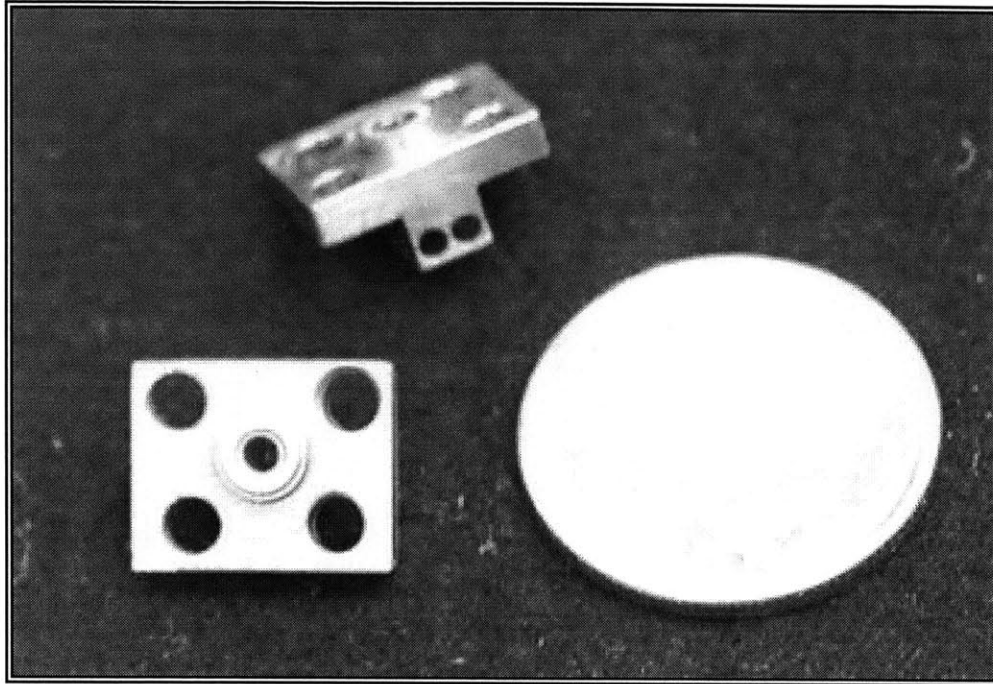


Figure 6.8: The precision, high-pressure flanges are shown for scale juxtaposed against a dime

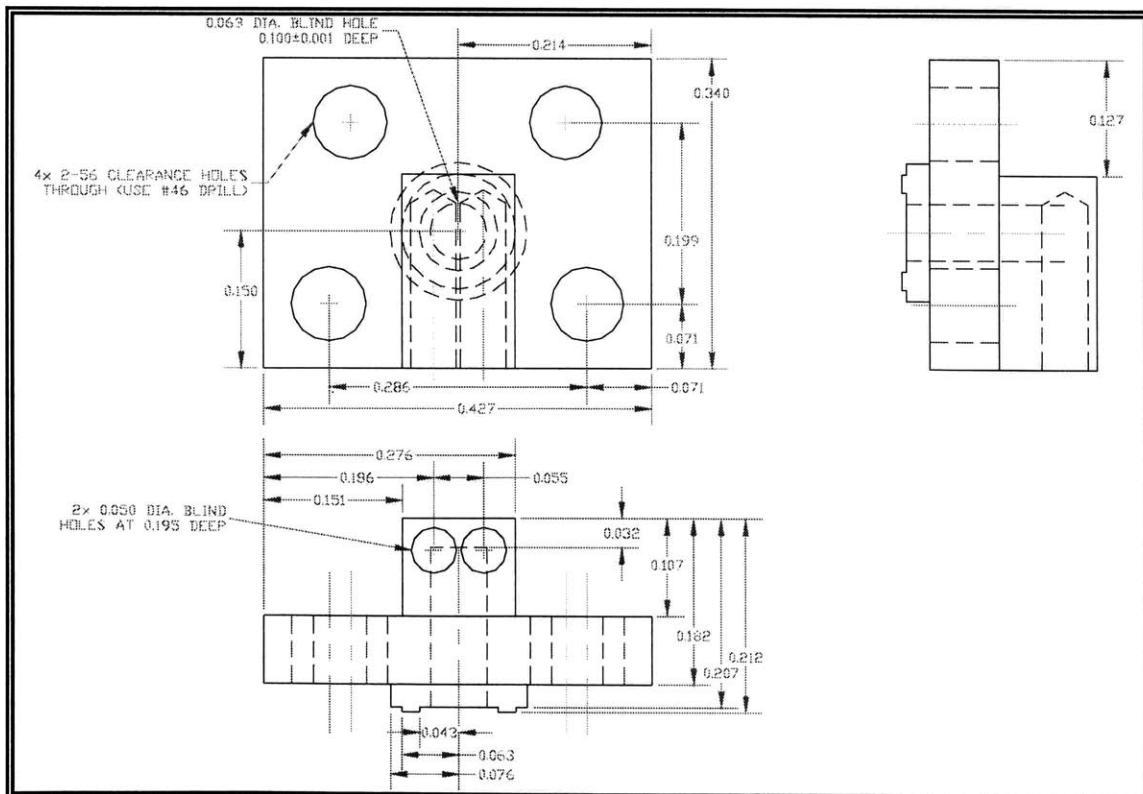


Figure 6.9: This technical drawing of the high-pressure flange reveals an intricate feature on the male portion of the part, a tiny ridge used for deforming a copper gasket seal

The second type of flange plugging into the high-pressure assembly is an electrical connector for the inlet valve leads, shown in a technical drawing in Figure 6.10. This part is designed to accommodate a small, sealed electrical connector epoxied inside. The flange screws into a female thread on the high-pressure reservoir, and it is sealed in place with LocTite® sealing agent. Once sealed, the flange itself cannot come out. However, the electrical connector allows the inlet valve power wires to be easily plugged in and taken out of the high-pressure reservoir.

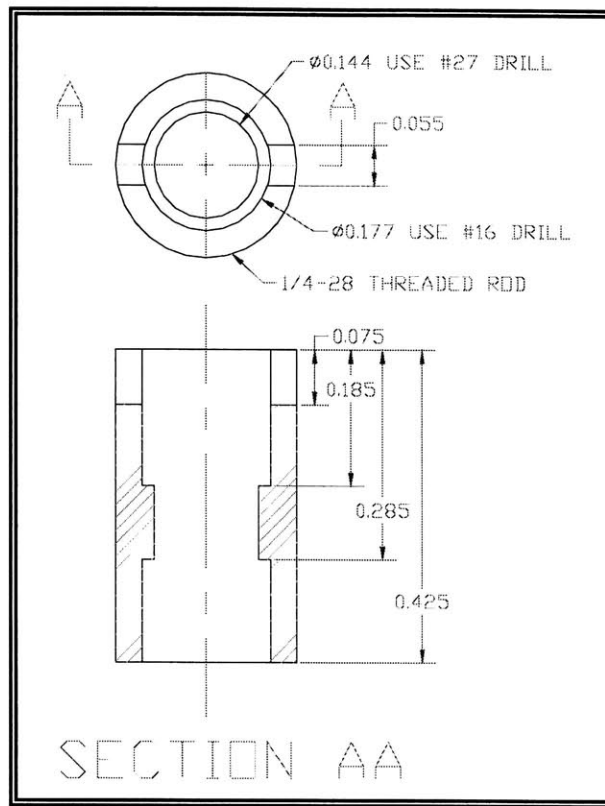


Figure 6.10: A plug of epoxy holds a tiny electrical connector in place on this fixture

6.2 THE COLD END HOUSING

The cold end housing consists of two parts: the housing wall and the pin bulkhead. Both parts are made out of non-ferrous material to prevent any disturbances to the magnetic field generated by the valves. The pin bulkhead, shown in Figure 6.11, is a cylindrical part that caps the cold end assembly. It contains 30 holes around the perimeter to accommodate 1/16-inch-diameter pins. As can be seen by the technical drawing in Figure 6.12, the part also has 12 threaded holes to accommodate 4-40 machine screws. When the cold end is assembled, these screws are used to camp down on the high-pressure bulkhead to squeeze the Indium seals tight within the cold end. The 30 pins interconnecting the pin bulkhead to the housing wall provide the reaction force against the housing wall as tightening the screws increases the pressure on the Indium seals.

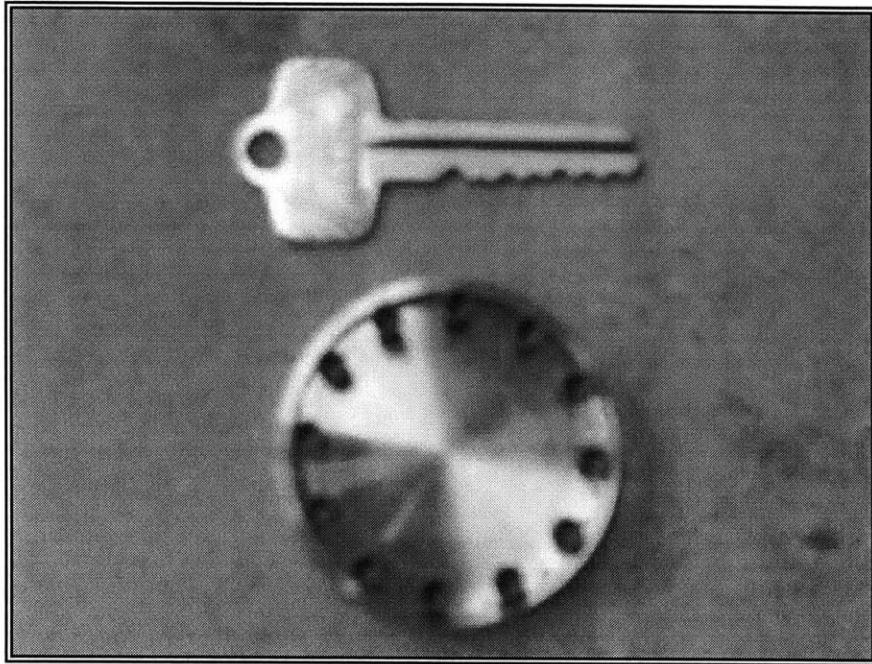


Figure 6.11: The pin bulkhead, pictured for scale against a key, provides the Indium squeezing force for the cold end's seals

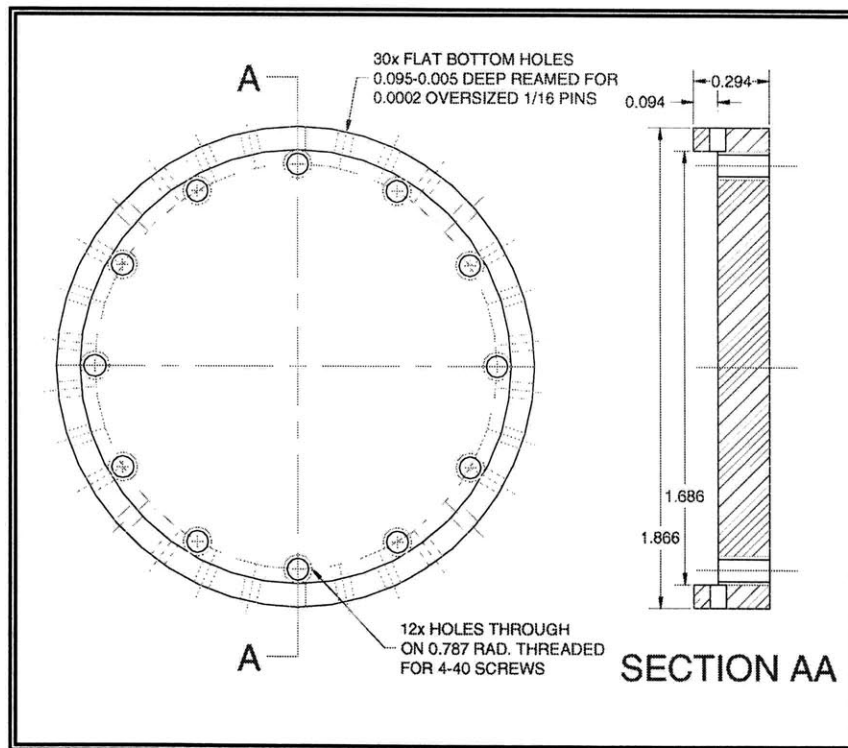


Figure 6.12: The 30 pinholes open only halfway onto the inner ridge. This geometry prevents the pins from falling out while allowing them to be pushed out from the inside for disassembly

The housing wall is a thin, hollow cylinder, making up the outer surface of the cold end. It provides axial alignment for all the internal parts. The housing wall has a number of holes and access ports to accommodate the various flanges, fluid supply tubes, and wires that cross from the cold end to the outside world. It also contains one of the surfaces that seals against the valve bulkhead with Indium to create the displacement volume for the expander. The top collar of the housing wall is designed with a weld preparation to join this piece with the honed that is the cylinder of the cryocooler. The bottom of the housing wall contains 30 1/16-inch diameter holes equally spaced around the perimeter. These holes accommodate pins that push through the pin bulkhead into the housing wall to interconnect the two parts. An image of this part is presented in Figure 6.13.

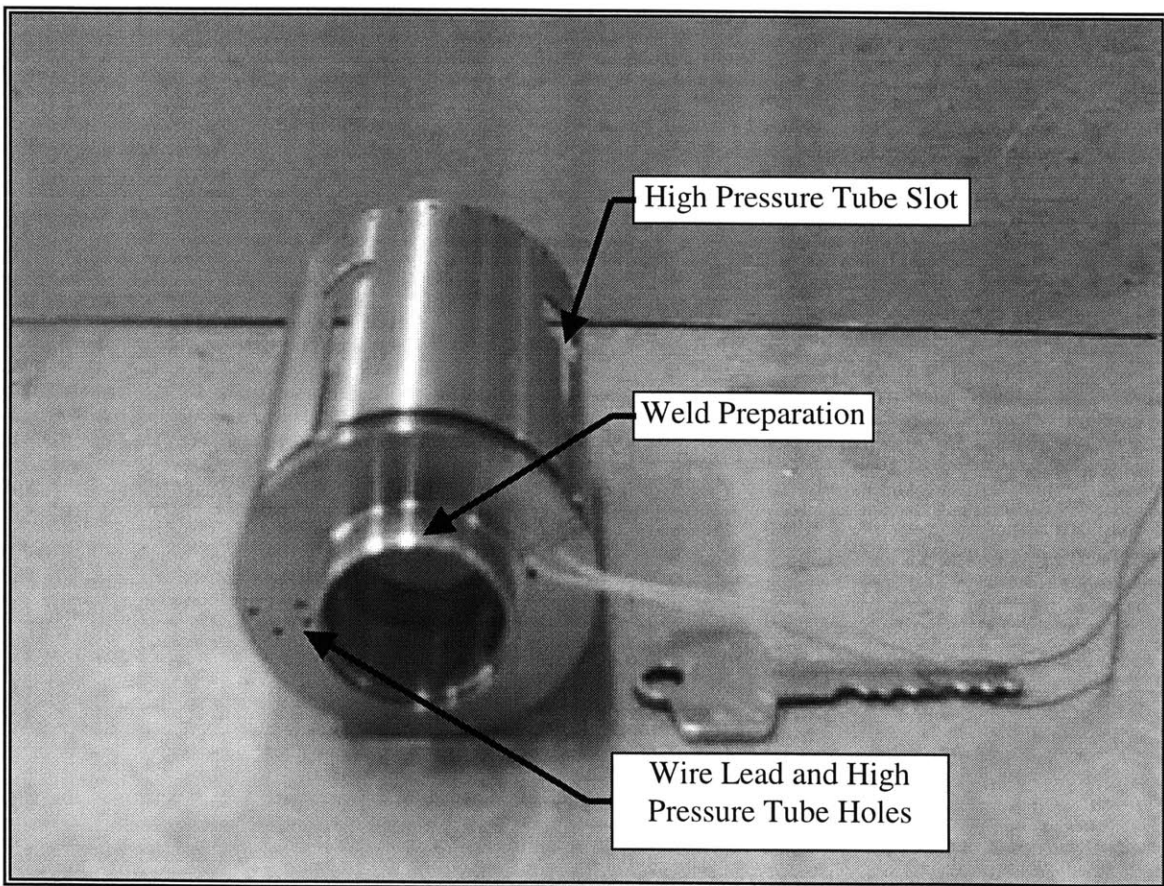


Figure 6.13: This top view of the housing wall shows the expander weld preparation in addition to the slots for the small, high-pressure gas tubes leading up to the flange ports

An important feature appearing in the technical drawing of the housing wall, Figure 6.14, is the low-pressure seal groove. This groove is machined into the collar above the main housing. The purpose of this seal is to separate the low entropy gas coming from the outlet valve from the higher-entropy gas going up the shell side of the heat exchanger. Both streams are low pressure and very cold, and a spring-loaded Teflon seal will be placed in the groove to assure the streams do not mix.

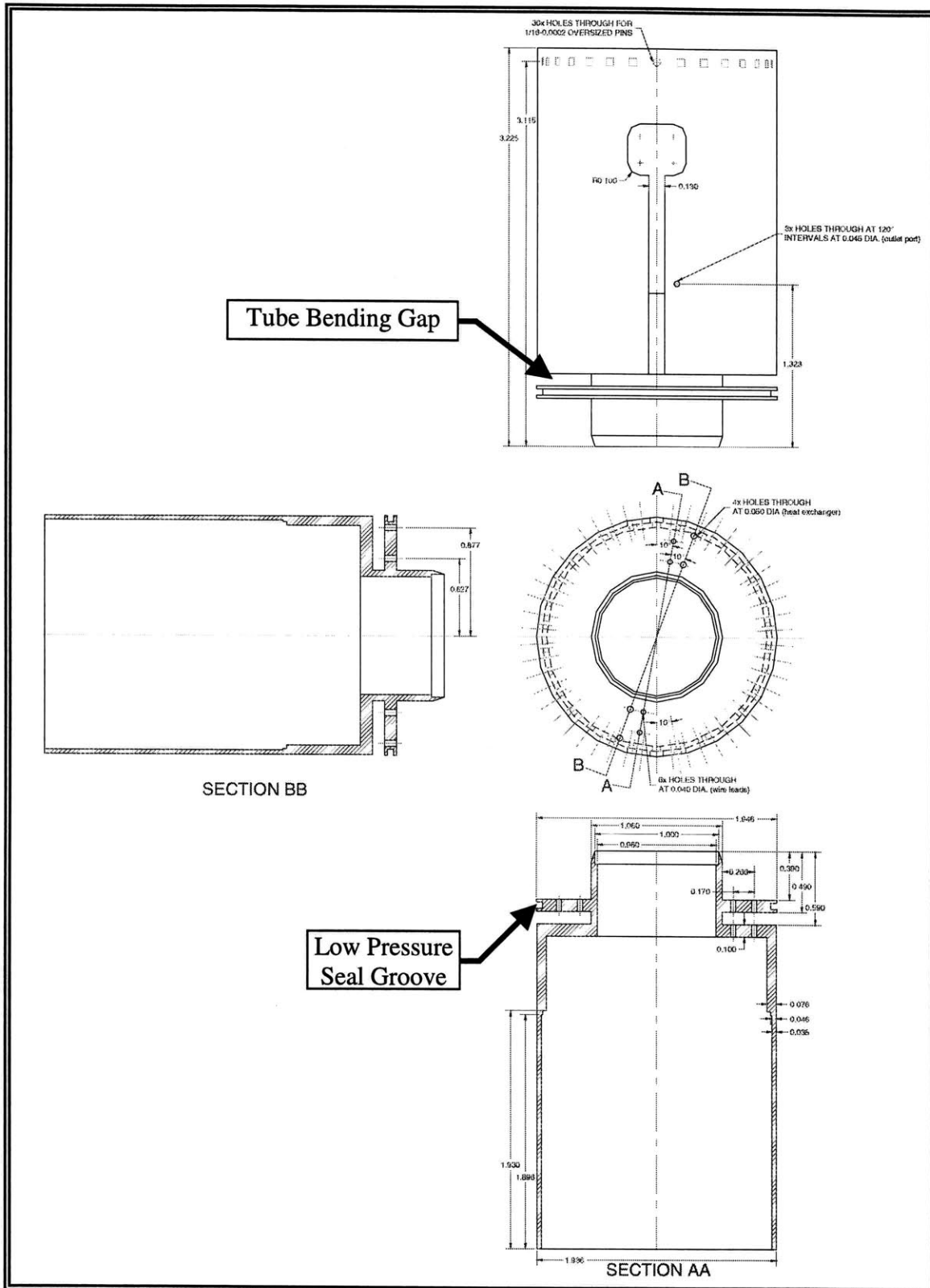


Figure 6.14: The housing wall has a very complex geometry with many holes and ports because it interacts with all other parts making up the cold end

Figure 6.14 also shows a 0.1-inch gap between the collar containing the Teflon seal and the rest of the housing wall. This gap is used as a space to bend the high-pressure capillary tubes emanating from the high-pressure flanges near the bottom of the cold end. The tubes are wrapped halfway around the housing wall and then threaded up through holes in the part where they finally attach to a manifold leading to the tube side of the cryocooler's heat exchanger.

This geometry is designed to allow enough tubing between the high-pressure flanges and the heat-exchanger manifold to elastically deform the tubes when the cold end needs to be disassembled. If the components of the cold end need to be removed, the high-pressure flanges are unscrewed from the high-pressure assembly. The flanges can then be sprayed outwards without bending the tubes because of the extra play provided in the additional tube length wrapped around the housing wall. With the flanges out of the way, the internal parts can be lifted out of the cold end.

In future iterations of the design, the gap in which the tubes are wrapped should be substantially wider than 0.1 inches. It was found that the current dimension is too tight to allow the tubes to make a 90-degree bend and be threaded through exiting holes to the heat exchanger manifold. There needs to be enough space in the gap to wrap two pairs of tubes halfway around the housing wall as well as allow for the passage of the wire leads from the outlet valve.

The outlet valve is permanently embedded in the top of the wall housing with LocTite® sealing agent. The valve leads snake through holes drilled in the housing to provide power for the valve to function. The lead holes are also sealed with LocTite®. In addition to holding the valve in place, LocTite® sealant serves to reduce dead volume around the outlet valve. Since the valve is designed to operate in the expander environment at the bottom of the expansion cylinder, dead volume around it can detract from the efficiency of the cryocooler.

6.2.1 Expander Space Dead Volume Minimization

The outlet valve is arranged in the cold end such that the cryocooler's piston travels through the inner bore of the annular valve all the way to the valve bulkhead. Given the arrangement of opposing valve and checking valve disks currently employed in the design, this configuration provides the best geometry to minimize the dead volume in the displacement volume of the expander.

Dead volume in cryogenic expanders, particularly those with high pressure ratios, is extremely detrimental to the expander performance. When the expander reaches the bottom of the exhaust stroke, the remaining gas in the dead volume is at a much lower pressure than the high-pressure charge gas. When the intake valve opens, the machine suffers severe entropy generation in the cold end as the high-pressure gas throttles into the low-pressure space. This entropy generation increases the level of entropy in the working fluid inside the expander and decreases the amount of entropy the working fluid can lift away from the load.

It is possible to recompress the gas in the dead volume up to the intake pressure, eliminating the effect of entropy generation across differential pressure. However, a portion of the exhaust stroke must be utilized for this recompression process. In expanders with high pressure ratios, the recompression stroke can be nearly the same length as the piston's entire travel, especially if the dead volume of gas requiring recompression is large. Thus, using recompression reduces the flow rate of low-entropy working fluid to the load.

In the machine built for this project, a compromise is struck between no recompression and total recompression on the exhaust stroke. Regardless, the dead volume in the displacement volume must be minimized to preserve the performance of the expander. The main contributors to dead volume in the expander are the inlet valve ports, the valve lift zone between the valve bulkhead and the outlet valve face, and the gap between the expander piston and the expander wall. The contribution of each dead volume to the total is tabulated in Table 6.1.

Table 6.1: Major contributors to cold end dead volume

Inlet Port Volume	Valve Lift Zone Volume	Piston Gap Volume
[in ³]	[in ³]	[in ³]
0.0013	0.0325	0.0856

Table 6.2 tabulates the ratio of total dead volume to the volume swept by one cycle of the expander. The ratio between these numbers is a significant 16.7 percent. In future designs of the cold end, more attention should be paid to reducing dead volume to improve cryocooler performance.

Table 6.2: Ratio of cold end dead to piston swept volumes

Total Dead Volume	Total Swept Volume	Dead/Swept Volume Ratio
[in ³]	[in ³]	[]
0.119	0.713	0.167

6.3 THE VALVE ASSEMBLY

The valve assembly consists of the inlet valve disk, the outlet valve disk, the spacer ring, and the valve bulkhead. The description and design of the valve disks is discussed in Chapter 2. The dynamic features of the valve bulkhead under pressure cycling and the role this part plays in valve sealing are described in Chapter 7. In addition, the valve spring action of the embedded permanent magnet array is discussed in Chapter 3. However, for completeness, a general description and images of the valve bulkhead and spacer ring are provided here in the context of their role in integrating the valves into the cold end. Both parts are made of non-ferrous metal so as not to disrupt the magnetic field generated by the cold end valves.

The spacer ring is a thin annular part that sits between the face of the outlet valve and the valve bulkhead in the expander space. A technical drawing of the ring is provided in Figure 6.15. The part's outer dimension allows it to fit loosely into the wall housing while its inner diameter provides the outlet valve disk just enough clearance to slip through without interference. The spacer ring has two primary functions. First, it keeps the outlet valve disk radially centered so the expander piston does not hit the valve disk during its stroke. Second, the spacer ring assures that the outlet valve lift cannot go below 0.010 inches because it provides a hard stop to the Indium squeezing process on the variable pressure seal if this threshold is reached.

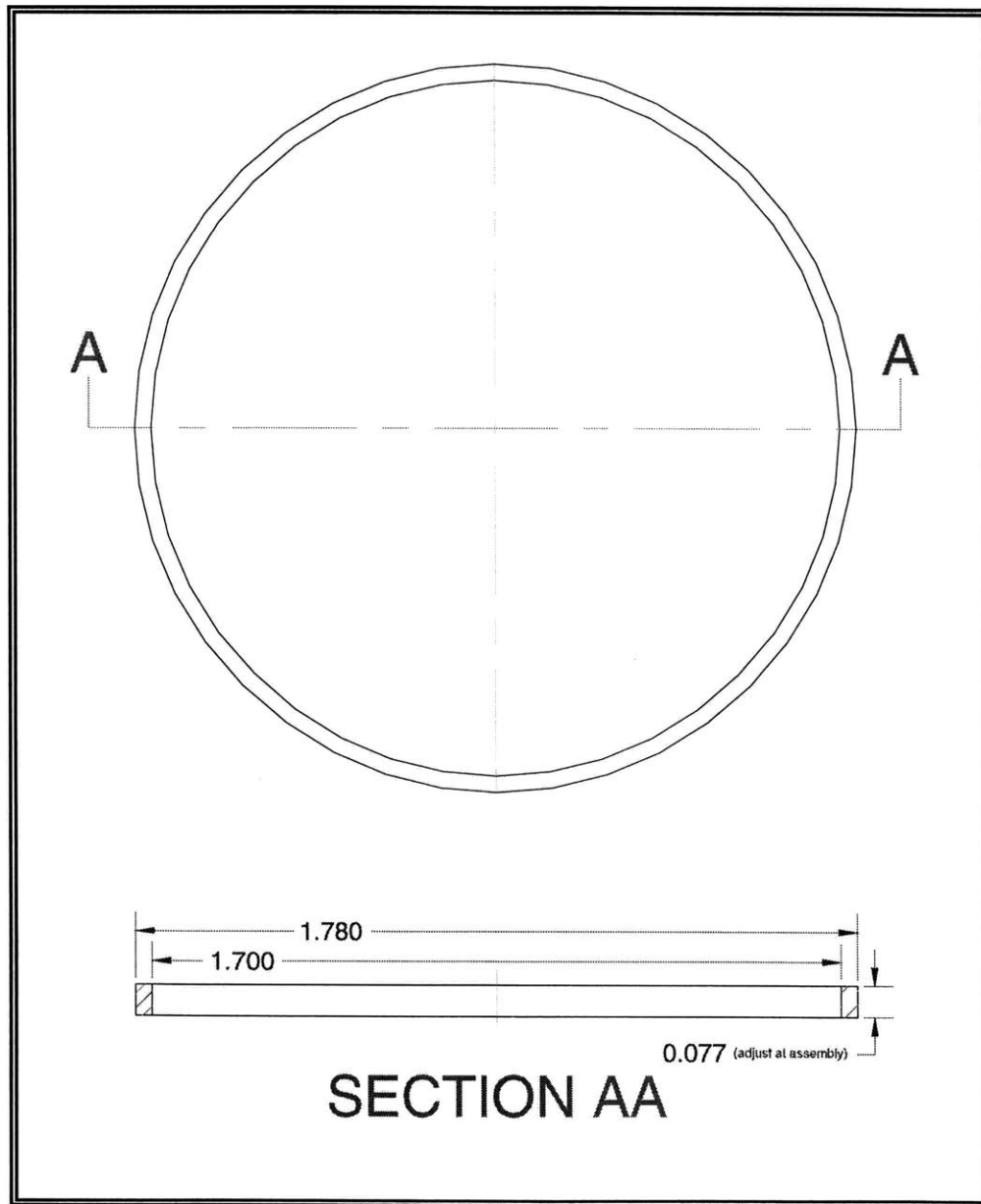


Figure 6.15: The height dimension of spacer ring can be adjusted by sanding to accurately regulate the minimum outlet valve lift

The valve bulkhead is a flat round disk that contains three inlet and three outlet valve ports drilled through it. A drawing of the bulkhead is given in Figure 6.16. This part's primary function is to maintain the pressure differential between the high-pressure assembly and the expander volume to assure no unwanted communication of working fluid occurs between the two. The valve bulkhead contains two sealing surfaces for Indium wire. One surface seals against the inlet valve housing component of the high-pressure assembly to maintain the high-pressure reservoir. The second opposing surface seals against a surface in the housing wall component of the cold end housing to seal the expander volume.

The bulkhead also supports 16 permanent magnets, eight on each side, that supply the closing force for the valves. The magnets are held in place by small dabs of epoxy placed in the magnet holes. The holes are machined to accommodate a good fit with the magnets. The magnets, along with the seats of the intake valve ports can be seen in the picture of the part in Figure 6.17. The valve seats are made of Kel-F plastic material and are held in place on the bulkhead by swages punched into the metal surrounding the seats.

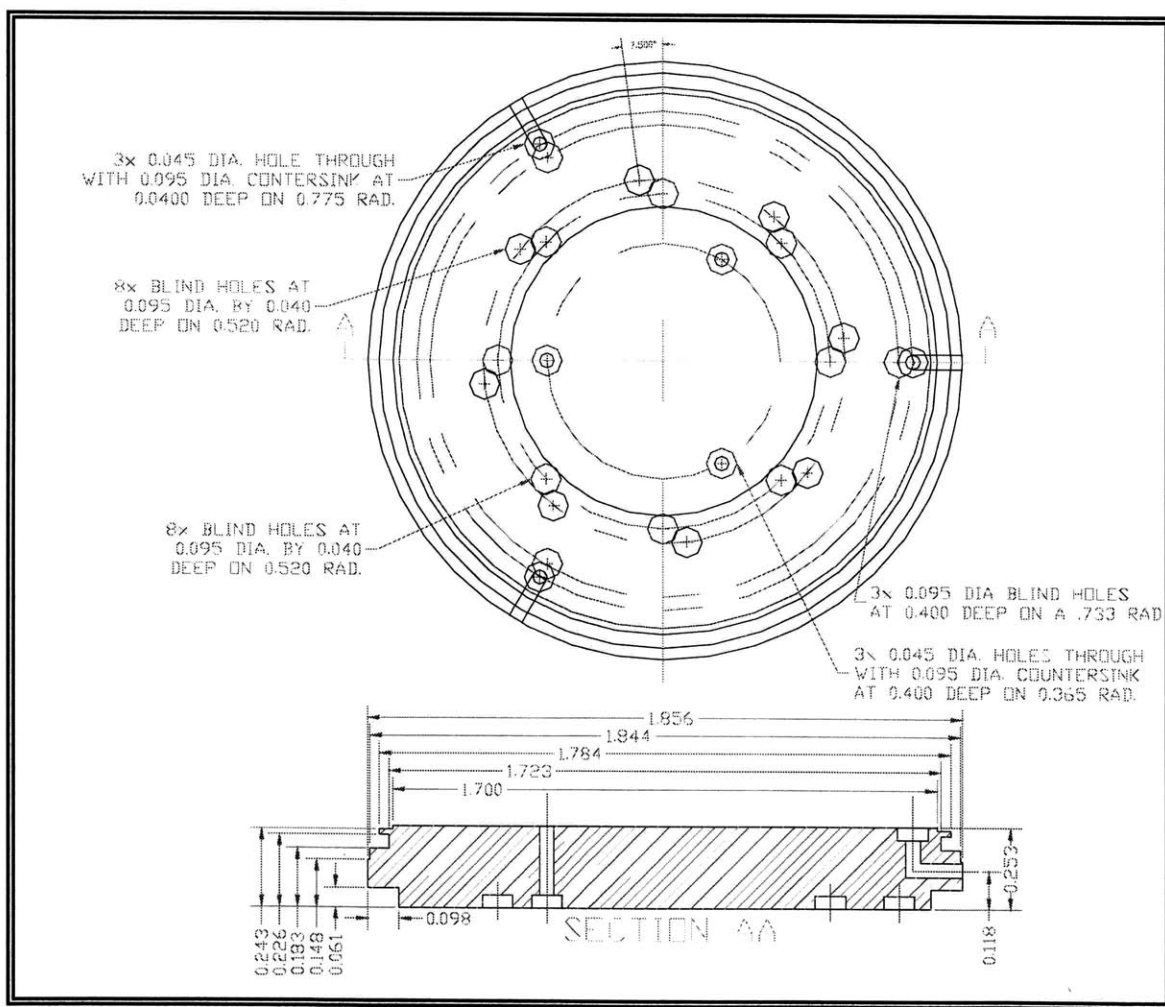


Figure 6.16: The valve bulkhead, which maintains pressure differentials the cold end, contains two sealing surfaces on opposing sides along its outer perimeter

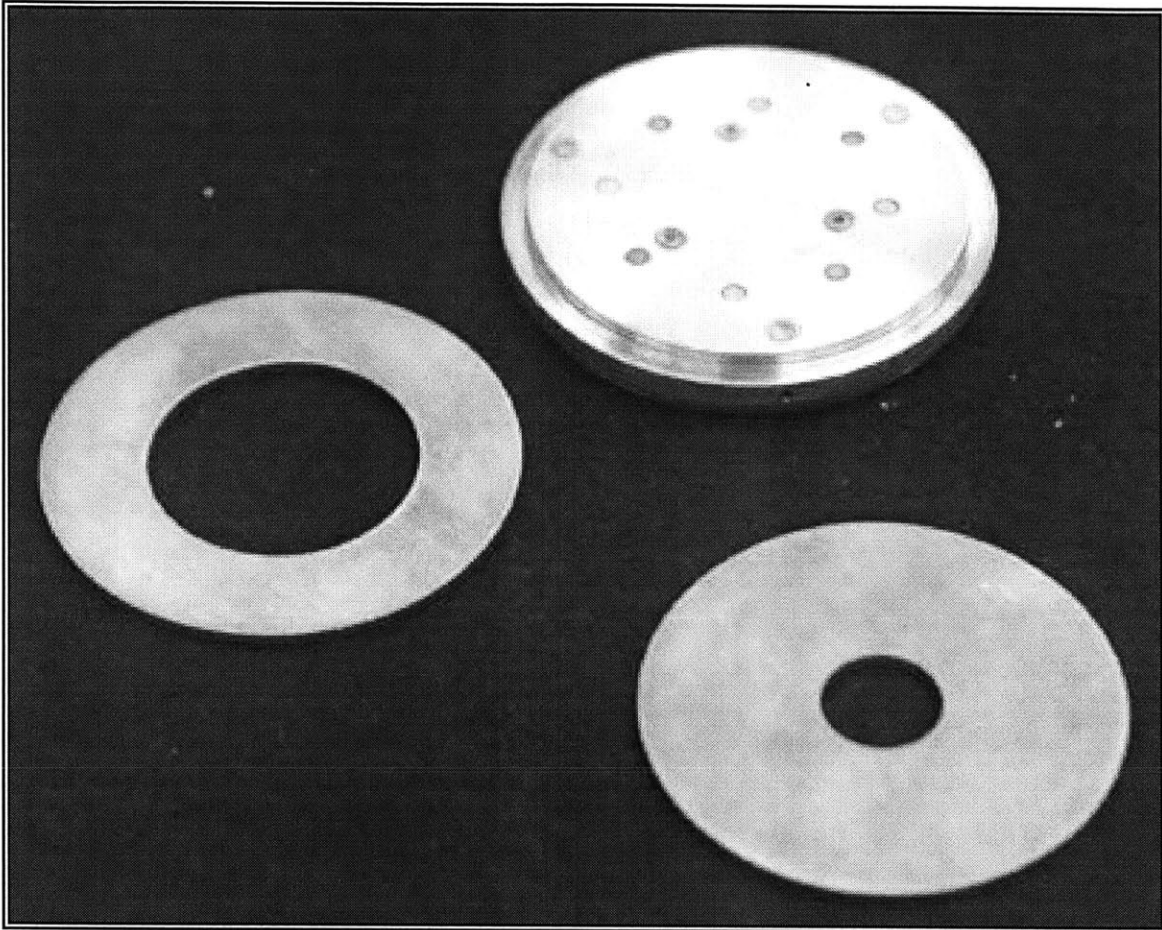


Figure 6.17: The valve bulkhead face that seals against the inlet valve is shown along with the polished sealing faces of both the inlet and outlet valves

6.3.1 Valve Seat Swaging Process

To assure the Kel-F valve seats stay affixed to the valve bulkhead, they are swaged in place by a pressure punching process that deforms the metal around the seats. After the seats are placed snugly within their holes in the valve bulkhead, the entire part is placed into the swaging fixture shown in Figure 6.18. This fixture allows the seats to be centered and clamped into place one at a time exactly below a punch of carbon steel.

Various subtly different punch geometries were tried to determine how to best swage the material. However, all the punches had the same basic features. They are cylindrical so as to fit within the swaging fixture, and they have flat ends, allowing them to be pushed evenly by a hydraulic press. The working end of the punches has a short protrusion that is hollow inside. It is wide enough to slip over the valve seat and contact the valve bulkhead's metal surface without damaging the seat. The working edge of the punch is tapered on the outside to create a sharp, metal-cutting surface. Two such punches are shown in Figure 6.19. Ultimately, it was found that punches fitting snugly around the Kel-F seats provide the best swage to hold the seats in place.

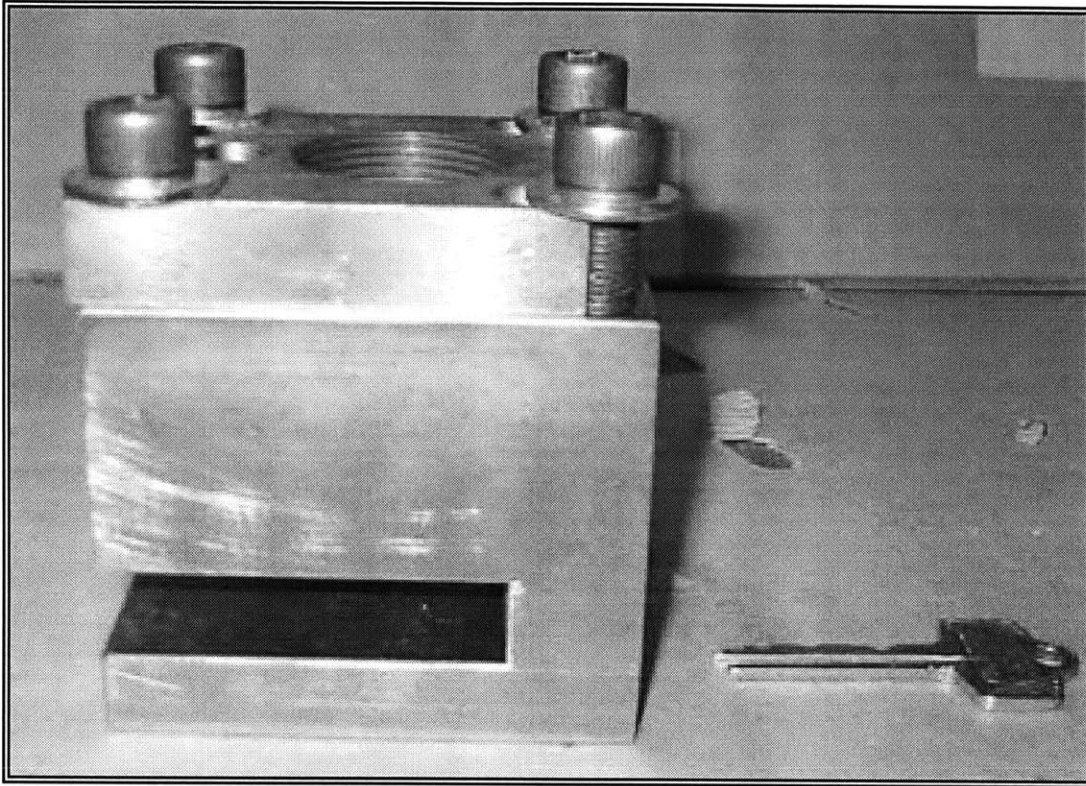


Figure 6.18: The punch fixture screws into the working end of a hydrologic press, generating the pressure required to deform and swage the metal around the seats

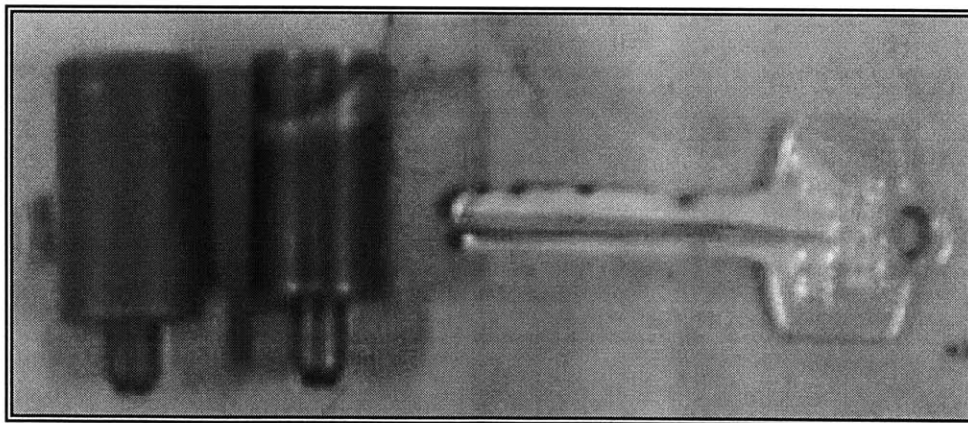


Figure 6.19: Two characteristic punches for swaging the Kel-F seats into the valve bulkhead are shown next to a key to demonstrate their scale

With the punch set over a seat to be swaged in place, a manually actuated hydraulic press is screwed into the threads atop of the swaging fixture. This press provides the pressure to cut and deform the metal around the seat so it bites into the Kel-F material, securing the seat in place. It was found that a pressure of 1500 pounds-per square-inch is ideal to cause swaging deformation, hydraulic pressures in excess of 2000 pounds-per square-inch damage the metal severely and distort the seat. Pressures less than 1000 pounds-per square-inch do not swage the metal enough to hold the seats in place. An image of the entire swaging apparatus is given in Figure 6.20.

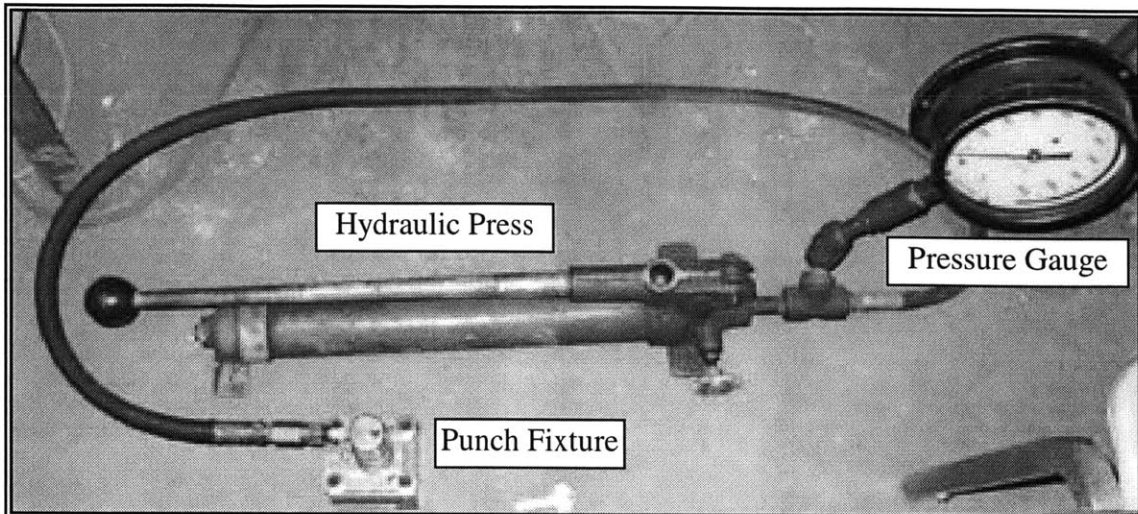


Figure 6.20: The manually actuated hydraulic press contains a gauge so the user can ascertain how much pressure is being applied during the swaging process

All seats on the valve bulkhead are swaged in succession. Once the swaging process is complete, it is important to ream out each valve port hole to assure the holes are the proper diameter after the swaging distortion.

6.4 FABRICATING INDIUM SEALS

All of the static seals in the cold end are created using gaskets of Indium metal. Indium, a pure element with atomic number of 49, is a very soft, silvery-white metal with a brilliant luster. A primary feature of the metal is its low melting point, 429.81 Kelvin. This property makes the material very malleable at room temperature and allows it to deform and flow easily when put under pressure. Indium also shows some affinity for sticking to steel surfaces.

Indium gaskets are used almost exclusively in experimental cryogenic machines because they have been shown to provide good sealing against cryogenic nitrogen and helium at very low temperature. Indium seals are formed by placing a gasket between two smooth surfaces and pushing the surfaces together under pressure. Most of the Indium squeezed out from between the two parts, but thin layer, on the order of 0.003 inches, remains adhered to the surfaces, creating a pressure-tight seal.

Normally, Indium is used to seal vessels about a foot in diameter. These applications require gaskets made of Indium wire about 0.25 inches in diameter. However, the cold end of the machine described in this paper requires seals for components about 2 inches in diameter. Thus, a process of extruding Indium wire at 0.020 inches in diameter was developed. Figure 6.21 shows a spool of Indium wire with a nominal diameter small enough to be utilized for seals in the cyocooler.

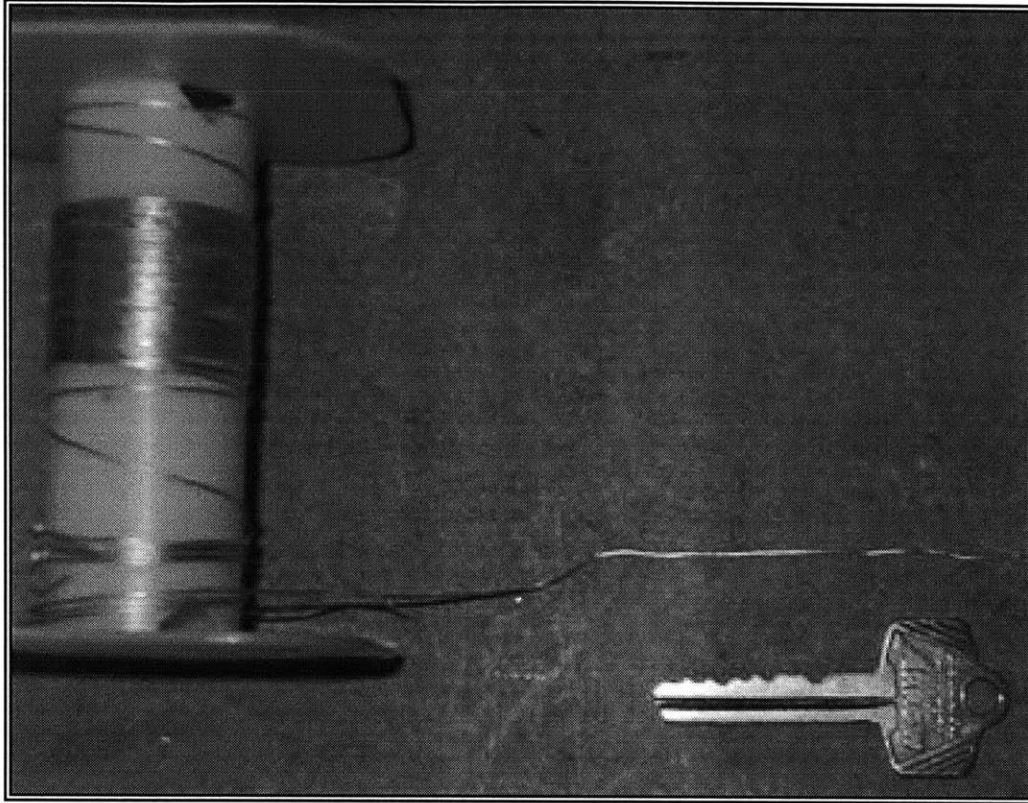


Figure 6.21: This spool of 0.020-inch diameter Indium wire was manufactured by extrusion.; one standard slug of Indium is enough for many feet of wire

This thin Indium wire is fabricated by extruding a slug of Indium using a die and a press. The slug is made by pouring molten Indium into a Teflon mold and allowing the metal to cool. The cooled cylindrical plug is then forced down a hole in the press assembly by a carbon steel pin. Screwed onto the working end of the press is a brass die with a 0.020-inch-diameter hole in the end. A close-up image of the die is presented in Figure 6.22.

The entire Indium extruder assembly is placed between the jaws of a standard bench top vice, and the vice is very slowly clamped down upon the extruder, as shown in Figure 6.23. The vice pushes the carbon-steel pin against the slug of Indium and causes a small wire of the metal to squeeze out of the die. The wire is protected from dirt by a paper towel laid over the vice. Once enough Indium has been squeezed out of the extruder, it can be wrapped onto a spool for storage.

It was found that the extrusion process happens very slowly, but the vice must be retightened periodically to assure continuous pressure remains on the Indium plug. It was also found that if too much pressure is applied, the Indium wire comes out too rapidly and begins to curl over on itself, making that stretch of wire useless for making seals.

The gaskets themselves are made by wrapping the extruded wire around a pre-machined groove in the sealing surface. The wire ends are crossed over, squished together until they stick, and then the excess is cut away with a sharp blade. The gasket is then ready to be squeezed between two sealing surfaces.

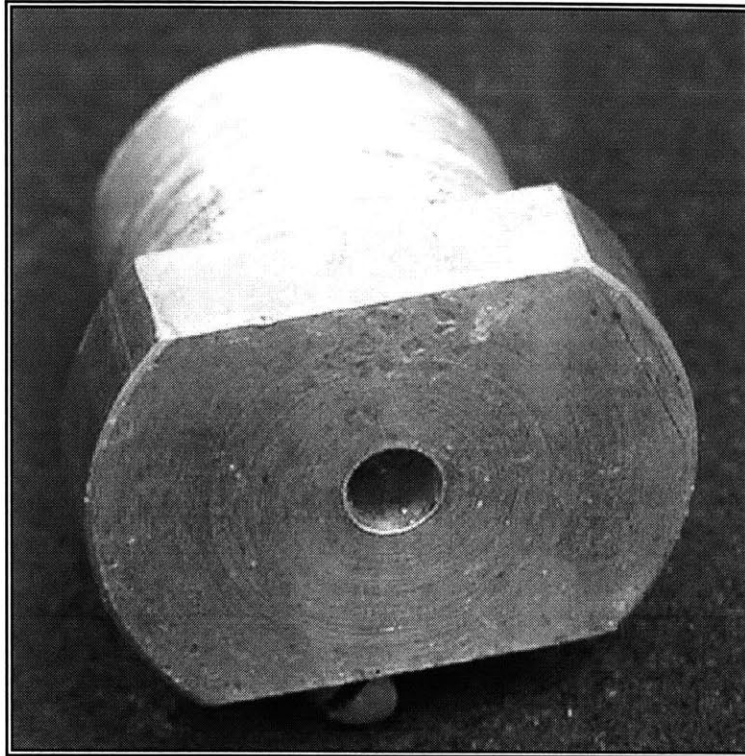


Figure 6.22: The exit hole in the die contains a 0.020-inch inner hole that sets the ultimate diameter of the wire

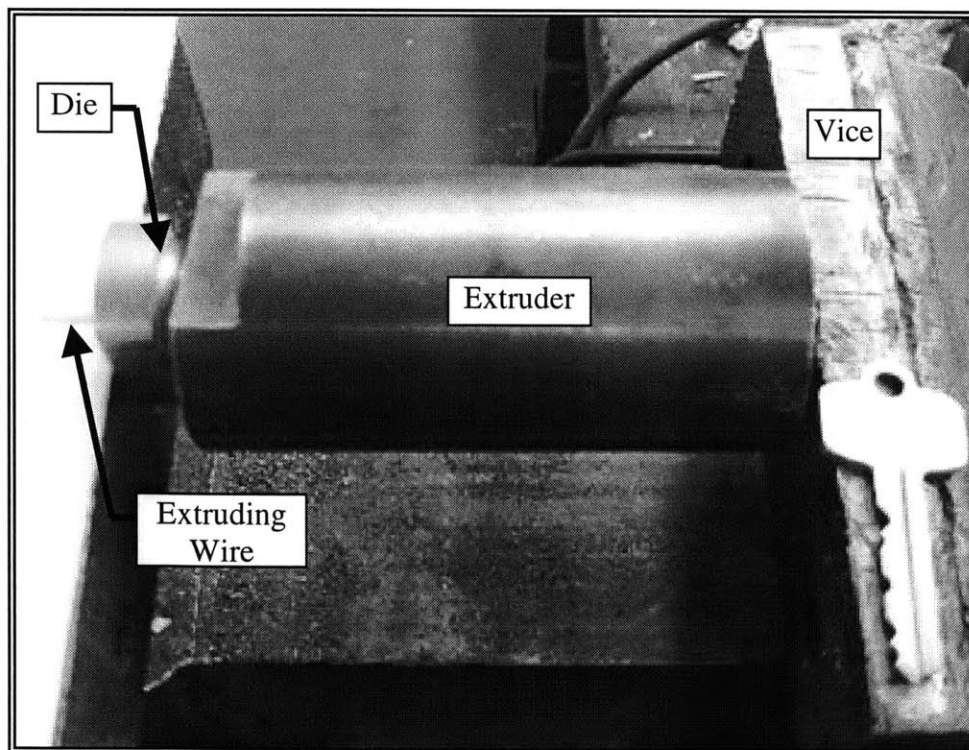


Figure 6.23: The assembly is clamped into a vice and squeezed; a strand of wire can be seen extruding out of the die on the left side of the image

7.0 VALVE DYNAMIC OPERATION

As the cold end operates, the valves experience a complex set of coupled internal dynamics as well as interactions with other components of the cryocooler. These multiple aspects of total operation can be broadly broken into a set of constitutive processes. Each process can be explored and characterized individually to enhance understanding of the total operation. These processes include mechanical dynamics; electromagnetic dynamics; thermodynamics, material stressing, compression, and deflection; fluid dynamics; and tribology.

It is important to note that although the dynamic processes are being treated individually here, they all interact in the context of the total operation of the system. The lack of coupling analysis is not meant to suggest that these interactions do not exist. Instead, the simplified, first-order analyses presented here represent bounding cases for the true behavior and effects of these complex interrelations.

7.1 VALVE DISK DYNAMICS AND OPERATIONAL TIME SCALES

To engender the proper flow of working fluid through the cold end, the valve disks must traverse a path that repeats once every cycle. In the starting position, a valve disk is sealed against three valve ports. It is pulled down onto the valve seats by button magnets embedded in the valve bulkhead acting like a valve spring. In most cases, the valve disk is also being pushed in the same direction by the pressure differential of the working fluid acting through the valve ports.

When it is time for a valve to open, a command current signal energizes the valve coil. Magnetic flux lines emanating from the valve coil link the valve disk to the valve yoke. This linkage generates a new force on the valve disk that overcomes the preexisting components. The valve disk begins to move towards the valve yoke. The valve disk traverses a 0.010-inch lift gap as working fluid rushes past it through the open valve ports. The gap is characterized by a magnetic field of increasing magnitude in the direction of the valve yoke. As the valve disk nears the valve yoke, this increasing field accelerates the valve disk faster. The movement of the valve disk towards the valve yoke also increases the inductance of the magnetic circuit, slowing any dynamic transients inherent in the electromagnetic processes.

The valve disk touches the valve yoke. Its kinetic energy is converted into potential energy deforming both parts. Under minute damped oscillations of both components, the valve disk is decelerated to rest. It remains there by virtue of a holding magnetic field induced through the valve yoke. When the time comes for the valve to close, the magnetic field is relaxed. The force induced by the button magnets on the valve disk again dominates, and the valve disk traverses the gap in the opposite direction. Coming to rest atop the valve seats, which deform to bring the valve disk to rest. The valve disk seals against the seats, and backpressure begins to build. This entire process is repeated once every second, at the cycling rate of the cold end.

Two important considerations arise when examining the valve disk excursion. First, it is significant to know how long the disks take to traverse the 0.01-inch gap to assure that the valves' mechanical action is much more rapid than the rate of the cycle. Second, the velocity with which the valve disks impact the valve seats when the valves close is important for considerations related to valve seat lifetime.

These two quantities can be determined simultaneously through a solution of Newton's second law applied to a single valve disk represented in the free body diagram, Figure 7.1. In general, the force induced on the valve disk by the valve yoke is a function of valve disk position, X , and valve coil current, I . In turn, both these variables are functions of time. These features are encompassed in Newton's second law, Equation 7.1

$$F(X(t), I(t)) = m \frac{dV}{dt} \quad (\text{Equation 7.1})$$

$$X(t) = X_o + Vdt$$

For this analysis, it is assumed that valve coil current is held constant. This assumption approximates the real situation because a sophisticated power supply, which is described in Section 7.4.1, has been built to meet this specification.

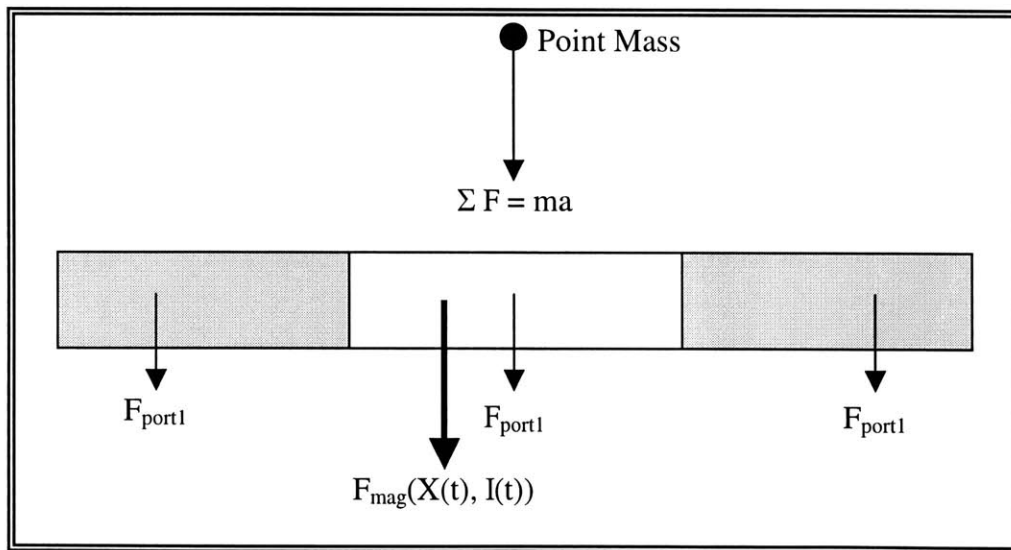


Figure 7.1: All of the forces imposed on the valve disk are encompassed in this simple free-body diagram force model

The solution to Equation 7.1 can be approximated by a stepwise solution where tiny iterative time steps are plugged into a discrete version of the equation. The system is then solved with values from the previous iteration to develop a new set of values. The process repeats from the initial conditions until enough time steps have elapsed for the valve disk model to traverse the 0.010-inch air gap. The related final values for time and disk velocity are recorded. Equations 7.2a and 7.2b, a modified version on Equation 7.1, are designed to carry out this iterative approach.

$$\Delta V_n = \frac{F(X(t)_n)}{m} \Delta t \quad (\text{Equation 7.2a})$$

$$V_{n+1} = V_n + \Delta V_n$$

$$\Delta X(t)_n = \Delta V_n \Delta t \quad (\text{Equation 7.2b})$$

$$X(t)_{n+1} = X(t)_n + \Delta X(t)_n$$

The most complex step in executing Equations 7.2a and 7.2b is determining the force exerted on the valve disk as a function of the disk's position in space. Section 5.2 shows that a series of surfaces can be developed using Quickfield, a finite element software model, to represent the force induced on the valve disk at various valve coil input currents. Each surface represents the valve's performance for a different combination of the valve's characteristic geometric tolerances. Ultimately, an upper limiting case and a lower limiting case are identified that effectively bound the recorded data. These bounds are curves representing the maximum and minimum force that can be applied to the valve disk when it is seated on the valve ports for any value of input current from 0 to 110 amp-turns.

Once these force-bounding models are identified, they can be exercised in Quickfield to develop curves for force imposed on the valve disk as a function of the disk's position. To generate these curves, the valve disk within the models is moved to a number of positions along its travel. The finite element simulation is used to return the static force imposed on the valve disk at each of these points. These data are used to generate a pair of bounding curves representing the force imposed on the valve during its travel.

Unlike the static test models described in Section 5.2, the valve simulations utilized here incorporate the permanent magnet model discussed in Section 3.4. The permanent magnets induce a force on the valve disk against the greater pull of the valve yoke. The permanent magnet model is utilized in this simulation because the magnets are present in the actual machine and have an effect on the valve's performance. These finite element simulations incorporate all the magnetic forces the valve disks experience in the actual machine. The value of the finite element code for this modeling exercise becomes apparent because the analytical quadratic relationship that exists relating force to distance is obscured by at least two factors. First, there is non-ideal leakage of flux detracting from the force imposed on the valve disk. Second, the superposition of the permanent magnets' field with the field of the valve yoke creates a force field of complex geometry that would be difficult to model analytically.

The force verses position curves generated through this modeling process are translated into continuous equations using a polynomial least squares fit approximation. The data points and the accompanying trend line equations are presented in Figure 7.2.

With reliable bounding equations for the force generated on the valve disk as a function of position, the iterative solution process is carried out using a simple code. The resulting spreadsheet is included in Appendix D of this document. As with any discrete iterative process, the accuracy of the result increases as the size of the iterative step decreases. Step sizes ranging from 0.0005 seconds to 0.000001 seconds were utilized to confirm the solution converged as the step size decreased.

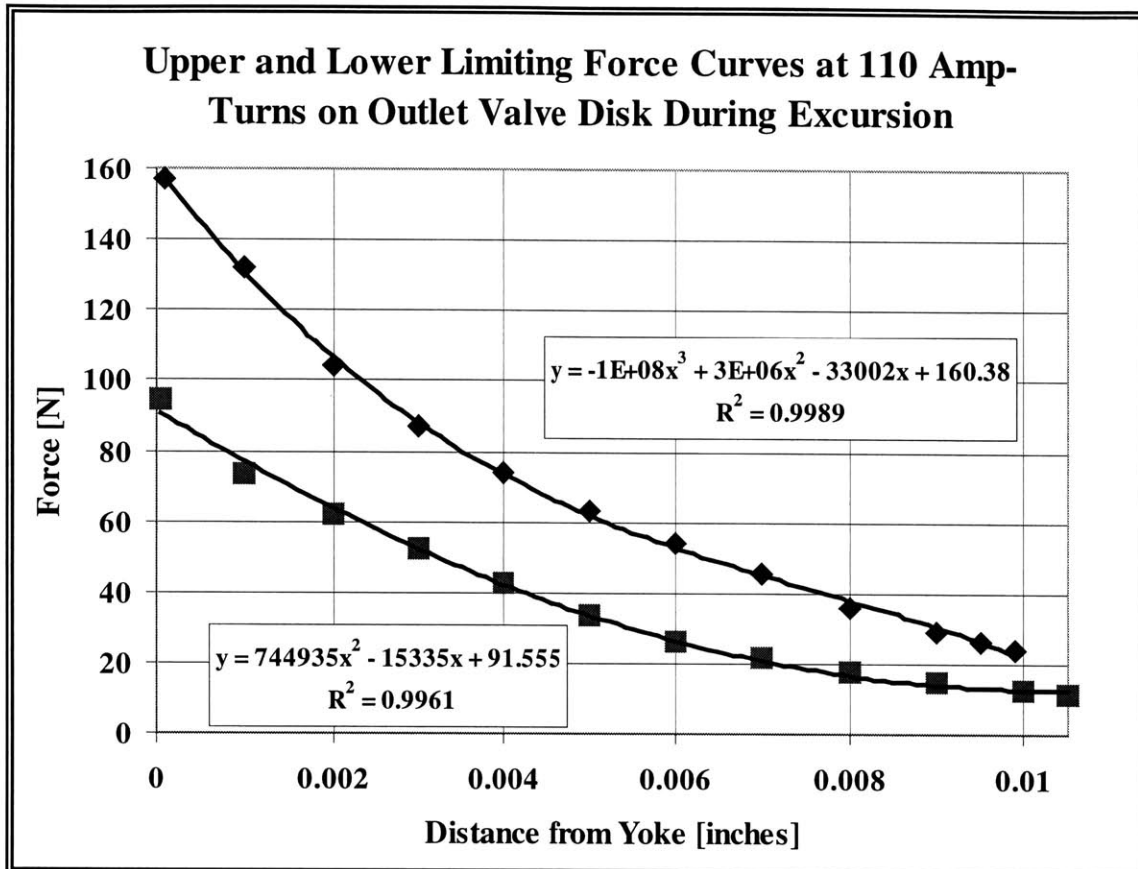


Figure 7.2: Upper and lower force bounds on the valve disk by the valve yoke's magnetic field show how force increases as the valve disk nears the valve yoke

The results of the iterative model are presented in Table 7.1 for the two finest step sizes utilized. At these small step increments, the total duration of valve movement has converged to three significant figures and the final disk velocities for each step size vary by less than 0.5 percent. This analysis shows that the travel time of the disk is bound between 2.27 and 3.37 milliseconds, which is much faster than any other mechanical process in the cycle. The final velocity of the disk is bound by 12.13 and 9.12 meters-per-second. The implications of these bounding valves are important when considering the impact pressure of the disk and the lifetime of the valve seats on the valve bulkhead.

Table 7.1: Bounding values on valve dynamic timescale and velocity

	Upper Limit		Lower Limit	
Time Step	Total Duration	Final Velocity	Total Duration	Final Velocity
[seconds]	[seconds]	[meters/second]	[seconds]	[meters/second]
5.0E-06	0.00227	12.17	0.00337	9.13
1.0E-06	0.00227	12.13	0.00337	9.12

7.2 VALVE SEAT SEALING EFFECTIVENESS

The inlet and outlet valve ports rest in the center of Kel-F plastic buttons embedded into the valve bulkhead. There are three ports associated with each valve. Proper sealing of the valve ports occurs when the valve disk comes into contact with the entire surface area of each valve seat. This condition means that the valve port itself is completely covered by the valve disk and the valve seat is experiencing a small level of elastic deformation under compression.

The valve disk, the valve seats, and the valve bulkhead are all significant components in assuring good valve port sealing. The valve seats experience dynamic elastic deformation as a favorable side effect of the sealing force applied from the valve disk. The valve bulkhead also experiences dynamic elastic deformation cycling resulting from the pressure difference it supports between the high-pressure reservoir and the variable pressure assembly. These pieces were designed to accommodate minimum valve port leakage. In the current configuration, there are three possible ways the valve ports could fail to seal owing to dynamic excursions.

If the valve ports fail to create a flat plane for the valve disk to seal upon, it is possible for the valve disk to sit cocked in some alternate plane and fail to cover all of the valve ports correctly. Designing only three valve ports for each valve eliminates the possibility of this situation because these three points make up the only plane on which the valve disk can come to rest.

The valve bulkhead could elastically bow so that its center interferes with the valve disk as is shown in Figure 7.3. In this case, the center edge of the annular valve disk must strike the valve bulkhead before the sealing face of the valve disk reaches the valve ports. This valve bulkhead bowing direction can only be experienced with the outlet valve because of the direction of the pressure gradient supported by the valve bulkhead. However, because the outlet valve disk is annular with large inner radius, a deflection of this type would cause a sealing failure only if the deflection was very large; on the order of 0.01 inches. Deflections this severe would introduce much more serious structural problems than a sealing failure. The valve bulkhead has been designed with enough thickness to prevent such severe bowing.

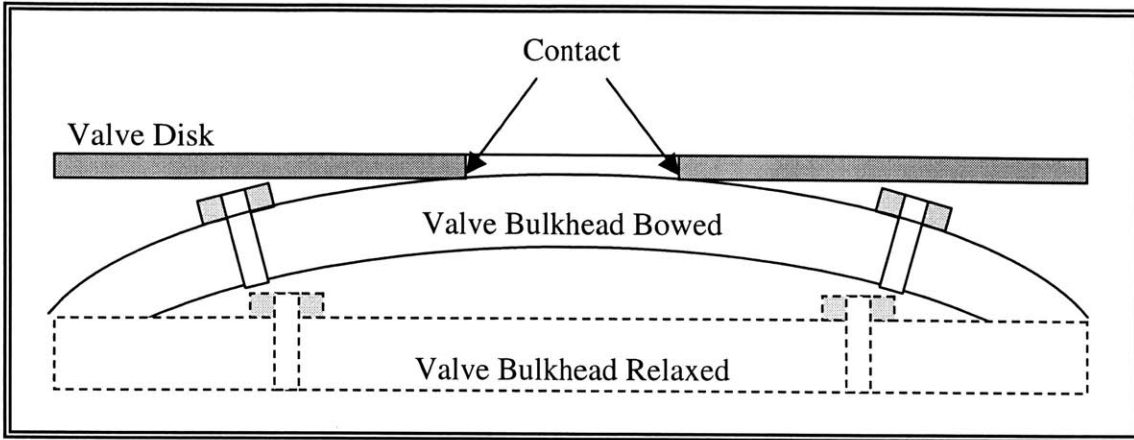


Figure 7.3: Bowing with its center upwards, the valve bulkhead contacts the valve disk retarding sealing. This type of contact can only occur with the outlet valve

The valve bulkhead could also elastically bow with its center inwards causing the outer edges of the valve disk to strike the outer radius of the valve bulkhead before the disk reaches the valve seats. This situation can only happen with the inlet valve because the pressure differential across the valve bulkhead always forces it to bow center down with respect to the inlet valve disk. In addition, the inlet valve seats are placed toward the center of the valve bulkhead where the deflection is more pronounced than on the outer radius.

In the prototype cold end, three bumpers were placed on the valve bulkhead at a radius outside the inlet valve ports. These bumpers were placed to prevent the valve disk from cocking when it seated, and they were lapped a few thousandths of an inch shorter than the valve seats to prevent interference with sealing. However, as shown in Figure 7.4, a sealing failure by center inward bowing of the valve bulkhead is exacerbated by the presence of the bumpers.

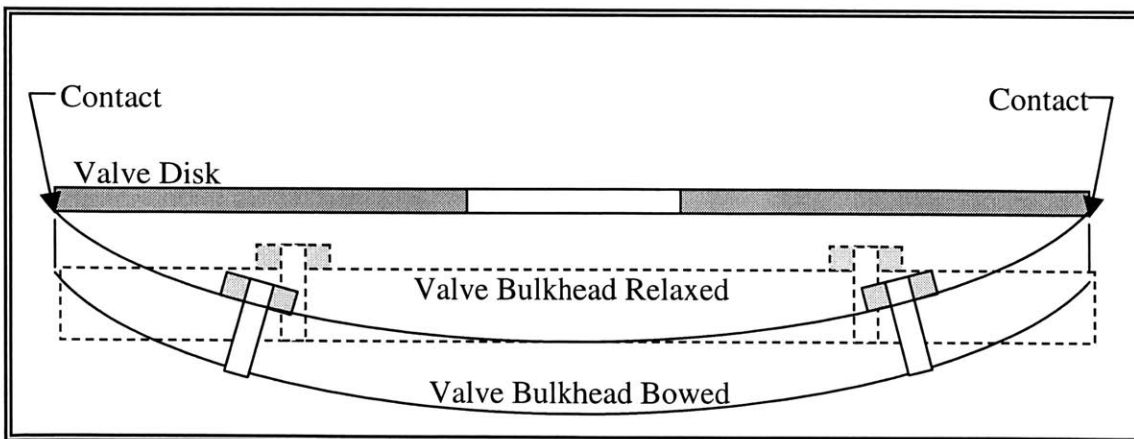


Figure 7.4: Bowing center downwards, the valve bulkhead pulls the inlet valve ports away from the valve disk, causing it to rest instead on the edge of the outer radius

A third sealing failure mode localized on the scale of the valve seats is also possible. Since the valve seats are embedded in the valve bulkhead, the bowing of the valve bulkhead causes the plane created by the valve seats to bow. In this situation, the valve disk impacts the valve seats at an angle severe enough that proper sealing does not occur. This situation is shown in Figure 7.5. This failure mode can occur both on the inlet and outlet valve sides of the valve bulkhead, but it is more likely to occur on the outlet valves because of their larger radial placement.

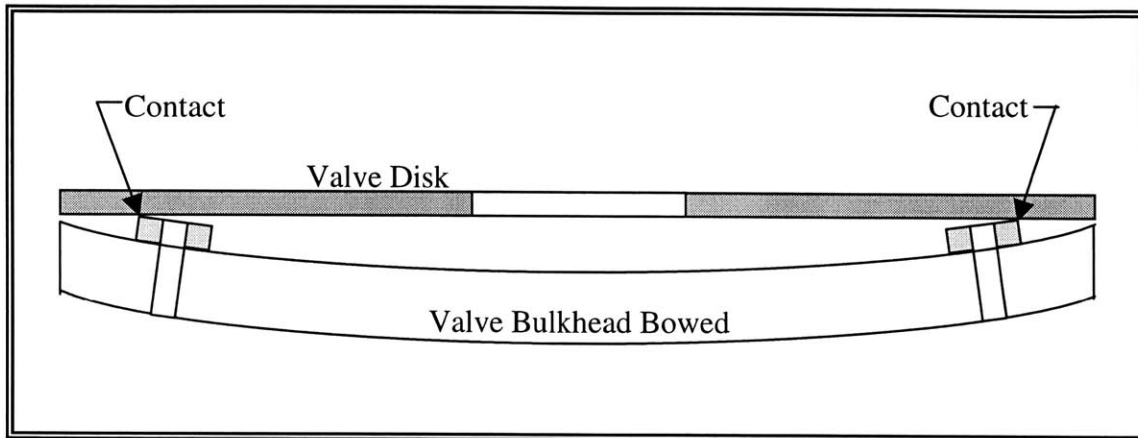


Figure 7.5: Bowing of the plane connecting the valve seats causes the valve disk to rest at an angle with respect to the seats, creating a localized leak

7.2.1 Valve Bulkhead Deflection Analysis

To determine whether any of the deformation sealing failure modes will occur during normal operation of the cold end, a deflection analysis is required. Using a standard model for static deflection, it is possible to estimate the extent of dynamic bowing of the valve bulkhead. The literature¹⁰ contains a set of mathematical models for metal plates and cylinders undergoing various types of loading. The results of these models can be superimposed to build up an accurate model of the static deformation for any complex set of loading conditions.

For the valve bulkhead model, the following loadings need to be superimposed: 1) uniform high pressure on the circular area enclosed by the high-pressure assembly; 2) low pressure on the area radially outward of the high-pressure assembly; 3) clamping pressure at the location of the high-pressure seal; and 4) variable pressure on the expander side of the valve bulkhead. To simplify the analysis, it is assumed that the valve bulkhead is a solid cylinder, and the various ports, magnet holes, and sealing groves are ignored. It is also assumed that all of the pressure loadings described above are bearing down against a simple support on the outer radius of the opposing side of the disk, representing the variable pressure space seal. To build up this loading profile, a set of simpler loads is superimposed through the summation described in Figure 7.6.

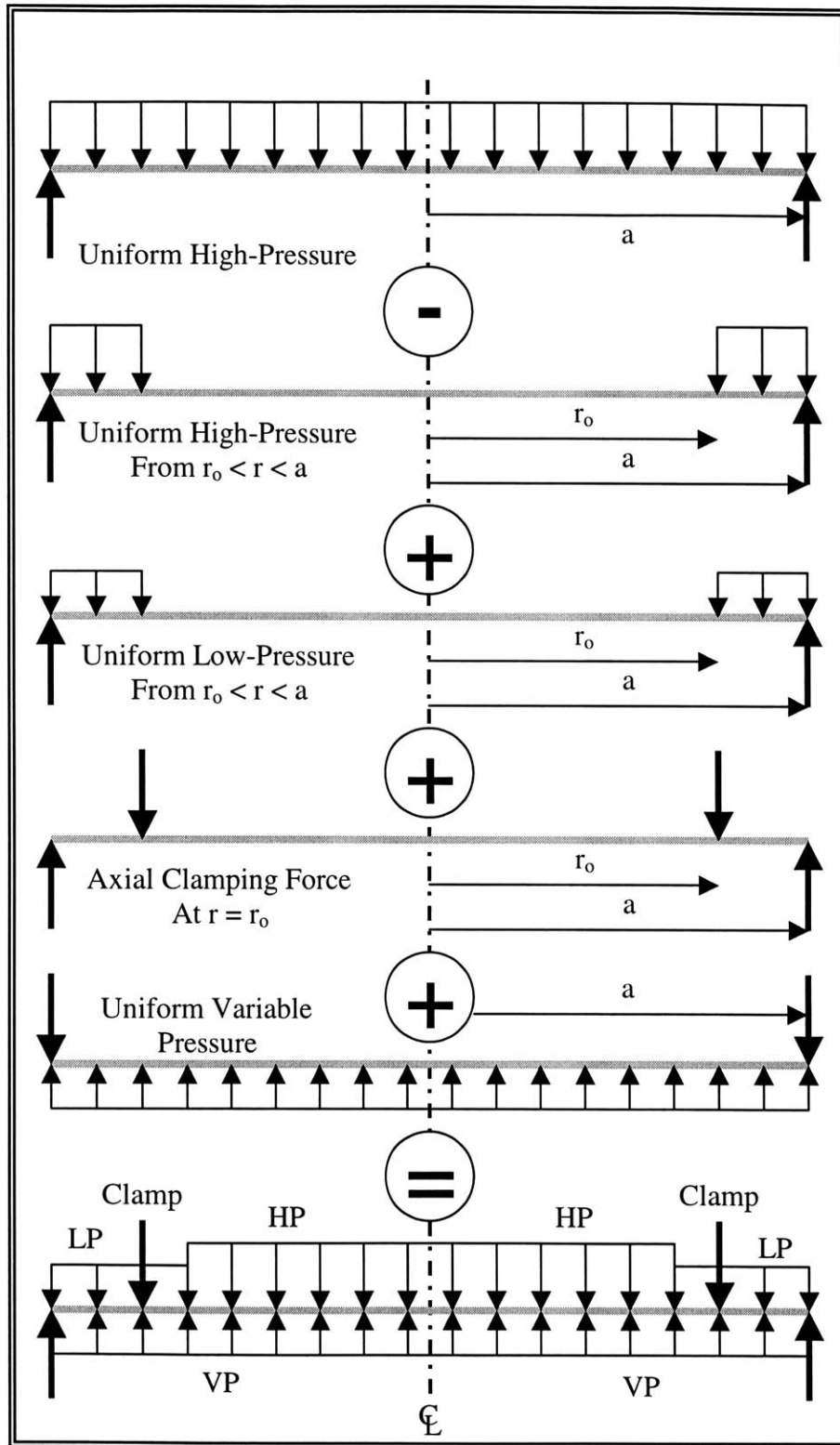


Figure 7.6: These five simple load cases must be mathematically superimposed to generate the final valve bulkhead load profile

The superposition model was encoded in a Microsoft Excel spreadsheet, which is provided in Appendix E of this document. The model was exercised through a range of discrete variable pressure values at increments of 25 pounds-per-square-inch. The range of variable pressure differentials, 10 pounds-per-square-inch through 250 pounds-per-square-inch, is representative of the pressure excursion the valve bulkhead will experience through one complete expander piston cycle.

The valve bulkhead load model returns the magnitude of vertical displacement at 21 discrete, independent, equally spaced locations from the center of the valve bulkhead along a radial straight line to the outer edge. Microsoft Excel is used to create smooth, continuous lines between these points, approximating the displacement of the valve bulkhead surface. Figure 7.7 provides a graphical representation for this series of results. If swept 360 degrees to create a series of symmetrical surfaces of rotation, these curves represent the approximate shape of the valve bulkhead surface for various pressure differentials across it. While the valve bulkhead will always be slightly deflected owing to the clamping force applied to it to crush the Indium seals, the maximum static deflection it can experience in this machine is about 0.0003 inches at the center.

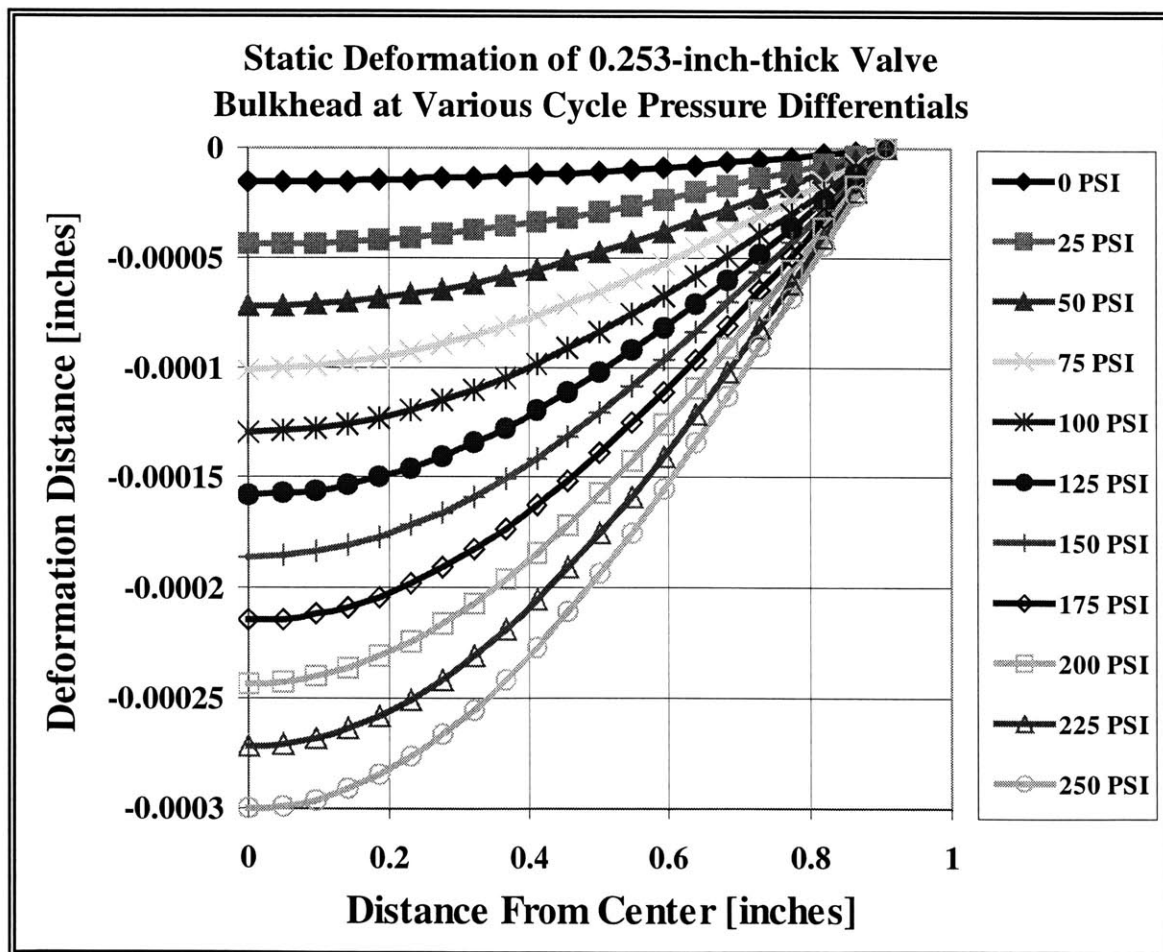


Figure 7.7: The static deformation shape of the valve bulkhead is predicted for a variety of pressure loads experienced during one piston expander cycle

The static analysis may only provide a partial picture of the valve bulkhead deformation. It is also important to look at the dynamics of the valve bulkhead deformation to assure the excursion of the plate is not dramatically increased by resonance with the driving force. In the dynamic regime, the valve bulkhead can be thought of as a thick circular plate oscillating at its fundamental frequency. For this type of oscillation, this geometry has an approximate natural frequency given by Equation 7.3⁸ where Y is the material's Young's modulus, ρ is the density, h is the part's height, and a is the outer radius.

$$\omega^2 = \frac{320}{9} \left(\frac{Y}{\rho} \right) \left(\frac{h^2}{a^2} \right) \quad (\text{Equation 7.3})$$

The driving force of the system is the variable pressure exerted on the valve bulkhead by the expander at a frequency of 1 Hz. In this first-order dynamic analysis, three types behaviors are possible. If the driving force is much lower than the valve bulkhead's natural frequency, the part will deform exactly as indicated in the static analysis. If the driving force is much higher than the natural frequency of the valve bulkhead, the part will deform to a static shape indicative of the time-averaged value of the pressure variation. If the driving force is nearly equal to the natural frequency of the valve bulkhead, the amplitude of deformation deflection will grow dramatically larger than suggested in the static case, and further analysis is required.

Using Equation 7.3, it is estimated that the natural frequency of the plate is about 8.7×10^4 Hz. Thus, the driving frequency is low enough that the valve bulkhead effectively deforms exactly as described by the static analysis. Given this result, the analysis indicates that the valve bulkhead will not deform vertically more than 0.0003 inches at its center. Since the valve seats stand 0.010 inches proud of the valve bulkhead, sealing failures due to valve disk-valve bulkhead impact will not occur. In addition, provided the inlet valve buttons are lapped more than 0.0003 inches shorter than the inlet valve seats, the buttons will not interfere with proper sealing. The disruption of the flat plane associated with the three valve seats created by the bending of the valve bulkhead does, however, merit additional analysis.

7.2.2 Valve Seat Deflection and Sealing Analysis

The valve seats are affixed to the surface of the valve bulkhead that dynamically bows with every pressure cycle. However, the valve seats are supposed to seal against a valve disk that is perfectly planar. This mismatch causes the valve disk to impact one edge of the valve seat before impacting the other edge. If the seats do not deform enough to allow the disk to come in contact with the entire surface of the valve seat, proper sealing will not occur. This situation is shown graphically in Figure 7.8.

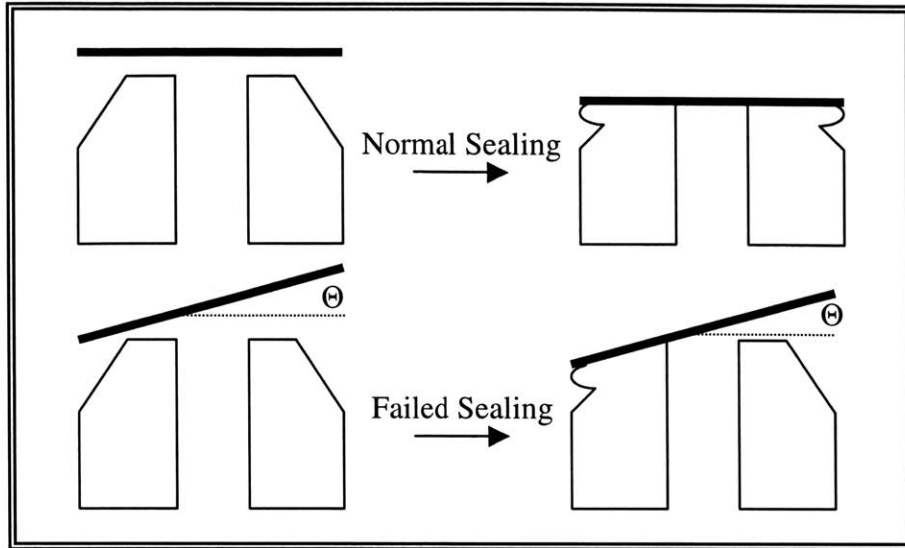


Figure 7.8: Proper valve port sealing juxtaposed against a leaking valve port demonstrates the importance of valve seat deformation

To build an analysis describing this type of sealing failure, the main variable is the slope at which the valve bulkhead is bending at the particular radial location of the valve seats. The greater the local slope, the more compliant the valve seat must be to assure proper sealing with the valve disk. Figure 7.9 demonstrates how severe valve bulkhead deformation slope can cause a sealing failure on the scale of a single valve port. In this case, the height g , the space between the valve seat edge and the valve disk, is substantial.

The static deformation analysis described above was utilized to estimate the slope of the surface of the valve bulkhead at various radial locations from the center to the outside edge. Figure 7.10 shows the slope deformation of the model for various characteristic pressures at increments of 25 pounds-per-square-inch.

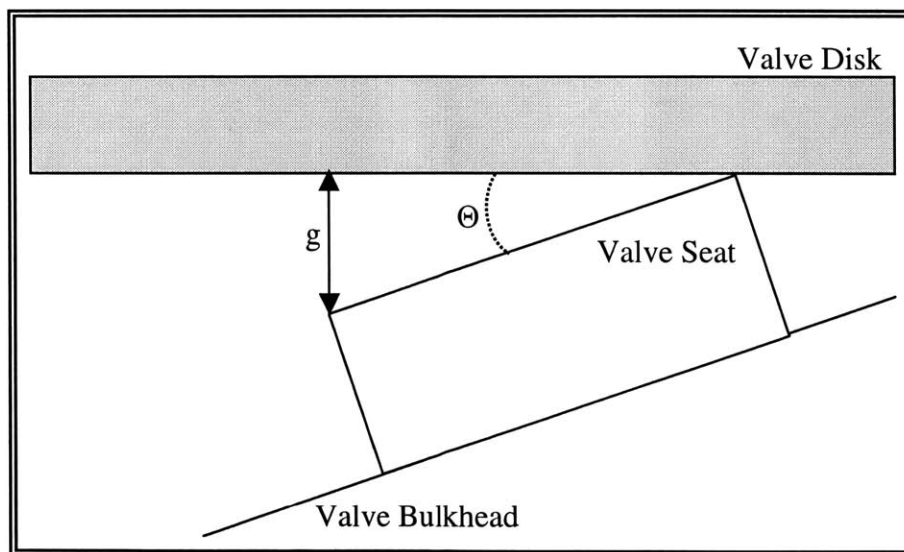


Figure 7.9: If the contact angle between the valve seat and the valve disk is severe, leakage occurs as characterized by the gap length, g

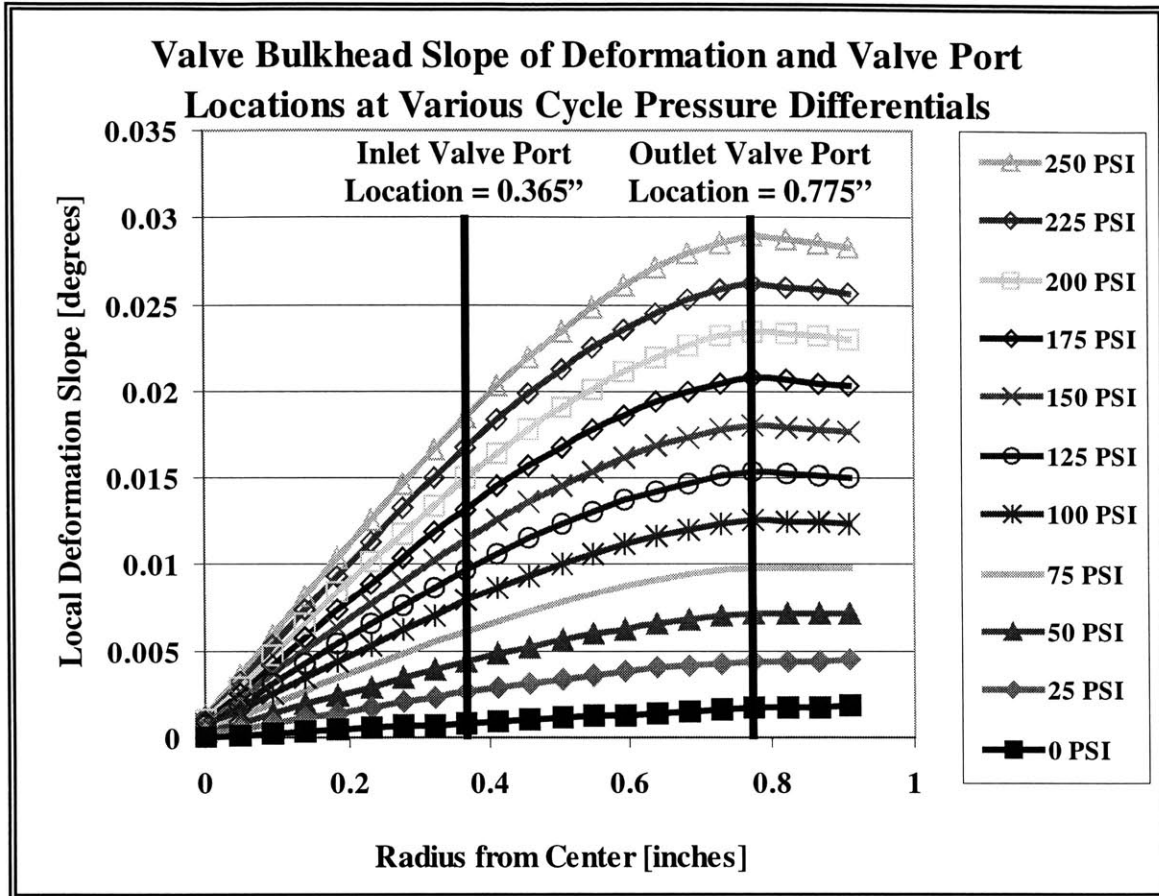


Figure 7.10: The radial locations of the valve ports with respect to the valve bulkhead deformation slope dictate the compliance the valve seats require to seal properly

The slope information guides the bounds of this analysis. With the reservoir pressure at a constant 265 pounds-per square-inch, the highest deformation slope occurs in the vicinity of the outlet valve port radius when the variable pressure space is discharged to 15 pounds-per square-inch. This situation represents a pressure differential across the valve bulkhead of 250 pounds-per square-inch. These conditions present the worst possible combination of sealing parameters, and it is assumed that if successful sealing is achieved for this case, all other cases will demonstrate effective sealing.

The deformation magnitude of a single valve seat for a particular input force can be approximated using Hooke's law, Equation 7.4, where F is the imposed force; A is the contact area; Y is the Young's modulus, taken for Kel-F at 10 Kelvin; L is the uncompressed length of the material, and δ is the deflected length of the material. The variable Y is fixed by the selection of Kel-F as the material, and the variable L is fixed by the geometry of the valve seats.

$$F = \left(\frac{AY}{L} \right) \delta \quad (\text{Equation 7.4})$$

The valve seats are at an angle with respect to the valve disk owing to the valve bulkhead slope. Thus, the contact area, A , is not merely the area of the valve seat. It is instead a complex function of the valve bulkhead slope and the deflection length of the valve seat. This relationship is shown qualitatively in Figure 7.11. Another aspect of this problem is that the valve seats will expand slightly in diameter as they are compressed and hence the value of A will increase slightly with valve seat deflection. However, to ease the complexity of the analysis, it is convenient to pick a constant upper bound for A . Assuming the valve seats seal for this upper bound on A , they should seal for all smaller values of A because it is in the numerator of the constant in Equation 7.4. For this analysis, the full frontal contact area of the valve seat was selected for the variable A and any additional increase in A due to deformation is assumed to be so small as to be

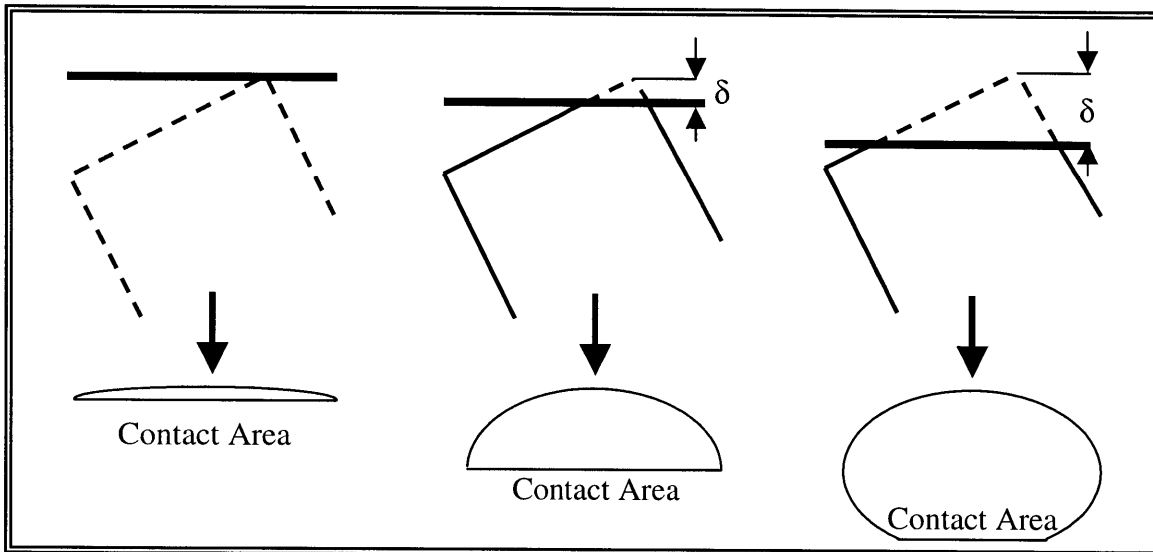


Figure 7.11: The contact area between the valve disk and valve seat is a complex function of slope and valve seat deformation neglected.

Given the bounding condition imposed upon A , Equation 7.4 becomes a simple linear relationship between imposed force and the valve seat deflection. For proper sealing to occur, the imposed force must create a deflection, δ , equal or greater than the height between the valve seat edge and the valve disk, g , caused by the slope in the valve bulkhead. This condition is characterized by Equation 7.5 where r_o is the radius of the valve seat and Θ is the valve bulkhead deflection slope at the local radial location of the valve seats. The constant $1/3$ is introduced to account for three valve seats.

$$\frac{F}{3} \left(\frac{L}{AY} \right) = \delta \geq g = 2r_o \sin(\Theta) \quad (\text{Equation 7.5})$$

The force pulling the valve disk onto the valve seats is derived from a combination of sources: 1) the magnetic force from the button magnets embedded in the valve bulkhead and 2) the pressure differential through the valve ports pulling the disk onto the seats. For the outlet valves, the pressure across the valve ports is variable. A bounding case of minimum force can be considered by ignoring the pressure differential across the ports. This assumption leaves only the force on the valve disk induced by the button magnets to assure proper sealing. In Section 3.4.2, the button magnet layout design is discussed. A value of about 1.75 newtons is postulated as the closing force induced by the button magnets on each valve disk. With all pertinent valves in place, the following values result:

$$\begin{aligned} \text{gap, } g &= 8.95 \times 10^{-5} \text{ inches} \\ \text{deflection, } \delta &= 2.28 \times 10^{-7} \text{ inches} \end{aligned}$$

This comparison indicates that the outlet valve does not seal under worst-case conditions. However, a more important conclusion should be drawn from the order of magnitude of the numbers involved. These values are much smaller than any machined tolerance on the valve bulkhead of the valve ports. In addition, lengths from 10^{-5} to 10^{-7} inches are on the order of the surface roughness features on each of the components. Thus, the deflection numbers are not a controlling factor in determining whether the valves leak.

Regardless, if carried through to estimate an upper bound in the leak rate, this calculation should compare the leakage through the valve bulkhead to the volume of material taken into the expander. The largest port area the gas could leak through is the circumference of the valve seat multiplied by the gap opening, g , in the worst-case situation. This area works out to about 1.4×10^{-5} square inches per port, or about 4.2×10^{-5} square inches overall. The maximum pressure ratio across the valve ports is about 18, and therefore the leakage should be treated as choked sonic flow. Applying a volume flow rate, Equation 7.6, to the choked flow, a maximum bound on the leak rate is found. The variable V is the speed of sound in helium at 10 Kelvin and A is the combined orifice area through which the fluid flows

$$\dot{Q} = VA \quad (\text{Equation 7.6})$$

The maximum volume leak rate can be found to be about 0.31 cubic-inches-per-second. Comparing this value to the expander swept volume rate on the intake stroke, about 1.57 cubic-inches-per-second, the maximum volume of fluid that could leak through the valves is about 20 percent of the swept volume rate.

This calculation is provided to demonstrate one rudimentary approximation to the valve leak rate. However, the use of deformation numbers compounded with multiple worst-case scenario bounds provides a gross overestimation of the true leakage rate. The actual valves will perform substantially better than predicted here.

In addition, there are several factors contributing to decreased leak rate that are not taken into account: 1) the flow goes subsonic over the portion of the stroke where the pressure ratio falls below 2. 2) The actual flow orifice is only about half the value utilized because of the contact between the valve disk and the edge of the valve seats. 3) The height g remains smaller than the taken value throughout most of the pressure cycle.

If the valves do prove to leak, one attractive class of remedies suggested by this analysis is to increase the valve seat deformation to the order of 10^{-4} inches to assure good sealing. The valve seats could be made more compliant under compression by either making them longer or changing the inner and outer radii to reduce their total contact area with the valve disk. In general, the valve bulkhead should be further increased in thickness to reduce its bowing under variable pressure and thus reduce the maximum gap height, g .

7.3 VALVE SEAT LIFETIME

A primary motivation in creating specialized cold-end valves is to assure that the duration of time between replacements is substantially longer than off-the-shelf solenoid valves designed for occasional use. Ultimately, the cryocooler may be deployed in situations where it will run uninterrupted for many months at a time for several years in a row between overhauls.

The main wear on the cold-end valves occurs when the valve disk impacts the valve seats. In stopping the valve disk, if the restoring pressure induced by the valve seats is substantially higher than the compressive yield strength of the valve seats, the valve seats will fail very quickly. To analyze this situation, the model shown in Figure 7.12 was developed. The system consists of the valve disk and the valve seats, and the seats are treated as three ideal springs in parallel. As the valve disk strikes the valve seats, the valve seats deform and convert the valve disk's kinetic energy into stored potential energy. The system then undergoes damped oscillation to dissipate the energy as heat. An energy balance on the original impact can determine the valve seat deflection distance, δ , generated to stop the valve disk. Equation 7.7 represents this relationship. This deflection can be plugged into the spring equation, Equation 7.4, to yield the maximum force imposed on the valve seats during the impact.

$$\frac{1}{2}mV^2 = \int_0^{\delta} Fdx \quad (\text{Equation 7.7})$$

This force result, when divided over the area of the valve seats yields an impact pressure. The impact pressure can be compared against the yield stress of Kel-F plastic to determine whether valve disk impacts will damage the valve seats over time.

To perform this impact pressure calculation, the minimum and maximum terminal velocities of the outlet valve disk, derived in Section 7.1, are utilized. These values are 9.12 and 12.13 meters-per-second respectively. Table 7.2 shows the results of the impact pressure analysis. This analysis shows that the values in the possible range of disk impact pressures are smaller than the yield strength of Kel-F plastic at 10 Kelvin⁶. Thus, the valve seats are expected to enjoy lifetimes substantially longer than those expected for off-the-shelf solenoid valves.

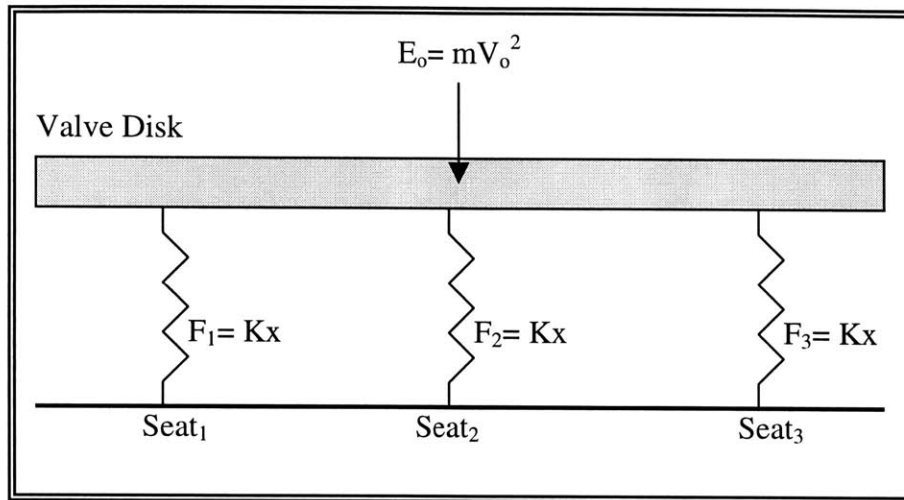


Figure 7.12: A first-order energy model of the valve disk and valve seat interaction represents the seats as simple springs

Table 7.2: Valve Seat Impact Pressure Versus Compressive Yield Strength

	Velocity	Impact Pressure	Kel-F Yield Strength @ 10K
	[m/s]	[N/m ²]	[N/m ²]
Min Disk Velocity	9.12	2.67x10 ⁹	7.2x10 ⁹
Max Disk Velocity	12.13	3.56x10 ⁹	7.2x10 ⁹

Inherent in this analysis is the assumption that the force felt by the valve disk at various positions along its traverse follows the curves in Figure 7.2. Since the electrical inductance of the valve changes with valve disk position, maintaining force-verses-position-function continuity requires a sophisticated power supply that can deliver high-voltage control signals much more rapidly than the valve's dynamics occur. If a sophisticated valve coil current control routine is employed, the force imposed on the valve disk at the end of its traverse can be instantly reduced. This drop in force will result reduced valve disk velocity at the end of its traverse. In turn, the impact pressure on the valve seats is reduced. Thus, active shaping of the control current will serve to further decrease the impact pressure endured by the valve seats, increasing their lifetime. Such a control routine requires a power supply that can regulate the valve disk current more rapidly than the valve disk moves regardless of electrical inductance changes imposed by the varying magnetic field geometry.

7.4 CONTROL, ENERGY CONSUMPTION, AND DISSIPATION

The electromagnetic dynamics of the valves and the couplings of related parameters with the system's thermodynamic and mechanical properties create an additional series of design constraints. Eliminating mechanical linkages in the cold end in favor of electromagnetic actuation requires sophisticated control electronics with enough robustness to force the valve disks to respond rapidly to commands signals. In addition, some of the energy required to maintain the magnetic fields actuating the valves dissipates as heat in the cold end. This dissipated energy must be quantified to assure it does not detract significantly from performance of the cold end.

Since the valves contain wound valve coils, they are inherent inductors in the control circuits in which they are wired. This inductance causes the valves to resist changes in current, and they will tend to lag behind any change in circuit current, even a control command. As an additional complication, valve coil inductance is a function of valve disk position. The speed of the valve coil's response is governed by the magnitude of voltage, ϵ , driving the command current through the valve coil.

A high-voltage bench top power supply has been built to allow precise regulation of the valve coil control current on timescales ten times faster than the mechanical speed of the valve disk traversing the 0.01-inch lift gap. This "smart" control current feature can be utilized to precisely shape the current and induced force on the valve disk.

7.4.1 Triple-R Valve and Energy Consumption

To open the valves, about 0.12 amps over 900 turns is required to energize the valve coils to about 110 amp-turns. Without any control routine in place, the opening current is held at 0.12 amps over the entire duration the valve remains open. This holding current has an associated joule-heating rate that goes as the coil resistance multiplied by the square of the input current. This energy is dissipated as heat in the cold end. Using the room temperature resistance measured for each valve coil, the joule heating of each valve can be calculated. Table 7.3 displays the pertinent energy dissipation characteristics of the valves.

Table 7.3: Joule Heating Dissipation in the Valve Coil at Room Temperature

	Resistance	Steady State Power Required	Valve "ON" Time	Heat Energy Dissipated
	[ohms]	[watts]	[seconds/cycle]	[Joules/cycle]
Inlet Valve	80	1.152	0.1	0.1152
Outlet Valve	91	1.310	0.4	0.524

As the cold end cools to its operating temperature of 10 Kelvin, the resistance of the copper in the wire drops dramatically. This property is measured via the residual resistance ratio (RRR) metric as represented in Equation 7.8. To obtain the resistance of wire at a given temperature, the resistance at room temperature is divided by the RRR.

$$RRR(T) = \frac{R_{273K}}{R_T} \quad (\text{Equation 7.8})$$

The RRR curve for any wire can be obtained by measuring the resistance across a length of wire at various cryogenic temperatures. As the purity of the copper in the wire increases, higher RRR values are achieved. Table 7.4 provides RRR measures for three grades of commercially available copper wire measured in the laboratory. A wire's RRR at 10 Kelvin is well approximated by the measured value at 4.2 Kelvin. Thus, a revised estimate of the valve's energy dissipation at operating temperature is presented in Table 7.5. Note that this energy dissipation approximation assumes that the coil is wound with high-purity copper wire. Table 7.5 shows that the valves together will dissipate about 0.0071 joules per cycle at 10 Kelvin, less than 0.1 percent of the 1 watt of heat lifted by the cold end per cycle.

Table 7.4: RRR for Grades of Commercial Wire

Wire Type	RRR(77K)	RRR(4.2K)
Standard Magnet Wire	6.17	32.42
Intermediate-Purity	7.03	48.38
High-Purity	8.23	89.96

Another path for heat to enter the cold end is via conduction down the valve wire leads. A gross upper estimate on conduction heat transfer down the valve leads from room temperature to 10 Kelvin suggests a loss of about 0.0273 watts-per-lead, or about 0.1092 watts total. This estimate was performed for a 32-gauge copper wire 20 centimeters in length with RRR=90 strung directly from 10 Kelvin to 300 Kelvin. In the actual machine, the cold valve wire leads will be thermally anchored to the stage above and the wire diameter will be greatly reduced. Regardless, conduction up the leads appears to be the most substantial thermal loss mechanism emanating from the valves.

Table 7.5: Joule Heating Dissipation at the Valve Coil at 10 Kelvin

	Resistance	Steady State Power Required	Valve "ON" Time	Heat Energy Dissipated
	[ohms]	[watts]	[seconds/cycle]	[Joules/cycle]
Inlet Valve	0.89	0.013	0.1	0.0013
Outlet Valve	1.01	0.015	0.4	0.0058

8.0 REFLECTIONS AND CONCLUSIONS

Throughout this thesis, a number of specific recommendations are made about areas of development that could benefit from additional work. Supplemental areas of study that would have been explored had more time been available are also outlined. To facilitate the easy continuation of this work, these suggestions are recapped here ordered by the chapter in which they appear in this thesis.

Chapter 2

An enhancement in the cold end design could arise if push rods through the valve ports are used to engender placement of the outlet valve outside the expander space. The current outlet valve yoke placement incurs a significant amount of expander dead volume. However, attempts to move the outlet valve yoke to the high-pressure part of the cold end using push rods will incur added mechanical complexity. An additional tradeoff will be the significantly increased mass of the valve's moving parts, which will cause slower valve operation. These consequences need to be evaluated to determine whether the push rod configuration is in fact more desirable than the current geometry.

Chapter 3

In general, the valves need to be redesigned utilizing knowledge gleaned from the prototype design process to better match their performance to the design requirements of the cold end. The valves, in their current configuration, are designed to open against 250 pound-per-square-inch of pressure across eight valve ports. However, the final valve bulkhead design calls for only three valve ports. Thus, the valves can be substantially reduced in size to better match this less demanding design requirement.

The iterative evolutionary design process yields a valve design that is highly dependant upon the order in which various parameters were exercised in the finite element model. There are a number of additional possible geometry perturbations that could yield better valve performance than achieved through the process described in this thesis. A complete exploration of the design space is possible using finite element modeling, but that process would be very time consuming. Future cold valve development should focus on the design space for valve coil aspect ratios between 1.5 and 6.5. There is more benefit to be gained from placing additional conductive coil material as near to the valve's outer diameter as possible.

The spacer ring on the outlet valve is essentially a vestigial component that the designer failed to remove from a previous design iteration. The use of Loctite® sealing agent to hold the outlet valve in the wall assembly makes the spacer ring obsolete. The function of centering the outlet valve disk can be taken over by the wall assembly with more thoughtful design. This improvement will reduce the cold end complexity as well as the expander dead volume.

The finite element model for the permanent magnet array that makes up the virtual valve spring is clearly poor. The overall ability of the model to predict the dynamic behavior of the valve disk will be enhanced if a more accurate refinement of the permanent magnet simulation is advanced. Force tests should also be run with the inlet valve magnet array and the inlet valve disk to provide another point of reference for the development of the permanent magnet model.

Chapter 5

Several important geometric tolerances are identified in Chapter 5, but it is impossible to isolate the valve performance loss contribution of each mechanism because their effects overlap. While it is possible to use characteristic values of these tolerances to bound the valve performance via finite element, it is impossible to develop a finite element model that represents the valve performance exactly until the extent of each tolerance is individually identified. Quantifying the effects of each tolerance on valve performance will require building special test rigs to isolate and measure the contribution of each tolerance. This data could then be used to build a more accurate finite element model of the valve.

Chapter 6

There are several simple geometric fixes in the cold end assembly that will improve the system's performance and ease of use. First, the 0.1-inch gap in the wall assembly used as bending space for the high-pressure capillary tubes should be made substantially wider than 0.1 inches. The current dimension is too tight to allow the tubes to make the required 90-degree bend. Second, the miniature flange facilitating the sealed connection between the high-pressure flanges and the high-pressure reservoir should be modified to accommodate Indium seals instead of copper.

In general, there is a large amount of unnecessary dead volume in the cold end arising from vestigial components and poor design decisions. In the future, more attention should be paid to reducing this dead volume to improve cryocooler performance.

Chapter 7

A simple deflection analysis shows that deflection lengths experienced by the valve bulkhead and valve seats during the cycle are too small to control whether the valve ports seal correctly. However, if valve leakage is a problem, modifications to these parts can be made to increase the influence of deflections to assure proper sealing is achieved. These measures include the following: 1) increasing the thickness of the valve bulkhead to decrease its bowing and 2) modifying the valve seats to increase their deformation compliance under compression by either making them longer or decreasing their contact surface area.

8.1 TECHNOLOGIES THIS WORK MAY ENABLE

The most significant direct development arising out of this body of work is the advancement of electromagnetic valves for cryogenic applications. To date, mechanically actuated valves have entirely dominated machines in the cryogenic domain. However, there are many cryogenic applications that may reap substantial operation and maintenance cost savings or cycle optimization and control benefits from retrofitting with electromagnetic valves. Adding to the number of viable demonstrations showing that electromagnetic valves are a feasible alternative in cryogenics, this work will help to open avenues for commercialization of this technology.

The most important contribution made through this work is pioneering the way to development of a small, reliable, efficient cryocooler capable of lifting one Watt of heat at 10 Kelvin with an input power of less than 1000 Watts. When the three-stage machine is ultimately constructed, it will represent a significant general advance in the field of cryogenics, and it will prove that a miniaturized machine running the Collins cycle can be competitive with existing cryogenic technologies. The Collins cycle may replace existing cryocoolers in many space-borne satellite applications from astronomy to surveillance because of the reduced power consumption this cycle affords for the same level of cooling. On the ground, this machine will have military and civilian applications ranging from enhanced night vision equipment for soldiers to ultra-precise sensor packages for industry. Perhaps the most lucrative potential application is in desktop computing. There may come a time when miniaturized Collins cycles become standard equipment for augmenting personal computers and providing cryogenically cooled supercomputing capabilities to the standard consumer.

The advent of the miniature Collins cycle cryocooler will also have applications in more exotic regimes of science and technology. Adding a fourth stage to the device will create a small, portable machine capable of liquefying helium at 4.2 Kelvin. Any application requiring low-temperature superconductors may then benefit from this advance. The magnet cooling systems in plasma fusion power plants, superconducting magnetic energy storage systems and, levitating trains may all be enhanced and economized by the availability of this technology. There is much ground still to cover, but the benefits and potential applications on the horizon make an alluring call for further work.

8.2 CONCLUSION

Through this research project, a design for a feasible cold end unit capable of executing the expander portion of one-stage of a multi-stage Collins cycle is presented. This machine has been built and tested, demonstrating the ability to condense water on its surface when running in contact with the outside environment on room temperature nitrogen.

The emphasis of this machine's development has been to create electromagnetic cryogenic valves and integrate them into the cold end. The difficulties and successes encountered during the development of this technology are catalogued and many suggestions are made pointing the way to potential improvements for the next phase of the machine's development.

A finite-element modeling method is used to explore the valve's design space using an evolutionary iterative process to cut down on the time to converge to a favorable solution. This process supplants pre-existing cryocooler electromagnetic valve design methodologies by allowing the experimenter to explore various geometries without having to build and test hardware.

A set of analysis tools based on the finite element modeling results are developed and presented to yield first-order approximations for several functions of the cold end including the following: electromagnetic, mechanical, dynamic, thermodynamic, and tribological. These performance calculations are instrumental in breaking down the various processes affecting the operation of the cold end, and it is recommended that they be used in the future as a baseline to develop more sophisticated cycle models and design rules. Along with these modeling tools, an experimental process for static benchmarking is described, and the sensitivity of the valve to various geometric tolerances is explored and modeled. It is demonstrated that the finite element modeling method can be utilized to reliably bound a set of experimental data.

There are three immediate next steps for this project that will facilitate advancement towards an operable three-stage Collins cycle cryocooler. First, the current working fluid, nitrogen, must be replaced with helium to assure the system will not leak severely using the more pervasive gas. Second, a helical recuperative heat exchanger, currently under development, must be installed over the expander to provide thermal isolation for the cold end from the outside environment. Third, a dewar to house the expander/heat-exchanger assembly must be devised to facilitate testing of the cold end at cryogenic temperatures. These steps will most likely require the experimenter to modify and rebuild most of the cold end components to comply with the demands of very low temperature.


REFERENCES

- 1) Ceridon, Kimi Malia, "Remote Cooling using Cold Electromagnetic Valves to Drive an External Flow Loop on a Gifford McMahon Cryocooler," MIT Master's Thesis, June 2001.
- 2) Crunkleton, James Alan, "A New Configuration for a Liquid Helium Temperature Cryocooler", MIT Doctoral Thesis, September 1987.
- 3) Crunkleton, J.A., "A New Configuration for a Small-Capacity, Liquid-Helium-Temperature Cryocooler," *Cryocooler 7*, Plenum Press, New York (1992), pp. 187-196.
- 4) Collins, S.C and Cannaday, R.L, Expansion Machines For Low Temperature Processes, Oxford University Press, London (1958).
- 5) Fitzgerald, A.E., Kingsly, C. Jr. and Kusko, A, Electric Machinery: The Processes, Devices, and Systems of Electromechanical Energy Conversion, 3rd Edition, McGraw-Hill Inc., New York (1961).
- 6) Hartwih, Günther, Polymer Properties at Room and Cryogenic Temperatures, Plenum Press, New York (1994).
- 7) Jones, R.E., Smith, J.L. Jr., "Design of Experimental Free Piston Cryogenic Expander," *Advances in Cryogenic Engineering*, Volume 45, Plenum Press, New York (2000), pp. 1485-1491.
- 8) Lord Rayleigh, The Theory of Sound, 2nd. Edition, Volume 1, Chapter IX, Macmillan, London (1926).
- 9) Scott, Russell B., Cryogenic Engineering, 3rd Edition, Met-Chem Research Inc., Boulder, Colorado (1963).
- 10) Young, W.C., Roark's Formulas for Stress and Strain, 6th Edition, McGraw-Hill Inc., New York (1989).

APPENDIX A – PARAMAGNETIC MATERIAL PROPERTIES

The following is manufacture's information for FR430, the paramagnetic material utilized to build the valve yokes and valve disks.

CARPENTER TECHNOLOGY CORPORATION
CARPENTER STEEL DIVISION



TECHNICAL DATA

CARPENTER 430FR SOLENOID QUALITY

Type analysis:

Carbon	0.06%
Manganese	0.50%
Silicon	1.25%
Phosphorus	0.02%
Sulfur	0.30%
Chromium	17.50%
Molybdenum	0.30%
Iron	Balance

DESCRIPTION:

Carpenter 430FR Solenoid Quality is a chromium iron alloy specially developed for solenoid valve magnetic core components which must operate in corrosive environments. When supplied in the mill annealed condition, the direct current basic magnetic properties are similar to Carpenter 430F Solenoid Quality; however, the hardness is slightly higher. The slightly higher hardness reduces cold work deformation (peening) that occurs during cyclic impacts between moving and stationary parts of the AC and DC magnetic circuits. Improved magnetic properties and lower residual magnetism are realized at round bar diameters greater than 0.375" (9.53 mm) and the degree of improvement is greater as the diameter increases.

Unannealed: Items are available in the unannealed condition when the size ordered cannot be supplied in the mill annealed condition and/or in the most magnetic soft condition. Depending upon requirements of the end product, parts must be heat treated to render the alloy more magnetically soft than as supplied.

Mill Annealed: Centerless ground bar items 0.375" (9.53 mm) round and larger are available at the hardness range of Rockwell B 80/88. In this condition, AC and DC magnetic properties are in the same range as that obtained when applying heat treatment to the alloy in the unannealed condition. Solenoid valve magnetic core components can be machined to sizes, chemically passivated, if necessary, and then can be assembled into the final product.

CORROSION RESISTANCE:

Carpenter 430FR, similar to Carpenter 430F Solenoid Quality, combats corrosion from atmosphere, fresh water, gases, common beverages, dairy products, etc. For best corrosion resistance, surfaces should be entirely free of oxide and foreign particles and subjected to a passivating process.

PHYSICAL CONSTANTS:

Specific gravity	7.59
Density — lb/in ³	0.274
kg/m ³	7584
Mean coefficient of thermal expansion	
10 ⁻⁶ /°F (32/1200°F)	6.6
10 ⁻⁶ /°C (0/699°C)	11.9
Electrical resistivity	
ohm-cir mil/ft	460
microhm-mm	760
Curie temperature	
°F	1220
°C	660

DIRECT CURRENT MAGNETIC PROPERTIES

Condition	Hardness Rockwell B	Maximum Permeability	From 10 K Gauss (1T)			
			H _c (Oe)	H _c A/cm	Br K Gauss*	Br T*
Mill Annealed	80/88	1100/2400	1.2/2.5	0.95/1.99	02.5/07.0	0.25/0.70
Full Anneal**	80/88	1100/2200	1.2/2.5	0.95/1.99	02.5/07.0	0.25/0.70

Intrinsic Magnetic Saturation 13.5 K Gauss (1.35T)

*Br value varies - as diameter decreases, Br increases.

**Annealed for 2 hours, 1500°F (816°C). Cooled approximately 70°F (21.1°C) per hour to below 800°F (427°C). Hydrogen or vacuum atmosphere is suggested to prevent surface discoloration during treatment.

Method of test - straight lengths ASTM A-341; solid rings ASTM A-596.

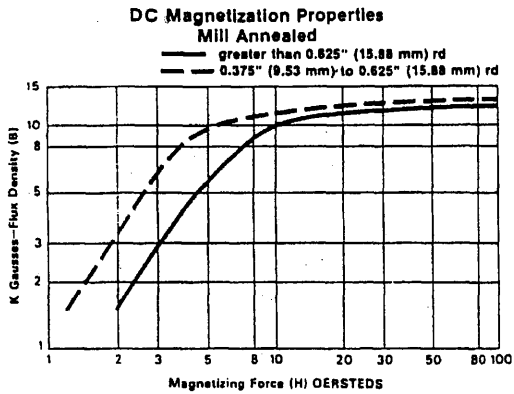
The information and data presented herein are typical or average values and are not a guarantee of maximum or minimum values. Applications specifically suggested for material described herein are made solely for the

purpose of illustration to enable the reader to make his own evaluation and are not intended as warranties, either express or implied, of fitness for these or other purposes.

ELECTRONIC ALLOYS 18

1-83/8M

Carpenter 430FR Solenoid Quality, Continued



HEAT TREATMENT:

Annealing for Magnetic Properties: 1550/1830°F (843/1000°C) 2 hours — cool 100°F (56°C) per hour to 800°F (427°C). Dry hydrogen or vacuum atmosphere is suggested to prevent surface oxidation.

Annealing to Soften: Heat uniformly to 1250/1400°F (677/760°C) — cool in air — Brinell approximately 170.

Hardening: Does not respond to hardening by heat treatment.

WORKABILITY:

Forging: Carpenter 430FR Solenoid Quality should be heated uniformly to 1500/1600°F (816/871°C) and then taken to the forging temperature of 1950/2100°F (1066/1149°C) as rapidly as possible. Do not soak at the forging temperature since this produces grain growth. Hot working operations should not be continued when the temperature has dropped below 1500°F (816°C). Forgings should be air cooled.

Cold Working: Carpenter 430FR Solenoid Quality will withstand moderate cold work, but is not recommended for cold upsetting. The main application for this steel is in solenoid cores that are machined to shape.

Welding: Responds fairly well to hell-arc and electron beam welding when weld bead is very narrow, such as 1/8" (3.2 mm) wide and 1/32" (0.8 mm) deep.

TYPICAL MECHANICAL PROPERTIES:
Tensile Test in 1" (25.4 mm) rd. bar

	Yield Strength 0.2% Offset		Tensile Strength		% Elongation in 2" (50.8 mm)	% Reduction of Area	Brinell Hardness
	ksi	MPa	ksi	MPa			
Mill Annealed (Rockwell B 86)	50	345	78	538	30	60	174

MACHINABILITY:

Operation	Hardness Rockwell B	Speed		Feed		Suggested Tool Material
		sfm	m/s	lpr	mm/r	
Turning	92 min	155	0.79	0.001"/0.003"	0.025/0.076	M-42
	92 max	130	0.66	0.002"/0.004"	0.051/0.102	M-42
Drilling	92 min	100	0.51	0.001"/0.005"	0.025/0.127	M-42
	92 max	90	0.46	0.001"/0.005"	0.025/0.127	M-42
Milling	92 min	125	0.64	0.003"/0.006"	0.076/0.152	M-2
	92 max	110	0.56	0.003"/0.006"	0.076/0.152	M-2
Tapping	92 min	30-35	0.15/0.18	—	—	M-1 or M-2
	92 max	25-30	0.13/0.15	—	—	M-1 or M-2

FORMS AVAILABLE:

Cold Drawn and Ground Bars
Wire and Wire Rods

APPENDIX B – STATIC FORCE DATA

The data from all of the static test rig force experiments on the outlet valve are presented here in tabular form. Over the course of the experiment, three different valve yokes were utilized to take the data because the valve design evolved during the process. All three valves are geometrically similar, but they are not identical. The type of valve utilized to take the data is denoted on the top of each table. Although the data presented in the body of the thesis is derived from the force tests on the final valve, all the data gathered from all three valves is presented here for completeness.

The main difference between the valves is that Prototype 1 and Prototype 2 are wound with 28-gauge wire with about 250 turns on the coil. The final valve is wound with 32-gauge wire with about 900 turns. This difference in the number of turns is reflected in the resistance measured for the coil. However, the number of amp-turns developed to energize the coil is not necessarily effected because valves with fewer turns can be energized with higher currents to reach the same amp-turn value as valves with more turns.

In the preliminary force rig experiments, only the current measured when the valve yoke dropped the weighted disk was recorded. As the experiment evolved it became evident that both the dropping current and the sticking current were important in bounding the true behavior of the valve disk. In the spirit of presenting all of the data, the early data which includes only the dropping current is presented along with the later data. The later data is identifiable because matrices holding the sticking current and dropping current data for a particular combination of variables are grouped together but separated by a thick gray line. The top header of each table denotes whether the data below is for the sticking condition of the dropping condition.

The data is organized by shim size in ascending order. The top header of each table denotes the shim size in inches.

Separation	0.0036"		Prototype 1					
Coil Voltage	Shunt Volts	Coil Amps	Amp-Turns	Power Drawn	Weight	Weight	Force	Resistance
[volts]	[millivolts]	[amps]	[amps]	[watts]	[grams]	[kilograms]	[N]	[ohms]
1.045	6.100	0.183	45.57	0.191	285	0.285	2.792	5.710
0.851	6.000	0.180	44.82	0.153	262	0.262	2.572	4.728
0.987	5.500	0.165	41.09	0.163	242	0.242	2.371	5.982
0.920	5.000	0.150	37.35	0.138	219	0.219	2.144	6.133
0.820	4.650	0.140	34.74	0.114	202	0.202	1.980	5.878

Separation	0.004"	drop	Prototype 2					
Coil Voltage	Shunt Volts	Coil Amps	Amp-Turns	Power Drawn	Weight	Weight	Force	Resistance
[volts]	[millivolts]	[amps]	[amps]	[watts]	[grams]	[kilograms]	[N]	[ohms]
0.479	3.000	0.090	19.80	0.043	66	0.066	0.652	5.322
0.687	4.300	0.129	28.38	0.089	152	0.152	1.493	5.326
0.722	4.500	0.135	29.70	0.097	207	0.207	2.028	5.348
0.984	6.100	0.183	40.26	0.180	269	0.269	2.636	5.377
Separation	0.004"	stick	Prototype 2					
Coil Voltage	Shunt Volts	Coil Amps	Amp-Turns	Power Drawn	Weight	Weight	Force	Resistance
[volts]	[millivolts]	[amps]	[amps]	[watts]	[grams]	[kilograms]	[N]	[ohms]
0.568	3.500	0.105	23.10	0.060	66	0.066	0.652	5.410
0.745	4.600	0.138	30.36	0.103	152	0.152	1.493	5.399
0.846	5.200	0.156	34.32	0.132	207	0.207	2.028	5.423
1.049	6.500	0.195	42.90	0.205	269	0.269	2.636	5.379

Separation	0.006"	drop	Prototype 2					
Coil Voltage	Shunt Volts	Coil Amps	Amp-Turns	Power Drawn	Weight	Weight	Force	Resistance
[volts]	[millivolts]	[amps]	[amps]	[watts]	[grams]	[kilograms]	[N]	[ohms]
0.496	3.100	0.093	20.46	0.046	66	0.066	0.652	5.333
0.717	4.500	0.135	29.70	0.097	152	0.152	1.493	5.311
0.748	4.600	0.138	30.36	0.103	207	0.207	2.028	5.420
0.913	5.600	0.168	36.96	0.153	269	0.269	2.636	5.435
Separation	0.006"	stick	Prototype 2					
Coil Voltage	Shunt Volts	Coil Amps	Amp-Turns	Power Drawn	Weight	Weight	Force	Resistance
[volts]	[millivolts]	[amps]	[amps]	[watts]	[grams]	[kilograms]	[N]	[ohms]
0.633	3.900	0.117	25.74	0.074	66	0.066	0.652	5.410
0.774	4.800	0.144	31.68	0.111	152	0.152	1.493	5.375
0.855	5.300	0.159	34.98	0.136	207	0.207	2.028	5.377
1.170	7.100	0.213	46.86	0.249	269	0.269	2.636	5.493

Separation	0.0075"		Prototype 1					
Coil Voltage	Shunt Volts	Coil Amps	Amp-Turns	Power Drawn	Weight	Weight	Force	Resistance
[volts]	[millivolts]	[amps]	[amps]	[watts]	[grams]	[kilograms]	[N]	[ohms]
1.447	8.000	0.240	59.76	1.920	285	0.285	2.792	6.029
1.627	8.750	0.263	65.36	2.297	262	0.262	2.572	6.198
1.677	9.000	0.270	67.23	2.430	242	0.242	2.372	6.211
1.104	7.000	0.210	52.29	1.470	219	0.219	2.144	5.257
0.973	5.500	0.165	41.09	0.908	202	0.202	1.981	5.897

Separation	0.0075"		Prototype 1					
Coil Voltage	Shunt Volts	Coil Amps	Amp-Turns	Power Drawn	Weight	Weight	Force	Resistance
[volts]	[millivolts]	[amps]	[amps]	[watts]	[grams]	[kilograms]	[N]	[ohms]
1.116	6.500	0.195	48.56	1.268	285	0.285	2.792	5.723
1.267	7.000	0.210	52.29	1.470	262	0.262	2.573	6.033
1.405	7.900	0.237	59.01	1.872	242	0.242	2.371	5.928
1.463	8.100	0.243	60.51	1.968	219	0.219	2.145	6.021
1.389	7.775	0.233	58.08	1.814	202	0.202	1.981	5.955

Separation	0.008	drop	Prototype 2					
Coil Voltage	Shunt Volts	Coil Amps	Amp-Turns	Power Drawn	Weight	Weight	Force	Resistance
[volts]	[millivolts]	[amps]	[amps]	[watts]	[grams]	[kilograms]	[N]	[ohms]
0.747	4.600	0.138	30.36	0.103	66	0.066	0.652	5.413
1.005	6.100	0.183	40.26	0.184	152	0.152	1.493	5.492
1.117	6.800	0.204	44.88	0.228	207	0.207	2.028	5.475
1.375	8.300	0.249	54.78	0.342	269	0.269	2.636	5.522
Separation	0.008	stick	Prototype 2					
Coil Voltage	Shunt Volts	Coil Amps	Amp-Turns	Power Drawn	Weight	Weight	Force	Resistance
[volts]	[millivolts]	[amps]	[amps]	[watts]	[grams]	[kilograms]	[N]	[ohms]
0.862	5.300	0.159	34.98	0.137	66	0.066	0.652	5.421
1.082	6.600	0.198	43.56	0.214	152	0.152	1.493	5.465
1.149	7.000	0.210	46.20	0.241	207	0.207	2.028	5.471
1.516	9.000	0.270	59.40	0.409	269	0.269	2.636	5.615

Separation	0.010	drop	Prototype 2					
Coil Voltage	Shunt Volts	Coil Amps	Amp-Turns	Power Drawn	Weight	Weight	Force	Resistance
[volts]	[millivolts]	[amps]	[amps]	[watts]	[grams]	[kilograms]	[N]	[ohms]
0.220	1.400	0.042	9.24	0.009	12	0.012	0.117	5.238
1.000	6.100	0.183	40.26	0.183	66	0.066	0.652	5.464
1.163	6.800	0.204	44.88	0.237	152	0.152	1.493	5.701
1.343	8.250	0.248	54.45	0.332	207	0.207	2.028	5.426
1.504	8.500	0.255	56.10	0.384	269	0.269	2.636	5.898
2.252	14.750	0.443	97.35	0.997	1120	1.120	10.987	5.089
2.317	15.000	0.450	99.00	1.043	1220	1.220	11.968	5.149
2.477	16.500	0.495	108.90	1.226	1320	1.320	12.949	5.004
Separation	0.010	stick	Prototype 2					
Coil Voltage	Shunt Volts	Coil Amps	Amp-Turns	Power Drawn	Weight	Weight	Force	Resistance
[volts]	[millivolts]	[amps]	[amps]	[watts]	[grams]	[kilograms]	[N]	[ohms]
0.246	1.550	0.047	10.23	0.011	12	0.012	0.117	5.290
1.084	6.700	0.201	44.22	0.218	66	0.066	0.652	5.393
1.349	7.700	0.231	50.82	0.312	152	0.152	1.493	5.840
1.410	8.600	0.258	56.76	0.364	207	0.207	2.028	5.465
1.584	9.500	0.285	62.70	0.451	269	0.269	2.636	5.558
2.351	15.500	0.465	102.30	1.093	1120	1.120	10.987	5.056
2.435	16.000	0.480	105.60	1.169	1220	1.220	11.968	5.073
2.570	17.000	0.510	112.20	1.311	1320	1.320	12.949	5.039

Separation	0.010	drop	Final Design					
Coil Voltage	Shunt Volts	Coil Amps	Amp-Turns	Power Drawn	Weight	Weight	Force	Resistance
[volts]	[millivolts]	[amps]	[amps]	[watts]	[grams]	[kilograms]	[N]	[ohms]
0.141	0.055	0.002	1.56	0.000	12	0.012	0.114	85.455
2.377	0.850	0.026	24.07	0.061	102	0.102	1.001	93.216
3.507	1.150	0.035	32.57	0.121	203	0.203	1.994	101.652
4.500	1.500	0.045	42.48	0.203	248	0.248	2.435	100.000
5.930	2.000	0.060	56.64	0.356	550	0.550	5.392	98.833
11.120	3.600	0.108	101.95	1.201	1335	1.335	13.093	102.963
Separation	0.010	stick	Final Design					
Coil Voltage	Shunt Volts	Coil Amps	Amp-Turns	Power Drawn	Weight	Weight	Force	Resistance
[volts]	[millivolts]	[amps]	[amps]	[watts]	[grams]	[kilograms]	[N]	[ohms]
0.481	0.150	0.005	4.25	0.002	12	0.012	0.114	106.889
3.632	1.200	0.036	33.98	0.131	102	0.102	1.001	100.889
3.990	1.350	0.041	38.23	0.162	203	0.203	1.994	98.519
5.350	1.800	0.054	50.98	0.289	248	0.248	2.435	99.074
7.280	2.200	0.066	62.30	0.480	550	0.550	5.392	110.303
12.990	4.200	0.126	118.94	1.637	1335	1.335	13.093	103.095

Separation	0.0108		Prototype 1					
Coil Voltage	Shunt Volts	Coil Amps	Amp-Turns	Power Drawn	Weight	Weight	Force	Resistance
[volts]	[millivolts]	[amps]	[amps]	[watts]	[grams]	[kilograms]	[N]	[ohms]
1.990	10.500	0.315	78.44	0.627	285	0.285	2.793	6.317
1.655	8.750	0.263	65.36	0.434	262	0.262	2.573	6.305
1.455	8.000	0.240	59.76	0.349	242	0.242	2.373	6.063
1.850	9.100	0.273	67.98	0.505	219	0.219	2.145	6.777
1.920	10.000	0.300	74.70	0.576	202	0.202	1.982	6.400

Separation	0.0108		Prototype 1					
Coil Voltage	Shunt Volts	Coil Amps	Amp-Turns	Power Drawn	Weight	Weight	Force	Resistance
[volts]	[millivolts]	[amps]	[amps]	[watts]	[grams]	[kilograms]	[N]	[ohms]
1.474	8.100	0.243	60.51	0.358	285	0.285	2.792	6.066
1.622	9.000	0.270	67.23	0.438	262	0.262	2.573	6.007
1.728	9.500	0.285	70.97	0.492	242	0.242	2.371	6.063
1.230	9.000	0.270	67.23	0.332	219	0.219	2.145	4.556
1.551	8.500	0.255	63.50	0.396	202	0.202	1.981	6.082

Separation	0.0120	drop	Prototype 2					
Coil Voltage	Shunt Volts	Coil Amps	Amp-Turns	Power Drawn	Weight	Weight	Force	Resistance
[volts]	[millivolts]	[amps]	[amps]	[watts]	[grams]	[kilograms]	[N]	[ohms]
0.257	1.600	0.048	10.56	0.012	12	0.012	0.117	5.354
0.938	5.800	0.174	38.28	0.163	66	0.066	0.652	5.391
1.179	7.300	0.219	48.18	0.258	152	0.152	1.493	5.384
1.382	8.500	0.255	56.10	0.352	207	0.207	2.028	5.420
1.720	11.000	0.330	72.60	0.568	269	0.269	2.636	5.212

Separation	0.0120	stick	Prototype 2					
Coil Voltage	Shunt Volts	Coil Amps	Amp-Turns	Power Drawn	Weight	Weight	Force	Resistance
[volts]	[millivolts]	[amps]	[amps]	[watts]	[grams]	[kilograms]	[N]	[ohms]
0.278	1.750	0.053	11.55	0.015	12	0.012	0.117	5.295
1.049	6.500	0.195	42.90	0.205	66	0.066	0.652	5.379
1.346	8.200	0.246	54.12	0.331	152	0.152	1.493	5.472
1.430	8.800	0.264	58.08	0.378	207	0.207	2.028	5.417
1.785	11.500	0.345	75.90	0.616	269	0.269	2.636	5.174

Separation	0.0144		Prototype 1					
Coil Voltage	Shunt Volts	Coil Amps	Amp-Turns	Power Drawn	Weight	Weight	Force	Resistance
[volts]	[millivolts]	[amps]	[amps]	[watts]	[grams]	[kilograms]	[N]	[ohms]
2.660	14.000	0.420	104.58	1.117	285	0.285	2.793	6.333
2.520	13.250	0.398	98.98	1.002	261	0.261	2.559	6.340
2.500	13.000	0.390	97.11	0.975	236	0.236	2.312	6.410
2.350	12.500	0.375	93.38	0.881	213	0.213	2.091	6.267
2.180	11.500	0.345	85.91	0.752	202	0.202	1.982	6.319

The data from all of the static test rig force experiments on the inlet valve is presented here in tabular form. Over the course of the experiment, two different valves were utilized to take the data because the valve design evolved during the process. The valve yokes are geometrically similar, but they are not identical. The type of valve utilized to take the data is denoted on the top of each table.

The main difference between the valves is that Prototype 1 is wound with 28-gauge wire with about 250 turns on the coil. The final valve is wound with 32-gauge wire with about 900 turns.

The following matrices contain performance data for the inlet valve. Matrices holding the sticking current and dropping current data for a particular combination of variables are grouped together but separated by a thick gray line. The top of each table denotes whether the data below is for the sticking condition or the dropping condition.

The data is organized by shim size in ascending order. The top of each table denotes the shim size in inches.

Separation	0.004"	drop	Prototype 1					
Coil Voltage	Shunt Volts	Coil Amps	Amp-Turns	Power Drawn	Weight	Weight	Force	Resistance
[volts]	[millivolts]	[amps]	[amps]	[watts]	[grams]	[kilograms]	[N]	[ohms]
0.479	3.000	0.090	19.80	0.043	66	0.066	0.652	5.322
0.687	4.300	0.129	28.38	0.089	152	0.152	1.493	5.326
0.722	4.500	0.135	29.70	0.097	207	0.207	2.028	5.348
0.984	6.100	0.183	40.26	0.180	269	0.269	2.636	5.377
Separation	0.004"	stick	Prototype 1					
Coil Voltage	Shunt Volts	Coil Amps	Amp-Turns	Power Drawn	Weight	Weight	Force	Resistance
[volts]	[millivolts]	[amps]	[amps]	[watts]	[grams]	[kilograms]	[N]	[ohms]
0.568	3.500	0.105	23.10	0.060	66	0.066	0.652	5.410
0.745	4.600	0.138	30.36	0.103	152	0.152	1.493	5.399
0.846	5.200	0.156	34.32	0.132	207	0.207	2.028	5.423
1.049	6.500	0.195	42.90	0.205	269	0.269	2.636	5.379

Separation	0.006"	drop	Prototype 1					
Coil Voltage	Shunt Volts	Coil Amps	Amp-Turns	Power Drawn	Weight	Weight	Force	Resistance
[volts]	[millivolts]	[amps]	[amps]	[watts]	[grams]	[kilograms]	[N]	[ohms]
0.496	3.100	0.093	20.46	0.046	66	0.066	0.652	5.333
0.717	4.500	0.135	29.70	0.097	152	0.152	1.493	5.311
0.748	4.600	0.138	30.36	0.103	207	0.207	2.028	5.420
0.913	5.600	0.168	36.96	0.153	269	0.269	2.636	5.435
Separation	0.006"	stick	Prototype 1					
Coil Voltage	Shunt Volts	Coil Amps	Amp-Turns	Power Drawn	Weight	Weight	Force	Resistance
[volts]	[millivolts]	[amps]	[amps]	[watts]	[grams]	[kilograms]	[N]	[ohms]
0.633	3.900	0.117	25.74	0.074	66	0.066	0.652	5.410
0.774	4.800	0.144	31.68	0.111	152	0.152	1.493	5.375
0.855	5.300	0.159	34.98	0.136	207	0.207	2.028	5.377
1.170	7.100	0.213	46.86	0.249	269	0.269	2.636	5.493

Separation	0.008"	drop	Prototype 1					
Coil Voltage	Shunt Volts	Coil Amps	Amp-Turns	Power Drawn	Weight	Weight	Force	Resistance
[volts]	[millivolts]	[amps]	[amps]	[watts]	[grams]	[kilograms]	[N]	[ohms]
0.747	4.600	0.138	30.36	0.103	66	0.066	0.652	5.413
1.005	6.100	0.183	40.26	0.184	152	0.152	1.493	5.492
1.117	6.800	0.204	44.88	0.228	207	0.207	2.028	5.475
1.375	8.300	0.249	54.78	0.342	269	0.269	2.636	5.522
Separation	0.008"	stick	Prototype 1					
Coil Voltage	Shunt Volts	Coil Amps	Amp-Turns	Power Drawn	Weight	Weight	Force	Resistance
[volts]	[millivolts]	[amps]	[amps]	[watts]	[grams]	[kilograms]	[N]	[ohms]
0.862	5.300	0.159	34.98	0.137	66	0.066	0.652	5.421
1.082	6.600	0.198	43.56	0.214	152	0.152	1.493	5.465
1.149	7.000	0.210	46.20	0.241	207	0.207	2.028	5.471
1.516	9.000	0.270	59.40	0.409	269	0.269	2.636	5.615

Separation	0.010"	drop	Prototype 1					
Coil Voltage	Shunt Volts	Coil Amps	Amp-Turns	Power Drawn	Weight	Weight	Force	Resistance
[volts]	[millivolts]	[amps]	[amps]	[watts]	[grams]	[kilograms]	[N]	[ohms]
0.220	1.400	0.042	9.24	0.009	12	0.012	0.117	5.238
1.000	6.100	0.183	40.26	0.183	66	0.066	0.652	5.464
1.163	6.800	0.204	44.88	0.237	152	0.152	1.493	5.701
1.343	8.250	0.248	54.45	0.332	207	0.207	2.028	5.426
1.504	8.500	0.255	56.10	0.384	269	0.269	2.636	5.898
2.252	14.750	0.443	97.35	0.997	1120	1.120	10.987	5.089
2.317	15.000	0.450	99.00	1.043	1220	1.220	11.968	5.149
2.477	16.500	0.495	108.90	1.226	1320	1.320	12.949	5.004
Separation	0.010"	stick	Prototype 1					
Coil Voltage	Shunt Volts	Coil Amps	Amp-Turns	Power Drawn	Weight	Weight	Force	Resistance
[volts]	[millivolts]	[amps]	[amps]	[watts]	[grams]	[kilograms]	[N]	[ohms]
0.246	1.550	0.047	10.23	0.011	12	0.012	0.117	5.290
1.084	6.700	0.201	44.22	0.218	66	0.066	0.652	5.393
1.349	7.700	0.231	50.82	0.312	152	0.152	1.493	5.840
1.410	8.600	0.258	56.76	0.364	207	0.207	2.028	5.465
1.584	9.500	0.285	62.70	0.451	269	0.269	2.636	5.558
2.351	15.500	0.465	102.30	1.093	1120	1.120	10.987	5.056
2.435	16.000	0.480	105.60	1.169	1220	1.220	11.968	5.073
2.570	17.000	0.510	112.20	1.311	1320	1.320	12.949	5.039

Separation	0.010"	drop	Final Design					
Coil Voltage	Shunt Volts	Coil Amps	Amp-Turns	Power Drawn	Weight	Weight	Force	Resistance
[volts]	[millivolts]	[amps]	[amps]	[watts]	[grams]	[kilograms]	[N]	[ohms]
0.852	0.350	0.011	9.54	0.009		0.000	0.000	81.143
3.100	1.300	0.039	35.45	0.121	65	0.065	0.641	79.487
3.156	1.300	0.039	35.45	0.123	65	0.065	0.641	80.923
4.170	1.800	0.054	49.09	0.225	120	0.120	1.175	77.222
5.700	2.250	0.068	61.36	0.385	221	0.221	2.169	84.444
6.030	2.500	0.075	68.18	0.452	383	0.383	3.758	80.400
6.680	2.650	0.080	72.27	0.531	383	0.383	3.758	84.025
8.790	3.550	0.107	96.81	0.936	691	0.691	6.775	82.535
8.910	3.700	0.111	100.90	0.989	850	0.850	8.341	80.270
9.730	3.950	0.119	107.72	1.153	850	0.850	8.341	82.110
10.220	4.150	0.125	113.17	1.272	1025	1.025	10.058	82.088
10.630	4.300	0.129	117.26	1.371	1158	1.158	11.359	82.403
11.350	4.600	0.138	125.44	1.566	1333	1.333	13.075	82.246
11.470	4.700	0.141	128.17	1.617	1333	1.333	13.075	81.348
13.810	5.600	0.168	152.71	2.320	1810	1.810	17.759	82.202
14.180	5.800	0.174	158.17	2.467	2118	2.118	20.776	81.494
15.250	6.100	0.183	166.35	2.791	2118	2.118	20.776	83.333
Separation	0.010"	stick	Final Design					
Coil Voltage	Shunt Volts	Coil Amps	Amp-Turns	Power Drawn	Weight	Weight	Force	Resistance
[volts]	[millivolts]	[amps]	[amps]	[watts]	[grams]	[kilograms]	[N]	[ohms]
1.234	0.520	0.016	14.18	0.019		0.000	0.000	79.103
3.206	1.350	0.041	36.81	0.130	65	0.065	0.641	79.160
3.213	1.550	0.047	42.27	0.149	65	0.065	0.641	69.097
4.280	1.850	0.056	50.45	0.238	120	0.120	1.175	77.117
5.780	2.300	0.069	62.72	0.399	221	0.221	2.169	83.768
6.110	2.550	0.077	69.54	0.467	383	0.383	3.758	79.869
6.900	2.750	0.083	74.99	0.569	383	0.383	3.758	83.636
8.900	3.600	0.108	98.17	0.961	691	0.691	6.775	82.407
9.280	3.900	0.117	106.35	1.086	850	0.850	8.341	79.316
10.130	4.100	0.123	111.81	1.246	850	0.850	8.341	82.358
10.310	4.200	0.126	114.53	1.299	1025	1.025	10.058	81.825
10.790	4.400	0.132	119.99	1.424	1158	1.158	11.359	81.742
11.670	4.850	0.146	132.26	1.698	1333	1.333	13.075	80.206
11.910	4.850	0.146	132.26	1.733	1333	1.333	13.075	81.856
14.570	6.100	0.183	166.35	2.666	1810	1.810	17.759	79.617
15.400	6.300	0.189	171.80	2.911	2118	2.118	20.776	81.481
16.010	6.450	0.194	175.89	3.098	2118	2.118	20.776	82.739

Separation	0.012"	drop	Prototype 1					
Coil Voltage	Shunt Volts	Coil Amps	Amp-Turns	Power Drawn	Weight	Weight	Force	Resistance
[volts]	[millivolts]	[amps]	[amps]	[watts]	[grams]	[kilograms]	[N]	[ohms]
0.257	1.600	0.048	10.56	0.012	12	0.012	0.117	5.354
0.938	5.800	0.174	38.28	0.163	66	0.066	0.652	5.391
1.179	7.300	0.219	48.18	0.258	152	0.152	1.493	5.384
1.382	8.500	0.255	56.10	0.352	207	0.207	2.028	5.420
1.720	11.000	0.330	72.60	0.568	269	0.269	2.636	5.212
Separation	0.012"	stick	Prototype 1					
Coil Voltage	Shunt Volts	Coil Amps	Amp-Turns	Power Drawn	Weight	Weight	Force	Resistance
[volts]	[millivolts]	[amps]	[amps]	[watts]	[grams]	[kilograms]	[N]	[ohms]
0.278	1.750	0.053	11.55	0.015	12	0.012	0.117	5.295
1.049	6.500	0.195	42.90	0.205	66	0.066	0.652	5.379
1.346	8.200	0.246	54.12	0.331	152	0.152	1.493	5.472
1.430	8.800	0.264	58.08	0.378	207	0.207	2.028	5.417
1.785	11.500	0.345	75.90	0.616	269	0.269	2.636	5.174

APPENDIX C – VALVE MODEL PERFORMANCE DATA

Once an idealized valve model was converged upon using the finite element code, it was desirable to test whether the actual behavior of the real valve could be captured using the computer simulation. Through the valve building, assembly, and testing processes, three major geometric tolerances emerged as unknowns that might affect the valve's performance.

Valve lift height is the distance the valve disk must travel from the valve seats to the face of the valve yoke when the valve coil is energized. Ideally, this distance is 0.010 inches. However, when the valve performance was tested, brass shims were utilized to simulate this gap by offsetting the valve disk from the valve yoke by the width of the shim. The shim width, as measured with a micrometer, has a tolerance of ± 0.0005 inches. Thus, the valve lift in the valve performance tests could range from 0.0095 inches to 0.0105 inches.

Axial offset represents the degree of axial misalignment between the valve spool and the valve cover when the two pieces are press fit together upon assembly. Although a step is machined into the valve cover causing it to seat firmly on the valve spool, there remains an uncertainty of about +0.003 inches, as measured with a caliper, between the alignment of both parts. In an attempt to minimize the negative effects of this tolerance, the two faces are lapped flush once they are assembled.

Interference gap is a term used to quantify the degree of roughness on the contact surfaces between the valve spool and the valve cover. The roughness at this contact reduces the actual interface area between the two parts through which magnetic flux travels. Effectively, an added resistance is introduced into the magnetic circuit by the interface. This resistance can be modeled as a very thin air gap separating the two components at their interface. It is estimated that the effective size of this gap may range from 0 to 0.003 inches.

The following tables contain valve performance data from the Quickfield finite element model for various characteristic combinations of the three geometric tolerances described above. The first set of data is all for a valve lift of 0.0095 inches. Data for the ideal model is presented first, followed by matrices of data for a range of characteristic axial offset and interference gap to various degrees.

Perfect Model	0.0095
Amp-Turns	Force
[amps]	[N]
2	0.0077406
25	1.2553
36	2.6809
43	3.8743
57	6.9248
80	13.839
102	22.715
110	26.494

Axial Offset = 0	Interface Gap = 0
Amp-Turns	Force
[amps]	[N]
2	0.0077304
25	1.2534
36	2.6762
43	3.8673
57	6.911
80	13.815
102	22.65
110	26.417

Axial Offset = 0.001	Interface Gap = 0
Amp-Turns	Force
[amps]	[N]
2	0.0070019
25	1.1345
36	2.4196
43	3.4964
57	6.2465
80	12.476
102	20.335
110	23.534

Axial Offset = 0	Interface Gap = 0.001
Amp-Turns	Force
[amps]	[N]
2	0.0068392
25	1.1026
36	2.3485
43	3.3936
57	6.0651
80	12.129
102	19.868
110	23.154

Axial Offset = 0.001	Interface Gap = 0.001
Amp-Turns	Force
[amps]	[N]
2	0.0061557
25	0.99008
36	2.1059
43	3.0428
57	5.4383
80	10.877
102	17.816
110	20.758

Axial Offset = 0	Interface Gap = 0.002
Amp-Turns	Force
[amps]	[N]
2	0.0061623
25	0.98886
36	2.1013
43	3.0354
57	4.4239
80	10.848
102	17.771
110	20.711

Axial Offset = 0.001	Interface Gap = 0.002
Amp-Turns	Force
[amps]	[N]
2	0.0055479
25	0.88816
36	1.8845
43	2.7218
57	4.8634
80	9.7282
102	15.94
110	18.578

Axial Offset = 0	Interface Gap = 0.003
Amp-Turns	Force
[amps]	[N]
2	0.0056002
25	0.89547
36	1.8987
43	2.7417
57	4.8979
80	9.7954
102	16.036
110	18.691

Axial Offset = 0.001	Interface Gap = 0.003
Amp-Turns	Force
[amps]	[N]
2	0.0050547
25	0.80652
36	1.7074
43	2.4648
57	4.4029
80	8.8072
102	14.428
110	16.814

Axial Offset = 0.002		Interface Gap = 0	
Amp-Turns	Force	Amp-Turns	Force
[amps]	[N]	[amps]	[N]
2	0.0063918	2	0.0058461
25	1.0329	25	0.094256
36	2.2006	36	2.0059
43	3.1798	43	2.8981
57	5.6811	57	5.1771
80	11.35	80	10.346
102	18.509	102	16.873
110	21.4	110	19.526

Axial Offset = 0.002		Interface Gap = 0.001	
Amp-Turns	Force	Amp-Turns	Force
[amps]	[N]	[amps]	[N]
2	0.0056054	2	0.0051122
25	0.89967	25	0.8189
36	1.9112	36	1.7376
43	2.7609	43	2.5098
57	4.9343	57	4.4854
80	9.8719	80	8.9738
102	16.161	102	14.694
110	18.824	110	17.116

Axial Offset = 0.002		Interface Gap = 0.002	
Amp-Turns	Force	Amp-Turns	Force
[amps]	[N]	[amps]	[N]
2	0.0050433	2	0.0045934
25	0.80577	25	0.73259
36	1.7076	36	1.5505
43	2.4658	43	2.2383
57	4.4059	57	3.9991
80	8.8139	80	8.0005
102	14.44	102	13.105
110	16.831	110	15.274

Axial Offset = 0.002		Interface Gap = 0.003	
Amp-Turns	Force	Amp-Turns	Force
[amps]	[N]	[amps]	[N]
2	0.0045978	2	0.0041887
25	0.73222	25	0.6661
36	1.5483	36	1.4067
43	2.2344	43	2.0294
57	3.9912	57	3.6245
80	7.9839	80	7.2502
102	13.08	102	11.88
110	15.245	110	13.844

The second set of data is all for a valve lift of 0.010 inches. Data for the ideal model is presented first, followed by matrices of data for a range of character axial offset and interference gap to various degrees.

Perfect Model	0.01
Amp-Turns	Force
[amps]	[N]
2	0.0070188
25	1.1345
36	2.4193
43	3.4955
57	6.2466
80	12.485
102	20.481
110	23.88

Axial Offset = 0	Interface Gap = 0
Amp-Turns	Force
[amps]	[N]
2	0.0070177
25	1.1338
36	2.2807
43	3.4938
57	6.2431
80	12.48
102	20.459
110	23.86

Axial Offset = 0.001	Interface Gap = 0
Amp-Turns	Force
[amps]	[N]
2	0.006396
25	1.0333
36	2.2012
43	3.1803
57	5.6815
80	11.351
102	18.529
110	21.478

Axial Offset = 0	Interface Gap = 0.001
Amp-Turns	Force
[amps]	[N]
2	0.0062798
25	1.0095
36	2.1473
43	3.1023
57	5.5439
80	11.087
102	18.163
110	21.166

Axial Offset = 0.001	Interface Gap = 0.001
Amp-Turns	Force
[amps]	[N]
2	0.0056511
25	0.90676
36	1.9264
43	2.7829
57	4.9733
80	9.9485
102	16.293
110	18.984

Axial Offset = 0	Interface Gap = 0.002
Amp-Turns	Force
[amps]	[N]
2	0.005675
25	0.90854
36	1.9282
43	2.7847
57	4.9753
80	9.9522
102	16.3
110	18.996

Axial Offset = 0.001	Interface Gap = 0.002
Amp-Turns	Force
[amps]	[N]
2	0.0051053
25	0.81561
36	1.7288
43	2.4963
57	4.4603
80	8.922
102	14.617
110	17.037

Axial Offset = 0	Interface Gap = 0.003
Amp-Turns	Force
[amps]	[N]
2	0.0051688
25	0.82482
36	1.7468
43	2.5217
57	4.5043
80	9.0096
102	14.747
110	17.188

Axial Offset = 0.001	Interface Gap = 0.003
Amp-Turns	Force
[amps]	[N]
2	0.0046599
25	0.74208
36	1.5695
43	2.2653
57	4.0464
80	8.0938
102	13.259
110	15.456

Axial Offset = 0.002	Interface Gap = 0
Amp-Turns [amps]	Force [N]
2	0.0058672
25	0.94554
36	2.0122
43	2.9071
57	5.1926
80	10.378
102	16.947
110	19.638

Axial Offset = 0.003	Interface Gap = 0
Amp-Turns [amps]	Force [N]
2	0.005371
25	0.86394
36	1.8363
43	2.65626
57	4.7378
80	9.4712
102	15.463
110	17.923

Axial Offset = 0.002	Interface Gap = 0.001
Amp-Turns [amps]	Force [N]
2	0.0051696
25	0.82798
36	1.7569
43	2.5377
57	4.5344
80	9.0703
102	14.86
110	17.316

Axial Offset = 0.003	Interface Gap = 0.001
Amp-Turns [amps]	Force [N]
2	0.0047141
25	0.75372
36	1.5974
43	2.3067
57	4.1221
80	8.2462
102	13.506
110	15.733

Axial Offset = 0.002	Interface Gap = 0.002
Amp-Turns [amps]	Force [N]
2	0.0046661
25	0.74416
36	1.5751
43	2.2738
57	4.062
80	8.1253
102	13.311
110	15.513

Axial Offset = 0.003	Interface Gap = 0.002
Amp-Turns [amps]	Force [N]
2	0.0042491
25	0.67674
36	1.4306
43	2.0648
57	3.6886
80	7.3787
102	12.091
110	14.089

Axial Offset = 0.002	Interface Gap = 0.003
Amp-Turns [amps]	Force [N]
2	0.0042535
25	0.67641
36	1.4284
43	2.0609
57	3.6808
80	7.3622
102	12.064
110	14.059

Axial Offset = 0.003	Interface Gap = 0.003
Amp-Turns [amps]	Force [N]
2	0.0038795
25	0.61624
36	1.2999
43	1.8749
57	3.3483
80	6.6969
102	10.976
110	12.79

The third set of data is all for a valve lift of 0.0105 inches. Data for the ideal model is presented first, followed by matrices of data for a range of character axial offset and interference gap to various degrees.

Perfect Model	0.0105
Amp-Turns	Force
[amps]	[N]
2	0.0064428
25	1.0379
36	2.2115
43	3.1951
57	5.7092
80	11.416
102	18.714
110	21.828

Axial Offset = 0		Interface Gap = 0		Axial Offset = 0.001		Interface Gap = 0	
Amp-Turns	Force	Amp-Turns	Force	Amp-Turns	Force	Amp-Turns	Force
[amps]	[N]	[amps]	[N]	[amps]	[N]	[amps]	[N]
2	0.0064428	2	0.0058509	2	0.0052042	2	0.0051053
25	1.0379	25	0.94254	25	0.83337	25	0.81561
36	2.2115	36	2.0057	36	1.7683	36	1.7288
43	3.1951	43	2.8975	43	2.554	43	2.4963
57	5.7092	57	5.176	57	4.5638	57	4.4603
80	11.416	80	10.344	80	9.1295	80	8.922
102	18.714	102	16.899	102	14.951	102	14.617
110	21.828	110	19.614	110	17.421	110	17.037

Axial Offset = 0		Interface Gap = 0.001		Axial Offset = 0.001		Interface Gap = 0.001	
Amp-Turns	Force	Amp-Turns	Force	Amp-Turns	Force	Amp-Turns	Force
[amps]	[N]	[amps]	[N]	[amps]	[N]	[amps]	[N]
2	0.0057564	2	0.0052042	2	0.0051053	2	0.0043097
25	0.92327	25	0.83337	25	0.81561	25	0.68545
36	1.9615	36	1.7683	36	1.7288	36	1.448
43	2.8334	43	2.554	43	2.4963	43	2.0893
57	5.0625	57	4.5638	57	4.4603	57	3.7316
80	10.127	80	9.1295	80	8.922	80	7.4637
102	16.576	102	14.951	102	14.617	102	12.229
110	19.313	110	17.421	110	17.037	110	14.252

Axial Offset = 0		Interface Gap = 0.002		Axial Offset = 0.001		Interface Gap = 0.002	
Amp-Turns	Force	Amp-Turns	Force	Amp-Turns	Force	Amp-Turns	Force
[amps]	[N]	[amps]	[N]	[amps]	[N]	[amps]	[N]
2	0.0052165	2	0.0051053	2	0.0051053	2	0.0043097
25	0.83354	25	0.81561	25	0.81561	25	0.68545
36	1.7668	36	1.7288	36	1.7288	36	1.448
43	2.5511	43	2.4963	43	2.4963	43	2.0893
57	4.5571	57	4.4603	57	4.4603	57	3.7316
80	9.116	80	8.922	80	8.922	80	7.4637
102	14.928	102	14.617	102	14.617	102	12.229
110	17.395	110	17.037	110	17.037	110	14.252

Axial Offset = 0		Interface Gap = 0.003		Axial Offset = 0.001		Interface Gap = 0.003	
Amp-Turns	Force	Amp-Turns	Force	Amp-Turns	Force	Amp-Turns	Force
[amps]	[N]	[amps]	[N]	[amps]	[N]	[amps]	[N]
2	0.0047613	2	0.0043097	2	0.0043097	2	0.0043097
25	0.75861	25	0.68545	25	0.68545	25	0.68545
36	1.6046	36	1.448	36	1.448	36	1.448
43	2.3158	43	2.0893	43	2.0893	43	2.0893
57	4.1359	57	3.7316	57	3.7316	57	3.7316
80	8.272	80	7.4637	80	7.4637	80	7.4637
102	13.541	102	12.229	102	12.229	102	12.229
110	15.78	110	14.252	110	14.252	110	14.252

Axial Offset = 0.002		Interface Gap = 0		Axial Offset = 0.003		Interface Gap = 0	
Amp-Turns	Force	Amp-Turns	Force	Amp-Turns	Force	Amp-Turns	Force
[amps]	[N]	[amps]	[N]	[amps]	[N]	[amps]	[N]
2	0.0053745	2	0.0050006	2	0.0043447	2	0.0039301
25	0.86417	25	0.80258	25	0.69372	25	0.62509
36	1.8372	36	1.7042	36	1.4683	36	1.32
43	2.654	43	2.4614	43	2.1198	43	1.9047
57	4.7409	57	4.3965	57	3.7875	57	3.4021
80	9.4752	80	8.7881	80	7.5756	80	6.8049
102	15.486	102	14.361	102	12.413	102	11.151
110	17.971	110	16.669	110	14.456	110	12.994

Axial Offset = 0.002		Interface Gap = 0.001		Axial Offset = 0.003		Interface Gap = 0.001	
Amp-Turns	Force	Amp-Turns	Force	Amp-Turns	Force	Amp-Turns	Force
[amps]	[N]	[amps]	[N]	[amps]	[N]	[amps]	[N]
2	0.0047398	2	0.0043447	2	0.0039301	2	0.003596
25	0.75765	25	0.69372	25	0.62509	25	0.57052
36	1.606	36	1.4683	36	1.32	36	1.2023
43	2.3193	43	2.1198	43	1.9047	43	1.7335
57	4.1446	57	3.7875	57	3.4021	57	3.0953
80	8.2908	80	7.5756	80	6.8049	80	6.191
102	13.58	102	12.413	102	11.151	102	10.147
110	15.826	110	14.456	110	12.994	110	11.824

Axial Offset = 0.002		Interface Gap = 0.002		Axial Offset = 0.003		Interface Gap = 0.002	
Amp-Turns	Force	Amp-Turns	Force	Amp-Turns	Force	Amp-Turns	Force
[amps]	[N]	[amps]	[N]	[amps]	[N]	[amps]	[N]
2	0.0042847	2	0.0039301	2	0.003596	2	0.003262
25	0.068242	25	0.62509	25	0.57052	25	0.5271
36	1.4429	36	1.32	36	1.2023	36	1.121
43	2.0826	43	1.9047	43	1.7335	43	1.615
57	3.7203	57	3.4021	57	3.0953	57	2.855
80	7.442	80	6.8049	80	6.191	80	5.715
102	12.194	102	11.151	102	10.147	102	9.355
110	14.21	110	12.994	110	11.824	110	10.95

Axial Offset = 0.002		Interface Gap = 0.003		Axial Offset = 0.003		Interface Gap = 0.003	
Amp-Turns	Force	Amp-Turns	Force	Amp-Turns	Force	Amp-Turns	Force
[amps]	[N]	[amps]	[N]	[amps]	[N]	[amps]	[N]
2	0.0039215	2	0.003596	2	0.003262	2	0.002928
25	0.62294	25	0.57052	25	0.5271	25	0.4837
36	1.3142	36	1.2023	36	1.121	36	1.04
43	1.8957	43	1.7335	43	1.615	43	1.5
57	3.3852	57	3.0953	57	2.855	57	2.635
80	6.7709	80	6.191	80	5.715	80	5.24
102	11.096	102	10.147	102	9.355	102	8.565
110	12.929	110	11.824	110	10.95	110	10.165

APPENDIX D - VALVE DISK DYNAMICS

Presented here is one of four Microsoft Excel spreadsheets developed to simulate in a stepwise fashion the traverse of the outlet valve disk as it moves between the valve seats and the valve yoke. This model is the execution of Equation 7.2 presented in the body of the thesis in combination with Figure 7.2.

$$\Delta V_n = \frac{F(X(t)_n)}{m} \Delta t \quad (\text{Equation 7.2a})$$

$$V_{n+1} = V_n + \Delta V_n$$

$$\Delta X(t)_n = \Delta V_n \Delta t \quad (\text{Equation 7.2b})$$

$$X(t)_{n+1} = X(t)_n + \Delta X(t)_n$$

This spreadsheet uses a time step of 0.000005 seconds and is calculated for the maximum force condition in Figure 7.2 developed from the bounding finite element models. The other three spreadsheets developed for the outlet valve represent the following situations: 1) a time step of 0.000005 seconds with the minimum force condition, 2) a 0.000001 second time step with the maximum force condition, and 3) a 0.000001 second time step with the minimum force condition. These spreadsheets have been left out because they are substantially longer than the one presented here and provide no additional useful information about this simulation process.

Volume	Density	Mass	Time Step
[m ³]	[kg/m ³]	[kg]	[seconds]
1.25985E-06	7584	0.009554739	0.000005

i	Time	Force	dV	V _{i+1}	dx	X _{i+1}
[]	[seconds]	[newtons]	[meters/second]	[meters/second]	[meters]	[meters]
0	0	30.16	0.015782745	0	0	0.01
1	0.000005	30.16	0.015782745	0.015782745	7.89137E-08	0.009999921
2	0.00001	30.16023848	0.015782869	0.031565614	1.57828E-07	0.009999763
3	0.000015	30.16071543	0.015783119	0.047348733	2.36744E-07	0.009999527
4	0.00002	30.16143087	0.015783493	0.063132227	3.15661E-07	0.009999211
5	0.000025	30.1623848	0.015783993	0.078916219	3.94581E-07	0.009998816
6	0.00003	30.16357723	0.015784617	0.094700836	4.73504E-07	0.009998343
7	0.000035	30.16500816	0.015785365	0.110486201	5.52431E-07	0.00999779
8	0.00004	30.1666776	0.015786239	0.12627244	6.31362E-07	0.009997159
9	0.000045	30.16858558	0.015787237	0.142059678	7.10298E-07	0.009996449
10	0.00005	30.1707321	0.015788361	0.157848038	7.8924E-07	0.009995659
11	0.000055	30.17311719	0.015789609	0.173637647	8.68188E-07	0.009994791
12	0.00006	30.17574086	0.015790982	0.189428629	9.47143E-07	0.009993844
13	0.000065	30.17860314	0.01579248	0.205221109	1.02611E-06	0.009992818
14	0.00007	30.18170404	0.015794102	0.221015211	1.10508E-06	0.009991713
15	0.000075	30.1850436	0.01579585	0.236811061	1.18406E-06	0.009990529
16	0.00008	30.18862185	0.015797722	0.252608784	1.26304E-06	0.009989266
17	0.000085	30.1924388	0.01579972	0.268408504	1.34204E-06	0.009987924
18	0.00009	30.19649451	0.015801842	0.284210346	1.42105E-06	0.009986503
19	0.000095	30.200789	0.01580409	0.300014435	1.50007E-06	0.009985003
20	0.0001	30.20532231	0.015806462	0.315820897	1.5791E-06	0.009983424

21	0.000105	30.21009448	0.015808959	0.331629856	1.65815E-06	0.009981765
22	0.00011	30.21510556	0.015811581	0.347441438	1.73721E-06	0.009980028
23	0.000115	30.22035559	0.015814329	0.363255767	1.81628E-06	0.009978212
24	0.00012	30.22584462	0.015817201	0.379072968	1.89536E-06	0.009976317
25	0.000125	30.2315727	0.015820199	0.394893166	1.97447E-06	0.009974342
26	0.00013	30.2375399	0.015823321	0.410716488	2.05358E-06	0.009972289
27	0.000135	30.24374627	0.015826569	0.426543057	2.13272E-06	0.009970156
28	0.00014	30.25019186	0.015829942	0.442372999	2.21186E-06	0.009967944
29	0.000145	30.25687675	0.01583344	0.458206439	2.29103E-06	0.009965653
30	0.00015	30.26380101	0.015837064	0.474043503	2.37022E-06	0.009963283
31	0.000155	30.27096471	0.015840813	0.489884316	2.44942E-06	0.009960833
32	0.00016	30.27836792	0.015844687	0.505729002	2.52865E-06	0.009958305
33	0.000165	30.28601072	0.015848686	0.521577688	2.60789E-06	0.009955697
34	0.00017	30.29389321	0.015852811	0.537430499	2.68715E-06	0.00995301
35	0.000175	30.30201546	0.015857061	0.553287561	2.76644E-06	0.009950243
36	0.00018	30.31037758	0.015861437	0.569148998	2.84574E-06	0.009947397
37	0.000185	30.31897966	0.015865939	0.585014937	2.92507E-06	0.009944472
38	0.00019	30.3278218	0.015870566	0.600885503	3.00443E-06	0.009941468
39	0.000195	30.33690411	0.015875319	0.616760821	3.0838E-06	0.009938384
40	0.0002	30.34622671	0.015880197	0.632641019	3.16321E-06	0.009935221
41	0.000205	30.3557897	0.015885202	0.64852622	3.24263E-06	0.009931978
42	0.00021	30.36559323	0.015890332	0.664416552	3.32208E-06	0.009928656
43	0.000215	30.3756374	0.015895588	0.68031214	3.40156E-06	0.009925255
44	0.00022	30.38592236	0.01590097	0.69621311	3.48107E-06	0.009921774
45	0.000225	30.39644825	0.015906478	0.712119588	3.5606E-06	0.009918213
46	0.00023	30.40721522	0.015912113	0.7280317	3.64016E-06	0.009914573
47	0.000235	30.41822341	0.015917873	0.743949573	3.71975E-06	0.009910853
48	0.00024	30.42947299	0.01592376	0.759873333	3.79937E-06	0.009907054
49	0.000245	30.44096413	0.015929773	0.775803107	3.87902E-06	0.009903175
50	0.00025	30.45269699	0.015935913	0.79173902	3.9587E-06	0.009899216
51	0.000255	30.46467177	0.01594218	0.807681199	4.03841E-06	0.009895178
52	0.00026	30.47688863	0.015948573	0.823629772	4.11815E-06	0.009891059
53	0.000265	30.48934779	0.015955093	0.839584865	4.19792E-06	0.009886861
54	0.00027	30.50204945	0.015961739	0.855546604	4.27773E-06	0.009882584
55	0.000275	30.51499382	0.015968513	0.871515117	4.35758E-06	0.009878226
56	0.00028	30.52818111	0.015975414	0.887490531	4.43745E-06	0.009873789
57	0.000285	30.54161156	0.015982442	0.903472973	4.51736E-06	0.009869271
58	0.00029	30.55528541	0.015989598	0.919462571	4.59731E-06	0.009864674
59	0.000295	30.5692029	0.015996881	0.935459452	4.6773E-06	0.009859997
60	0.0003	30.58336428	0.016004291	0.951463743	4.75732E-06	0.009855239
61	0.000305	30.59776984	0.01601183	0.967475573	4.83738E-06	0.009850402
62	0.00031	30.61241983	0.016019496	0.983495069	4.91748E-06	0.009845485
63	0.000315	30.62731455	0.016027291	0.99952236	4.99761E-06	0.009840487
64	0.00032	30.6424543	0.016035213	1.015557573	5.07779E-06	0.009835409
65	0.000325	30.65783938	0.016043264	1.031600837	5.158E-06	0.009830251
66	0.00033	30.67347012	0.016051444	1.047652281	5.23826E-06	0.009825013
67	0.000335	30.68934684	0.016059752	1.063712033	5.31856E-06	0.009819694
68	0.00034	30.70546988	0.016068189	1.079780223	5.3989E-06	0.009814295
69	0.000345	30.72183961	0.016076756	1.095856978	5.47928E-06	0.009808816
70	0.00035	30.73845639	0.016085451	1.111942429	5.55971E-06	0.009803256
71	0.000355	30.75532059	0.016094276	1.128036706	5.64018E-06	0.009797616
72	0.00036	30.77243262	0.016103231	1.144139937	5.7207E-06	0.009791896
73	0.000365	30.78979287	0.016112316	1.160252252	5.80126E-06	0.009786094
74	0.00037	30.80740178	0.01612153	1.176373783	5.88187E-06	0.009780212
75	0.000375	30.82525976	0.016130875	1.192504658	5.96252E-06	0.00977425

76	0.00038	30.84336728	0.016140351	1.208645009	6.04323E-06	0.009768207
77	0.000385	30.8617248	0.016149958	1.224794967	6.12397E-06	0.009762083
78	0.00039	30.88033279	0.016159695	1.240954662	6.20477E-06	0.009755878
79	0.000395	30.89919175	0.016169564	1.257124226	6.28562E-06	0.009749592
80	0.0004	30.9183022	0.016179565	1.273303791	6.36652E-06	0.009743226
81	0.000405	30.93766465	0.016189697	1.289493488	6.44747E-06	0.009736778
82	0.00041	30.95727966	0.016199962	1.305693449	6.52847E-06	0.00973025
83	0.000415	30.97714778	0.016210359	1.321903808	6.60952E-06	0.00972364
84	0.00042	30.99726959	0.016220888	1.338124696	6.69062E-06	0.00971695
85	0.000425	31.01764569	0.016231551	1.354356247	6.77178E-06	0.009710178
86	0.00043	31.0382767	0.016242347	1.370598594	6.85299E-06	0.009703325
87	0.000435	31.05916325	0.016253277	1.386851872	6.93426E-06	0.009696391
88	0.00044	31.08030599	0.016264341	1.403116213	7.01558E-06	0.009689375
89	0.000445	31.1017056	0.01627554	1.419391753	7.09696E-06	0.009682278
90	0.00045	31.12336277	0.016286873	1.435678626	7.17839E-06	0.0096751
91	0.000455	31.14527822	0.016298341	1.451976967	7.25988E-06	0.00966784
92	0.00046	31.16745267	0.016309945	1.468286912	7.34143E-06	0.009660498
93	0.000465	31.18988689	0.016321685	1.484608597	7.42304E-06	0.009653075
94	0.00047	31.21258166	0.016333561	1.500942158	7.50471E-06	0.009645571
95	0.000475	31.23553777	0.016345574	1.517287732	7.58644E-06	0.009637984
96	0.00048	31.25875605	0.016357724	1.533645457	7.66823E-06	0.009630316
97	0.000485	31.28223736	0.016370012	1.550015469	7.75008E-06	0.009622566
98	0.00049	31.30598255	0.016382438	1.566397907	7.83199E-06	0.009614734
99	0.000495	31.32999253	0.016395002	1.582792909	7.91396E-06	0.00960682
100	0.0005	31.35426822	0.016407706	1.599200615	7.996E-06	0.009598824
101	0.000505	31.37881057	0.016420549	1.615621164	8.07811E-06	0.009590746
102	0.00051	31.40362054	0.016433532	1.632054696	8.16027E-06	0.009582586
103	0.000515	31.42869915	0.016446656	1.648501351	8.24251E-06	0.009574343
104	0.00052	31.4540474	0.01645992	1.664961272	8.32481E-06	0.009566018
105	0.000525	31.47966637	0.016473327	1.681434599	8.40717E-06	0.009557611
106	0.00053	31.50555713	0.016486875	1.697921474	8.48961E-06	0.009549122
107	0.000535	31.53172208	0.016500567	1.714422041	8.57211E-06	0.009540549
108	0.00054	31.55815851	0.016514402	1.730936443	8.65468E-06	0.009531895
109	0.000545	31.58487144	0.016528381	1.747464823	8.73732E-06	0.009523157
110	0.00055	31.61186078	0.016542504	1.764007328	8.82004E-06	0.009514337
111	0.000555	31.63912777	0.016556773	1.780564101	8.90282E-06	0.009505435
112	0.00056	31.66667368	0.016571188	1.797135288	8.98568E-06	0.009496449
113	0.000565	31.69449981	0.016585749	1.813721038	9.06861E-06	0.00948738
114	0.00057	31.72260747	0.016600458	1.830321496	9.15161E-06	0.009478229
115	0.000575	31.75099804	0.016615315	1.84693681	9.23468E-06	0.009468994
116	0.00058	31.77967291	0.01663032	1.863567131	9.31784E-06	0.009459676
117	0.000585	31.80863352	0.016645475	1.880212606	9.40106E-06	0.009450275
118	0.00059	31.83788134	0.016660781	1.896873387	9.48437E-06	0.009440791
119	0.000595	31.86741786	0.016676237	1.913549625	9.56775E-06	0.009431223
120	0.0006	31.89724463	0.016691846	1.93024147	9.65121E-06	0.009421572
121	0.000605	31.92736323	0.016707607	1.946949077	9.73475E-06	0.009411837
122	0.00061	31.95777529	0.016723521	1.963672598	9.81836E-06	0.009402019
123	0.000615	31.98848244	0.016739591	1.980412189	9.90206E-06	0.009392117
124	0.00062	32.01948639	0.016755815	1.997168004	9.98584E-06	0.009382131
125	0.000625	32.05078888	0.016772196	2.013940199	1.00697E-05	0.009372061
126	0.00063	32.08239169	0.016788733	2.030728933	1.01536E-05	0.009361907
127	0.000635	32.11429662	0.016805429	2.047534362	1.02377E-05	0.00935167
128	0.00064	32.14650556	0.016822284	2.064356646	1.03218E-05	0.009341348
129	0.000645	32.17902039	0.016839299	2.081195945	1.0406E-05	0.009330942
130	0.00065	32.21184308	0.016856475	2.09805242	1.04903E-05	0.009320452

131	0.000655	32.24497561	0.016873814	2.114926234	1.05746E-05	0.009309877
132	0.00066	32.27842002	0.016891315	2.131817549	1.06591E-05	0.009299218
133	0.000665	32.31217841	0.016908981	2.14872653	1.07436E-05	0.009288474
134	0.00067	32.3462529	0.016926812	2.165653342	1.08283E-05	0.009277646
135	0.000675	32.38064568	0.01694481	2.182598151	1.0913E-05	0.009266733
136	0.00068	32.41535898	0.016962975	2.199561127	1.09978E-05	0.009255735
137	0.000685	32.45039508	0.01698131	2.216542436	1.10827E-05	0.009244653
138	0.00069	32.48575631	0.016999814	2.233542251	1.11677E-05	0.009233485
139	0.000695	32.52144506	0.01701849	2.250560741	1.12528E-05	0.00922232
140	0.0007	32.55746375	0.017037339	2.267598079	1.1338E-05	0.009210894
141	0.000705	32.59381488	0.017056361	2.284654441	1.14233E-05	0.009199471
142	0.00071	32.63050099	0.017075559	2.30173	1.15086E-05	0.009187962
143	0.000715	32.66752468	0.017094934	2.318824934	1.15941E-05	0.009176368
144	0.00072	32.7048886	0.017114486	2.33593942	1.16797E-05	0.009164688
145	0.000725	32.74259545	0.017134218	2.353073638	1.17654E-05	0.009152923
146	0.00073	32.78064802	0.017154131	2.370227769	1.18511E-05	0.009141072
147	0.000735	32.81904911	0.017174227	2.387401996	1.1937E-05	0.009129135
148	0.00074	32.85780163	0.017194506	2.404596502	1.2023E-05	0.009117112
149	0.000745	32.89690852	0.01721497	2.421811472	1.21091E-05	0.009105003
150	0.00075	32.93637277	0.017235622	2.439047094	1.21952E-05	0.009092808
151	0.000755	32.97619748	0.017256462	2.456303556	1.22815E-05	0.009080526
152	0.00076	33.01638576	0.017277493	2.473581049	1.23679E-05	0.009068158
153	0.000765	33.05694082	0.017298715	2.490879765	1.24544E-05	0.009055704
154	0.00077	33.09786593	0.017320132	2.508199896	1.2541E-05	0.009043163
155	0.000775	33.13916441	0.017341743	2.525541639	1.26277E-05	0.009030535
156	0.00078	33.18083966	0.017363552	2.542905191	1.27145E-05	0.00901782
157	0.000785	33.22289515	0.017385559	2.56029075	1.28015E-05	0.009005019
158	0.00079	33.26533442	0.017407768	2.577698518	1.28885E-05	0.008992131
159	0.000795	33.30816107	0.017430179	2.595128697	1.29756E-05	0.008979155
160	0.0008	33.35137879	0.017452795	2.612581492	1.30629E-05	0.008966092
161	0.000805	33.39499134	0.017475617	2.63005711	1.31503E-05	0.008952942
162	0.00081	33.43900253	0.017498648	2.647555758	1.32378E-05	0.008939704
163	0.000815	33.48341627	0.01752189	2.665077648	1.33254E-05	0.008926379
164	0.00082	33.52823654	0.017545345	2.682622993	1.34131E-05	0.008912965
165	0.000825	33.5734674	0.017569014	2.700192007	1.3501E-05	0.008899464
166	0.00083	33.61911299	0.0175929	2.717784907	1.35889E-05	0.008885876
167	0.000835	33.66517753	0.017617006	2.735401913	1.3677E-05	0.008872198
168	0.00084	33.7116653	0.017641333	2.753043246	1.37652E-05	0.008858433
169	0.000845	33.7585807	0.017665884	2.77070913	1.38535E-05	0.00884458
170	0.00085	33.80592818	0.017690661	2.788399791	1.3942E-05	0.008830638
171	0.000855	33.8537123	0.017715666	2.806115457	1.40306E-05	0.008816607
172	0.00086	33.9019377	0.017740903	2.82385636	1.41193E-05	0.008802488
173	0.000865	33.9506091	0.017766372	2.841622733	1.42081E-05	0.00878828
174	0.00087	33.99973131	0.017792078	2.859414811	1.42971E-05	0.008773983
175	0.000875	34.04930923	0.017818022	2.877232833	1.43862E-05	0.008759597
176	0.00088	34.09934787	0.017844208	2.895077041	1.44754E-05	0.008745121
177	0.000885	34.14985232	0.017870637	2.912947677	1.45647E-05	0.008730556
178	0.00089	34.20082774	0.017897312	2.930844989	1.46542E-05	0.008715902
179	0.000895	34.25227944	0.017924237	2.948769226	1.47438E-05	0.008701158
180	0.0009	34.30421277	0.017951413	2.966720639	1.48336E-05	0.008686325
181	0.000905	34.35663323	0.017978845	2.984699485	1.49235E-05	0.008671401
182	0.00091	34.40954637	0.018006535	3.002706019	1.50135E-05	0.008656388
183	0.000915	34.46295789	0.018034485	3.020740504	1.51037E-05	0.008641284
184	0.00092	34.51687357	0.018062699	3.038803203	1.5194E-05	0.00862609
185	0.000925	34.57129928	0.01809118	3.056894383	1.52845E-05	0.008610806

186	0.00093	34.62624102	0.018119931	3.075014314	1.53751E-05	0.00859543
187	0.000935	34.6817049	0.018148955	3.093163269	1.54658E-05	0.008579965
188	0.00094	34.73769711	0.018178256	3.111341526	1.55567E-05	0.008564408
189	0.000945	34.79422399	0.018207837	3.129549362	1.56477E-05	0.00854876
190	0.00095	34.85129197	0.0182377	3.147787062	1.57389E-05	0.008533021
191	0.000955	34.90890758	0.018267851	3.166054913	1.58303E-05	0.008517191
192	0.00096	34.96707751	0.018298291	3.184353204	1.59218E-05	0.008501269
193	0.000965	35.02580852	0.018329025	3.202682229	1.60134E-05	0.008485256
194	0.00097	35.08510753	0.018360056	3.221042285	1.61052E-05	0.008469151
195	0.000975	35.14498154	0.018391388	3.239433673	1.61972E-05	0.008452953
196	0.00098	35.20543771	0.018423025	3.257856698	1.62893E-05	0.008436664
197	0.000985	35.26648331	0.01845497	3.276311669	1.63816E-05	0.008420283
198	0.00099	35.32812573	0.018487228	3.294798896	1.6474E-05	0.008403809
199	0.000995	35.3903725	0.018519801	3.313318698	1.65666E-05	0.008387242
200	0.001	35.45323127	0.018552695	3.331871393	1.66594E-05	0.008370583
201	0.001005	35.51670982	0.018585914	3.350457307	1.67523E-05	0.00835383
202	0.00101	35.58081609	0.018619461	3.369076768	1.68454E-05	0.008336985
203	0.001015	35.64555812	0.01865334	3.387730108	1.69387E-05	0.008320046
204	0.00102	35.71094411	0.018687557	3.406417665	1.70321E-05	0.008303014
205	0.001025	35.77698239	0.018722115	3.425139779	1.71257E-05	0.008285889
206	0.00103	35.84368144	0.018757018	3.443896798	1.72195E-05	0.008268669
207	0.001035	35.91104988	0.018792272	3.46268907	1.73134E-05	0.008251356
208	0.00104	35.97909648	0.018827881	3.481516951	1.74076E-05	0.008233948
209	0.001045	36.04783014	0.018863849	3.5003808	1.75019E-05	0.008216446
210	0.00105	36.11725994	0.018900182	3.519280982	1.75964E-05	0.00819885
211	0.001055	36.18739508	0.018936884	3.538217866	1.76911E-05	0.008181159
212	0.00106	36.25824495	0.01897396	3.557191826	1.7786E-05	0.008163373
213	0.001065	36.32981906	0.019011414	3.57620324	1.7881E-05	0.008145492
214	0.00107	36.4021271	0.019049253	3.595252493	1.79763E-05	0.008127515
215	0.001075	36.47517893	0.019087481	3.614339975	1.80717E-05	0.008109444
216	0.00108	36.54898454	0.019126104	3.633466078	1.81673E-05	0.008091276
217	0.001085	36.62355413	0.019165126	3.652631204	1.82632E-05	0.008073013
218	0.00109	36.69889803	0.019204554	3.671835758	1.83592E-05	0.008054654
219	0.001095	36.77502676	0.019244392	3.69108015	1.84554E-05	0.008036199
220	0.0011	36.85195101	0.019284646	3.710364796	1.85518E-05	0.008017647
221	0.001105	36.92968165	0.019325323	3.729690119	1.86485E-05	0.007998998
222	0.00111	37.00822971	0.019366427	3.749056546	1.87453E-05	0.007980253
223	0.001115	37.08760643	0.019407965	3.768464511	1.88423E-05	0.007961411
224	0.00112	37.16782321	0.019449942	3.787914453	1.89396E-05	0.007942471
225	0.001125	37.24889164	0.019492366	3.807406819	1.9037E-05	0.007923434
226	0.00113	37.3308235	0.019535241	3.826942059	1.91347E-05	0.007904299
227	0.001135	37.41363077	0.019578574	3.846520633	1.92326E-05	0.007885067
228	0.00114	37.49732562	0.019622371	3.866143004	1.93307E-05	0.007865736
229	0.001145	37.58192041	0.019666664	3.885809644	1.9429E-05	0.007846307
230	0.00115	37.6674277	0.019711386	3.90552103	1.95276E-05	0.007826779
231	0.001155	37.75386026	0.019756616	3.925277646	1.96264E-05	0.007807153
232	0.00116	37.84123106	0.019802337	3.945079983	1.97254E-05	0.007787428
233	0.001165	37.92955329	0.019848556	3.964928539	1.98246E-05	0.007767603
234	0.00117	38.01884033	0.01989528	3.984823819	1.99241E-05	0.007747679
235	0.001175	38.1091058	0.019942516	4.004766335	2.00238E-05	0.007727655
236	0.00118	38.20036352	0.019990271	4.024756606	2.01238E-05	0.007707531
237	0.001185	38.29262753	0.020038553	4.044795159	2.0224E-05	0.007687307
238	0.00119	38.38591211	0.020087369	4.064882528	2.03244E-05	0.007666983
239	0.001195	38.48023175	0.020136727	4.085019255	2.04251E-05	0.007646558
240	0.0012	38.57560118	0.020186633	4.105205888	2.0526E-05	0.007626032

241	0.001205	38.67203537	0.020237097	4.125442986	2.06272E-05	0.007605405
242	0.00121	38.76954951	0.020288127	4.145731112	2.07287E-05	0.007584676
243	0.001215	38.86815904	0.020339729	4.166070842	2.08304E-05	0.007563846
244	0.00122	38.96787966	0.020391913	4.186462754	2.09323E-05	0.007542913
245	0.001225	39.06872729	0.020444687	4.206907441	2.10345E-05	0.007521879
246	0.00123	39.17071813	0.020498058	4.227405499	2.1137E-05	0.007500742
247	0.001235	39.2738686	0.020552037	4.247957537	2.12398E-05	0.007479502
248	0.00124	39.37819542	0.020606631	4.268564168	2.13428E-05	0.007458159
249	0.001245	39.48371555	0.02066185	4.289226018	2.14461E-05	0.007436713
250	0.00125	39.59044621	0.020717702	4.30994372	2.15497E-05	0.007415163
251	0.001255	39.69840492	0.020774197	4.330717918	2.16536E-05	0.00739351
252	0.00126	39.80760944	0.020831344	4.351549262	2.17577E-05	0.007371752
253	0.001265	39.91807784	0.020889152	4.372438414	2.18622E-05	0.00734989
254	0.00127	40.02982844	0.020947631	4.393386045	2.19669E-05	0.007327923
255	0.001275	40.14287989	0.021006791	4.414392836	2.2072E-05	0.007305851
256	0.00128	40.2572511	0.021066642	4.435459478	2.21773E-05	0.007283673
257	0.001285	40.37296128	0.021127193	4.456586671	2.22829E-05	0.007261391
258	0.00129	40.49002995	0.021188455	4.477775126	2.23889E-05	0.007239002
259	0.001295	40.60847693	0.021250438	4.499025564	2.24951E-05	0.007216507
260	0.0013	40.72832235	0.021313154	4.520338718	2.26017E-05	0.007193905
261	0.001305	40.84958666	0.021376611	4.541715329	2.27086E-05	0.007171196
262	0.00131	40.97229062	0.021440822	4.563156151	2.28158E-05	0.00714838
263	0.001315	41.09645532	0.021505798	4.584661949	2.29233E-05	0.007125457
264	0.00132	41.22210219	0.021571549	4.606233498	2.30312E-05	0.007102426
265	0.001325	41.34925296	0.021638087	4.627871585	2.31394E-05	0.007079287
266	0.00133	41.47792974	0.021705424	4.649577008	2.32479E-05	0.007056039
267	0.001335	41.60815495	0.02177357	4.671350579	2.33568E-05	0.007032682
268	0.00134	41.7399514	0.02184254	4.693193119	2.3466E-05	0.007009216
269	0.001345	41.8733422	0.021912343	4.715105462	2.35755E-05	0.006985641
270	0.00135	42.00835088	0.021982993	4.737088455	2.36854E-05	0.006961955
271	0.001355	42.14500129	0.022054502	4.759142957	2.37957E-05	0.006938159
272	0.00136	42.28331768	0.022126883	4.781269841	2.39063E-05	0.006914253
273	0.001365	42.42332466	0.022200149	4.80346999	2.40173E-05	0.006890236
274	0.00137	42.56504723	0.022274313	4.825744303	2.41287E-05	0.006866107
275	0.001375	42.70851079	0.022349387	4.84809369	2.42405E-05	0.006841866
276	0.00138	42.85374113	0.022425386	4.870519076	2.43526E-05	0.006817514
277	0.001385	43.00076442	0.022502324	4.8930214	2.44651E-05	0.006793049
278	0.00139	43.14960727	0.022580213	4.915601613	2.4578E-05	0.006768471
279	0.001395	43.3002967	0.022659069	4.938260683	2.46913E-05	0.006743779
280	0.0014	43.45286013	0.022738906	4.960999588	2.4805E-05	0.006718974
281	0.001405	43.60732542	0.022819737	4.983819326	2.49191E-05	0.006694055
282	0.00141	43.76372088	0.022901579	5.006720905	2.50336E-05	0.006669022
283	0.001415	43.92207524	0.022984446	5.029705351	2.51485E-05	0.006643873
284	0.00142	44.08241769	0.023068354	5.052773705	2.52639E-05	0.006618609
285	0.001425	44.24477788	0.023153317	5.075927021	2.53796E-05	0.00659323
286	0.00143	44.4091859	0.023239351	5.099166373	2.54958E-05	0.006567734
287	0.001435	44.57567235	0.023326474	5.122492847	2.56125E-05	0.006542121
288	0.00144	44.74426828	0.0234147	5.145907547	2.57295E-05	0.006516392
289	0.001445	44.91500523	0.023504047	5.169411594	2.58471E-05	0.006490545
290	0.00145	45.08791524	0.023594531	5.193006125	2.5965E-05	0.00646458
291	0.001455	45.26303086	0.023686169	5.216692294	2.60835E-05	0.006438496
292	0.00146	45.44038514	0.023778979	5.240471273	2.62024E-05	0.006412294
293	0.001465	45.62001165	0.023872977	5.26434425	2.63217E-05	0.006385972
294	0.00147	45.80194449	0.023968183	5.288312433	2.64416E-05	0.006359531
295	0.001475	45.9862183	0.024064613	5.312377046	2.65619E-05	0.006332969

296	0.00148	46.17286827	0.024162287	5.336539334	2.66827E-05	0.006306286
297	0.001485	46.36193013	0.024261224	5.360800557	2.6804E-05	0.006279482
298	0.00149	46.55344018	0.024361441	5.385161998	2.69258E-05	0.006252556
299	0.001495	46.74743531	0.024462959	5.409624957	2.70481E-05	0.006225508
300	0.0015	46.94395297	0.024565796	5.434190753	2.7171E-05	0.006198337
301	0.001505	47.14303122	0.024669974	5.458860728	2.72943E-05	0.006171043
302	0.00151	47.34470871	0.024775512	5.48363624	2.74182E-05	0.006143625
303	0.001515	47.54902471	0.024882431	5.508518671	2.75426E-05	0.006116082
304	0.00152	47.75601912	0.024990751	5.533509422	2.76675E-05	0.006088415
305	0.001525	47.96573247	0.025100494	5.558609916	2.7793E-05	0.006060622
306	0.00153	48.17820594	0.025211682	5.583821598	2.79191E-05	0.006032702
307	0.001535	48.39348136	0.025324336	5.609145934	2.80457E-05	0.006004657
308	0.00154	48.61160122	0.025438478	5.634584411	2.81729E-05	0.005976484
309	0.001545	48.83260872	0.025554131	5.660138542	2.83007E-05	0.005948183
310	0.00155	49.05654773	0.025671319	5.685809861	2.8429E-05	0.005919754
311	0.001555	49.28346282	0.025790063	5.711599924	2.8558E-05	0.005891196
312	0.00156	49.51339929	0.025910389	5.737510313	2.86876E-05	0.005862508
313	0.001565	49.74640316	0.02603232	5.763542634	2.88177E-05	0.005833691
314	0.00157	49.9825212	0.026155881	5.789698515	2.89485E-05	0.005804742
315	0.001575	50.22180093	0.026281096	5.815979611	2.90799E-05	0.005775662
316	0.00158	50.46429064	0.026407991	5.842387602	2.92119E-05	0.00574645
317	0.001585	50.71003941	0.026536592	5.868924193	2.93446E-05	0.005717106
318	0.00159	50.95909709	0.026666924	5.895591117	2.9478E-05	0.005687628
319	0.001595	51.21151437	0.026799014	5.922390131	2.9612E-05	0.005658016
320	0.0016	51.46734277	0.026932889	5.94932302	2.97466E-05	0.005628269
321	0.001605	51.72663461	0.027068576	5.976391596	2.9882E-05	0.005598387
322	0.00161	51.98944311	0.027206104	6.0035977	3.0018E-05	0.005568369
323	0.001615	52.25582233	0.027345501	6.030943201	3.01547E-05	0.005538215
324	0.00162	52.52582725	0.027486794	6.058429995	3.02921E-05	0.005507922
325	0.001625	52.79951372	0.027630015	6.08606001	3.04303E-05	0.005477492
326	0.00163	53.07693852	0.027775191	6.113835201	3.05692E-05	0.005446923
327	0.001635	53.35815939	0.027922354	6.141757556	3.07088E-05	0.005416214
328	0.00164	53.643235	0.028071534	6.16982909	3.08491E-05	0.005385365
329	0.001645	53.932225	0.028222763	6.198051853	3.09903E-05	0.005354375
330	0.00165	54.22519003	0.028376072	6.226427925	3.11321E-05	0.005323243
331	0.001655	54.52219174	0.028531493	6.254959418	3.12748E-05	0.005291968
332	0.00166	54.82329282	0.028689059	6.283648477	3.14182E-05	0.00526055
333	0.001665	55.12855699	0.028848804	6.312497282	3.15625E-05	0.005228987
334	0.00167	55.43804904	0.029010762	6.341508043	3.17075E-05	0.00519728
335	0.001675	55.75183487	0.029174966	6.370683009	3.18534E-05	0.005165426
336	0.00168	56.06998147	0.029341452	6.400024462	3.20001E-05	0.005133426
337	0.001685	56.39255696	0.029510256	6.429534718	3.21477E-05	0.005101278
338	0.00169	56.71963063	0.029681414	6.459216132	3.22961E-05	0.005068982
339	0.001695	57.05127292	0.029854963	6.489071094	3.24454E-05	0.005036537
340	0.0017	57.38755548	0.030030939	6.519102034	3.25955E-05	0.005003941
341	0.001705	57.72855118	0.030209383	6.549311417	3.27466E-05	0.004971195
342	0.00171	58.07433415	0.030390331	6.579701748	3.28985E-05	0.004938296
343	0.001715	58.42497976	0.030573824	6.610275572	3.30514E-05	0.004905245
344	0.00172	58.7805647	0.030759902	6.641035474	3.32052E-05	0.00487204
345	0.001725	59.14116696	0.030948605	6.671984079	3.33599E-05	0.00483868
346	0.00173	59.5068659	0.031139976	6.703124055	3.35156E-05	0.004805164
347	0.001735	59.87774222	0.031334056	6.73445811	3.36723E-05	0.004771492
348	0.00174	60.25387805	0.031530888	6.765988998	3.38299E-05	0.004737662
349	0.001745	60.63535693	0.031730516	6.797719514	3.39886E-05	0.004703673
350	0.00175	61.02226387	0.031932984	6.829652498	3.41483E-05	0.004669525

351	0.001755	61.41468536	0.032138339	6.861790837	3.4309E-05	0.004635216
352	0.00176	61.81270941	0.032346625	6.894137462	3.44707E-05	0.004600746
353	0.001765	62.21642557	0.03255789	6.926695352	3.46335E-05	0.004566112
354	0.00177	62.62592497	0.032772181	6.959467533	3.47973E-05	0.004531315
355	0.001775	63.04130037	0.032989547	6.99245708	3.49623E-05	0.004496352
356	0.00178	63.46264615	0.033210038	7.025667118	3.51283E-05	0.004461224
357	0.001785	63.89005839	0.033433703	7.059100821	3.52955E-05	0.004425929
358	0.00179	64.32363486	0.033660594	7.092761414	3.54638E-05	0.004390465
359	0.001795	64.7634751	0.033890762	7.126652177	3.56333E-05	0.004354832
360	0.0018	65.20968043	0.034124262	7.160776438	3.58039E-05	0.004319028
361	0.001805	65.662354	0.034361146	7.195137584	3.59757E-05	0.004283052
362	0.00181	66.12160079	0.03460147	7.229739055	3.61487E-05	0.004246903
363	0.001815	66.58752773	0.03484529	7.264584345	3.63229E-05	0.00421058
364	0.00182	67.06024365	0.035092663	7.299677007	3.64984E-05	0.004174082
365	0.001825	67.53985938	0.035343646	7.335020653	3.66751E-05	0.004137407
366	0.00183	68.02648777	0.035598299	7.370618951	3.68531E-05	0.004100554
367	0.001835	68.52024376	0.035856681	7.406475633	3.70324E-05	0.004063521
368	0.00184	69.02124436	0.036118855	7.442594488	3.7213E-05	0.004026308
369	0.001845	69.52960877	0.036384883	7.478979371	3.73949E-05	0.003988914
370	0.00185	70.04545838	0.036654827	7.515634198	3.75782E-05	0.003951335
371	0.001855	70.56891686	0.036928753	7.552562951	3.77628E-05	0.003913573
372	0.00186	71.10011014	0.037206727	7.589769678	3.79488E-05	0.003875624
373	0.001865	71.63916653	0.037488815	7.627258493	3.81363E-05	0.003837487
374	0.00187	72.18621674	0.037775087	7.66503358	3.83252E-05	0.003799162
375	0.001875	72.74139394	0.038065612	7.703099192	3.85155E-05	0.003760647
376	0.00188	73.3048338	0.03836046	7.741459652	3.87073E-05	0.003721939
377	0.001885	73.87667456	0.038659705	7.780119356	3.89006E-05	0.003683039
378	0.00189	74.4570571	0.038963419	7.819082775	3.90954E-05	0.003643943
379	0.001895	75.04612496	0.039271679	7.858354454	3.92918E-05	0.003604652
380	0.0019	75.64402445	0.03958456	7.897939014	3.94897E-05	0.003565162
381	0.001905	76.25090465	0.03990214	7.937841154	3.96892E-05	0.003525473
382	0.00191	76.86691755	0.0402245	7.978065655	3.98903E-05	0.003485582
383	0.001915	77.49221804	0.04055172	8.018617375	4.00931E-05	0.003445489
384	0.00192	78.12696404	0.040883883	8.059501259	4.02975E-05	0.003405192
385	0.001925	78.77131651	0.041221073	8.100722332	4.05036E-05	0.003364688
386	0.00193	79.42543957	0.041563376	8.142285708	4.07114E-05	0.003323977
387	0.001935	80.08950055	0.04191088	8.184196588	4.0921E-05	0.003283056
388	0.00194	80.76367006	0.042263673	8.226460261	4.11323E-05	0.003241924
389	0.001945	81.44812208	0.042621847	8.269082109	4.13454E-05	0.003200578
390	0.00195	82.14303402	0.042985495	8.312067604	4.15603E-05	0.003159018
391	0.001955	82.84858684	0.043354711	8.355422315	4.17771E-05	0.003117241
392	0.00196	83.56496508	0.043729592	8.399151907	4.19958E-05	0.003075245
393	0.001965	84.29235697	0.044110237	8.443262144	4.22163E-05	0.003033029
394	0.00197	85.03095452	0.044496745	8.48775889	4.24388E-05	0.00299059
395	0.001975	85.78095361	0.04488922	8.53264811	4.26632E-05	0.002947927
396	0.00198	86.54255409	0.045287766	8.577935876	4.28897E-05	0.002905037
397	0.001985	87.31595984	0.04569249	8.623628366	4.31181E-05	0.002861919
398	0.00199	88.10137891	0.0461035	8.669731866	4.33487E-05	0.00281857
399	0.001995	88.89902359	0.046520908	8.716252775	4.35813E-05	0.002774989
400	0.002	89.70911053	0.046944827	8.763197602	4.3816E-05	0.002731173
401	0.002005	90.53186083	0.047375373	8.810572974	4.40529E-05	0.00268712
402	0.00201	91.36750017	0.047812663	8.858385638	4.42919E-05	0.002642828
403	0.002015	92.2162589	0.048256819	8.906642457	4.45332E-05	0.002598295
404	0.00202	93.07837218	0.048707964	8.95535042	4.47768E-05	0.002553518
405	0.002025	93.95408006	0.049166222	9.004516642	4.50226E-05	0.002508495

406	0.00203	94.84362764	0.049631723	9.054148365	4.52707E-05	0.002463225
407	0.002035	95.74726518	0.050104597	9.104252962	4.55213E-05	0.002417703
408	0.00204	96.66524822	0.050584978	9.154837939	4.57742E-05	0.002371929
409	0.002045	97.59783773	0.051073002	9.205910942	4.60296E-05	0.0023259
410	0.00205	98.54530022	0.05156881	9.257479752	4.62874E-05	0.002279612
411	0.002055	99.50790791	0.052072543	9.309552295	4.65478E-05	0.002233065
412	0.00206	100.4859389	0.052584347	9.362136642	4.68107E-05	0.002186254
413	0.002065	101.4796771	0.053104371	9.415241013	4.70762E-05	0.002139178
414	0.00207	102.4894129	0.053632766	9.46887378	4.73444E-05	0.002091833
415	0.002075	103.5154426	0.054169688	9.523043468	4.76152E-05	0.002044218
416	0.00208	104.5580693	0.054715295	9.577758763	4.78888E-05	0.001996329
417	0.002085	105.6176025	0.05526975	9.633028513	4.81651E-05	0.001948164
418	0.00209	106.6943586	0.055833217	9.68886173	4.84443E-05	0.00189972
419	0.002095	107.7886609	0.056405866	9.745267595	4.87263E-05	0.001850994
420	0.0021	108.9008399	0.05698787	9.802255465	4.90113E-05	0.001801982
421	0.002105	110.0312336	0.057579405	9.85983487	4.92992E-05	0.001752683
422	0.00211	111.1801872	0.058180653	9.918015524	4.95901E-05	0.001703093
423	0.002115	112.348054	0.058791799	9.976807322	4.9884E-05	0.001653209
424	0.00212	113.535195	0.05941303	10.03622035	5.01811E-05	0.001603028
425	0.002125	114.7419794	0.060044541	10.09626489	5.04813E-05	0.001552547
426	0.00213	115.9687849	0.060686529	10.15695142	5.07848E-05	0.001501762
427	0.002135	117.2159975	0.061339196	10.21829062	5.10915E-05	0.00145067
428	0.00214	118.4840125	0.062002749	10.28029337	5.14015E-05	0.001399269
429	0.002145	119.7732337	0.062677399	10.34297077	5.17149E-05	0.001347554
430	0.00215	121.0840747	0.063363363	10.40633413	5.20317E-05	0.001295522
431	0.002155	122.4169585	0.064060862	10.47039499	5.2352E-05	0.00124317
432	0.00216	123.7723177	0.064770122	10.53516511	5.26758E-05	0.001190495
433	0.002165	125.1505954	0.065491376	10.60065649	5.30033E-05	0.001137491
434	0.00217	126.5522448	0.06622486	10.66688135	5.33344E-05	0.001084157
435	0.002175	127.9777298	0.066970817	10.73385217	5.36693E-05	0.001030488
436	0.00218	129.4275253	0.067729495	10.80158166	5.40079E-05	0.00097648
437	0.002185	130.9021176	0.06850115	10.87008281	5.43504E-05	0.000922129
438	0.00219	132.4020042	0.069286042	10.93936885	5.46968E-05	0.000867432
439	0.002195	133.927695	0.070084437	11.00945329	5.50473E-05	0.000812385
440	0.0022	135.4797118	0.070896608	11.0803499	5.54017E-05	0.000756983
441	0.002205	137.0585891	0.071722835	11.15207273	5.57604E-05	0.000701223
442	0.00221	138.6648743	0.072563405	11.22463614	5.61232E-05	0.0006451
443	0.002215	140.2991282	0.073418611	11.29805475	5.64903E-05	0.00058861
444	0.00222	141.9619253	0.074288754	11.3723435	5.68617E-05	0.000531748
445	0.002225	143.6538542	0.075174141	11.44751765	5.72376E-05	0.00047451
446	0.00223	145.3755179	0.076075089	11.52359273	5.7618E-05	0.000416892
447	0.002235	147.1275344	0.07699192	11.60058465	5.80029E-05	0.000358889
448	0.00224	148.9105371	0.077924966	11.67850962	5.83925E-05	0.000300497
449	0.002245	150.7251752	0.078874567	11.75738419	5.87869E-05	0.00024171
450	0.00225	152.5721142	0.079841072	11.83722526	5.91861E-05	0.000182524
451	0.002255	154.4520363	0.080824836	11.9180501	5.95903E-05	0.000122934
452	0.00226	156.365641	0.081826226	11.99987632	5.99994E-05	6.29342E-05
453	0.002265	158.3136456	0.082845618	12.08272194	6.04136E-05	2.52054E-06
454	0.00227	160.2967857	0.083883396	12.16660534	6.0833E-05	-5.83125E-05
i	Time	Force	dV	V _{i+1}	dx	X _{i+1}
[]	[seconds]	[newtons]	[meters/second]	[meters/second]	[meters]	[meters]

The final result is determined at the step for which the valve disk displacement turns negative, meaning the valve disk has traversed at least 0.010 inches by the end of this time step. For the terminal time step, the speed sheet relays the time required for the valve disk to complete the traverse and the velocity of the valve disk as it passes through the 0.010-inch mark.

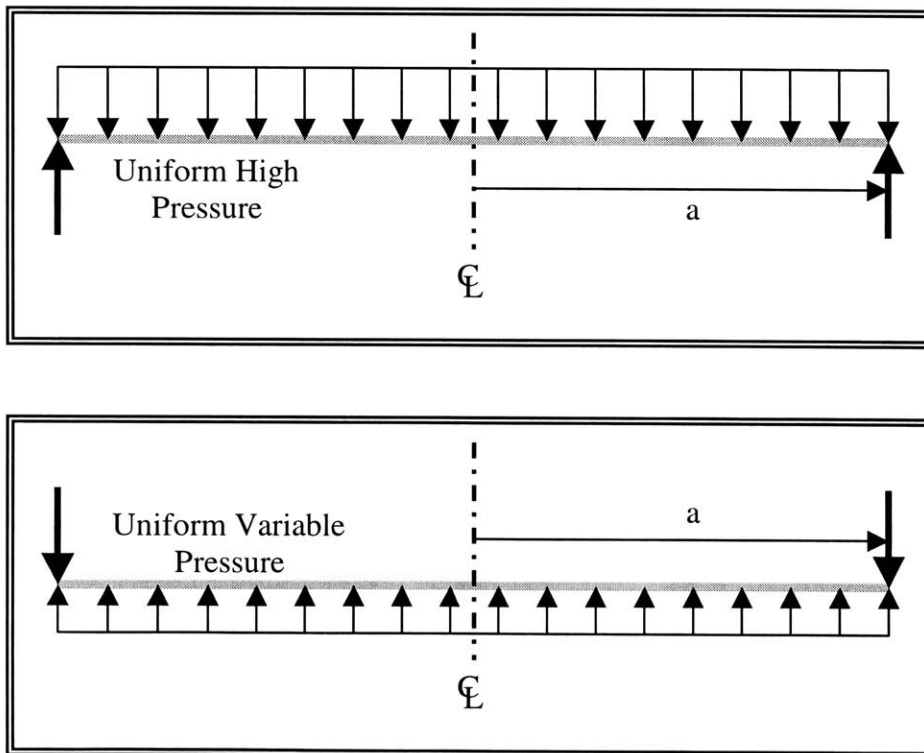
APPENDIX E - VALVE BULKHEAD DEFORMATION ANALYSIS

To develop the valve bulkhead deformation analysis presented in Chapter 7, solutions for various loading profiles on a flat circular plate were utilized in linear combination. The valve bulkhead is assumed to approach a simply supported flat circular plate of constant thickness. This assumption neglects the blind and through holes in the plate for the valve ports and permanent magnets, and it also ignores the features for the Indium seals on the outside radius.

The formulas used to determine the shape and the slope of the valve bulkhead under loading are found in Reference 10, Roark's Formulas for Stress & Strain. A review of the cases used for each load type is presented here. All formulas are for flat circular plates of constant thickness.

Uniform Pressure Across Entire Surface

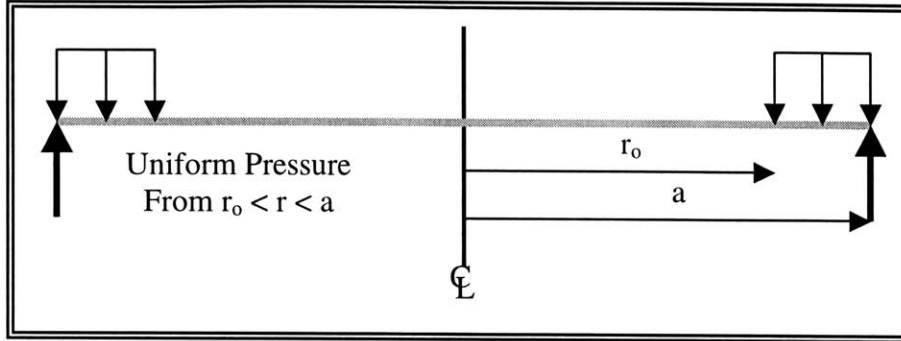
This formula set is used for the uniform high-pressure and the variable pressure components.



The formulas for this case appear on page 429 of Reference 10, Table 24, Case Number 10. A special case of this formula is used where $r_o = 0$. For the variable pressure component, the value of load was exercised through a range values characteristic of a full expander cycle. Individual spread sheets were developed to represent each of these characteristic values.

Uniform Pressure Across Partial Surface

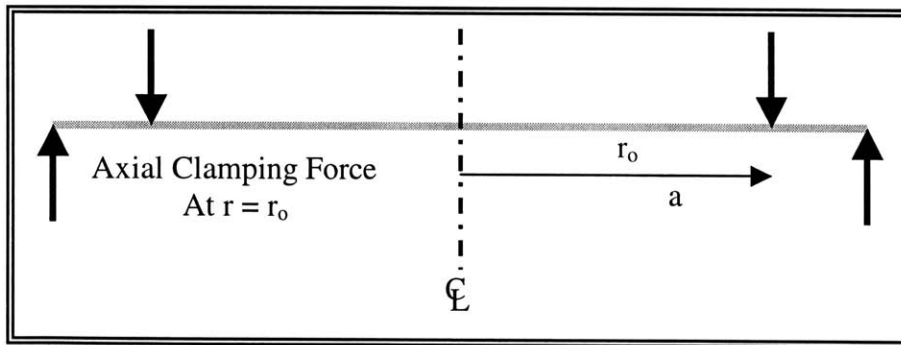
This formula set is used to subtract a high-pressure region and add a low-pressure region on the outer diameter of the valve bulkhead.



The formulas for this case appear on page 429 of Reference 10, Table 24, Case Number 10. The value r_0 is set at 0.83 inches, which is the radius of the high-pressure assembly contact with the valve bulkhead at the Indium seal.

Clamping Pressure

This formula set represents the annular line pressure load imposed on the valve bulkhead as the high-pressure assembly is clamped down upon it to make a tight Indium seal.



The formulas for this case appear on page 429 of Reference 10, Table 24, Case Number 9. The value r_0 is set at 0.83 inches, which is the radius of the high-pressure assembly contact with the valve bulkhead at the Indium seal.

Deformation Calculation Process

The formulas specified above were coded into a Microsoft Excel spreadsheet and exercised for a characteristic set of points along the valve bulkhead surface to generate the deformation profile Figure 7.7 and the deformation slope profile in Figure 7.10. This spreadsheet analysis was copied and repeated for each characteristic value of variable pressure to generate a complete picture of the valve bulkhead deformation profile.

Included herein are the results for each of the deformation components. These solutions are added together via superposition to arrive at the final deformation data, which is presented at the end of this appendix.

Variable Uniform Pressure

Pressure Load	Pressure Load	Outer Radius	Elastic Modulus	Plate Thickness	Poisson's Ratio	Flexural Rigidity
[lb/in ²]	[N/m ²]	[m]	[N/m ²]	[m]	[-]	[Nm]
265	1827111.4	0.0235712	1.93053E+11	0.0064262	0.3	4691.557995

Point #	Radius	Displacement	Radius	Displacement
[-]	[m]	[m]	[in]	[in]
0	0	7.65821E-06	0	0.000301504
1	0.001240589	7.63181E-06	0.048842008	0.000300464
2	0.002419149	7.55797E-06	0.095241915	0.000297557
3	0.003597709	7.43706E-06	0.141641822	0.000292797
4	0.004776269	7.26981E-06	0.188041729	0.000286212
5	0.005954829	7.05721E-06	0.234441636	0.000277842
6	0.007133389	6.80054E-06	0.280841544	0.000267737
7	0.008311949	6.50138E-06	0.327241451	0.000255959
8	0.009490509	6.16157E-06	0.373641358	0.000242581
9	0.010669069	5.78323E-06	0.420041265	0.000227686
10	0.011847629	5.36878E-06	0.466441172	0.000211369
11	0.013026189	4.92091E-06	0.51284108	0.000193736
12	0.014204749	4.44258E-06	0.559240987	0.000174904
13	0.015383309	3.93706E-06	0.605640894	0.000155002
14	0.016561869	3.40789E-06	0.652040801	0.000134169
15	0.017740429	2.85887E-06	0.698440708	0.000112554
16	0.018918989	2.29412E-06	0.744840616	9.03195E-05
17	0.020097549	1.71801E-06	0.791240523	6.7638E-05
18	0.021276109	1.13521E-06	0.83764043	4.46931E-05
19	0.022454669	5.5066E-07	0.884040337	2.16795E-05
20	0.0235712	0	0.927998144	0

Uniform High Pressure

Pressure Load	Outer Radius	Elastic Modulus	Plate Thickness	Poisson's Ratio	Flexural Rigidity
[N/m ²]	[m]	[N/m ²]	[m]	[]	[Nm]
1827110.68	0.0235712	1.93053E+11	0.0064262	0.3	4691.557995
Point #	Radius	Displacement	Radis	Displacement	
[]	[m]	[m]	[in]	[in]	
0	0	-7.65821E-06	0	-0.000301504	
1	0.001240589	-7.6318E-06	0.048842008	-0.000300464	
2	0.002419149	-7.55796E-06	0.095241915	-0.000297557	
3	0.003597709	-7.43706E-06	0.141641822	-0.000292797	
4	0.004776269	-7.2698E-06	0.188041729	-0.000286212	
5	0.005954829	-7.0572E-06	0.234441636	-0.000277842	
6	0.007133389	-6.80054E-06	0.280841544	-0.000267737	
7	0.008311949	-6.50138E-06	0.327241451	-0.000255959	
8	0.009490509	-6.16157E-06	0.373641358	-0.000242581	
9	0.010669069	-5.78323E-06	0.420041265	-0.000227686	
10	0.011847629	-5.36878E-06	0.466441172	-0.000211369	
11	0.013026189	-4.9209E-06	0.51284108	-0.000193736	
12	0.014204749	-4.44258E-06	0.559240987	-0.000174904	
13	0.015383309	-3.93706E-06	0.605640894	-0.000155002	
14	0.016561869	-3.40789E-06	0.652040801	-0.000134168	
15	0.017740429	-2.85887E-06	0.698440708	-0.000112554	
16	0.018918989	-2.29412E-06	0.744840616	-9.03194E-05	
17	0.020097549	-1.71801E-06	0.791240523	-6.7638E-05	
18	0.021276109	-1.13521E-06	0.83764043	-4.46931E-05	
19	0.022454669	-5.50659E-07	0.884040337	-2.16795E-05	
20	0.0235712	0	0.927998144	0	

Uniform Annular High Pressure

Pressure Load	Pressure Radius	Outer Radius	Elastic Modulus	Plate Thickness	Poisson's Ratio	Flexural Rigidity
[N/m ²]	[m]	[m]	[N/m ²]	[m]	[-]	[Nm]
1827110.68	0.021082	0.0235712	1.93053E+11	0.0064262	0.3	4691.557995
L17	L11					
[-]	[-]					
0.005244285	4.95709E-06					
Point #	Radius	G11	r-ro	Displacement	Radius	Displacement
[-]	[m]	[-]	[m]	[m]	[in]	[in]
0	0	n/a	-0.021082	-2.41891E-07	0	-9.52323E-06
1	0.001240589	8370.247026	-0.019841411	-2.41219E-07	0.048842008	-9.49678E-06
2	0.002419149	355.1516734	-0.018662851	-2.39336E-07	0.095241915	-9.42267E-06
3	0.003597709	47.93257897	-0.017484291	-2.36241E-07	0.141641822	-9.30083E-06
4	0.004776269	10.41838667	-0.016305731	-2.31934E-07	0.188041729	-9.13125E-06
5	0.005954829	2.919273363	-0.015127171	-2.26414E-07	0.234441636	-8.91393E-06
6	0.007133389	0.95137963	-0.013948611	-2.19682E-07	0.280841544	-8.64889E-06
7	0.008311949	0.340308641	-0.012770051	-2.11738E-07	0.327241451	-8.33611E-06
8	0.009490509	0.128650557	-0.011591491	-2.02581E-07	0.373641358	-7.97559E-06
9	0.010669069	0.049968189	-0.010412931	-1.92211E-07	0.420041265	-7.56735E-06
10	0.011847629	0.019460039	-0.009234371	-1.80629E-07	0.466441172	-7.11137E-06
11	0.013026189	0.007416022	-0.008055811	-1.67835E-07	0.51284108	-6.60765E-06
12	0.014204749	0.002687929	-0.006877251	-1.53828E-07	0.559240987	-6.05621E-06
13	0.015383309	0.000891609	-0.005698691	-1.38609E-07	0.605640894	-5.45703E-06
14	0.016561869	0.000254875	-0.004520131	-1.22177E-07	0.652040801	-4.81011E-06
15	0.017740429	5.62279E-05	-0.003341571	-1.04533E-07	0.698440708	-4.11547E-06
16	0.018918989	7.43591E-06	-0.002163011	-8.60475E-08	0.744840616	-3.38769E-06
17	0.020097549	2.44522E-07	-0.000984451	-6.56231E-08	0.791240523	-2.58358E-06
18	0.021276109	2.87618E-10	0.000194109	-4.43262E-08	0.83764043	-1.74512E-06
19	0.022454669	5.67419E-07	0.001372669	-2.18886E-08	0.884040337	-8.61753E-07
20	0.0235712	4.95709E-06	0.0024892	5.36633E-23	0.927998144	2.11273E-21

Uniform Annular Low Pressure

Pressure Load	Pressure Radius	Outer Radius	Elastic Modulus	Plate Thickness	Poisson's Ratio	Flexural Rigidity
[N/m ²]	[m]	[m]	[N/m ²]	[m]	[]	[Nm]
103421.36	0.021082	0.0235712	1.93053E+11	0.0064262	0.3	4691.557995
L17	L11					
[]	[]					
0.005244285	4.95709E-06					
Point #	Radius	G11	r-ro	Displacement	Radius	Displacement
[]	[m]	[]	[m]	[m]	[in]	[in]
0	0	n/a	-0.021082	-1.36919E-08	0	-5.39051E-07
1	0.001240589	8370.247026	-0.019841411	-1.36539E-08	0.048842008	-5.37554E-07
2	0.002419149	355.1516734	-0.018662851	-1.35473E-08	0.095241915	-5.33359E-07
3	0.003597709	47.93257897	-0.017484291	-1.33722E-08	0.141641822	-5.26462E-07
4	0.004776269	10.41838667	-0.016305731	-1.31283E-08	0.188041729	-5.16863E-07
5	0.005954829	2.919273363	-0.015127171	-1.28159E-08	0.234441636	-5.04562E-07
6	0.007133389	0.95137963	-0.013948611	-1.24348E-08	0.280841544	-4.8956E-07
7	0.008311949	0.340308641	-0.012770051	-1.19851E-08	0.327241451	-4.71855E-07
8	0.009490509	0.128650557	-0.011591491	-1.14668E-08	0.373641358	-4.51449E-07
9	0.010669069	0.049968189	-0.010412931	-1.08799E-08	0.420041265	-4.2834E-07
10	0.011847629	0.019460039	-0.009234371	-1.02243E-08	0.466441172	-4.0253E-07
11	0.013026189	0.007416022	-0.008055811	-9.50008E-09	0.51284108	-3.74018E-07
12	0.014204749	0.002687929	-0.006877251	-8.70724E-09	0.559240987	-3.42804E-07
13	0.015383309	0.000891609	-0.005698691	-7.84578E-09	0.605640894	-3.08888E-07
14	0.016561869	0.000254875	-0.004520131	-6.91569E-09	0.652040801	-2.72271E-07
15	0.017740429	5.62279E-05	-0.003341571	-5.91696E-09	0.698440708	-2.32951E-07
16	0.018918989	7.43591E-06	-0.002163011	-4.87061E-09	0.744840616	-1.91756E-07
17	0.020097549	2.44522E-07	-0.000984451	-3.71452E-09	0.791240523	-1.4624E-07
18	0.021276109	2.87618E-10	0.000194109	-2.50903E-09	0.83764043	-9.87805E-08
19	0.022454669	5.67419E-07	0.001372669	-1.23898E-09	0.884040337	-4.87784E-08
20	0.0235712	4.95709E-06	0.0024892	-2.2489E-24	0.927998144	-8.85391E-23

Annular Clamping Pressure

Force Load	Radius of Application	Outer Radius	Elastic Modulus	Plate Thickness	Poisson's Ratio	Flexural Rigidity
[N]	[m]	[m]	[N/m ²]	[m]	[]	[Nm]
1335	0.021082	0.0235712	1.93053E+11	0.0064262	0.3	4691.557995
L9	L3					
0.09619549	0.000185572					

Point #	Radius	G3	r-ro	Displacement	Radius	Displacement
[]	[m]	[]	[m]	[m]	[in]	[in]
0	0	n/a	-0.021082	-1.37185E-07	0	-5.40098E-06
1	0.001240589	-2264.892855	-0.019841411	-1.36803E-07	0.048842008	-5.38594E-06
2	0.002419149	-199.6544254	-0.018662851	-1.35733E-07	0.095241915	-5.3438E-06
3	0.003597709	-42.69433129	-0.017484291	-1.33973E-07	0.141641822	-5.27452E-06
4	0.004776269	-13.16350149	-0.016305731	-1.31524E-07	0.188041729	-5.1781E-06
5	0.005954829	-4.935096951	-0.015127171	-1.28385E-07	0.234441636	-5.05453E-06
6	0.007133389	-2.079207511	-0.013948611	-1.24558E-07	0.280841544	-4.90383E-06
7	0.008311949	-0.9416686	-0.012770051	-1.2004E-07	0.327241451	-4.72598E-06
8	0.009490509	-0.445376782	-0.011591491	-1.14834E-07	0.373641358	-4.521E-06
9	0.010669069	-0.215282803	-0.010412931	-1.08938E-07	0.420041265	-4.28887E-06
10	0.011847629	-0.10439806	-0.009234371	-1.02352E-07	0.466441172	-4.0296E-06
11	0.013026189	-0.049859265	-0.008055811	-9.50773E-08	0.51284108	-3.74319E-06
12	0.014204749	-0.022952762	-0.006877251	-8.71131E-08	0.559240987	-3.42964E-06
13	0.015383309	-0.009894088	-0.005698691	-7.84596E-08	0.605640894	-3.08895E-06
14	0.016561869	-0.003817174	-0.004520131	-6.91166E-08	0.652040801	-2.72112E-06
15	0.017740429	-0.001213273	-0.003341571	-5.90843E-08	0.698440708	-2.32615E-06
16	0.018918989	-0.000262852	-0.002163011	-4.83629E-08	0.744840616	-1.90405E-06
17	0.020097549	-2.00614E-05	-0.000984451	-3.70703E-08	0.791240523	-1.45946E-06
18	0.021276109	1.25986E-07	0.000194109	-2.55425E-08	0.83764043	-1.00561E-06
19	0.022454669	3.68881E-05	0.001372669	-1.20611E-08	0.884040337	-4.74845E-07
20	0.0235712	0.000185572	0.0024892	6.91548E-10	0.927998144	2.72262E-08

Superposition Result

Radius [inches]	Displacement [inches]	Slope [radians]	Slope [degrees]
0	-1.54631E-05	9.44577E-07	5.41203E-05
0.047894641	-1.54202E-05	2.64718E-06	0.000151672
0.09339455	-1.52997E-05	4.35214E-06	0.000249359
0.138894459	-1.51017E-05	6.0571E-06	0.000347046
0.184394368	-1.48261E-05	7.76207E-06	0.000444734
0.229894277	-1.44729E-05	9.46703E-06	0.000542421
0.275394186	-1.40422E-05	1.1172E-05	0.000640108
0.320894095	-1.35338E-05	1.2877E-05	0.000737795
0.366394004	-1.29479E-05	1.45819E-05	0.000835483
0.411893913	-1.22845E-05	1.62869E-05	0.00093317
0.457393822	-1.15434E-05	1.79919E-05	0.001030857
0.502893731	-1.07248E-05	1.96968E-05	0.001128545
0.54839364	-9.82859E-06	2.14018E-05	0.001226233
0.593893549	-8.85481E-06	2.31068E-05	0.00132392
0.639393458	-7.80345E-06	2.48117E-05	0.001421608
0.684893367	-6.67452E-06	2.61772E-05	0.001499844
0.730393276	-5.48346E-06	2.84441E-05	0.001629729
0.775893185	-4.18925E-06	2.94453E-05	0.001687091
0.821393094	-2.84949E-06	0.00019364	0.011094737
0.866893003	-1.38537E-06	0.000357834	0.020502382
0.90999818	2.72262E-08	0.000522028	0.029910027

APPENDIX F - VALVE SEALING AND DEFORMATION CALCULATIONS

To determine whether the valve ports in the valve bulkhead properly seal while the valve bulkhead undergoes dynamic deformation, Equation 7.5 was developed from Hooke's law. To meet the sealing criteria, the total valve seat deformation, δ , must be greater than the gap created by the angle of contact between the valve disk and the valve seat.

$$\frac{F}{3} \left(\frac{L}{AY} \right) = \delta \geq g = 2r_o \sin(\Theta) \quad (\text{Equation 7.5})$$

Physical values representing the upper bound and the lower bound case are plugged into this equation as follows to yield the results reported in this thesis. From Chapter 3, the total sealing force of the button magnets is found to be about 1.75 newtons. According to Reference 6, the Elastic Modulus of Kel-F plastic at 10 Kelvin is 7.2×10^9 newtons-per-square-meter, or about 4.65×10^6 newtons-per-square-inch.

Upper Bound Limit

According to the deflection analysis in Chapter 7, the largest contact angle, Θ , is about 0.027 degrees for the largest pressure difference in the cycle at the location of the outlet valve ports.

$$\pi \left(\left(\frac{0.095}{2} \right)^2 - \left(\frac{0.045}{2} \right)^2 \right) = 0.0055 = A$$

$$2(0.095) \sin(.027) = 8.95 * 10^{-5} = g$$

$$\frac{1.75}{3} \left(\frac{0.01}{(.0055)(4.64 * 10^6)} \right) = 2.28 * 10^{-7} = \delta$$

$$\begin{aligned} \text{gap, } g &= 8.95 \times 10^{-5} \text{ inches} \\ \text{deflection, } \delta &= 2.28 \times 10^{-7} \text{ inches} \end{aligned}$$

Lower Bound Limit

According to the deflection analysis in Chapter 7, the smallest contact angle, Θ , encountered in the cycle is about 0.027 degrees for the largest pressure difference in the cycle at the location of the outlet valve ports is 0.0017 degrees. In addition, the force imposed on the valve disk increased by 1.19 newtons owing to the pressure difference across the valve ports providing back pressure sealing on the valve disk.

$$2(0.095)\sin(.0017) = 6.64 * 10^{-6} = g$$

$$\frac{2.94}{3} \left(\frac{0.01}{(.0055)(4.64 * 10^6)} \right) = 3.84 * 10^{-7} = \delta$$

gap, $g = 6.64 \times 10^{-6}$ inches
deflection, $\delta = 3.84 \times 10^{-7}$ inches

This analysis predicts that the valve ports will not seal properly seal under any circumstances. However, the order of magnitude of the deformation numbers shows that deformation is not a controlling factor in valve port sealing.